Circulating Fluidized Bed Combustion of Western Canadian Fuels

by

J.R. Grace, C.M.H. Brereton, C.J. Lim, R. Legros, J. Zhao, R.C. Senior, R.L. Wu, J.R. Muir and R. Engman

Department of Chemical Engineering
2216 Main Mall
Vancouver, BC
V6T 1W5

Final Report, Prepared for Energy Mines and Resources Canada
Under contract 52SS.23440-7-9136

August 1989

MICROMEDIA

Abstract

This report describes tests carried out during the 1987–89 period in the 152 mm square × 7.3 m tall UBC pilot scale circulating fluidized bed combustion unit. The unit was first modified to increase its flexibility, safety and capability by adding analyzers, providing a tapered bottom section, installing a baghouse, introducing novel multi-point solids and gas sampling systems, incorporating return of solids captured in the secondary cyclone and a series of other changes described in the report.

Combustion tests were then carried out with Highvale coal (a subbituminous Alberta coal), Minto coal (a high sulphur bituminous coal from New Brunswick), Poplar River lignite from Saskatchewan, an anthracitic coal from Mt. Klappan, BC and two pitches derived from upgrading of unconventional crudes. Calcining tests were also conducted using a calcium carbonate of direct interest to the pulp and paper industry. Typical operating conditions were temperatures from 800–950°C, superficial gas velocities of 5–9 m/s, solids circulation rates of 20–100 kg/m^2 s and solids feed rates of 15–25 kg/h. The secondary/primary air ratio was varied from about 0.3 to 2.

Circulating fluidized bed combustion was found to be well suited to each of the fuels investigated, despite their very different properties. The provision of recycle of solids from the secondary cyclone led to significant improvements in combustion efficiency and in sulphur capture. On the other hand, the introduction of the secondary air in such a way that swirl was created inside the riser had little influence on the performance of the combustor for the conditions studied.

NO_x emissions were generally in the range 100–200 ppm, and increased with increasing Ca:S molar ratio. CO emissions were usually of the order of 100 ppm, but with considerable scatter. Relatively uniform temperatures were obtained for all fuels. A product of uniform size and favorable reactivity was obtained in the calcining trial.

Gas samples withdrawn from the riser showed that there are pronounced lateral gradients in CFBC systems associated with the tendency of solids to be conveyed upwards in dilute flow in the core, while there is downflow in an annular region near the wall. The result is that oxygen is lower near the wall, while higher levels of CO and CH_4 are measured near the wall than in the core. A more complex pattern occurs for NO_x with the wall region showing higher levels than the core at the bottom where NO_x tends to be generated and lower levels near the wall in the upper regions where reduction occurs due to carbon and reducing gases.

Axial suspension density profiles derived from differential pressure measurements under combustion conditions show similar trends to those determined under room temperature conditions. Preliminary capacitance probe results obtained at high temperature after modifying the dielectric used to insulate the needle from the sheath also show similar traces to those produced in a low temperature cold model unit. Erosion probes inserted into the combustor from the side show clearly the core-annular structure of solids flow in the high temperature CFBC riser.

Analysis of the solids residues withdrawn under inert conditions during runs with the high sulphur Minto coal indicate that efficient recirculation of solids captured in the secondary cyclone results in significantly lower proportions of calcium sulphide than in earlier runs where there was no return of these solids. When there was no recirculation of solids from the secondary cyclone, the proportion of CaS was much higher in the finest material caught in the baghouse and secondary cyclone, but the concentration was quite uniform at seven different sampling positions, including the above two, when proper recycle was established.

Further heat transfer results showed that the membrane wall gave lower heat transfer coefficients than a single tube for similar operating conditions. Radiation plays a strong role, especially for dilute conditions. As in earlier work, local heat transfer was found to decrease with increasing distance downward along the heat transfer surface.

Preliminarily measurements indicated levels of N_2O to be of the order of 10– 60 ppm, but further work is required to confirm these values and to show the mechanisms which lead to formation and destruction of N_2O.

Initial steps have also been taken to develop a comprehensive model to predict reaction rates in CFBC risers. The model is based on a two-zone concept with interchange between a wall region and the core. Most of the conceptual and hydrodynamic aspects of the model have been worked out.

Some preliminary transient measurements have also been obtained as a first step in developing combustor control strategies and models. Some radial profiles of gas concentration determined in the secondary cyclone at a single level show higher CO concentrations near the wall of the cyclone than in the core.

Sommaire

Ce rapport décrit les essais de combustion qui ont eu lieu de 1987–1989 dans une installation pilote de combustion à l'Université de la Colombie Britannique. L'installation, qui a une section transversale carrée de 152 mm de diamètre et une hauteur de 7.3 m, fut l'objet de plusieurs modifications ayant pour but d'accroitre sa flexibilité, sa sécurité et sa capacité. Celles-ci incluent l'addition de nouveaux instruments analytiques, une nouvelle section inférieure conique, l'installation d'un filtre à sacs, la possibilité de retourner les solides capturés par le cyclone secondaire, un nouveau système d'échantillonnage des gaz et plusieurs autres changements qui sont décris dans le rapport.

Les essais de combustion ont été exécuté avec quatre types de charbon, soit un sous-bitumineux (Highvale) d'Alberta, un lignite de Poplar River en Saskatchewan, un anthracite de Mt. Klappan en Colombie Britannique et un bitumineux à haute teneur en soufre de la Nouvelle Ecosse (Minto), ainsi qu'avec deux bitumes produits lors de procédés de revalorisation des huiles lourdes. Les essais de calcination ont été conduit avec un carbonate de calcium provenant d'une usine de Pâtes et Papier. Les conditions d'opération étaient typiquement une température de 800–950°C, une vitesse superficielle de fluidisation de 5–9 m/s, une circulation de solides à un taux de 20–100 kg/m^2s et un débit de combustible de 15–25 kg/h. Le rapport des débits d'air secondaire et d'air primaire fut varié entre 0.3 et 2.0.

En dépit de leurs propriétés différentes, chacun des combustibles à l'essai était bien adapté pour la combustion en lit fluidisé circulant. Le retour des solides capturés par le cyclone secondaire eut un effet significatif sur le rendement de combustion ainsi que sur la capture du soufre par le calcaire. L'introduction d'un tourbillon dans le réacteur, par contre, n'eut aucun effet sur la performance du système pour les conditions étudiées.

Les émissions de NO_x étaient généralement entre 100–200 ppm, et avaient tendence à augmenter aver l'augmentation du rapport Ca:S. Les émissions de CO étaient habituellement aux alentours de 100 ppm, mais avaient tendance à varier beaucoup. Les profils de température étaient relativement uniformes pour tous les combustibles. Le produit obtenu lors de l'essai de calcination consistait de particules de taille uniforme et de réactivité remarquable.

L'analyse des gaz en provenance de différents endroits du réacteur a montré qu'il existe des gradients latéraux de concentration qui sont dût au fait que les solides voyagent de bas en haut en phase diluée dans le noyau, pendant qu'il y a un mouvement global de haut en bas dans la région annulaire près des parois. Ceci résulte en une concentration d'oxygène plus basse et des niveaux de CO et CH_4 plus élevés près des parois qu'au centre du réacteur. Pour les NO_x, les résultats sont un peu plus complexes, avec une plus grande concentration près des parois pour la partie inférieure du réacteur où le NO_x tend à être généré, et des concentrations plus faibles dans les parties supérieures où il y a réduction des NO_x à cause de la présence de carbone et de gaz réducteurs à ces niveaux.

Les profils axiaux de densité, qui ont été dérivé des pertes de pression mesurées à différents niveaux du réacteur opérant à températures de combustion, étaient similaires à ceux obtenus

à température ambiante. Plusieurs sondes introduites à différents niveaux ont montré des patrons d'érosion qui mettent en évidence la structure noyau-anneau du flux de solides dans un réacteur à lit circulant à hautes températures.

L'analyse des résidues obtenus lors de l'essai de combustion avec le charbon à haute teneur en soufre (Minto) a indiqué qu'une recirculation efficace des solides capturés par le cyclone secondaire résulte en une diminution importante du niveau de CaS. Sans recirculation secondaire, les proportions de CaS étaient beaucoup plus grandes dans les fractions de solides capturés dans le filtre à sacs et dans le cyclone secondaire. Les concentrations de CaS étaient, par contre, très uniformes dans les échantillons de solides pris à sept locations, incluant les deux énumérées plus haut, quand la recirculation secondaire était établit.

Il a été montré que les coefficients de transfert de chaleur sont inférieurs pour la membrane tubulaire que pour un simple tube exposé à des conditions similaires. Le transfert de chaleur par radiation joue un rôle très important, surtout à faible concentration de solides. Comme auparavant, le coefficient de transfert de chaleur local diminuait avec la distance verticale mesurée depuis le haut de la membrane tubulaire.

Une étude préliminaire a indiqué que les niveaux de N_2O dans le réacteur de combustion à lit circulant sont de l'ordre de 10–60 ppm, mais d'autres essais sont requis pour confirmer ces résultats et pour élucider le mécanisme de formation et de destruction du N_2O.

Les premiers pas ont été pris vers le développement d'un modèle mathématique capable de prédire les taux de réaction dans un système de combustion à lit circulant. Le modèle est basé sur un concept de deux phases, avec intéractions entre une région annulaire près des parois et un noyau au centre. Presque tous les aspects hydrodynamiques et conceptuels ont été résolu.

L'étude des réponses transitoires du système a été amorcé afin de développer une stratégie de contrôle pour les réacteurs à lit circulant. Quelques profils radiaux de concentration de gaz, obtenus à un seul niveau du cyclone secondaire, ont démontré que la concentration de CO près de la paroi est supérieure à celle mesurée au centre du cyclone.

Contents

ABSTRACT ii

SOMMAIRE iv

LIST OF TABLES ix

LIST OF FIGURES xi

ACKNOWLEDGEMENTS xiv

1 INTRODUCTION 1

2 THE EXPERIMENTAL FACILITIES 2
- 2.1 The Reactor Shaft 2
- 2.2 Fuel Feed System 8
- 2.3 Heat Transfer Surfaces 10
- 2.4 Solids Recycle Systems 10
- 2.5 Gas Exit and Analysis 13
- 2.6 Solids Sampling System 16
- 2.7 Instrumentation and Data Acquisition 16
- 2.8 Properties of Fuels, Sorbents and Inert Particles 21

3 MULTIFUEL COMBUSTION TRIALS 28
- 3.1 Experimental Procedure 28
  - 3.1.1 Start-up of the Unit 28
  - 3.1.2 Solids sampling procedures 29
  - 3.1.3 Gas sampling procedure 29
- 3.2 Results of Combustion Trials 29
  - 3.2.1 Highvale coal tests 29
  - 3.2.2 Minto coal tests 31
  - 3.2.3 Anthracite tests 34
  - 3.2.4 Lignite tests 38
  - 3.2.5 Pitch combustion tests 41

3.2.6 Calcination of calcium carbonate 54

4 GASEOUS POLLUTANT EMISSIONS 60
4.1 Multipoint Gas Sampling System 60
4.2 NO_x Emission Results 64
4.2.1 Effect of temperature 64
4.2.2 Effect of excess air ratio 66
4.2.3 Effect of staged combustion 66
4.2.4 Effect of Ca:S ratio 67
4.2.5 Fuel character and NO_x emission 67
4.3 SO_2 Emission and Sulphur Capture 68
4.4 Gas Concentration Profiles 68
4.4.1 NO_x concentration profiles at outer wall 69
4.4.2 Profiles at other radial positions 70
4.4.3 Other gas concentration profiles 71

5 HYDRODYNAMIC STUDIES IN THE CFBC PILOT PLANT 74
5.1 Suspension Density Profiles in the Riser 74
5.2 Capacitance Probe Study 77
5.3 Erosion Probe Results 78

6 SOLID RESIDUES FROM HIGH SULPHUR COAL 82
6.1 Background 82
6.2 Test Procedures 82
6.3 Experimental Results 83

7 HEAT TRANSFER STUDIES 87
7.1 Membrane Wall 87
7.2 Results 87

8 PRELIMINARY RESULTS OF FURTHER STUDIES 93
8.1 Determination of N_2O Emission Levels 93
8.2 Development of a CFBC Reactor Model 94
8.3 Transient Studies and Initial Work on Control Strategies 99
8.4 Study of Combustion Behaviour in Cyclone 101

9 CONCLUSIONS AND RECOMMENDATIONS 103
9.1 Conclusions 103
9.2 Recommendations 104

REFERENCES 106

APPENDICES 111

A Report on N_2O Measurement By Dr. K.C. Teo 111

B Output of Computer Program for Predictions of Axial Density Profiles in Riser 136

C Characterization of Solid Residues by Ortech International 140

List of Tables

2.1 Summary of Modifications in UBC-CFBC Facility During 1987–89 Contract Period. 5
2.2 Proximate and Ultimate Analyses of Solid Fuels. 23
2.3 Properties of Pitch Materials Tested. 24
2.4 Physical Properties of Particulate Materials. 25
2.5 Chemical Analyses of Limestones and Inerts. 26
2.6 Ash Composition of Fuels. 27

3.1 Chronology of Combustion Trials. 30
3.2 Operating Conditions and Combustion Results for Highvale Coal 32
3.3 Operating Conditions and Combustion Results for Minto Coal 35
3.4 NO_x Emissions from Combustion of Minto Coal (3% oxygen, sec./prim. air ratio = 1). 36
3.5 Operating Conditions and Combustion Results for Anthracite Coal 39
3.6 Carbon Content in CFBC for Anthracite Combustion Trial. (Conditions are described in Table 3.1, C in wt%) 41
3.7 Operating Conditions and Combustion Results for Lignite Coal (Run #15) . 42
3.8 Operating Conditions and Combustion Results for CANMET Pitch 44
3.9 Chemical Analysis of Samples from Run #17 – CANMET Pitch/Texlime. (See Table 3.8 for operating conditions). 47
3.10 Vanadium Mass Balance for CANMET Pitch Combustion Trial (Condition C6 in Table 3.8.) 49
3.11 Operating Conditions and Combustion Results for H-Oil Pitch 51
3.12 Chemical Analysis of Samples from Run #20 – H-Oil pitch/Texlime limestone (For conditions see Table 3.9). 52
3.13 Vanadium Mass Balance for H-Oil Pitch Combustion Trial (Entire Run #17). 54
3.14 Pros and Cons of Fluidized Bed Versus Rotary Kiln Calciners. 55
3.15 Operating Conditions and Results for Calcination Trial 56

4.1 Key Features of Gas Analyzers. 63
4.2 NO_x Emissions from Combustion of Anthracite (3% oxygen). 67

4.3 NO_x Emissions and Fuel Nitrogen-Volatiles Products, V_N (T = 820–880°C; Excess air = 10–25%; Secondary-to-primary air ratio = 0.5– 2.0; Superficial gas velocity = 7–10 m/s). 68

5.1 Particle Size Distribution of Bed Materials at the End of the Hydrodynamic Run (Run #21). 75

6.1 Key Details of Runs Where Solids Characterization was Carried Out. Further details are given in Table 3.3. 84
6.2 Chemical Analyses (% by mass) of Solid Samples. 85

7.1 Particle Size Analyses of Bed Materials for the Heat Transfer Runs 88

List of Figures

2.1 Simplified schematic diagram of circulating fluidized bed combustion facility (UBC). 3
2.2 View of principal refractory-lined reactor column. 4
2.3 Primary air distributor. 7
2.4 Secondary air port configuration. All dimensions are in mm. 7
2.5 Liquid fuel feeding system. 8
2.6 Atomizing nozzle for pitch feeding. All dimensions are in mm. 9
2.7 (a) Plan view and (b) section view of membrane wall heat transfer surface. All dimensions are in mm. 11
2.8 Hairpin configuration of the new heat transfer section. 12
2.9 Quartz window and calorimetric section for measuring solids circulation rate. All dimensions are in mm. (Ta_i: air temperature; Ts_i: average solids temperature). 14
2.10 Eductor configuration for secondary solids return. 15
2.11 Locations of solids sampling ports. 17
2.12 Top of reactor solids sampling system and operating procedure. 18
2.13 Nitrogen purged solids sampling system and operating procedure. 19
2.14 Thermocouple and pressure tap locations in CFBC reactor system. 20
2.15 Particle size distributions of solids fuels, sorbents and inert sand. 22

3.1 Typical temperature profile during Highvale combustion trials (Run #11, Condition 1; see Table 3.2 for operating conditions). 33
3.2 Sulphur capture versus Ca:S molar ratio for Minto coal combustion trials. 36
3.3 Particle size distribution of solids sampled from various locations during a Minto combustion trial (Run #16, Condition 1; see Table 3.3 for operating conditions). 37
3.4 Typical temperature profile during Anthracite coal combustion trials (Run #7, Condition 1; see Table 3.5 for operating conditions). 40
3.5 Sulphur capture versus Ca:S molar ratio for CANMET and H-Oil pitch combustion trails. 45

3.6 NO_x emission versus Ca:S molar ratio for CANMET and H-oil pitch combustion trials. (Secondary to primary air ratio = 0.77–0.86; superficial gas velocity = 8.2–8.8 m/s; see Tables 3.8 and 3.9 for operating conditions.) . . 46
3.7 Overall mass balance and typical temperature profile for the calcination trial. 57
3.8 Particle size distributions of $CaCO_3$ feed and CaO product. 58

4.1 Vertical gas sampling positions and sampling trains. 1. Sampling port; 2. Sampling probe extending into reactor; 3. Gas filter; 4. Flexible stainless steel tubing; 5. Heat exchanger; 6. Dryer; 7. Control Panel. Note that only one of the five sampling trains is shown. 61
4.2 Gas sampling system. 1. Reactor; 2. Primary cyclone; 3. Secondary cyclone; 4. Gas filter; 5. Heat exchanger; 6. Water trap; 7. Dryer; 8. Control valve; 9. Manifold; 10. Rotameter; 11. Control panel; 12. Three-way valve. 62
4.3 Gas probe with outer water-cooling. 63
4.4 Temperature effect on NO_x emission for Highvale coal at U=8.4 m/s, Secondary/primary air ratio = 1.0. 64
4.5 NO_x emission and bed temperature versus time after step decrease in fuel feed rate: U = 6.0 m/s, oxygen in flue gas = 9.5%, secondary/primary air ratio = 1.6. (Lignite Run #15) 65
4.6 NO_x emission vs. excess air ratio for Highvale coal: U = 8.0 m/s, T = 870 °C, secondary/primary air ratio = 1.0. 66
4.7 Axial NO_x concentrations at the wall for two secondary-to-primary air ratios for lignite combustion: U = 8.5 m/s, T = 870°C, oxygen in flue gas = 3.0%. 69
4.8 NO_x concentration profiles for Minto coal combustion: U = 7.6 m/s, T = 890°C, secondary to primary air ratio = 1.07, Ca/S = 3.0, oxygen in flue gas = 3.0%. 70
4.9 Oxygen concentration profiles for Minto coal combustion: U = 7.6 m/s, T = 890°C, secondary to primary air ratio = 1.07, Ca/S = 3.0, oxygen in flue gas = 3.0%. 71
4.10 CO concentration profiles for Minto coal combustion: U = 7.6 m/s, T = 890°C, secondary to primary air ratio = 1.07, Ca/S = 3.0, oxygen in flue gas = 3.0%. 72
4.11 SO_2 concentration profiles for Minto coal combustion: U = 7.6 m/s, T = 890°C, secondary to primary air ratio = 1.07, Ca/S = 3.0, oxygen in flue gas = 3.0%. 73

5.1 Axial density profiles. Silica sand particles and Highvale coal; temperature = 838–876°C; secondary to primary air ratio = 0.8–1.0. 76
5.2 Capacitance probe used for high temperature work. All dimensions in mm. . 78
5.3 Time trace of density measured at the wall of the reactor, (Height = 4.1 m above primary air distribution) from capacitance probe. (Temperature = 860°C; superficial velocity = 7.5 m/s; secondary to primary air ratio = 1.0). 79

5.4 Typical erosion patterns observed after 24 hour exposure (Highvale coal, Temperature = 840–890°C; G_s = 60 kg/m^2s; 304 stainless steel). 80

5.5 Erosion in the cooling tube region of the combustor after 24 hour exposure (Highvale coal; Temperature = 840–890°C; G_s = 60 kg/m^2s; 304 stainless steel). 81

7.1 Overall heat transfer coefficient for the membrane wall versus suspension density at three suspension temperatures: Bottom line: Run #6, C1 in Table 7.1; U=7.5 m/s. Other lines: Run #6, C2 in Table 7.1; U=8.8–9.5 m/s. 89

7.2 Cross-plot of overall heat transfer coefficient versus suspension temperature for membrane wall at four suspension density levels. 90

7.3 Local heat transfer coefficient along membrane wall versus z for two suspension temperatures. ρ_{susp} = 54 kg/m^3, Run #6, C1 in Table 7.1. 91

8.1 CFBC reactor model schematic. 96

8.2 Riser cross-section showing streamer distribution. 97

8.3 Comparison between predicted and experimental density profile. 98

8.4 Transient response to a step decrease in heat removal of 8.1 kW. 100

8.5 Radial CO concentration profile for secondary cyclone at a level of 203 mm below the top. Conditions: Superficial velocity = 7.5 m/s; Secondary to primary air ratio = 1.0; Reactor temperature = 872°C; Fuel: Highvale coal. 102

Acknowledgements

The authors are grateful to Hugh Ackroyd and Dr. Hongzhong Li, both of whom participated in the experimental work described in this report. We are also indebted to Dr. E.J. Anthony of E.M.R., who was both helpful and encouraging in his role as scientific authority for the project. We also wish to thank Roger Quan, who carried out a number of the analyses and participated in some of the fuel preparation tasks. The roles of Kurt Bose in the Pulp and Paper Centre workshop and of John Baranowsky and his staff in the Chemical Engineering workshop are also acknowledged with gratitude.

Chapter 1

INTRODUCTION

Circulating fluidized bed combustion (CFBC) continues to become a favoured technique for burning a wide range of coals, biomass and residues. CFBC boilers and power generation facilities are being installed or operated worldwide.

There is particular interest in this relatively new technology in Canada. A 22 MWe demonstration unit, partially funded by the Government of Canada, has been operated by New Brunswick Power at Chatham, New Brunswick since 1987. Nova Scotia Power is planning to construct a 150 MWe unit, probably the largest in the world, in the early 1990's, and it is considering a second such unit and retrofitting of several conventional power boilers to operate in the CFBC mode. New Brunswick Power is also considering large scale CFBC units for the 1990's. In Western Canada, a number of fuels such as residues from tar sands and heavy oil operations, woodwastes and certain coals seem to be ideal candidates for future CFBC installations.

While CFBC appears to be gaining in popularity, there continue to be many aspects of the performance of circulating fluidized beds which are not well understood and which could slow the effective utilization of the technology in Canada and in other countries. A number of these issues have been addressed in the Contract whose results are presented in the present report.

A 152 mm × 152 mm square × 7.32 m tall CFBC pilot plant unit has been operated in the Pulp and Paper Centre at the University of British Columbia (UBC) since late 1986. In a previous contract (Grace and Lim, 1987), preliminary information was obtained with a series of Canadian fuels, primarily Minto coal from New Brunswick, woodwastes (hogfuel and sawdust) and pitch derived from the CANMET hydrocracking demonstration unit operated by Petrocan in Montreal East. The data included heat transfer coefficients for both membrane cooling surfaces and for a vertical tube at different radial positions. Sulphur capture was determined as a function of the operating conditions for the high sulphur coal and for the pitch. NO_x levels were determined for each of the fuels tested and the solid wastes were examined for their calcium sulphide content. In the case of the pitch trials, the distribution of vanadium and nickel in the solid wastes was also determined. Various other measurements such as temperature profiles and solids densities derived from pressure measurements were also reported.

Chapter 2

THE EXPERIMENTAL FACILITIES

A diagram of the modified UBC–CFBC pilot plant is presented in Figure 2.1. Extensive modifications to the facilities were completed between August 1988 and January 1989. The extension equipment and modifications are summarized in Table 2.1. All the combustion trials and other tests presented in this report were performed in the experimental system described in the following sections.

2.1 The Reactor Shaft

The principal reactor shaft or riser is composed of five refractory-lined flanged sections providing a chamber of 152 mm square cross-section with an overall height of 7.32 m. A view of the reactor is shown in Figure 2.2. The refractory is erosion resistant and held in place by pins welded to the outside steel walls. The bottom section, which has stainless steel walls, is tapered gradually on the inside from a 51 mm × 152 mm cross-section at the bottom to 152 mm × 152 mm over its 1.22 m height. This feature is to provide a high acceleration region which helps to prevent agglomeration and sintering. Pressure taps and thermocouples are located at 610 mm maximum intervals along opposite east and west faces of the column. In addition, there are a series of twelve regularly spaced 41 mm diameter ports which can be used as viewing ports, for withdrawal of gas and/or solids samples or for insertion of probes and feed nozzles.

The distributor and plenum chamber are suspended from the bottom of the reactor for easy removal. Primary air is introduced to the bottom of the reactor through a novel distributor shown in Figure 2.3. This distributor has twenty 9.5 mm diameter orifices drilled at 30 and 50 degrees to the horizontal axis. Located at the centre of the base is a 38 mm tube which allows easy removal of agglomerates or sintered solids. The plenum chamber is also equipped with a drain pipe for removal of solids that might flow back through the distributor during shut down. For start-up of the unit, the primary air is preheated in the external burner by combustion of natural gas.

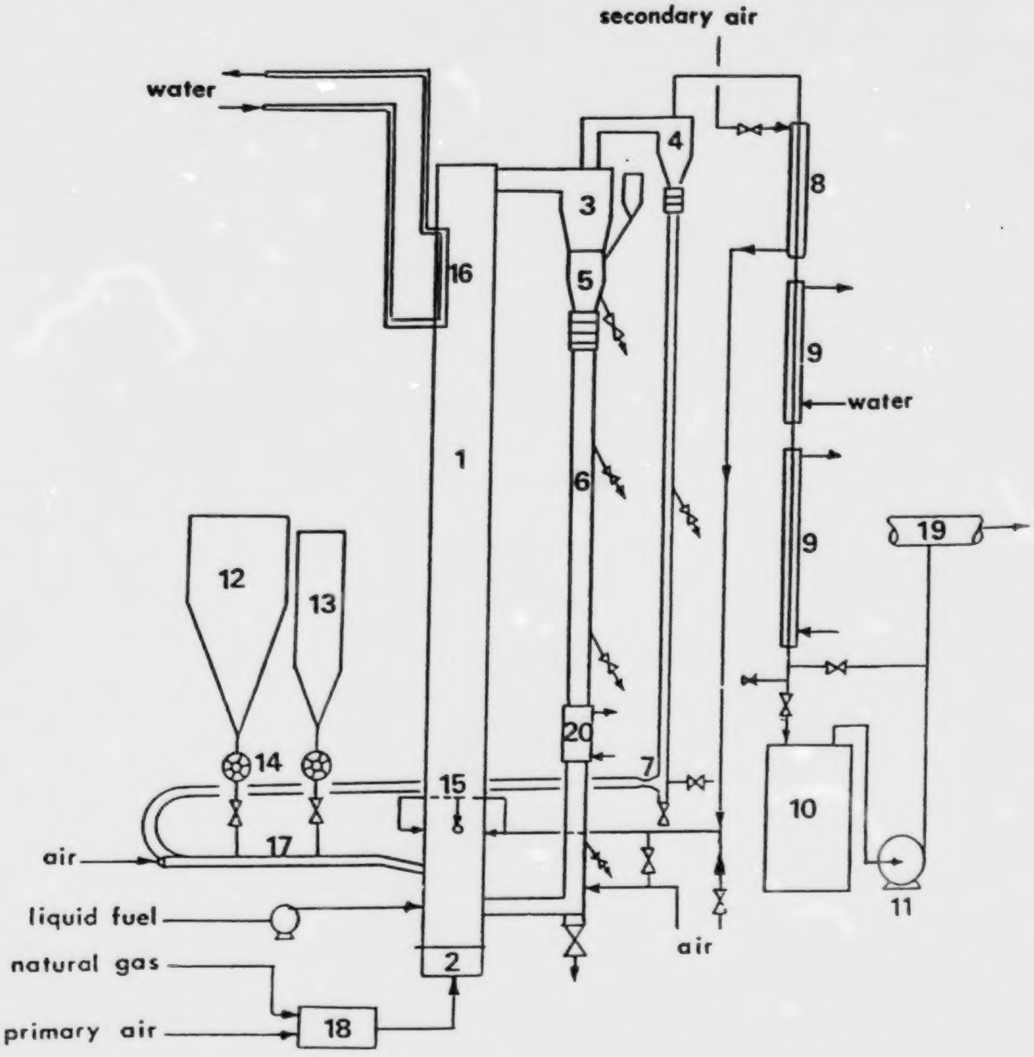
secondary air
water
4
8
3
16
5
9
water
1
6
9
19
12
13
20
14
7
15
10
air
17
liquid fuel
11
natural gas
2
air
primary air
18

1. Reactor; 2. Windox; 3. Primary cyclone; 4. Secondary cyclone; 5. Recycle hopper; 6. Standpipe; 7. Eductor; 8. Secondary air preheater; 9. Flue gas coolers; 10. Baghouse; 11. Induced draught fan; 12. Fuel hopper; 13. Sorbent hopper; 14. Rotary values; 15. Secondary air ports; 16. Membrane wall; 17. Pneumatic feed line; 18. External burner; 19. Ventilation; 20. Calorimetric section

FIGURE 2.1: Simplified schematic diagram of circulating fluidized bed combustion facility (UBC).

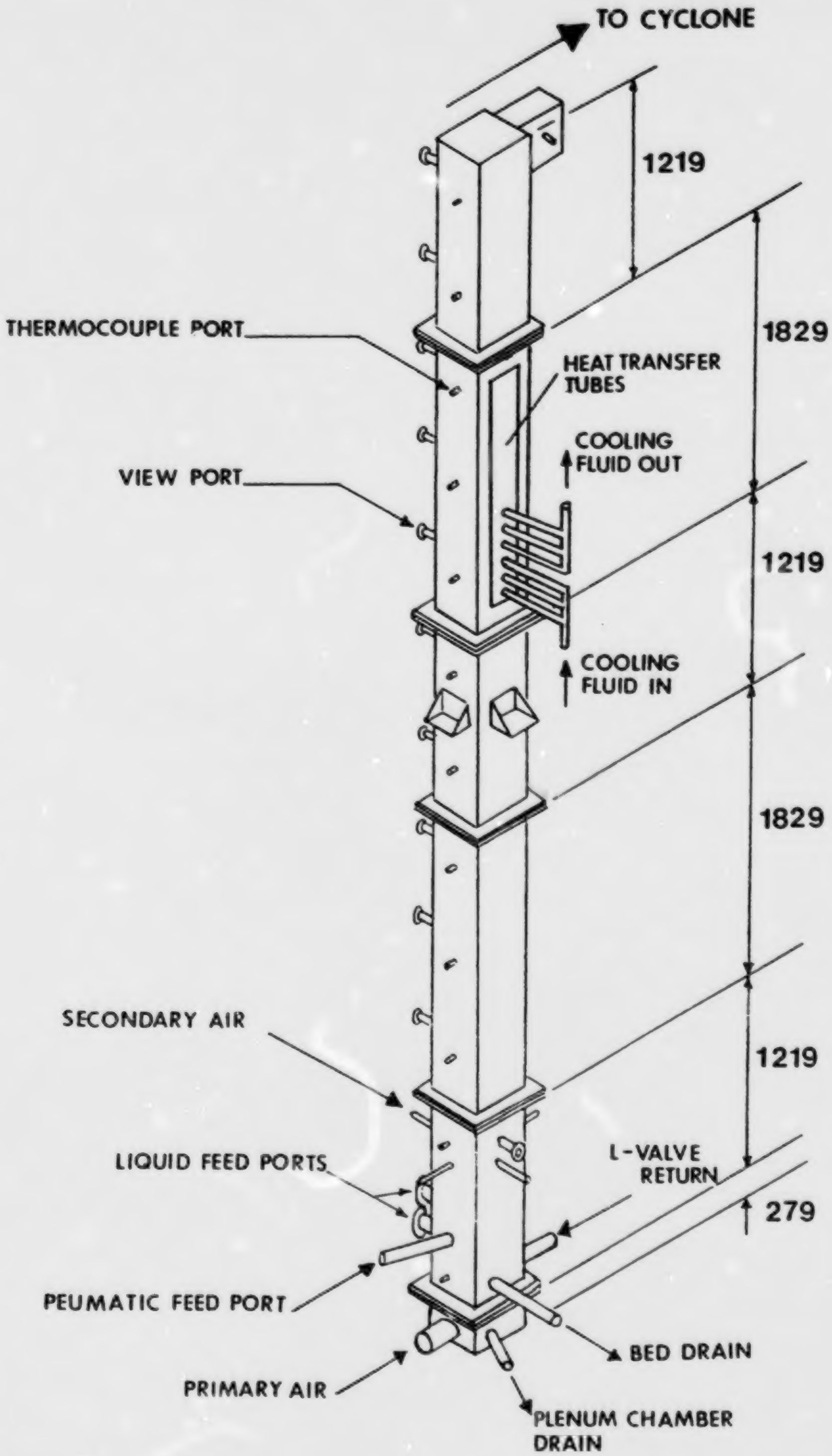
TO CYCLONE
1219
1829
1219
1829
1219
279
THERMOCOUPLE PORT
HEAT TRANSFER TUBES
COOLING FLUID OUT
VIEW PORT
COOLING FLUID IN
SECONDARY AIR
LIQUID FEED PORTS
L-VALVE RETURN
PEUMATIC FEED PORT
BED DRAIN
PRIMARY AIR
PLENUM CHAMBER DRAIN

FIGURE 2.2: View of principal refractory-lined reactor column.

TABLE 2.1: Summary of Modifications in UBC-CFBC Facility During 1987–89 Contract Period.

Modification	Justification
Baghouse installed	Capture of fines; more representative results
Reactor bottom changed to tapered section	Better able to deal with agglomerating fuels
Offset in standpipe from primary cyclone removed	Smoother recirculation
Secondary air preheating by heat exchange with flue gases	Increased flexibility and broader range of superficial velocity over which steady state operation can be maintained
Insulation improved	Faster start-up; greater flexibility and range of superficial velocity
Stainless steel hairpin cooling tubes capable of replacing membrane surface	Greater range of fuels and operating conditions
Stainless steel secondary cyclone replaces carbon steel secondary cyclone	Improved burnup of carbon monoxide and unburned carbon
Return system for solids captured in secondary cyclone	Improved sulphur capture and combustion efficiency
Analyzers for determination of CO, CO_2 and CH_4	On-line measurements of carbon monoxide, carbon dioxide and unburnt hydrocarbons
Improved (paramagnetic) oxygen analyzer	Continuous on-line oxygen measurements; greater accuracy
Improved SO_2 analyzer	Greater accuracy
Multipoint analysis system	Ability to obtain in-reactor axial and radial concentration profiles

TABLE 2.1· Summary of Modifications in UBC-CFBC Facility During 1987–89 Contract Period (continued)

Modification	Justification
Improved solids sampling system	Ability to take solids samples at different locations under a nitrogen purge for accurate determination of local solids composition
New solids feed hopper and load cells	Greater accuracy and more reliable feeding of solid fuels
Differential pressure transducers	Improved data acquisition and greater accuracy
Valve to control system pressure	Ability to maintain positive pressure in sample lines, hence improving accuracy
Improvements in pitch feed system including steam and new atomizer	More reliable and steady feeding of pitch and other liquids
Better support for thermal expansion	Greater safety and flexibility

Secondary air is fed to the reactor through four ports of diameter 35 mm located 0.9 m above the primary air distributor. This secondary air can either be injected through two pairs of directly opposed orifices (ports a,b,d and e in Figure 2.4) or through four off-centre ports (ports b,c,e and f in Figure 2.4) in order to create swirl in the reactor. The secondary air can also be preheated in the first flue gas cooling tubular heat exchanger. The primary and secondary air are metered (using rotameters) and controlled separately so that the ratio of their flows can be varied with a fixed total air flow.

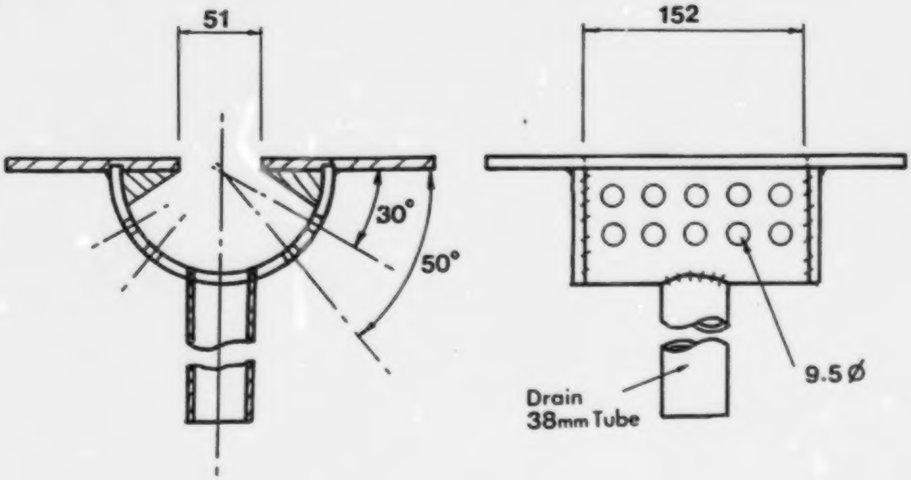
51
30°
50°
152
9.5 Ø
Drain
38mm Tube

FIGURE 2.3: Primary air distributor.

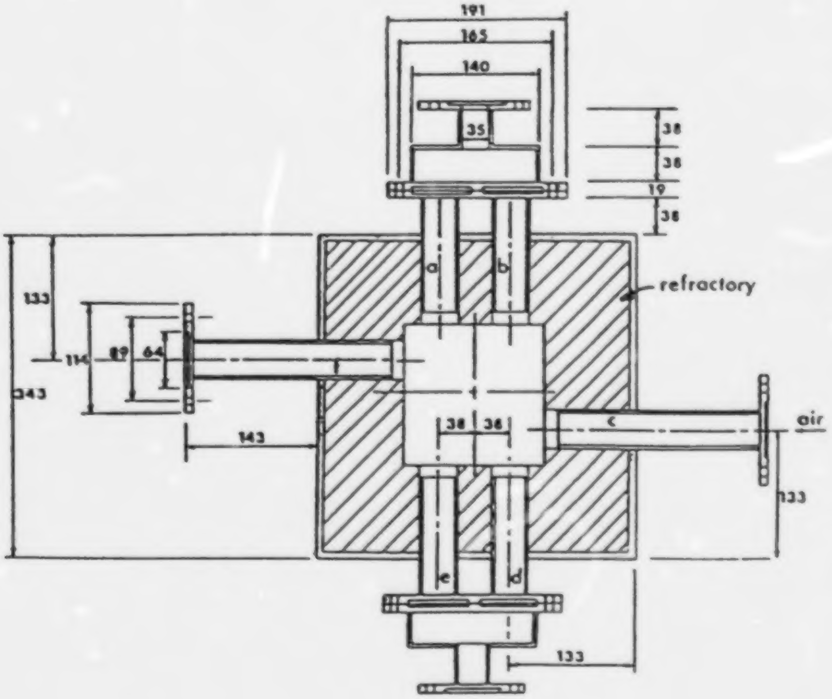
191
165
140
35
38
38
19
38
a
b
refractory
133
114
89
64
343
f
143
38
38
c
air
133
e
d
133

FIGURE 2.4: Secondary air port configuration. All dimensions are in mm.

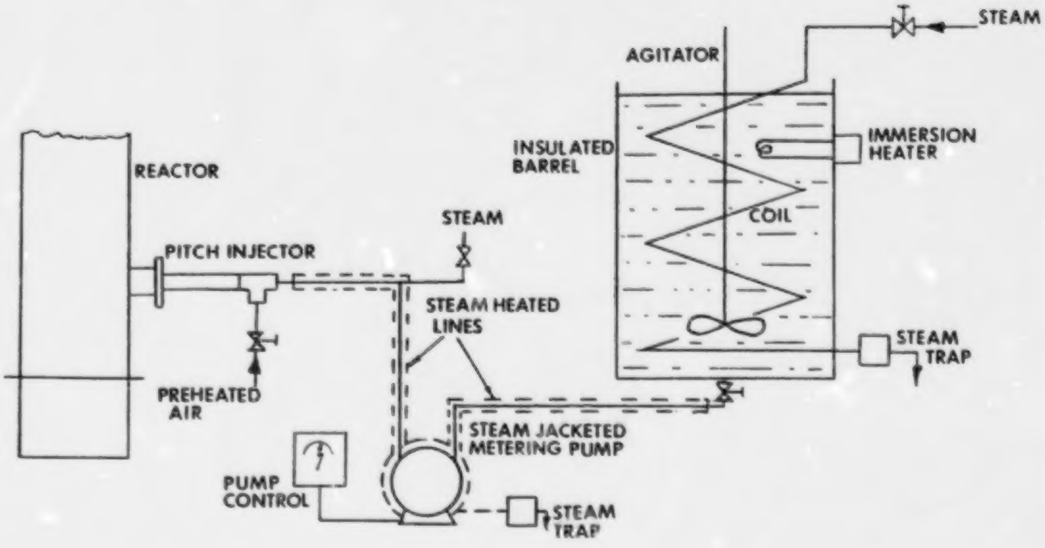
STEAM
AGITATOR
INSULATED BARREL
IMMERSION HEATER
REACTOR
STEAM
COIL
PITCH INJECTOR
STEAM HEATED LINES
STEAM TRAP
PREHEATED AIR
STEAM JACKETED METERING PUMP
PUMP CONTROL
STEAM TRAP

FIGURE 2.5: Liquid fuel feeding system.

2.2 Fuel Feed System

The feed system varies according to the type of fuel burned. For coal feeding, the system consists of two sealed hoppers (one for coal, the other for sorbent). For most cases where a sorbent (usually limestone) is required, it has been found more convenient to premix the coal/sorbent to the specified Ca:S ratio and to use only one of the hoppers. The fuel capacity is 2 drums of coal (approx. 360 kg) for the large hopper and 1 drum (approx. 180 kg) for the smaller one. The coal or coal/sorbent mixture is pneumatically fed through a 38 mm pipe entering the reactor at an angle of 15 degrees downward to the horizontal. The pneumatic conveying air comes from the secondary return system and/or directly from the main compressed air line. The solids feed rates are controlled by means of rotary valves, one per hopper, with rubber impellers and a transparent front to allow visual verification that the feeder is operating properly at all times. The larger hopper is mounted on load cells which allow the feed rate to be determined accurately.

For combustion of pitch materials, it was decided to feed the fuel as a liquid into the reactor. Both pitches have melting temperatures in the range 120–150°C. The feeding system is shown schematically in Figure 2.5. The key components of this system are as follows:

Heated reservoir: This vessel of volume 0.17 m^3 has two separate sources of heat which can provide together enough heat to bring the contents to temperatures above 150°C. Heat is supplied constantly by an immersed steam coil of surface area approximately 1.2 m^2. The steam pressure is adjusted to 550 kPa abs. or 155°C. To accelerate the initial

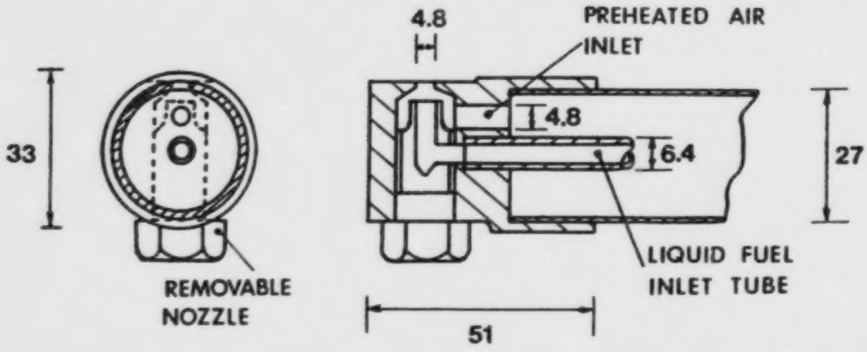

FIGURE 2.6: Atomizing nozzle for pitch feeding. All dimensions are in mm.

melting, a 3.0 kW electrical immersion heater was used. The outside of the reservoir is insulated using fiberfrax wool. A ventilation hood with a small vacuum is placed over the top of the vessel. A small (1/2 HP) Lighting mixer is installed at the top of the vessel to keep the contents in constant motion. The reservoir is supported on a load cell type weigh scale with a digital readout to allow the flow rate of fuel to be estimated. Melted pitch from a second vessel can be added to the main reservoir periodically via a heated connecting pipe. This second vessel consisted simply of a drum with two 3.0 kW barrel heaters attached to the outside and insulated with fiberfrax wool.

Piping system: The piping system was modified to eliminate all valves. Each section of pipe is steam traced and kept as short as possible. The steam pressure is also maintained at 550 kPa abs. (155°C).

Metering pump: A Roto-King Model C32 internal gear pump driven by a variable speed DC motor is used to control the flow rate of pitch. A steam jacket was welded onto the pump casing to maintain its temperature at 155°C.

Nozzle: After the experience gained during previous pitch runs (Grace and Lim, 1987), a new atomizing nozzle which allows easy clean up was built. This is shown in Figure 2.6. The atomizing air is heated in the calorimetric section above the L-valve. Constant air temperature and pressure are maintained to avoid variation in the fuel feedrate.

2.3 Heat Transfer Surfaces

In earlier work, it was found that too much heat was lost through the walls of the reactor to allow the use of membrane wall heat transfer sections. Some modifications to reduce the heat losses were incorporated in the system. These included replacing the bottom section with a stainless steel wall section which can be further insulated on the outside, elimination of several flanges on the standpipe, and addition of refractory to the previous heat transfer sections. These changes reduced the heat losses sufficiently for a single membrane wall to be returned to the reactor. The membrane heat transfer surface consists of four vertical stainless steel tubes of 21.3 mm OD and 13.9 mm ID, separated by longitudinal flat fins welded along their lengths as shown in Figure 2.7. Thermocouples are positioned at 152 mm intervals inside one of the central tubes and at the inlet and outlet of the cooling water in order that heat transfer coefficients can be determined for different intervals. The cooling surface has a total exposed area of 0.30 m^2 and a projected surface area of 0.23 m^2. With this surface in place, it was possible to run high calorific fuel (HHV> 28 MJ/kg) at a minimum gas superficial velocity of 6 m/s while maintaining the reactor temperature above 850°C.

During combustion trials of low calorific fuels with high moisture contents such as lignite coal, it was not possible to run at a low load condition (6 m/s) and maintain the reactor temperature above 850°C. A new heat transfer section was therefore built. This section contained three heavy-wall stainless steel tubes of 12.7 mm OD and 9.4 mm ID, in a hairpin configuration as shown in Figure 2.8. Water or air can be used as cooling fluid in one, two or three tubes at a time. This allowed heat removal rates to be varied from 0 to approximately 20 kW, without problems from thermal expansion since the tube bundle can expand freely inside the reactor. The heat transfer surface has a total exposed area of 0.34 m^2. This configuration was used for all the trials after October 1988 (Run 10 and following runs).

2.4 Solids Recycle Systems

Gas and entrained solids leaving the top of the reactor enter a refractory-lined medium-efficiency primary cyclone of inside diameter 305 mm. Solids captured in the primary cyclone drop into a conical recycle hopper. Make-up inert particles can also be added in this vessel from a small external hopper. From the bottom of the vessel, the solids descend in moving packed bed flow in a 102 mm ID, 4.72 m long externally insulated stainless steel standpipe, forming the vertical leg of an L-valve. There is a bellows-type expansion joint between the top of the standpipe and the bottom of the recycle hopper to allow for thermal expansion. The solids are returned to the reactor 152 mm above the primary air distributor through the horizontal section of the L-valve which is 790 mm long and 102 mm diameter. The circulation rate is controlled by the amount of aeration air fed to the L-valve at a single point, 102 mm above the horizontal axis of the L-valve. The circulation rate of solids can be measured by calorimetry or by visual determination of the solids descent velocity through a quartz window (see Figure 2.9). The calorimetric section consists of a 584 mm long jacketed section of the standpipe beginning 1.06 m above the bottom of the L-valve. Cooling air is passed through the jacket which is insulated on the outside. Determination of the coolant flow rate and its inlet and outlet temperatures allows the total heat exchange to be calculated. By measuring the solids temperature entering and leaving the jacketed section of pipe and ignoring the

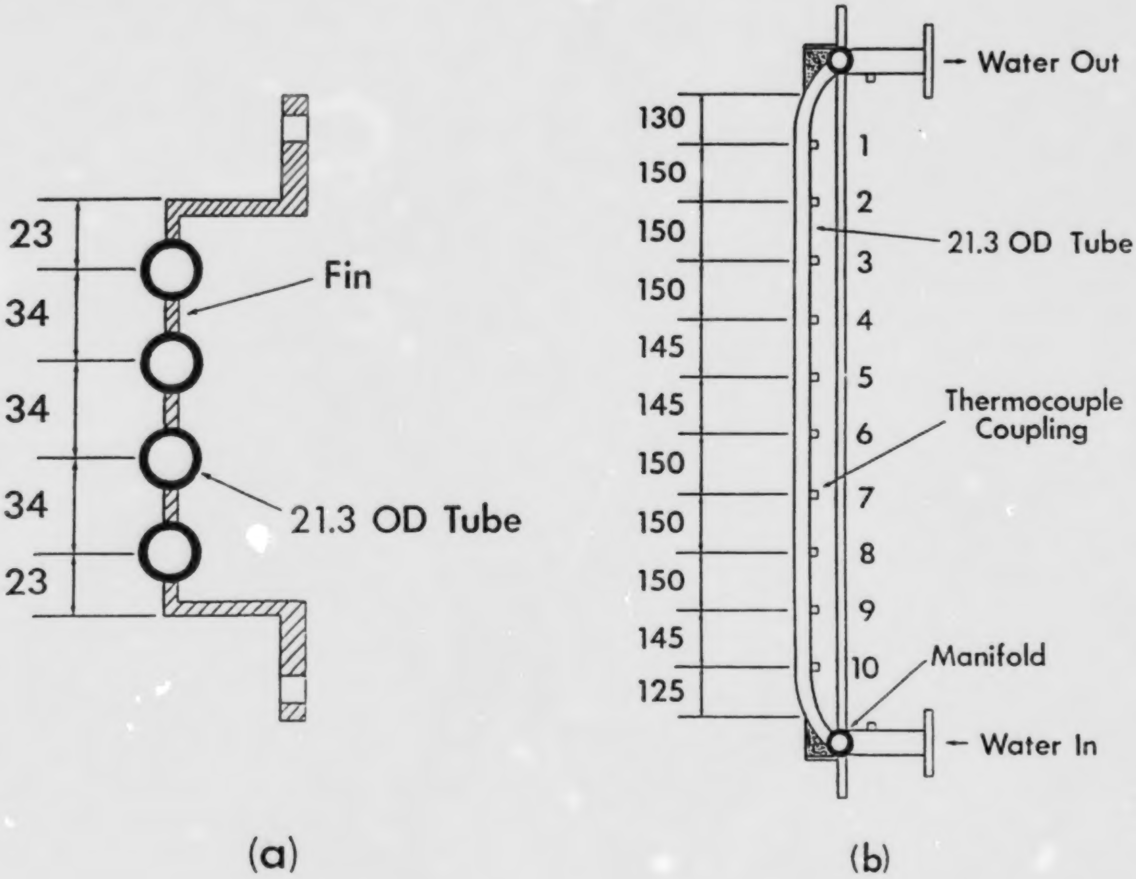
23
34
34
34
23
Fin
21.3 OD Tube
(a)
130
150
150
150
145
145
150
150
150
145
125
1
2
3
4
5
6
7
8
9
10
Water Out
21.3 OD Tube
Thermocouple Coupling
Manifold
Water In
(b)

FIGURE 2.7: (a) Plan view and (b) section view of membrane wall heat transfer surface. All dimensions are in mm.

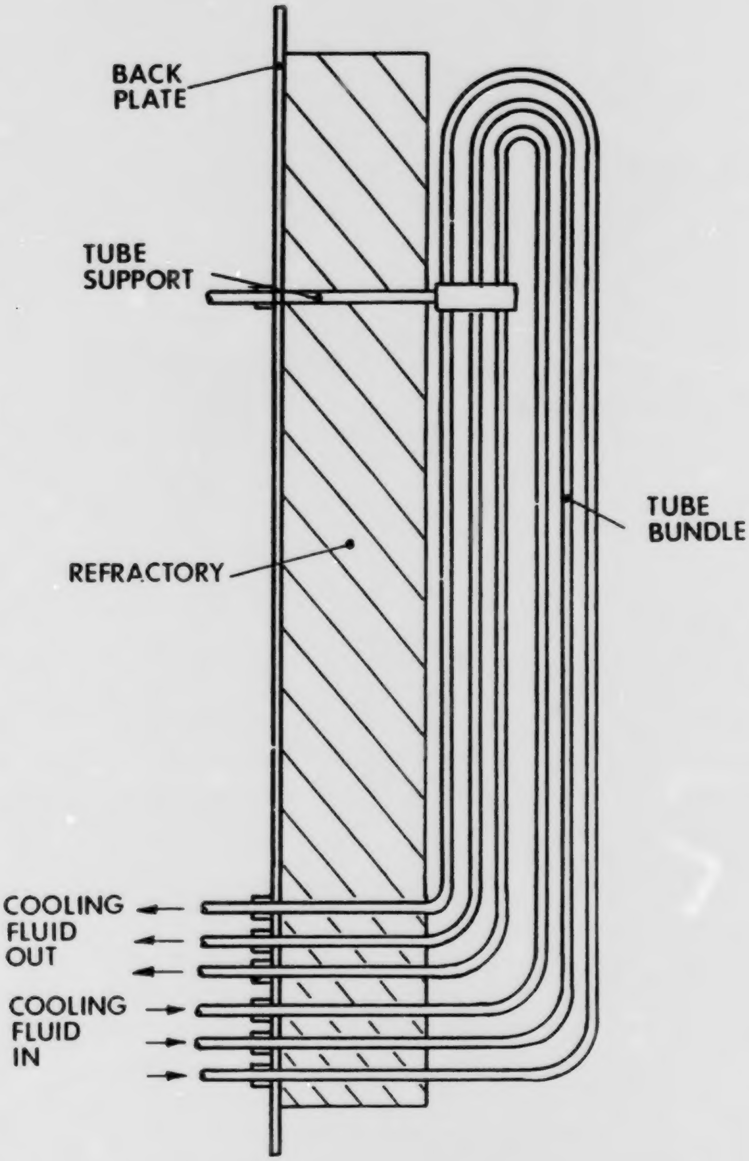
BACK PLATE
TUBE SUPPORT
TUBE BUNDLE
REFRACTORY
COOLING FLUID OUT
COOLING FLUID IN

FIGURE 2.8: Hairpin configuration of the new heat transfer section.

contribution of interstitial gas to the energy loss, it is then possible to estimate the mass flow rate of solids (Burkell *et al.*, 1988). The solids temperature is measured at four radial positions (at R=0, 25mm, 37.5mm and 50mm) along half the diameter of the standpipe. Numerical integration then provides a more accurate determination of the average solids temperatures necessary for the heat balance.

Because of the way the quartz window was built in the modified standpipe, it was not possible to obtain steady and reliable flows of solids against the glass. While the window was very useful for ensuring the state of flow of solids and provided an early indication if the inventory of solids was too low, it could not be used to determine the solids circulation rate as in previous work (Grace and Lim, 1987, Burkell *et al.*, 1988). The calorimetric technique was used to determine all the solids circulating rates given in this report.

Gas and entrained solids leaving the primary cyclone are directed to a 203 mm ID, high efficiency secondary cyclone. This cyclone is made of stainless steel and is insulated externally. Solids captured in the secondary cyclone fall into a 76 mm diameter dipleg. Early attempts were made to return the particles captured in the secondary cyclone to the bottom of the riser via a "V-valve" (Li and Kwauk, 1981). However, it was found that the solids were so fine that it was impossible to prevent flow reversal and emptying of the return leg during disturbances of the system.

Greater success in continuously returning the solids captured in the secondary cyclone was achieved with a jet eductor system, as shown in Figure 2.10. The purpose of the eductor is to enable the solids from the secondary cyclone, together with a small amount of gas, to be returned to the reactor bottom which is at a higher pressure. A small amount of air is fed to the distributor (see Figure 2.10) to keep the solids fluidized, while the baffle forces the solids to be entrained from the bottom of the eductor only. Larger particles, which might obstruct the venturi section, fall onto the distributor. The distributor can be rotated to allow removal of solids through the ball valve located below. The air fed to the eductor nozzle, together with what is entrained from the base of the cyclone, is then used as pneumatic gas flow for solid fuel feeding. The oxygen or carbon dioxide concentration can be measured in the dipleg to ensure that the air introduced in the eductor and by the distributor are drawn downward so that the performance of the secondary cyclone is not adversely affected.

2.5 Gas Exit and Analysis

Gas leaving the secondary cyclone is cooled in double-pipe type heat exchangers. The first of these heat exchangers is used as the secondary air preheater, while the other two are simply water cooled. The third heat exchanger also offers the possibility of further cooling with the help of three independently controlled internal water-cooled coils. Particulate solids are then removed from the flue gas in the baghouse before the flue gas enters an exhaust duct connected to an induced draught fan. The flue gas is then directed into the building ventilation duct. The I.D. fan creates a negative pressure in the baghouse which eliminates the risk of flue gas leaking into the lab.

Gas samples taken from the reactor at five axial positions, between the two cyclones and

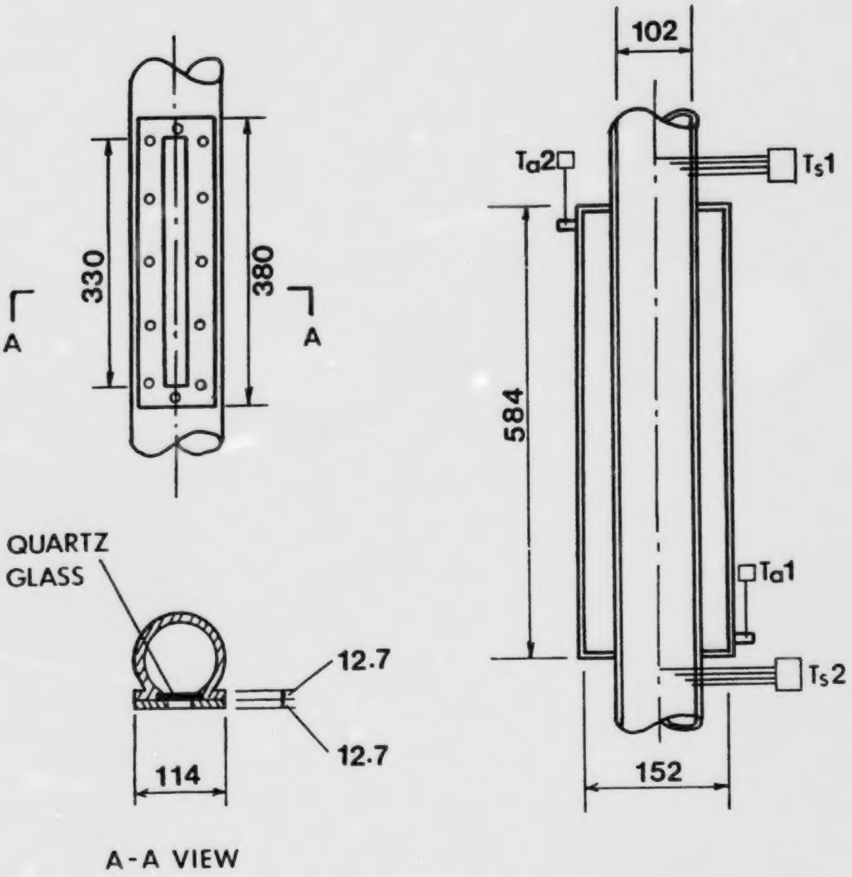
102
Ta2
Ts1
330
380
A
A
584
QUARTZ GLASS
Ta1
12.7
12.7
Ts2
114
152
A-A VIEW

FIGURE 2.9: Quartz window and calorimetric section for measuring solids circulation rate. All dimensions are in mm. (Ta_i: air temperature; Ts_i: average solids temperature).

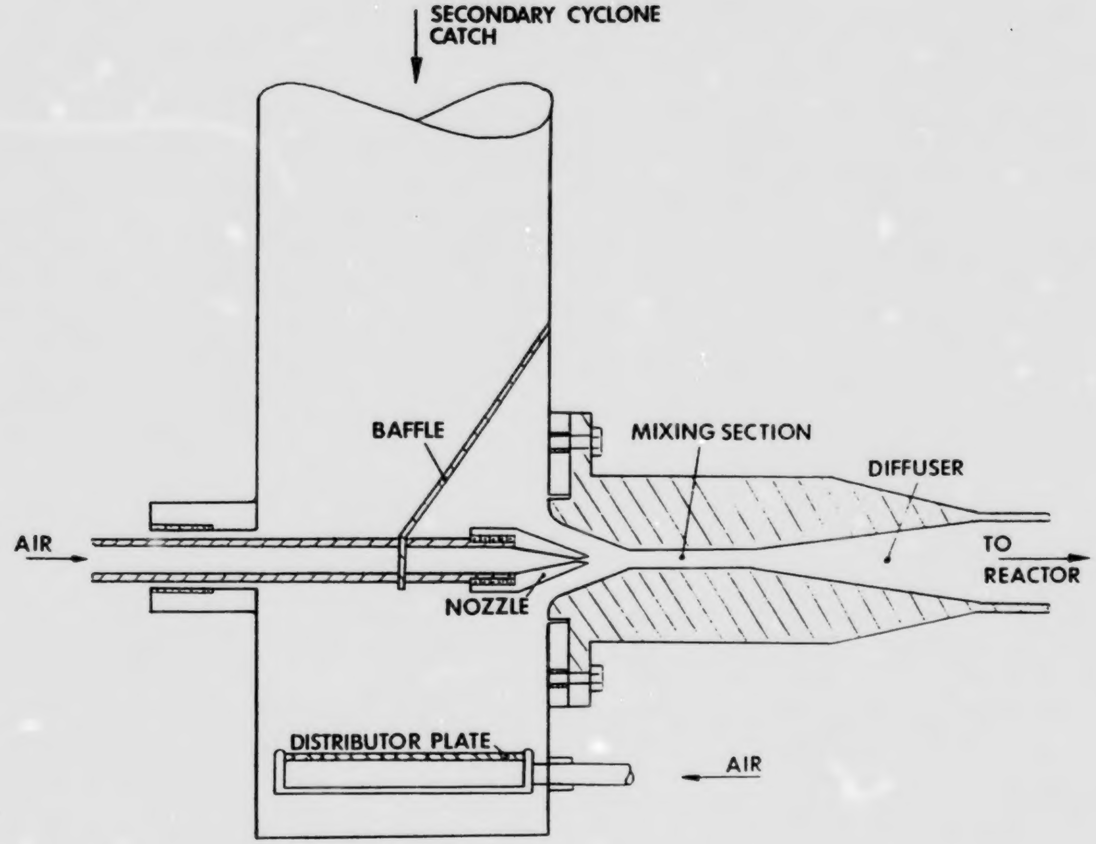
SECONDARY CYCLONE CATCH
BAFFLE
MIXING SECTION
DIFFUSER
AIR
TO REACTOR
NOZZLE
DISTRIBUTOR PLATE
AIR

FIGURE 2.10: Eductor configuration for secondary solids return.

from the flue gas after the first heat exchanger can be monitored continuously for O_2, CO_2, CO, SO_2, NO_x and unburned hydrocarbons. The gas sampling probes and analytical instruments are described in more detail in Chapter 4.

2.6 Solids Sampling System

Solids samples can be withdrawn from seven positions in the reactor system (see Figure 2.11): (1) from the bottom of the reactor shaft through a ball valve; (2) from the top of the reactor using a catching device permitting sampling across the entire cross-section as shown in Figure 2.12; (3) obliquely from the recycle hopper below the primary cyclone; (4) from one of three positions on the standpipe, near the top, in the middle and just above the L-valve aeration air port; (5) from the L-valve corner below the aeration point; (6) from the secondary cyclone return leg after passing the rotating distributor plate below the eductor; (7) from the baghouse. All the sampling points except the baghouse can be fitted with N_2-purged sampling receivers as shown in Figure 2.13, allowing the solids to be withdrawn and cooled under inert conditions to prevent oxidation or other reactions outside the reactor.

2.7 Instrumentation and Data Acquisition

The system instrumentation consists of the following:

(a) flowmeters for measuring all air and water flow rates;

(b) thermocouples throughout the entire system to allow measurement of temperature profiles (see Figure 2.14);

(c) pressure transducers connected to pressure taps on the main reactor to allow measurement of pressure profiles (see Figure 2.14);

(d) load cells supporting fuel hoppers to determine the solid and sorbent fuel feedrates;

(e) gas analyzers, as described above and in Chapter 4.

Data acquisition is provided by an AT&T 6300 PC equipped with a Metrabyte interface permitting up to 4000 samples per second in BASIC language and up to eight multiplexer boards with 16 channels on each board. Electrical outputs from thermocouples, pressure transducers and gas analyzers can be stored and processed in the computer. The load cells are connected through summation boxes to digital readouts. Air and water flow rates are read from calibrated rotameters.

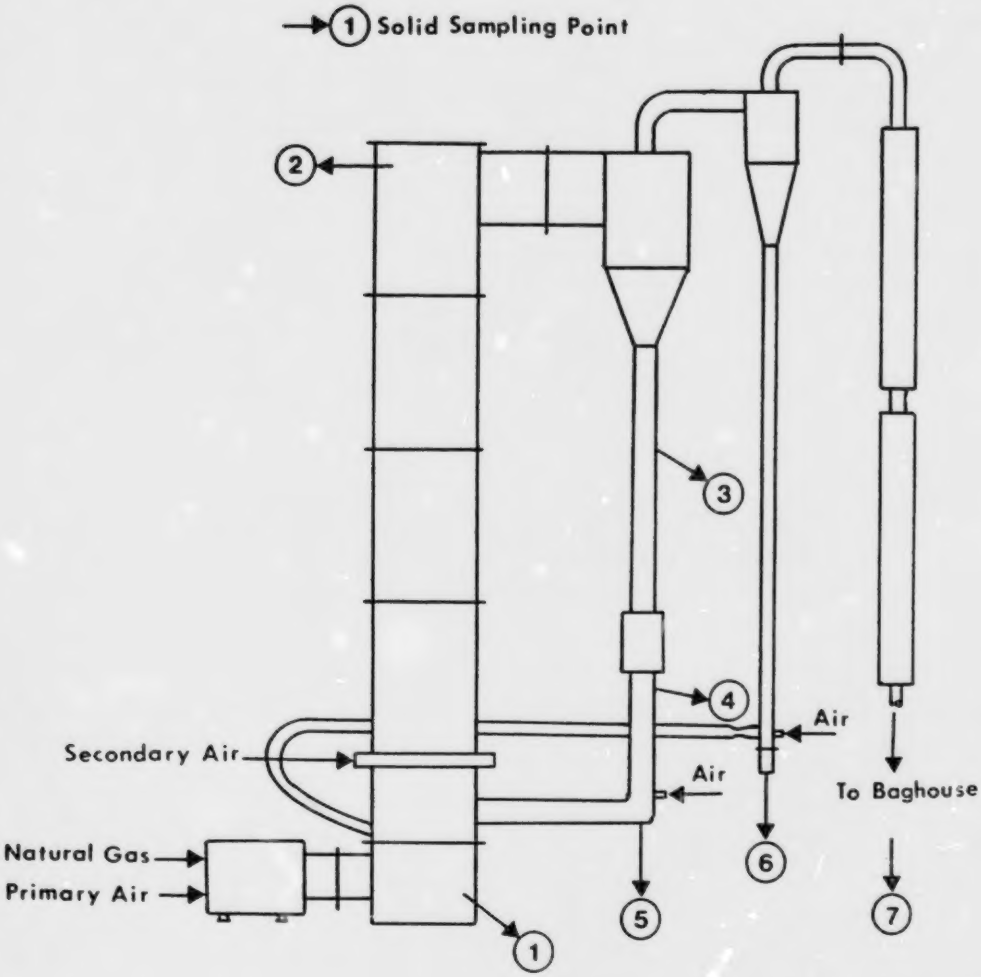

1 Solid Sampling Point
2
3
4
Air
Secondary Air
Air
To Baghouse
Natural Gas
Primary Air
5
6
7
1

FIGURE 2.11: Locations of solids sampling ports.

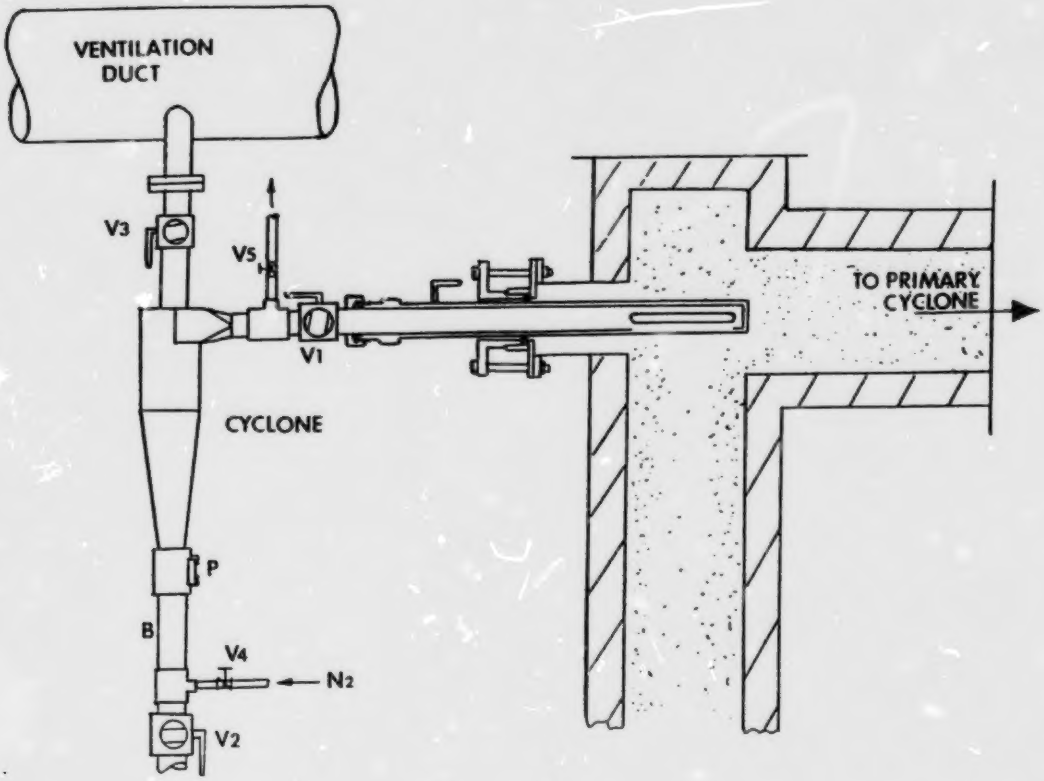
VENTILATION DUCT
V3
V5
V1
TO PRIMARY CYCLONE
CYCLONE
P
B
V4
N2
V2

Procedure

- Insert double pipe inside the reactor as shown above.
- Open V3.
- Open V4 and V5 and purge the sampling port with N_2.
- Open V1 slowly and fill the bottle (B) until solids reach the view port (P).
- Close V1 and leave solids to cool under N_2 (V3 closed, V4 and V5 open).
- Retract double pipe out of the reactor (150 mm).
- When cool, place N_2 flushed plastic bag at the outlet and open V2.
- Seal plastic bag and close V4 and V5. The port is now ready for the next sampling.

FIGURE 2.12: Top of reactor solids sampling system and operating procedure.

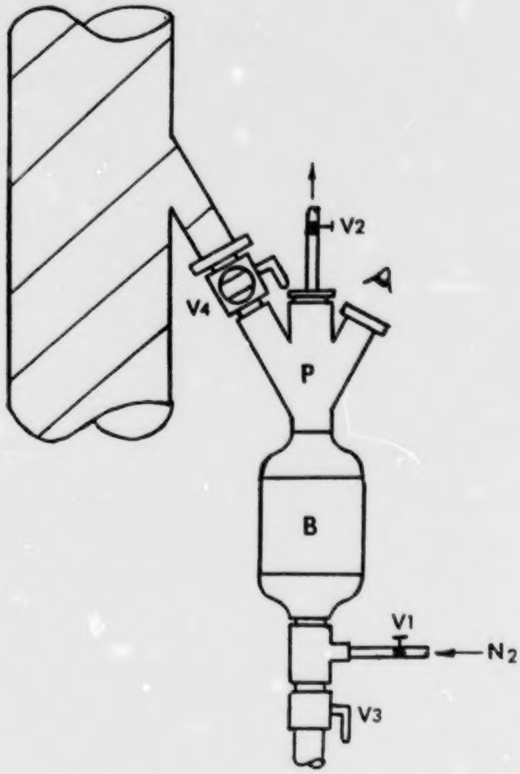

Procedure

- Open V3 and V4 to purge sampling line.
- When hot solids come out, close V4.
- When sampling port empty, close V3.
- Open V1 and V2 to purge sampling port with N_2.
- Leaving N_2 on, open V4 and fille the bottle (B) until solids reach the view port (P).
- Close V4 and leave solids to cool under N_2.
- When cool, place N_2 flushed plastic bag at the outlet and open V3.
- Seal plastic bag and close V1 and V2. The port is now ready for the next sampling.

FIGURE 2.13: Nitrogen purged solids sampling system and operating procedure.

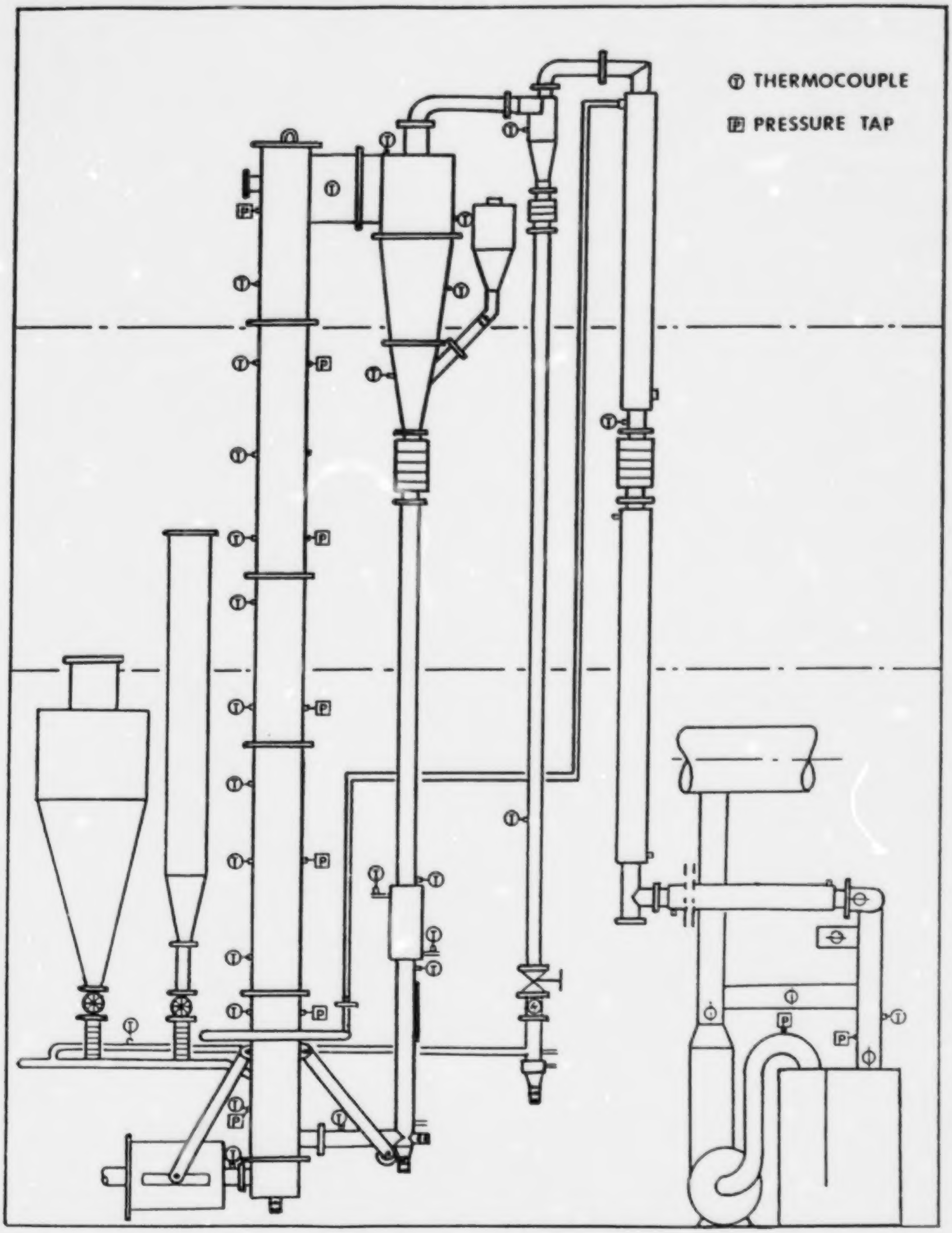
Ⓣ THERMOCOUPLE
Ⓟ PRESSURE TAP

FIGURE 2.14: Thermocouple and pressure tap locations in CFBC reactor system.

2.8 Properties of Fuels, Sorbents and Inert Particles

Combustion trials were carried out with a number of different solid fuels (four coals) as well as with two different pitches derived from oil upgrading operations. Proximate and ultimate analyses of the solid fuels are presented in Table 2.2. Important chemical and physical properties of the two pitches appear in Table 2.3. Physical properties of the sorbents and sands used during the combustion trials and other tests are provided in Table 2.4, while their chemical analyses are given in Table 2.5. All of these materials as fed belong in Geldart group B both at room temperature, according to the criteria established by Geldart (1973), and at the operating temperature and pressure of the combustor, using the criteria proposed by Grace (1986). The ash compositions of all fuels are presented in Table 2.6. Particle size distributions for the various particulate fuels, limestones and inert particulate materials fed to the unit before or during the combustion runs appear in Figure 2.15. Most of the physical properties were determined at U.B.C., with particle size analyses being by sieving and, for the smallest particles, a Coulter-type Counter. Proximate and ultimate analyses and ash analyses were carried out at the Centre for Mineral and Energy Technology (CANMET) in Ottawa, and generally show good agreement with previous reported values (*e.g.* Tibbets and Montgomery, 1976; Becker and Code, 1983; Becker *et al.*, 1987a; Becker *et al.*, 1987b) for the same materials.

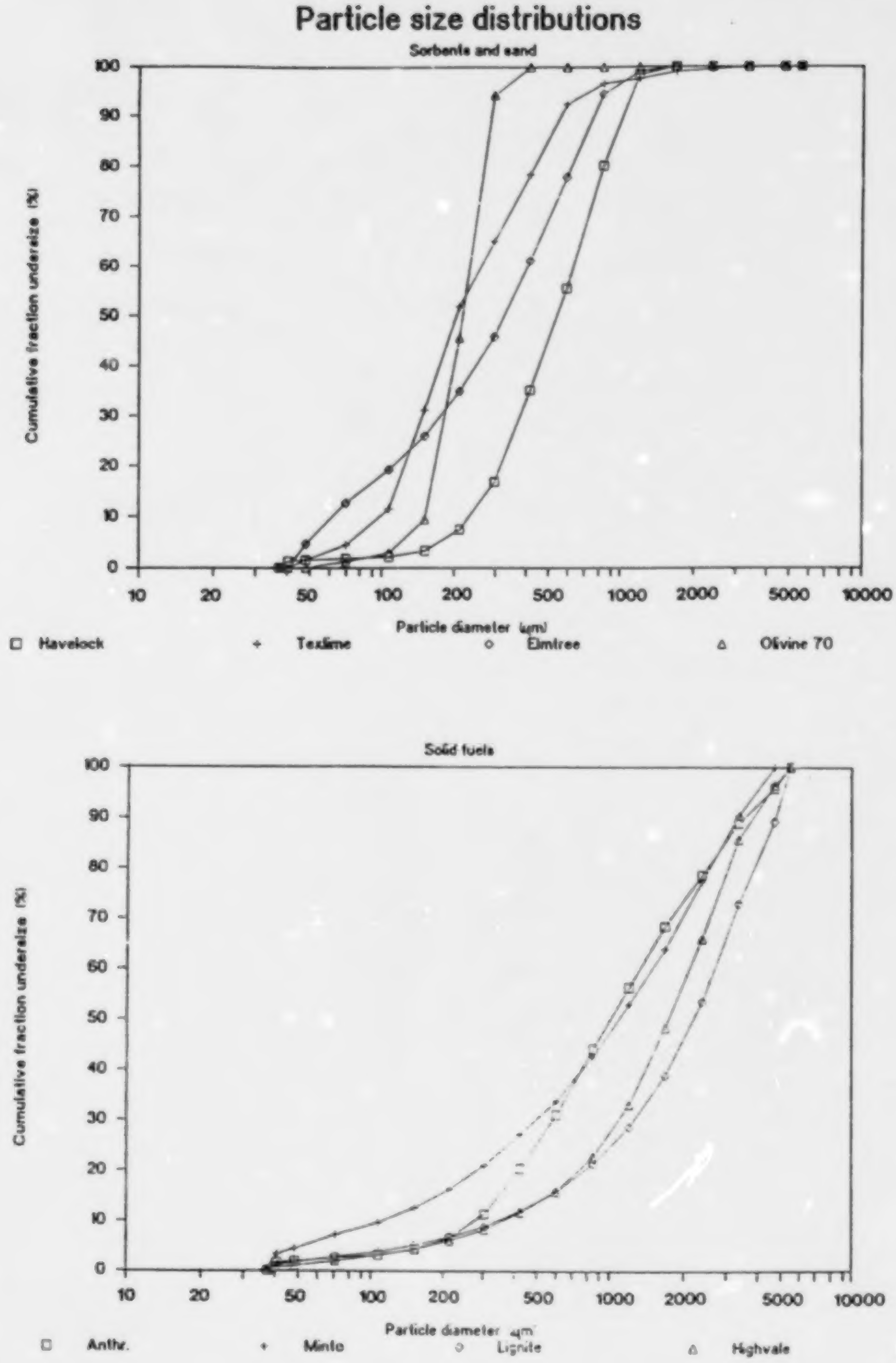

FIGURE 2.15: Particle size distributions of solids fuels, sorbents and inert sand.

TABLE 2.2: Proximate and Ultimate Analyses of Solid Fuels.

	Highvale Coal	Minto Coal	Lignite Coal	Anthracite Coal
Proximate Analyses (as received)				
Volatile Matter	30.5	33.1	35.1	7.0
Fixed Carbon	42.1	47.2	37.0	74.5
Ash	12.2	17.5	12.4	16.4
Moisture	15.2	2.2	15.5	2.1
Ultimate Analyses (dry basis)				
Carbon	62.4	66.0	59.0	77.5
Hydrogen	3.6	4.2	3.6	2.0
Nitrogen	0.8	0.8	0.7	0.9
Sulphur	0.2	6.6	0.9	0.5
Oxygen (by difference)	18.7	4.5	21.1	2.4
Ash	14.3	17.9	14.7	16.7
Higher Heating Value (MJ/kg)	24.0	27.8	24.0	28.4

TABLE 2.3: Properties of Pitch Materials Tested.

	CANMET Pitch	H-Oil Pitch
Proximate Analyses:		
Volatile Matter	67.7	—
Fixed Carbon	30.2	—
Ash	2.0	0.07
Moisture	0.1	0.01
Ultimate Analyses (dry basis)		
Carbon	86.2	86.4
Hydrogen	7.1	7.9
Nitrogen	1.1	1.0
Sulphur	2.8	2.3
Oxygen (by diff.)	1.0	2.3
Ash	1.8	0.1
Physical Properties:		
Density at 15°C, kg/m^3	1120	1131
API Gravity, 60/60°F	< 0	—
PI, wt. %	55.1	—
TI, wt. %	20.0	—
Asphaltenes, wt. %	35.1	—
CCR by MCR (RCR), %	56.4	43.2
GCD Data, % yield:		
- IBP/204°C	0.0	—
- 204°/343°C	1.0	15.7
- 343°/524°C	10.5	—
- 524°C +	88.5	84.3

TABLE 2.4: Physical Properties of Particulate Materials.

A)	Inert Materials	Olivine 70 Sand	Sand Used in Hydrodynamic Tests
	Particle density, kg/m^3	3066	2650
	Mean particle diameter, μm	241	148
	Voidage at minimum fluidization	0.46	0.43
	Minimum fluidization velocity at room temperature, m/s	0.090	0.021

B)	Sorbent	Elmtree Limestone	Texlime Limestone	Havelock Limestone
	Particle density, kg/m^3	2400	2500	2730
	Mean particle diameter, μm	210	214	454
	Voidage at minimum fluidization	0.44	0.43	0.47

TABLE 2.5: Chemical Analyses of Limestones and Inerts.

	Elmtree	Texlime	Havelock	Olivine Sand
CaO	54.32	55.97	53.55	0.41
SiO_2	0.00	1.03	1.77	41.48
MgO	0.60	0.37	0.30	48.08
Fe_2O_3	0.56	0.25	1.05	8.58
Al_2O_3	1.43	0.00	0.00	0.76
SO_3	n/a	0.33	0.20	0.54
Na_2O	0.05	0.03	0.01	0.05
K_2O	n/a	0.28	0.28	0.01
BaO	0.01	0.00	0.00	0.03
SrO	0.03	0.09	0.00	0.01
MnO_2	0.08	0.01	n/a	0.00
TiO_2	0.11	0.02	0.03	0.00
NiO	0.00	0.00	0.24	0.33
V_2O_5	0.00	0.03	0.01	0.00
P_2O_5	n/a	0.00	0.00	0.00

TABLE 2.6: Ash Composition of Fuels.

	Highvale Coal	Minto Coal	Lignite Coal	Anthracite Coal	CANMET Pitch	H-oil Pitch
SiO_2	45.73	37.04	36.25	59.22	21.4	16.3
Al_2O_3	26.57	12.33	21.75	17.90	8.2	7.0
Fe_2O_3	4.78	39.00	4.02	8.88	44.9	24.0
CaO	15.61	3.69	17.97	2.64	6.8	3.5
MgO	1.02	0.75	4.89	2.80	5.4	3.7
Na_2O	2.50	0.14	0.89	1.44	1.1	1.9
K_2O	0.35	1.23	1.14	0.97	0.3	1.1
TiO_2	0.69	0.64	0.59	1.15	0.7	0.7
P_2O_5	0.00	1.54	0.60	0.65	0.0	0.0
SO_3	1.71	0.97	5.47	1.52	4.2	0.0
V_2O_5	0.01	0.03	0.02	0.05	3.6	25.5
NiO	0.00	0.00	0.00	0.00	1.1	12.0
BaO	0.42	0.00	0.41	0.12	n/a	n/a
SrO	0.09	0.00	0.20	0.10	n/a	n/a
CoO_3	n/a	n/a	n/a	n/a	0.0	0.6
MoO_3	n/a	n/a	n/a	n/a	0.0	3.9
ZnO	n/a	n/a	n/a	n/a	0.0	0.2

Chapter 3

MULTIFUEL COMBUSTION TRIALS

3.1 Experimental Procedure

3.1.1 Start-up of the Unit

Before starting up the CFBC pilot plant, approximately 100 kg of inert materials, in most cases Olivine 70 sand with a mean particle size of 241 microns, is charged to the recycle hopper at the top of the standpipe through the small external hopper. This amount of material is sufficient to fill the primary recycle loop standpipe and the recycle hopper. The fuel hoppers are then filled with the appropriate fuels or combination of fuel/sorbent. Other preparatory actions include cleaning the baghouse, replacing faulty thermocouples and generally checking the entire system.

The complete start-up procedure is performed in two stages. During the first stage, the primary air is preheated in an external natural gas burner to a temperature of 950°C. The superficial velocity in the reactor is maintained above 6 m/s and the inert solids are circulated through the primary recycle loop. Solids caught in the secondary cyclone are simply discharged at the bottom of the dipleg. A period of approximately 90 minutes is necessary to bring the overall temperature to 380°C. During the entire start-up period, secondary air ports, the pneumatic feed line and gas sampling ports are kept free of solids by small amounts of purge air. Cooling water flows to the in-bed heat exchanger and flue gas coolers are initiated when the temperatures in those vicinities exceed 150°C.

During the second stage, the solids circulation rate is decreased until the temperature near the bottom of the reactor reaches 550°C. Highvale coal was generally used as a start-up fuel since it ignites and burns at a reasonable rate even at this low temperature. The coal was pneumatically fed into the reactor. The secondary recycle loop is initiated using the eductor system to recirculate the unburned carbon fines collected in the secondary cyclone. At first, considerable CO and unburned carbon particles are produced because of the low combustion temperature. From visual observations through the quartz window above the L-valve, the carbon loading can be seen to diminish as the temperature in the reactor increases. The solids circulation is kept to the maximum rate permissible while maintaining a temperature of at least 550° C in the lower part of the reactor. A period of 3 to 4 hours is necessary to bring the overall system up to 850°C, during which the coal feedrate is gradually increased while the natural gas is decreased.

The overall heat-up period now takes approximately 5 hours compared to 10–13 hours before the modifications to the CFBC (see Chapter 1). This is due in part to the new low pressure drop distributor, which allows higher through-put of primary air during the first stage of start-up, and also to the changes in operating procedures related to the initial coal firing and the improved thermal insulation of the system. Once the required temperature is reached, the particular fuel to be tested is fed and the Highvale coal feed is terminated. Primary, secondary and L-valve air are adjusted to predetermined values. The fuel feedrate is also adjusted to keep the O_2 level in the flue gas in the range 3–4% by volume (dry basis).

3.1.2 Solids sampling procedures

As mentioned in Chapter 2, solids samples can be withdrawn from six positions in the reactor system under a nitrogen-blanket. The sampling devices are illustrated in Figures 2.12 and 2.13 with their respective operating procedures. After the samples have been cooled under a nitrogen purge, they are transferred to nitrogen purged plastic bags and sealed. When a nitrogen blanket is not required, the sampling devices are disconnected from the ports. The solids samples can then be collected in stainless steel receivers. The initial discharges are discarded in all cases to avoid materials that have been sitting in the pipe above the valve. The samples are quickly covered with insulating materials to avoid contact with air during the cooling period. After cooling, the samples are transferred to plastic containers and sealed. Baghouse samples are obtained by removing the bottom drawer and replacing it with an empty one. The solids accumulated are then weighted and a sample is transferred to a plastic jar. The unwanted ash and other solids wastes are then discarded safely into drums ready for disposal.

3.1.3 Gas sampling procedure

A complete and detailed description of the gas sampling system and procedure is presented in Section 4.1. All results presented in this Chapter pertain only to the flue gas (before and after secondary cyclone). The axial gas concentration results obtained with the multipoint gas sampling system are presented and discussed in Chapter 4.

3.2 Results of Combustion Trials

A chronology of the various fuel combustion trials and other runs conducted during the course of the contract is provided in Table 3.1. The duration of each run includes the start-up period. Results are presented in this report only for runs where useful results were obtained.

3.2.1 Highvale coal tests

Highvale is a subbituminous coal from Alberta. It is the "best behaved" fuel burned in our unit so far, and, as already noted, its behaviour is ideal for the start-up period where a fuel which can ignite and burn at temperatures around 550° C is useful. Some of the results presented here for Highvale were obtained during different runs, after the start-up period

TABLE 3.1: Chronology of Combustion Trials.

Mo./Yr.	Fuel/Sorbent (Run #)	Duration (h)	Comments
3/88	Minto coal/Elmtree (24%) Texlime (76%) (Run #3)	43	Successful run, 1 condition No secondary recycle
3/88	Gulf Anthracite coal/None (Run #4)	9	Preliminary results for Anthracite coal. No secondary recycle.
5/88	Highvale coal/None (Run #6)	17	Heat transfer data obtained at T = 870°C and 700°C
7/88	Gulf Anthracite coal/None (Run #7)	22	Successful run. No secondary recycle.
8/88	Highvale coal/None (Run #9)	16	T = 760°C, swirl in secondary air injection. Eductor system working (2 conditions)
9/88	Highvale coal/None (Run #10)	16	T = 760°C, no swirl, secondary return. New heat transfer section
10/88	Highvale coal/None (Run #11)	16	T = 870°C, no swirl, secondary return.
10/88	Highvale coal/None (Run #12)	16	T = 870°C, swirl, secondary return.
10/88	Gulf Anthracite coal/None (Run #14)	37	Successful run with secondary return operating. (5 conditions)
11/88	Poplar river lignite/None (Run #15)	30	Successful run with secondary return. (4 conditions)
12/88	Minto coal/Havelock (Run #16)	53	6 conditions, secondary return operating.
2/89	CANMET pitch/Texlime (Run #17)	37	6 conditions, secondary return operating.
2/89	H-Oil pitch/Texlime (Run #18)	22	Leak in secondary air heat exchanger, 1 condition.
3/89	H-Oil pitch/Texlime (Run #20)	33	Successful run. 5 conditions. Secondary return operating.
4/89	Highvale/None (Run #21)	17	Hydrodynamics results.
4/89	Highvale/None (Run #22)	8	Additional data on Highvale. Leak in heat transfer tubes.
6/89	Calcination of Carbonate (Run #23)	23	Obtained calcined product. Burned diesel oil.

while still burning Highvale. Four independent runs burning solely Highvale were conducted to: (1) observe the combustion characteristics of this coal in a CFBC, and (2) investigate the effects of swirl introduced in the reactor by the secondary air jets. Results of these four runs are presented in Table 3.2.

In general, the combustion tests with Highvale showed very stable operation and temperature uniformity throughout the reactor loop as indicated in Figure 3.1, which presents a typical observed temperature profile. As expected NO_x emissions are very dependant on the reactor temperature, with values ranging from 70–92 ppm at 760°C to around 200 ppm at 870°C. The rate of increase is approximately 1.1 ppm/C, much lower than values observed in some bubbling beds. Gibbs *et al.* (1975) reported that in the range 650–850°C, NO_x increases linearly with temperature at a rate of 2.6 ppm/C. The effect of excess air on NO_x emissions was also studied using Highvale coal as fuel and the results are discussed in Chapter 4.

The combustion efficiency based on carbon conversion were always very high for Highvale coal. Values ranging from 95.9–97.9% at 760°C and up to 98.8–99.4% at 870°C were obtained in the CFBC with secondary recycle. Virtually complete CO burnout was achieved at temperatures above 850°C, where CO emissions were below 30 ppm, while values around 430 ppm were observed at the lower reactor temperature of 760°C. Highvale coal has a substantial calcium content in the ash resulting in an intrinsic Ca:S molar ratio of 5.7. The SO_2 emissions were in the range 0–28 ppm, meaning that there was 86–100% inherent sulphur capture.

The swirl created by the secondary air jets did not have any noticeable effect on the combustion characteristics. It was not possible to conclude from the results obtained whether or nor the introduction of swirl had any significant effect on the radial mixing in the reactor.

3.2.2 Minto coal tests

One of the concerns regarding the combustion of high sulphur fuels in circulating fluidized bed is related to the disposal of the solid residues. Large amounts of sorbent (in this case limestone: 98% $CaCO_3$) are used to react with the SO_2 formed during combustion. The major product is calcium sulphate, but smaller amounts of sulphide may also occur, especially if there is little or no oxygen present. In conventional bubbling beds, the sulphur capture reactions favour formation of sulphates because of the largely oxidizing atmosphere. However, in a CFBC a portion of the bed material may reside for a period of time in the return loop as a slow moving packed bed or fluidized bed. During this period, the solids are only mildly aerated and reducing conditions may prevail, allowing the formation of calcium sulphide instead of calcium sulphate. Use of staged combustion generates a further reducing zone below the level at which secondary air is introduced. Sulphide is undesirable in CFBC residues because it reacts with acidified water to generate H_2S. The H_2S is highly toxic and has an extremely unpleasant odour. There is interest in developing sufficient data to establish whether calcium sulphide will be present in CFBC residues in significant levels, and if so, to develop strategies to minimise its formation.

TABLE 3.2: Operating Conditions and Combustion Results for Highvale Coal

Run #	9		10		11		12	
	Swirl		No Swirl		No Swirl		Swirl	
Condition	1	2	1	2	1	2	1	2
U primary zone (m/s)	3.6	2.4	3.8	2.4	3.8	3.1	3.9	3.3
U secondary zone (m/s)	6.5	7.0	6.6	6.8	8.1	9.3	8.1	9.5
Secondary/primary air ratio (—)	0.83	1.89	0.71	1.84	1.11	1.99	1.11	1.86
Coal feed rate (kg/h)	30.7	30.8	29.7	29.6	25.9	29.2	25.9	30.5
Average suspension density (kg/m^3)	128	157	120	123	121	121	208	154
Temperature at bottom of reactor (°C)	752	751	753	759	861	890	877	876
Temperature at top of reactor (°C)	758	760	755	764	868	898	882	886
Temperature in L-valve return (°C)	756	758	756	766	874	903	890	895
Temperature in secondary cyclone (°C)	784	778	799	765	844	895	856	887
Recycle of secondary cyclone catch	yes	yes	yes	yes	yes	yes	yes	yes
Flue Gas Concentration								
O_2 (%)	2.3	3.0	3.6	3.3	3.2	3.0	3.1	3.0
CO_2 corrected to 3% O_2 (%)	16.6	16.3	18.8	16.0	16.4	16.3	16.1	16.1
CO corrected to 3% O_2 (ppm)	417	330	331	437	32	24	23	19
SO_2 corrected to 3% O_2 (ppm)	16	28	7	7	6	12	0	0
NO_x corrected to 3% O_2 (ppm)	70	74	88	92	190	208	208	195
CH_4 corrected to 3% O_2 (%)	0	0	0	0	0	0	0	0
Excess air level (%)	12.1	16.4	20.3	18.3	17.7	16.4	17.0	16.4
Combustion efficiency (%)	95.9	97.2	97.4	97.9	99.4	99.4	98.8	99.0
Mean Particle Size (μm) for								
Bed drain solids	189	174	182	170	192	181	181	188
Secondary cyclone catch	25	40	48	58	46	47	54	54
Baghouse catch	18	19	19	12	13	11	13	13

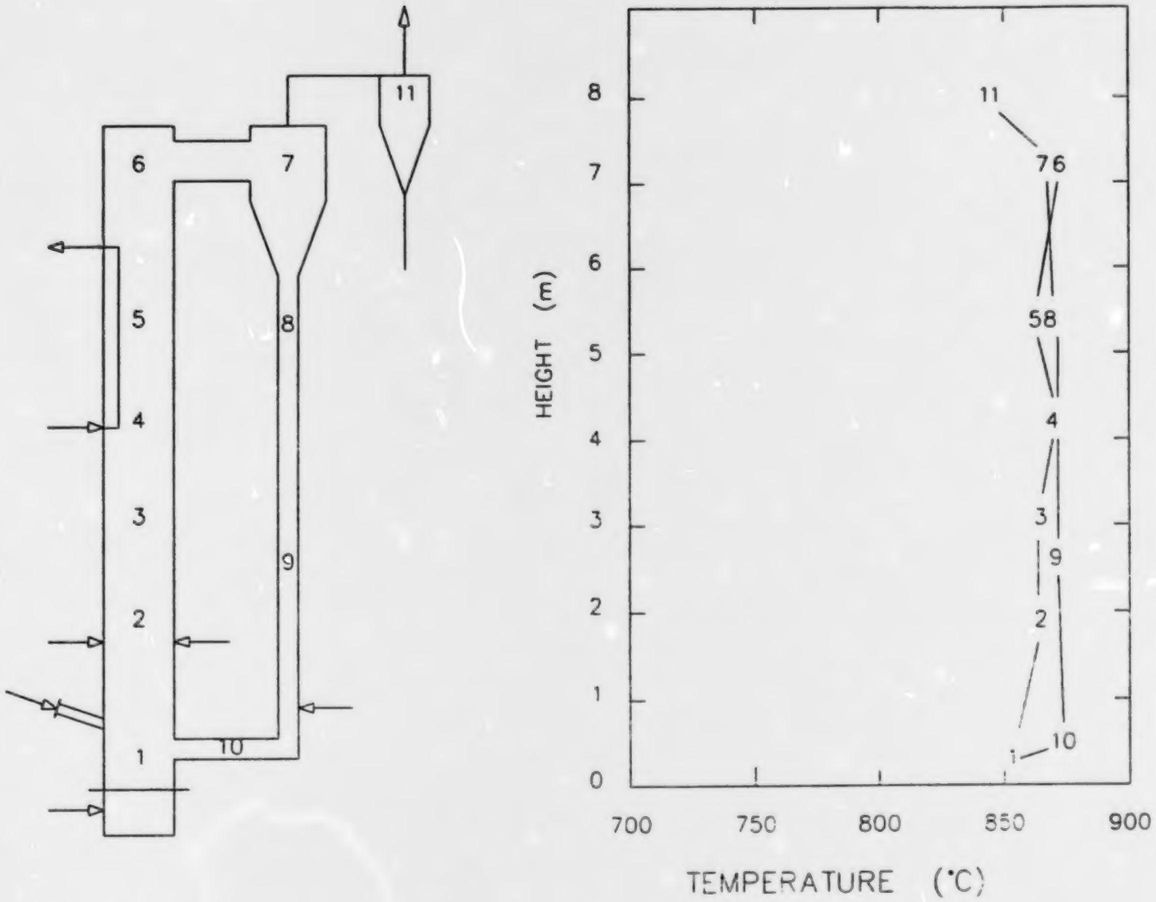

FIGURE 3.1: Typical temperature profile during Highvale combustion trials (Run #11, Condition 1; see Table 3.2 for operating conditions).

The first focus of the two combustion trials of Minto coal was to examine sulphide levels at different points in the CFBC loop under conditions corresponding to operation of the 22 MWe Chatham demonstration CFB boiler in New Brunswick. Minto is a high sulphur, bituminous high-volatile A (ASTM Classification) from New Brunswick. During the first run, the sorbent used was a mixture of 76% Texlime and 24% Elmtree. In the second trial, the sorbent was a fine Havelock limestone from New Brunswick. The properties and chemical compositions of these sorbents can be found in Chapter 2.

During the first run, a single operating condition, corresponding quite closely to the Chatham unit, was maintained for three solids inventory turnovers, a period of time sufficiently long to achieve solids composition steady-state. During the second trial, six conditions were maintained. Table 3.3 shows a summary of the operating conditions and the main combustion results for the two Minto trials. Characterization of the solids samples taken during the trials is considered in Chapter 6.

The main difference between the two trials was in the inclusion of the secondary cyclone catch recycle in the later one. Sulphur captures are plotted in Figure 3.2, together with the results obtained in previous tests (Grace and Lim, 1987) before the reactor was modified. It is seen that the results obtained in the modified CFBC without secondary recycle, using Havelock or a mixture of Texlime/Elmtree limestones as sorbents, fall very closely to those obtained previously. However, the introduction of secondary recycle caused a very significant improvement in sulphur capture. The particle size distributions of materials taken at different points around the system are shown in Figure 3.3. It seems that the fraction collected in the secondary cyclone, which had an average particle size around 40 microns, is responsible for much improved sulphur capture when it is returned to the reactor. The baghouse catch has a mean particle size of 19 microns.

The NO_x emissions were somewhat higher than for the other coals tested in our unit, with levels in the range 125–218 ppm. These emissions are strongly influenced by the presence of limestone due to the catalytic effects of limestone on reactions involving nitrogen species. Table 3.4 shows that the NO_x emissions almost doubled when the molar Ca:S ratio increased from 0 to 3.0 for the conditions described. Combustion efficiencies were also greatly improved with secondary recycle where values as high as 97% were obtained.

3.2.3 Anthracite tests

The anthracitic coal burned in our unit was from the Mt Klappan region of British Columbia. It is considered a low reactivity coal. However, Gulf Canada, which owns considerable stocks of this coal, is interested in developing the resource and is currently looking for economical ways of utilizing the material. Bubbling and circulating fluidized beds are natural focal points for this development because of the low reactivity and low volatiles content which preclude pulverized firing. Burnout would likely be low in a pulverized system and it might not be possible to maintain stable flames. In addition, NO_x emissions might not meet environmental standards. Sulphur emissions are not a concern with this coal because of the low sulphur content (0.4% by weight). Tests in bubbling beds at Queen's University (Becker *et al.*, 1987a) gave combustion efficiencies of the order of 90% at bed temperature between

TABLE 3.3: Operating Conditions and Combustion Results for Minto Coal

	Run #3	Run #16					
Condition	C1	1	2	3	4	5	6
U primary zone (m/s)	3.8	4.4	3.0	3.0	4.5	3.7	3.8
U secondary zone (m/s)	8.4	8.6	8.7	8.7	8.8	7.7	7.8
Secondary/primary air ratio	1.22	0.96	1.91	1.91	0.96	1.07	1.07
Coal feed rate (kg/h)	20.9	19.6	20.0	19.8	18.8	17.5	18.1
Limestone feed rate (kg/h)	12.7	12.1	12.4	7.4	7.0	6.5	11.2
Ca:S molar ratio	3.0	3.0	3.0	1.8	1.8	1.8	3.0
Average suspension density (kg/m^3)	—	166	165	122	136	159	161
Temperature at bottom of reactor (°C)	875	880	893	896	904	872	895
Temperature at top of reactor (°C)	—	887	895	893	880	868	890
Temperature in L-valve return (°C)	882	883	889	889	892	860	877
Temperature in secondary cyclone (°C)	853	853	860	869	876	852	839
Recycle of secondary cyclone catch	no	yes	yes	yes	yes	yes	no
Flue Gas Concentration							
O_2 (%)	2.6	3.5	3.1	3.3	4.2	3.7	3.1
CO_2 corrected to 3% O_2 (%)	—	16.8	16.7	16.5	16.6	16.5	16.9
CO corrected to 3% O_2 (ppm)	67	85	67	89	92	97	58
SO_2 corrected to 3% O_2 (ppm)	680	46	51	705	785	452	512
NO_x corrected to 3% O_2 (ppm)	142	224	218	175	188	165	177
CH_4 corrected to 3% O_2 (%)	0.015	0	0	0	0	0	0
Sulphur capture (%)	88.6	99.2	99.1	87.7	86.2	92.1	91.0
Calcium utilization (%)	33	33	33	48	48	51	30
Excess air level (%)	14.7	19.4	16.8	18.1	24.3	20.8	16.8
Combustion efficiency (%)	92.9	96.3	—	97.1	—	94.1	—
Mean Particle Size (μm) for							
Bed drain solids	187	201	—	—	—	210	—
L-valve solids	193	179	—	192	—	—	—
Secondary cyclone catch	—	43	49	67	—	66	—
Baghouse catch	33	19	—	21	—	23	—

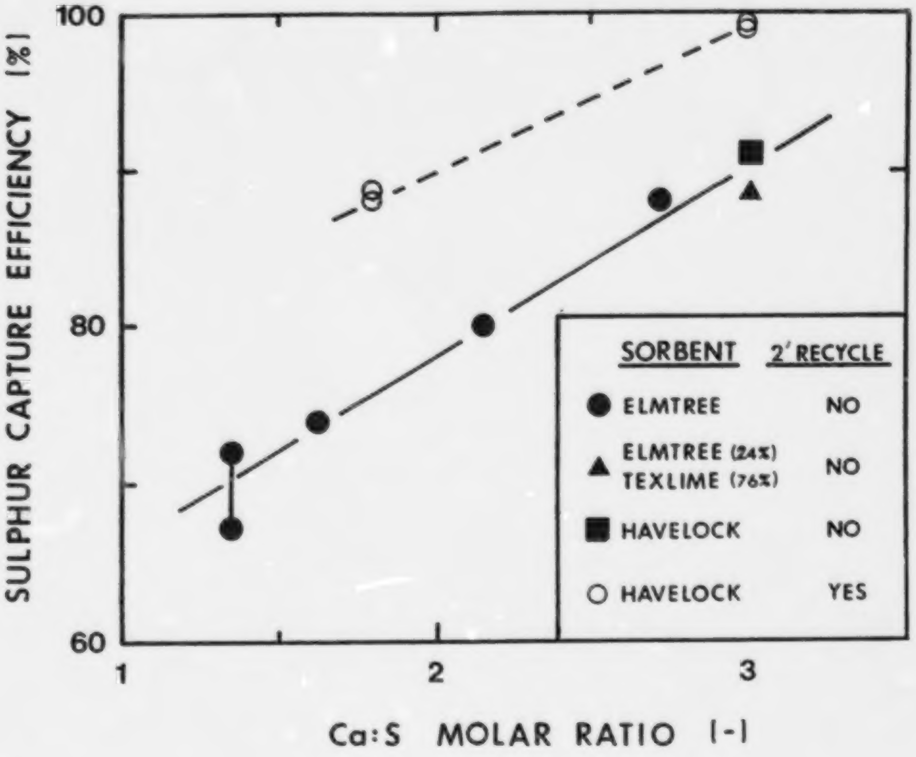

FIGURE 3.2: Sulphur capture versus Ca:S molar ratio for Minto coal combustion trials.

TABLE 3.4: NO_x Emissions from Combustion of Minto Coal (3% oxygen, sec./prim. air ratio = 1).

Superficial Gas Velocity (m/s)	Bed Temperature (°C)	Ca/S	Sulphur Capture (%)	NO_x (ppm)
8.3	880	0	—	127
8.4	900	1.8	87.0	160
8.3	882	3.0	99.2	218

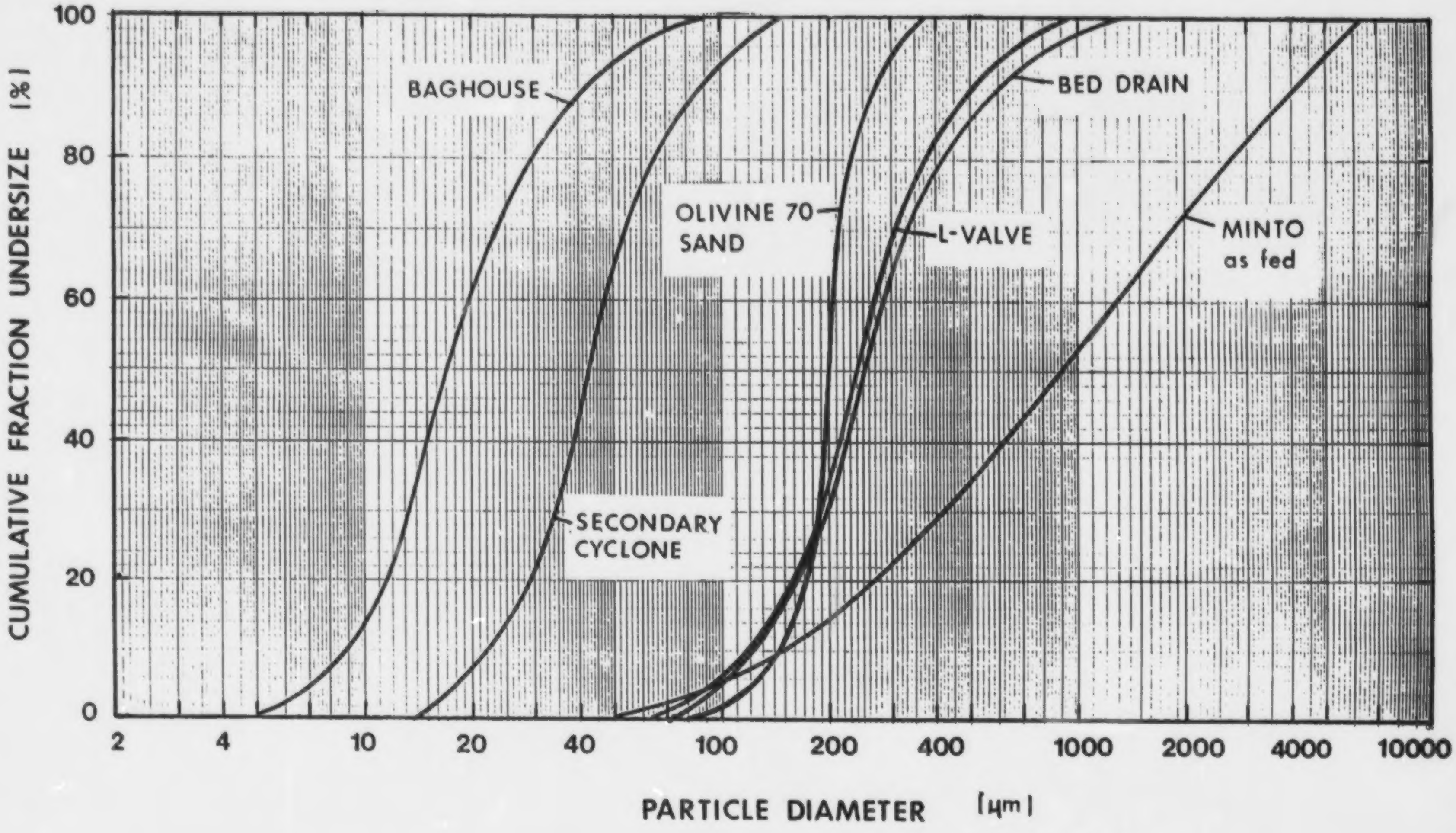

FIGURE 3.3: Particle size distribution of solids sampled from various locations during a Minto combustion trial (Run #16, Condition 1; see Table 3.3 for operating conditions).

890–900°C. The relative high temperature needed to achieve 90% combustion efficiency is a measure of the lack of reactivity of the coal.

The operating conditions and the results observed during the anthracite combustion trial (Run 14) are presented in Table 3.5. The results of a preliminary combustion trial (Run 7, July 1988) performed without secondary cyclone catch recycle, are also included in Table 3.5. The carbon loading in the primary return, secondary return and baghouse catch appear in Table 3.6. These values were the highest encountered in our unit, much higher than for more reactive coals. These levels of char loading in the system make load variations much slower than with more reactive fuels. The low reactivity meant that special attention to feeding must be paid to avoid char overloading in the system, which could lead to an uncontrolled temperature increase later when this material starts to burn.

The combustion efficiency was greatly improved when the fines captured in the secondary cyclone were recycled to the base of the reactor. The initial value of 92.9% obtained without secondary recycle was improved to 96–97.6% with secondary recycle at reactor temperatures always below 890°C. Even higher combustion efficiencies can be expected at higher temperatures (900°C or above). CO emissions were relatively high, 250–590 ppm at the higher load conditions (U=7.8 m/s) due to the low char reactivity and the lower secondary cyclone temperature which did not provide the appropriate environment for more complete CO burnout. However, the CO emissions were reduced below the 120 ppm level as the load was reduced (U=6 m/s). This suggests that an increased residence time in the reactor for a taller unit would reduce the CO emissions to lower levels. NO_x emissions were very low, around 100 ppm and below. Sulphur dioxide emissions were also favourable, with levels in the range 160–200 ppm. The temperature profiles were also very uniform over the reactor loop as illustrated in Figure 3.4.

3.2.4 Lignite tests

Poplar River lignite has a lower calorific value, combined with a higher moisture content than the other fuels examined, as shown in Table 2.2. In order to burn this fuel in our unit at a reasonable operating level (U=8 m/s), while maintaining a bed temperature above 850°C, it was necessary to modify the heat removal section in the reactor. The membrane wall configuration did not allow us to run without internal reactor cooling due to the risk of damage to the tubes from excessive thermal stresses. The new heat transfer section with the tube bundle described in Chapter 2 (see Figure 2.8), was used during the lignite combustion trials. It was then possible to operate at two different operating conditions (U=8 m/s and U=7 m/s) and two secondary-to-primary air ratios for the higher load conditions. The lower load conditions resulted in a lower reactor temperature even without heat removal from the reactor. The results and conditions of the trial are presented in Table 3.7.

In general, Poplar River lignite posed no particular problems in our unit and appears to be well suited to CFBC technology. Uniform temperature profiles throughout the entire loop were observed and combustion efficiency results showed excellent reactivity of the char (combustion efficiency $\geq$ 99.5% even in the low load case and at 800°C). Despite no sorbent being used during the trial, the SO_2 emissions always appeared to be below 20 ppm, suggest-

TABLE 3.5: Operating Conditions and Combustion Results for Anthracite Coal

	Run #14					Run #7
Condition	1	2	3	4	5	1
U primary zone (m/s)	3.9	5.2	2.6	2.0	3.1	3.8
U secondary zone (m/s)	7.7	7.8	7.9	6.0	6.2	7.8
Secondary/primary air ratio	1.0	0.5	2.02	2.02	1.0	1.0
Coal feed rate (kg/h)	18.3	18.4	18.0	13.4	13.9	18.7
Solids circulation flux (kg/m^{2}s)	42	40	48	—	46	—
Average suspension density (kg/m^3)	178	157	178	133	166	107
Temperature at bottom of reactor (°C)	856	859	867	861	864	843
Temperature at top of reactor (°C)	863	866	877	867	876	854
Temperature in L-valve return (°C)	875	872	881	869	880	841
Temperature in secondary cyclone (°C)	859	859	858	831	861	846
Recycle of secondary cyclone catch	yes	yes	yes	yes	yes	no
Flue Gas Concentration						
O_2 (%)	2.8	2.4	2.8	3.5	3.2	4.7
CO_2 corrected to 3% O_2 (%)	16.4	16.2	16.7	16.5	16.4	16.5
CO corrected to 3% O_2 (ppm)	241	489	586	115	108	420
SO_2 corrected to 3% O_2 (ppm)	—	124	158	203	—	—
NO_x corrected to 3% O_2 (ppm)	74	77	100	86	94	125
CH_4 corrected to 3% O_2 (%)	0	0	0	0.017	0.172	0
Excess air level (%)	15.2	12.7	15.2	19.7	17.7	28.4
Combustion efficiency (%)	96.7	97.0	96.5	97.6	97.1	92.9
Mean Particle Size (μm) for						
Bed drain solids	200	207	—	—	—	215
L-valve solids	188	199	192	183	188	—
Secondary cyclone catch	53	48	52	63	67	42
Baghouse catch	26	16	13	15	15	17

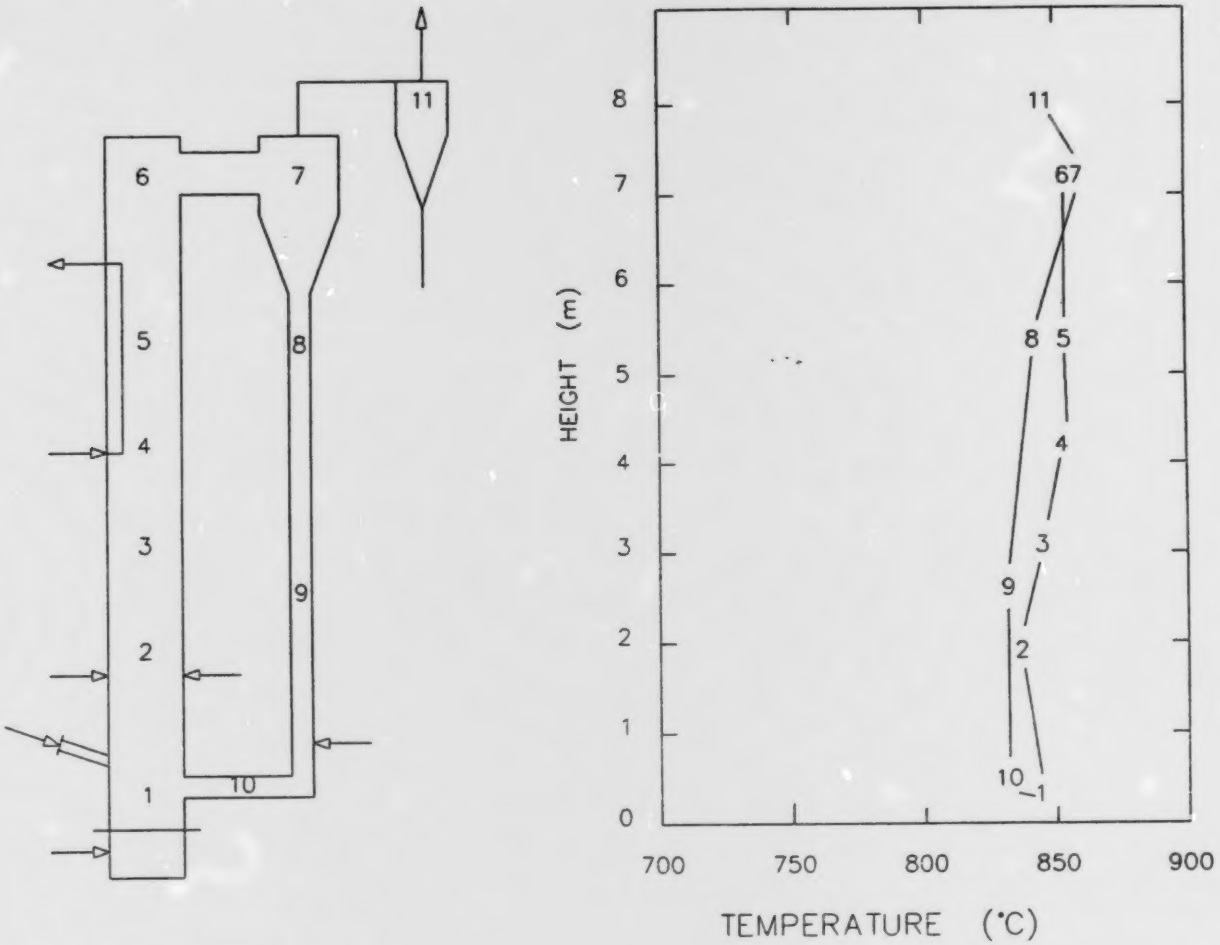

FIGURE 3.4: Typical temperature profile during Anthracite coal combustion trials (Run #7, Condition 1; see Table 3.5 for operating conditions).

TABLE 3.6: Carbon Content in CFBC for Anthracite Combustion Trial. (Conditions are described in Table 3.1, C in wt%)

Condition	Bed/L-Valve Drain	Secondary Cyclone Catch	Baghouse
Run 7–C1	4.54	32.2	24.3
Run 14–C1	3.33	10.5	14.9
Run 14–C2	2.58	11.3	13.8
Run 14–C3	2.00	5.9	15.9
Run 14–C4	1.32	6.8	10.9
Run 14–C5	4.42	13.8	13.4

ing an inherent sulphur capture of 97%. Tests with an improved SO_2 analysis system will be carried out in the future to see whether this finding is confirmed. The NO_x emissions were generally below 135 ppm at 870°C and as low as 89 ppm at 800°C.

The effect of temperature on NO_x formation could also be observed after a fuel step change experiment. The fuel feed rate was suddenly cut from 26 kg/h to 18 kg/h. The bed temperature and the NO_x emissions are plotted as functions of time after the step change in Figure 4.5. Both curves are seen to follow closely the same patterns, with NO_x emissions decreasing from 190 ppm at 850°C to 106 ppm at 725°C. The oxygen concentration in the flue gas rapidly reached a constant value of 9.9%, which explains the higher NO_x emissions at this higher excess air level. CO burnout was almost complete, with emissions always below 50 ppm at 870°C and only up to 77 ppm at 800°C. This again indicates excellent char reactivity.

3.2.5 Pitch combustion tests

The pitch materials (often referred to as tars) tested in this work constitute the bottom fractions or residues from efforts to upgrade unconventional crude hydrocarbons like heavy oils and tar sands bitumen. The materials, referred to here as pitch, tend to be high in asphaltenes and other high molecular weight hydrocarbons, often aromatics. They also tend to be high in sulphur and to be the repository of most of the heavy metals which were present in the original hydrocarbon material from which they were derived. Two main aspects are therefore of interest for the pitch combustion trials in our unit. First, it is important to determine whether CFBC technology can provide a suitable technique for disposing safely and cleanly of potentially troublesome pitch materials, while recovering some energy. Second the fate of the heavy metals during combustion needs to be examined.

TABLE 3.7: Operating Conditions and Combustion Results for Lignite Coal (Run #15)

Conditions	1	2	3	4
U primary zone (m/s)	4.1	2.9	3.0	2.9
U secondary zone (m/s)	8.4	8.8	6.9	8.6
Secondary/primary air ratio	1.07	2.03	1.28	2.00
Coal feed rate (kg/h)	26.4	27.8	22.6	27.2
Average suspension density (kg/m^3)	103	156	163	n/a
Temperature at bottom of reactor (°C)	869	875	801	876
Temperature at top of reactor (°C)	874	878	801	886
Temperature in L-valve return (°C)	880	886	810	887
Temperature in secondary cyclone (°C)	845	886	776	841
Recycle of secondary cyclone catch	yes	yes	yes	yes
Flue Gas Concentration				
O_2 (%)	3.3	3.2	3.8	3.3
CO_2 corrected to 3% O_2 (%)	18.1	17.6	16.4	18.0
CO corrected to 3% O_2 (ppm)	46	51	77	49
SO_2 corrected to 3% O_2 (ppm)	3	0	20	20
NO_x corrected to 3% O_2 (ppm)	132	131	89	134
CH_4 corrected to 3% O_2 (%)	0	0	0	0
Excess air level (%)	18.5	17.8	21.9	18.5
Combustion efficiency (%)	99.5	99.5	99.5	99.6
Mean Particle Size (μm) for				
Bed drain solids	197	159	166	159
L-valve solids	190	158	161	170
Secondary cyclone catch	33	43	41	59
Baghouse catch	12	13	13	15

Previous tests, conducted in our unit before the modifications described in Chapter 1 and 2, are described by Grace and Lim (1987). These tests were inconclusive on where the heavy metals ended up since there was no baghouse at the time to collect the fine fractions of solids escaping the system. Since then, a baghouse has been installed as described in Chapter 2. The feeding system was also modified (see Section 2.2). In brief, the entire pitch feed piping system was steam traced to maintain a uniform temperature of 155° C and a metering pump was used to control the pitch flow rate.

During the tests conducted under this contract, two pitches were burned in our combustion unit. Their properties are listed in Section 2.8. The sorbent used in these trials was Texlime limestone (see Tables 2.4 and 2.5 for properties).

CANMET pitch tests

The first pitch tested after installation of a baghouse was obtained from the CANMET Hydrocracking Demonstration Unit in the Petro-Canada Montreal-East refinery. The operating conditions and the results of the combustion trial are presented in Table 3.8. Full recycle of the secondary cyclone catch was maintained throughout the trial. The combustion efficiency was very high, always above 99.7%. The sulphur capture efficiencies are plotted in Figure 3.5 as a function of Ca:S molar ratio. The results once again show remarkably little influence of the Ca:S ratio on the sulphur capture over the range studied. Similar results were obtained during previous runs in our unit reported by Grace and Lim (1987).

NO_x emissions were a little higher than those obtained during the tests with solid fuels. The presence of limestone seems to have a significant effect on NO_x emissions as shown in Figure 3.6, where the NO_x levels are plotted as a function of Ca:S molar ratio. In this figure, the average reactor temperatures are indicated, while the secondary-to-primary air ratio was always in the range 0.77–0.86. CO levels were always low, with values in a narrow range, from 120–168 ppm, except in one case where the concentration reached 340 ppm.

The fate of the heavy metals, such as those present in CANMET pitch (nickel and vanadium), is of special interest because they form highly corrosive and somewhat toxic compounds when released in the gaseous phase during combustion. It is therefore desirable that these elements remain in the solid residue. It has been shown that more than 90% of the Ni and V ended up in the waste solids streams during small scale CFBC trials for two fuels, Syncrude coke and Minto coal (Hamer *et al.*, 1987). Metals contents of the solids samples collected during the CANMET pitch trial (Run #17) were therefore measured to investigate the issue of heavy metal emissions. The analyses are presented in Table 3.9. The analyses of the Olivine sand, Texlime limestone and CANMET pitch ash are also included in Table 3.9.

TABLE 3.8: Operating Conditions and Combustion Results for CANMET Pitch

	Run #17					
Conditions	Baseline	1	2	4	5	6
U primary zone (m/s)	4.7	4.9	3.0	4.5	4.6	2.9
U secondary zone (m/s)	8.7	8.8	8.3	8.4	8.5	8.3
Secondary/primary air ratio (—)	0.83	0.80	1.77	0.85	0.86	1.87
Pitch feed rate (kg/h)	14.8	15.1	14.0	13.0	14.0	13.4
Limestone feed rate (kg/h)	0	3.3	3.1	1.5	4.8	4.6
Ca:S molar ratio	0	2.50	2.50	1.30	3.90	3.90
Average suspension density (kg/m^3)	155	195	168	165	201	189
Temperature at bottom of reactor (°C)	895	905	882	873	864	874
Temperature at top of reactor (°C)	880	885	867	880	886	886
Temperature in L-valve return (°C)	891	835	817	856	843	854
Temperature in secondary cyclone (°C)	856	856	831	869	910	889
Recycle of secondary cyclone catch	yes	yes	yes	yes	yes	yes
Flue Gas Concentration						
O_2 (%)	3.2	3.0	3.5	5.0	3.8	3.9
CO_2 corrected to 3% O_2 (%)	14.9	16.0	15.3	15.0	16.7	15.1
CO corrected to 3% O_2 (ppm)	168	120	124	167	340	121
SO_2 corrected to 3% O_2 (ppm)	1182	225	179	319	255	256
NO_x corrected to 3% O_2 (ppm)	145	165	165	139	215	202
CH_4 corrected to 3% O_2 (%)	0.013	0.002	0.002	0.005	0.12	0.004
Sulphur capture (%)	—	87.6	90.1	82.4	85.9	85.9
Calcium utilization (%)	—	35	36	63	22	22
Excess air level (%)	17.3	16.0	19.2	30.4	21.2	21.9
Combustion efficiency (%)	99.9	99.9	99.9	99.9	99.7	99.7
Mean Particle Size (μm) for						
Bed drain solids	—	—	—	—	—	—
L-valve solids	188	—	193	184	—	173
Secondary cyclone catch	59	—	55	47	—	43
Baghouse catch	19	—	13	14	—	19

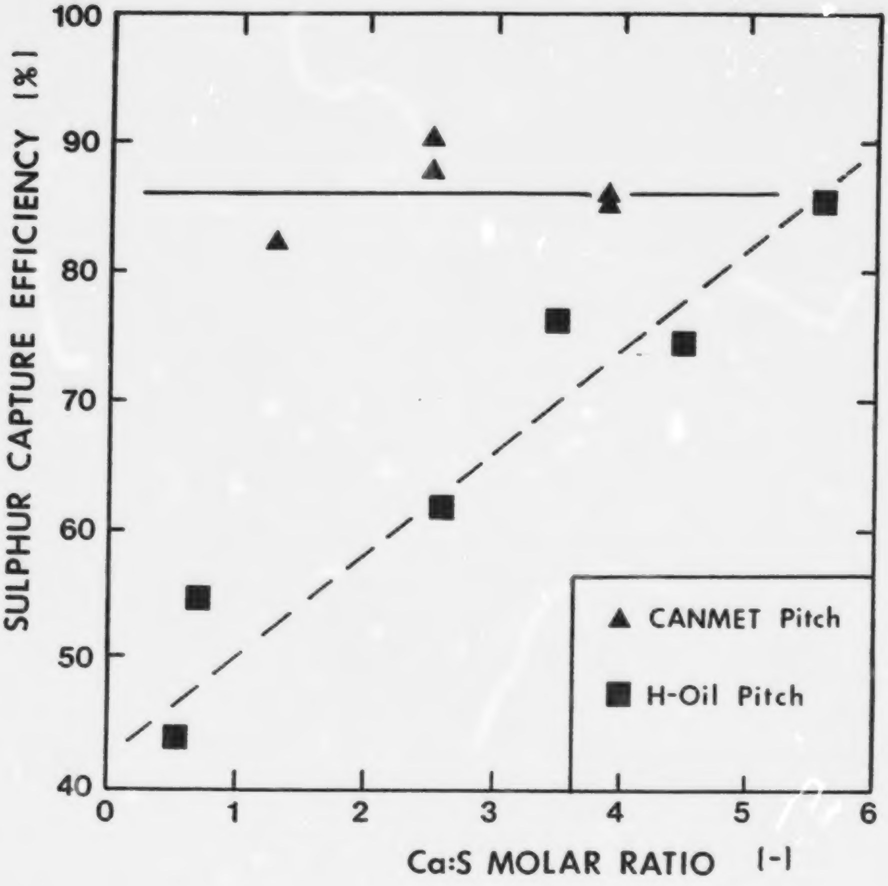

FIGURE 3.5: Sulphur capture versus Ca:S molar ratio for CANMET and H-Oil pitch combustion trails.

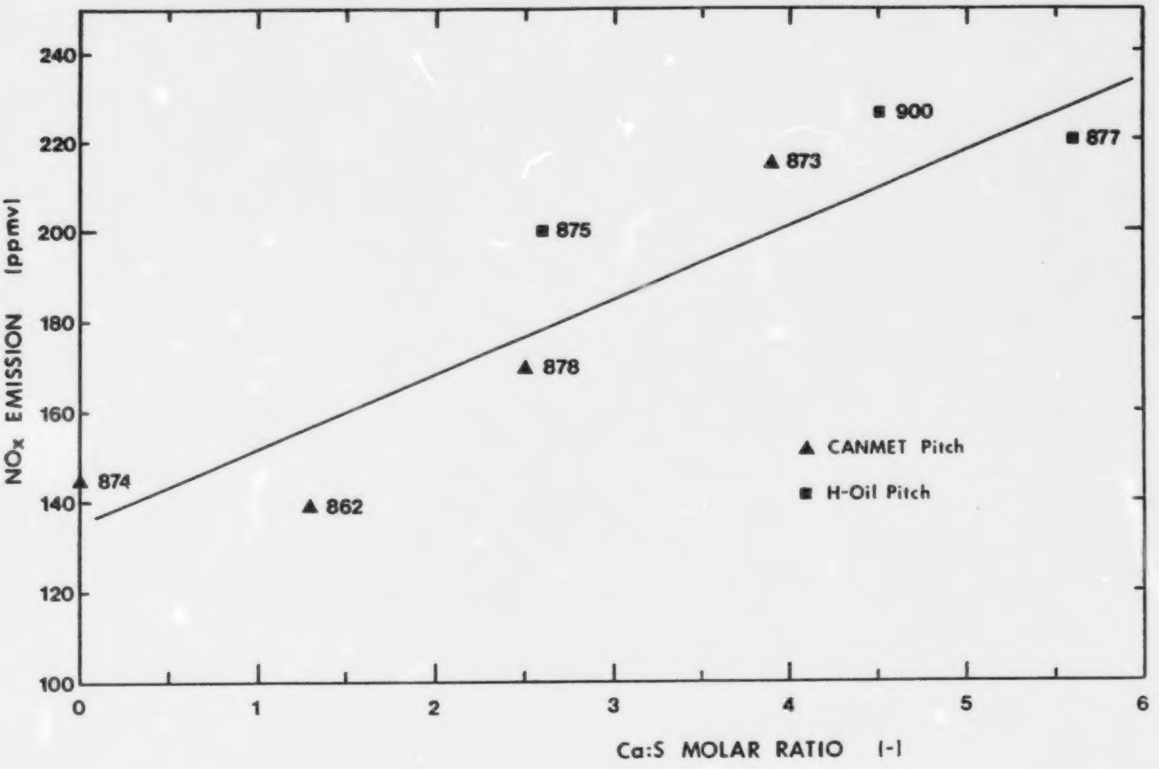

FIGURE 3.6: NO_x emission versus Ca:S molar ratio for CANMET and H-oil pitch combustion trials. (Secondary to primary air ratio = 0.77–0.86; superficial gas velocity = 8.2–8.8 m/s; see Tables 3.8 and 3.9 for operating conditions.)

TABLE 3.9: Chemical Analysis of Samples from Run #17 – CANMET Pitch/Texlime. (See Table 3.8 for operating conditions).

	BASELINE			TEST C2		
	L-VALVE	2'CYCL.	BAGHOUSE	L-VALVE	2'CYCL.	BAGHOUSE
SiO_2	42.25	45.6	36.8	40.93	20.97	27.85
Al_2O_3	2.01	13.25	16.74	2.11	6.1	11.09
Fe_2O_3	8.49	7.83	8.91	8.7	3.79	8.51
TiO_2	0.04	0.3	0.57	0.05	0.15	0.41
P_2O_5	0.33	0.13	0.24	0.16	0.17	0.3
CaO	1.58	7.97	14.22	3.01	43.05	22.73
MgO	44.71	22.08	10.58	43.88	9.21	9.75
SO_3	0.04	1.0	1.91	0.67	8.1	2.48
Na_2O	0.16	1.55	2.5	0.2	0.68	1.45
K_2O	0	0.36	0.45	0.08	0.24	0.26
BaO	0	0.14	0.47	0	0.05	0.27
SrO	0	0.02	0.13	0	0.08	0.09
V_2O_5	0	0.07	0.12	0.05	0.05	0.21
NiO	0.27	0.17	0.11	0.31	0.05	0.11
LOF	0	0.71	6.29	0.21	8.07	14.02
SUM	99.88	101.18	100.04	100.36	100.76	99.53

	TEST C4			TEST C6		
	L-VALVE	2'CYCL.	BAGHOUSE	L-VALVE	2'CYCL.	BAGHOUSE
SiO_2	39.76	19.03	19.27	39.65	16.38	17.01
Al_2O_3	4.2	6.68	7.89	2.75	4.95	6.67
Fe_2O_3	7.63	3.47	4.41	8.24	3.18	6.12
TiO_2	0.07	0.17	0.23	0.07	0.12	0.25
P_2O_5	0.78	0.1	0.09	0.94	0.14	0.14
CaO	5.62	46.81	43.73	7.11	50.3	36.79
MgO	37.97	5.83	4.61	38.32	6.37	5.37
SO_3	1.08	0.83	8.82	1.0	9.33	3.23
Na_2O	0.23	0.68	0.82	0.21	0.55	0.71
K_2O	0.04	0.22	0.21	0.04	0.21	0.19
BaO	0	0.06	0.11	0	0.04	0.11
SrO	0	0.09	0.09	0	0.09	0.08
V_2O_5	0.04	0.08	0.14	0.06	0.08	0.23
NiO	0.28	0.05	0.07	0.28	0.05	0.1
LOF	0.91	6.65	11.14	1.19	7.46	23.2
SUM	98.61	90.75	101.63	99.86	99.25	100.2

Table 3.9 (con't): Chemical Analysis of Samples from Run 17 – CANMET Pitch/Texlime.

	OLIVINE	TEXLIME	ASH
SiO_2	41.48	0	21.4
Al_2O_3	0.76	0.62	8.2
Fe_2O_3	8.58	0.45	44.9
TiO_2	0	0	0.7
P_2O_5	0	0	0
CaO	0.41	54.57	6.8
MgO	48.08	0.34	5.4
SO_3	0.54	1.17	4.2
Na_2O	0.05	0.05	1.1
K_2O	0.01	0.16	0.3
BaO	0.03	0.03	0
SrO	0.01	0.1	0
V_2O_5	0	0	3.6
NiO	0.33	0.01	1.1
LOF	0	42.9	2.3
SUM	100.28	100.4	100.0

TABLE 3.10: Vanadium Mass Balance for CANMET Pitch Combustion Trial (Condition C6 in Table 3.8.)

Pitch feed rate:	13.4 kg/h
Limestone feed rate:	4.6 kg/h
Waste produced:	3.6 kg/h
% V_2O_5 in Baghouse stream:	0.23%
% V_2O_5 in Pitch feed:	0.065%
V_2O_5 in	= 8.68 g/h
V_2O_5 out	= 8.28 g/h
V_2O_5 out/in	= 95%

The amount of magnesium oxide in each stream is a good indication of the fraction of Olivine sand in each sample. In general, the analyses of the L-valve samples, which represent the primary recycle loop, are very similar to pure Olivine sand, while the secondary cyclone catch consists mainly of calcined limestone (CaO). The amount of vanadium is relatively small in these two streams with an average of 0.05% and 0.07% for the primary and secondary recycle loop respectively. The finer baghouse stream which shows an average value of 0.18% in vanadium was the only waste stream throughout the entire trial. A vanadium mass balance for the last condition (C6) which corresponds as much as possible to steady-state condition is presented in Table 3.10. Most of the vanadium can be accounted for during the last period of the combustion trial. This suggests that the vanadium remains in the solid phase and is mostly found in the finest particulate fractions at steady-state. It was not possible to calculate the Ni mass balance because of the relatively large amount already present in the Olivine sand (0.33%) used as start-up materials.

H-Oil pitch tests

The Alberta Oil Sands Technology and Research Authority (AOSTRA) has been promoting the development of upgrading technology for a number of years. Tests have been conducted using a variety of upgrading processes developed in a number of countries to determine which can best meet the needs of oil sands bitumen. The second pitch tested in our work was a byproduct of one such test, carried out with the H-Oil Process developed by Hydrocarbon Research Incorporated.

Previous tests with this fuel in our unit before the installation of a baghouse were unsuccessful due to problems with the building ventilation system. Since the modifications to our equipment and by providing tighter control of the pitch feedrate by means of a metering positive displacement pump, two successful trials were achieved. The H-Oil pitch was less viscous and easier to handle than the CANMET pitch at the temperature maintained in the feed piping system (155°C). The formation of clouds of fine fly ash observed in previous trials with this pitch were only produced when there were substoichiometric conditions in the reactor. They could be eliminated completely by maintaining strict control of the excess air level.

The operating conditions and the results of the successful trials are presented in Table 3.11. The first noticeable result is that the combustion efficiency was consistently above 99.9%. Sulphur capture results are plotted in Figure 3.5, together with values obtained in previous runs (Grace and Lim, 1987). As expected, the capture efficiency increased with the Ca:S ratio. However, the actual values were much lower than for Minto coal or for CANMET pitch, possibly reflecting different sulphur compounds in the different fuels. The SO_2 emissions were found to be very sensitive to the operating conditions. Fluctuations in solids circulation rates and hence in suspension densities would result in large fluctuations in SO_2 emissions. The feedrate of sorbent was very low, of the order of 2 kg/h. Small changes in primary and secondary solids recycle rates could have caused large changes in the sorbent-to-pitch ratio in the reactor. This could explain the surprisingly small recorded influence of Ca:S on sulphur capture observed for the CANMET pitch.

Solids samples taken during the H-Oil pitch combustion trial (Run #20) were also analyzed for metals contents. The results are presented in Table 3.12, together with the Olivine sand, Texlime limestone and ash analyses. Once again it appears that the finest baghouse stream contains the highest concentration of vanadium, while the concentrations in the primary and secondary loops remain essentially constant at 0.04% and 0.07% wt of V respectively. The overall vanadium mass balance for the entire combustion trials (27.4 hours) is illustrated in Table 3.13. The accountability for vanadium is greater than 100% which is probably due to an error in the ash content of the pitch which was taken as being 0.1%. However, it appears that the heavy metal vanadium remains in the solid phase and does not devolatilize in the reactor.

TABLE 3.11: Operating Conditions and Combustion Results for H-Oil Pitch

	Run #18		Run #20			
Conditions	BL	C1	BL	2	3	4
U primary zone (m/s)	5.4	4.8	4.1	4.6	4.8	4.9
U secondary zone (m/s)	9.2	6.4	7.5	8.2	8.5	8.8
Secondary/primary air ratio	0.70	0.32	0.82	0.81	0.77	0.80
Pitch feed rate (kg/h)	14.5	10.4	13.9	13.5	13.5	14.0
Limestone feed rate (kg/h)	0	2.7	0	2.6	5.5	4.6
Ca:S molar ratio	0	3.50	0	2.60	5.60	4.50
Average suspension density (kg/m^3)	140	139	155	143	150	243
Temperature at bottom of reactor (°C)	889	882	761	864	877	900
Temperature at top of reactor (°C)	897	880	759	882	890	908
Temperature in L-valve return (°C)	902	890	773	875	881	892
Temperature in secondary cyclone (°C)	844	832	748	872	—	—
Recycle of secondary cyclone catch	yes	yes	yes	yes	yes	yes
Flue Gas Concentration						
O_2 (%)	3.6	3.2	3.2	3.5	4.0	3.7
CO_2 corrected to 3% O_2 (%)	13.8	14.5	16.8	17.1	16.8	16.6
CO corrected to 3% O_2 (ppm)	125	116	157	123	163	133
SO_2 corrected to 3% O_2 (ppm)	1110	351	986	562	214	375
NO_x corrected to 3% O_2 (ppm)	184	167	118	203	221	228
CH_4 corrected to 3% O_2 (%)	0.016	0.003	0.003	0	0	0.001
Sulphur capture (%)	—	76.1	—	61.7	85.4	74.5
Calcium utilization (%)	—	22	—	24	15	17
Excess air level (%)	19.8	17.2	17.2	19.1	22.5	20.5
Combustion efficiency (%)	—	—	99.9+	99.9+	—	99.9+
Mean Particle Size (μm) for						
L-valve solids	—	—	191	178	185	198
Secondary cyclone catch	—	—	44	58	71	81
Baghouse catch	—	—	15	23	22	29

TABLE 3.12: Chemical Analysis of Samples from Run #20 – H-Oil pitch/Texlime limestone (For conditions see Table 3.9).

	BASELINE			C1		
	L-VALVE	2'CYCL.	BAGHOUSE	L-VALVE	2'CYCL.	BAGHOUSE
SiO_2	41.01	40.6	29.69	39.85	22.85	26.0
Al_2O_3	0.65	8.77	7.98	0.69	4.06	6.14
Fe_2O_3	8.75	5.6	5.5	8.03	3.32	4.43
TiO_2	0.02	0.17	0.33	0.01	0.08	0.21
P_2O_5	0.53	0.27	0.21	1.54	0	0.24
CaO	0.53	11.7	17.19	2.12	39.68	26.24
MgO	48.41	20.97	16.39	44.29	14.57	13.06
SO_3	0.7	4.16	5.78	0.75	8.47	11.17
Na_2O	0.04	0.71	0.99	0.05	0.32	0.68
K_2O	0.01	0.15	0.15	0	0.14	0.11
BaO	0	0.06	0.2	0	0	0.12
SrO	0	0.01	0.05	0	0.05	0.06
V_2O_5	0.05	0.19	0.29	0.08	0.13	0.18
NiO	0.34	0.2	0.33	0.3	0.12	0.14
LOF	0	6.11	15.96	0.71	7.2	10.39
SUM	101.04	99.67	101.04	98.42	100.99	99.17

	C2			C3		
	L-VALVE	2'CYCL.	BAGHOUSE	L-VALVE	2'CYCL.	BAGHOUSE
SiO_2	39.06	18.15	17.35	38.21	16.09	8.23
Al_2O_3	0.85	2.49	3.65	1.14	1.59	1.47
Fe_2O_3	8.05	2.87	3.09	7.85	2.73	1.47
TiO_2	0.02	0.06	0.12	0.02	0.04	0.06
P_2O_5	1.07	0.42	0.45	0.98	0.22	0.01
CaO	2.29	43.87	40.41	3.88	49.22	57.84
MgO	44.4	13.57	10.64	43.61	13.62	4.77
SO_3	0.71	10.21	12.87	1.08	8.74	12.24
Na_2O	0.08	0.23	0.43	0.11	0.17	0.18
K_2O	0	0.12	0.13	0	0.12	0.13
BaO	0	0	0.04	0	0	0
SrO	0	0.06	0.07	0	0.07	0.1
V_2O_5	0.04	0.09	0.15	0.05	0.07	0.09
NiO	0.31	0.12	0.11	0.31	0.09	0.05
LOF	0.07	7.42	9.13	0.37	7.79	12.87
SUM	96.95	99.68	98.64	97.61	100.56	99.51

Table 3.12 (con't): Chemical Analysis of Samples from Run #20 – H-Oil pitch/Texlime limestone (For conditions see Table 3.9).

	C4					
	L-VALVE	2'CYCL.	BAGHOUSE	OLIVINE	TEXLIME	ASH
SiO_2	39.69	21.18	11.11	41.48	0	16.3
Al_2O_3	0.44	0.99	0.5	0.76	0.62	7.0
Fe_2O_3	8.16	3.93	2.6	8.58	0.45	24.0
TiO_2	0.01	0.03	0.03	0	0	0.7
P_2O_5	0.99	0.5	0.18	0	0	0
CaO	3.26	38.13	54.02	0.41	54.57	3.5
MgO	44.59	20.71	10.37	48.08	0.34	3.7
SO_3	0.71	7.24	11.15	0.54	1.17	0
Na_2O	0.06	0.12	0.08	0.05	0.05	1.9
K_2O	0	0.1	0.11	0.01	0.16	1.1
BaO	0	0	0	0.03	0.03	0
SrO	0	0.05	0.09	0.01	0.1	0
V_2O_5	0.04	0.07	0.11	0	0	25.5
NiO	0.33	0.14	0.29	0.33	0.01	12.0
LOF	0	6.09	10.09	0	42.9	2.8
SUM	98.28	99.28	100.73	100.28	100.4	98.5

TABLE 3.13: Vanadium Mass Balance for H-Oil Pitch Combustion Trial (Entire Run #20).

Length of combustion trial:			27.4 hours
Average pitch feed rate:			13.8 kg/h
Total amount of V_2O_5 in: (Based on 0.1% ash)			96.5 g
	B/H drain (kg)	% V_2O_5 in B/H (% wt)	Total V_2O_5 (g)
Baseline	3.2	0.29	9.3
C1	6.0	0.18	10.8
C2	5.8	0.15	8.7
C3	23.5	0.09	21.2
C4	31.3	0.11	34.4
Total amount of V_2O_5 out in Baghouse stream:			84.4 g
Total amount of V_2O_5 remaining in reactor:			40 g
Accountability of V (V_{in}/V_{out}):			129%

3.2.6 Calcination of calcium carbonate

Part of the Kraft process in a pulp mill involves the conversion of spent cooking chemicals into a suitable form for re-use in the pulping stage. The chemistry of the overall operation known as "recauticization" is simply:

$$CaO + H_2O + Na_2CO_3 \rightarrow 2NaOH + CaCO_3 \tag{3.1}$$

where the sodium carbonate formed in the digesters is converted into sodium hydroxide. The latter is separated from the calcium carbonate in "white liquor clarifiers" before being returned to the digesters. The calcium carbonate is then dried and calcined at a temperature of about 900°C to form CaO which is used for reaction (Equation 3.1).

Fluidized bed calciners are in use in Canada, Japan and the United States for the calcination of calcium carbonate in pulp mills, a duty which is also commonly performed in large rotary kilns. "Fluo-Solids" calciners have been reported to be more thermally efficient and easier to operate (Potkins, 1970). In a fluidized bed calciner, calcination of fine calcium carbonate results in spherical pellets of calcium oxide which are dense, hard and highly reactive. When pre-dried calcium carbonate is fed into the bottom of the fluidized bed at a calcination

TABLE 3.14: Pros and Cons of Fluidized Bed Versus Rotary Kiln Calciners.

PROS	CONS
Good lime quality Quick shut down and start-up Easy control Thermal savings	More electrical energy needed More sensitive to sodium content

temperature of about 900°C, calcination of the small particles is almost instantaneous, and the presence of inerts, which melt at this temperature (Na compounds), causes the particles to adhere to one another. The pros and cons of fluid bed versus rotary kiln calciners are presented in Table 3.14. Circulating fluidized bed technology, with its increased throughput per unit area and good turndown ratio, offers a possible alternative for the next generation of calcination systems. It is notable that CFB calciners have been used for calcination of aluminum ores and phosphates for some time (Reh, 1986).

In view of these factors and the importance of pulp production in BC, one run was conducted in which the UBC–CFBC unit was adapted for calcination of calcium carbonate. The carbonate was obtained from the Pulp Division of Crestbrook Forest Industry Ltd. located near Cranbrook, BC. The calcium carbonate was pneumatically fed into the reactor. Diesel fuel obtained from Esso Canada Ltd. was employed as the fuel and was fed from the liquid feed port through an atomizing nozzle. It was burned to maintain the reactor temperature above 870°C. The unit was operated without secondary recycle, at a superficial velocity of 7.6 m/s and a temperature in the range of 890–920°C. A summary of the operating conditions and results for the calcination trial is presented in Table 3.15. Silica sand ($dp=148\mu m$) was used as the start-up bed material. The product was discharged from the L-valve and bed drains.

The trial lasted 17.5 hours, during which time an average of 17.4 kg/h of calcium carbonate was fed to the reactor. Figure 3.7 shows the mass balance averaged over the entire trial, together with a typical temperature profile. The product collected from the primary loop (L-valve and bed drains) was remarkably uniform in size. The particle size distribution of the calcium carbonate fed and of the calcium oxide product discharged from the reactor are shown in Figure 3.8. It was not possible to obtain a product free of contaminants (sand and ash) in a trial of such short duration, but it was easy to separate the product from the inerts outside the reactor. The pellets of CaO did not grow much larger than 1 mm in the CFBC, as opposed to particles of up to 4 mm obtained in the Crestbrook Fluo-Solids calciner. The smaller, more uniform pellets appear to be excellent for use in the pulp mill. Dorris (1989) observed during a typical slaking test in green liquor that the lime produced in our unit was

TABLE 3.15: Operating Conditions and Results for Calcination Trial

U Primary Zone	(m/s)	4.2
U Secondary Zone	(m/s)	7.6
Secondary/Primary Air Ratio	(–)	0.8
Diesel Fuel Feed Rate	(kg/h)	9.1
Carbonate Feed Rate	(kg/h)	17.4
Average Suspension Density	(kg/m^3)	180
Temperature at Bottom of Reactor	(°C)	899
Temperature at Top of Reactor	(°C)	921
Temperature in L-valve Return	(°C)	894
Temperature in Secondary Cyclone	(°C)	885
Recycle of Secondary Cyclone Catch		No
Flue Gas Analysis		
O_2	(%)	5.6
CO_2	(%)	14.2
CO	(ppm)	57
SO_2	(ppm)	0
NO_x	(ppm)	13
CH_4	(%)	0
Excess air level	(%)	33.8

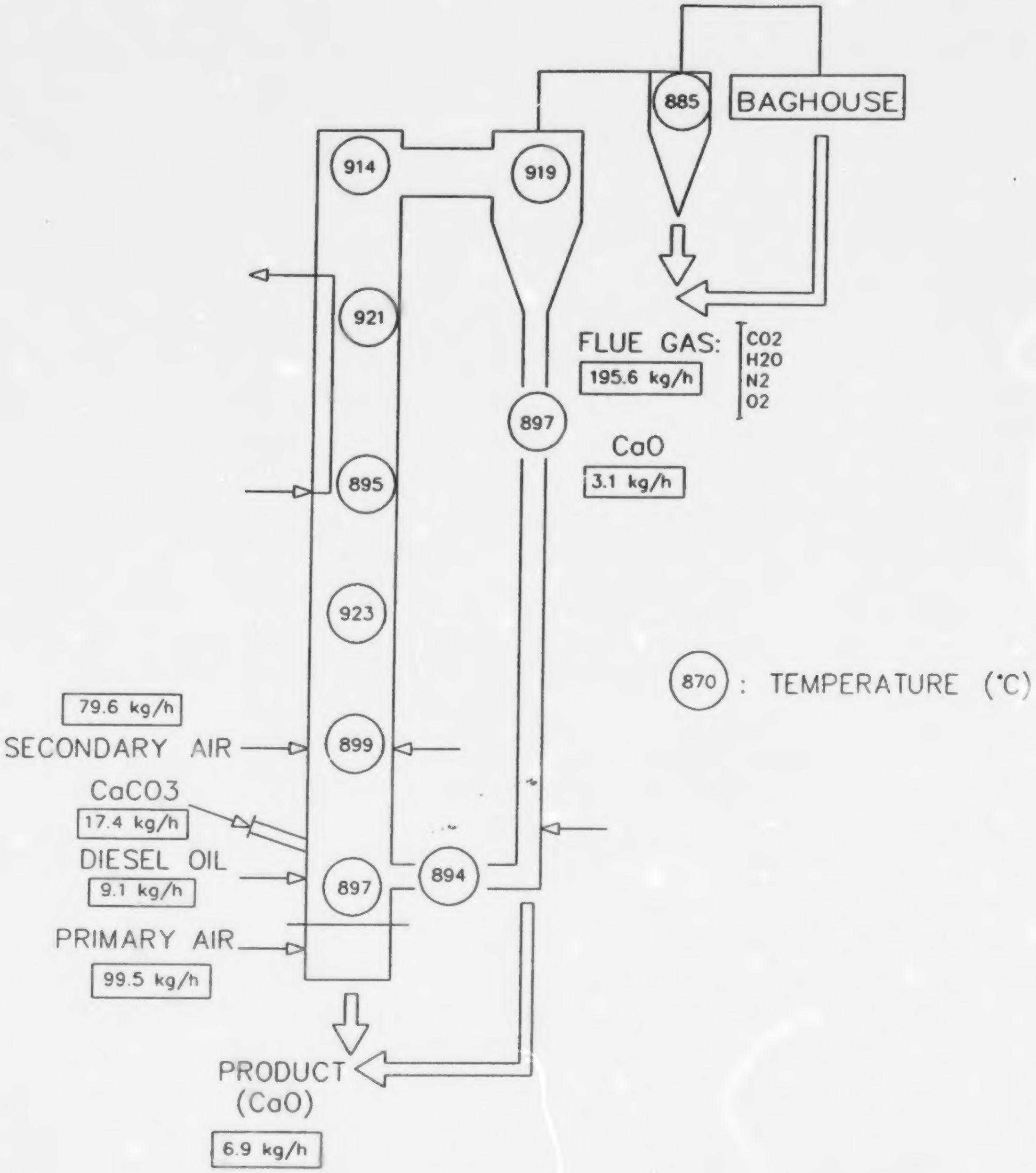
885
BAGHOUSE
914
919
921
FLUE GAS:
195.6 kg/h
CO2
H2O
N2
O2
897
CaO
3.1 kg/h
895
923
870 : TEMPERATURE (°C)
79.6 kg/h
SECONDARY AIR
899
CaCO3
17.4 kg/h
DIESEL OIL
9.1 kg/h
897
894
PRIMARY AIR
99.5 kg/h
PRODUCT
(CaO)
6.9 kg/h

FIGURE 3.7: Overall mass balance and typical temperature profile for the calcination trial.

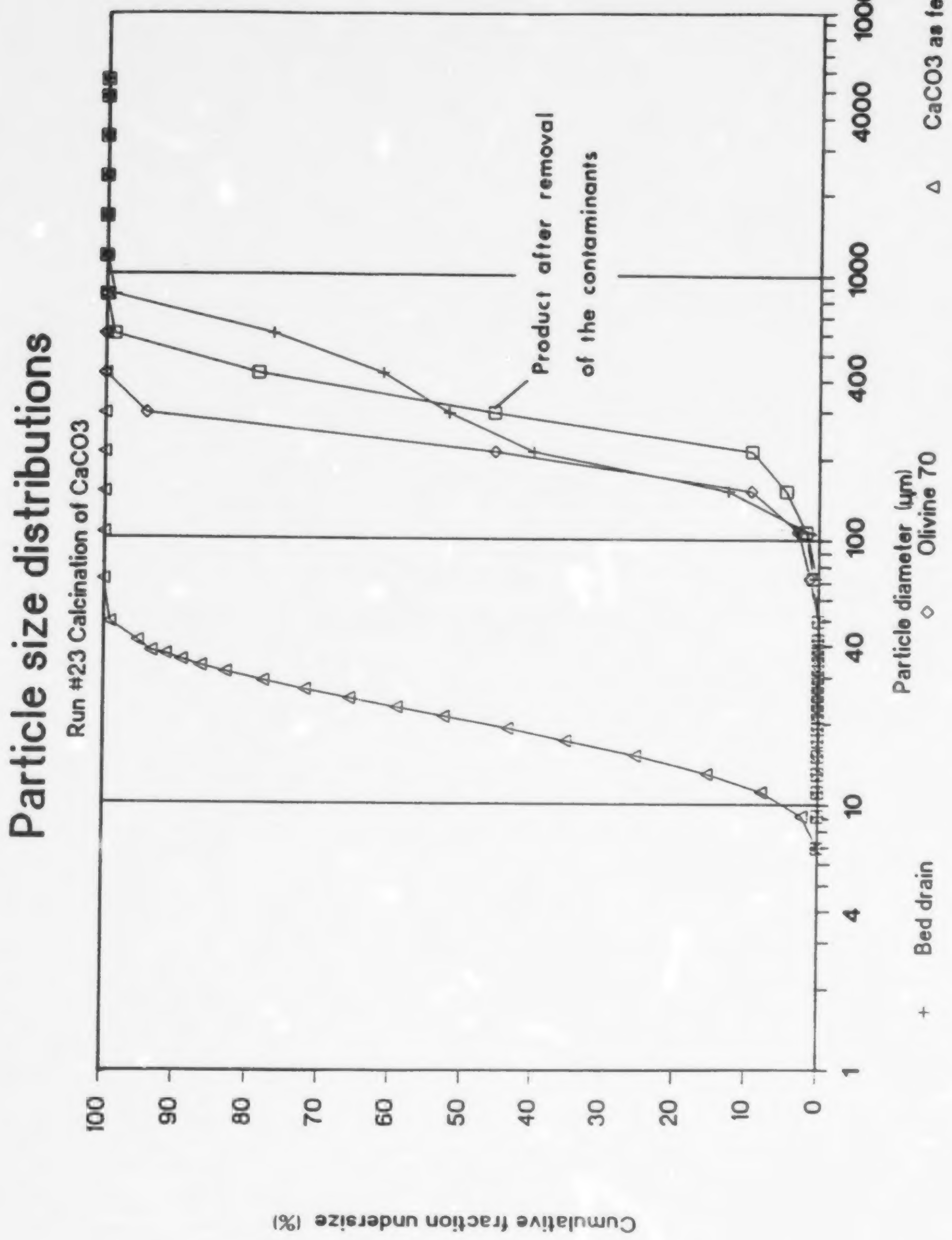

FIGURE 3.8: Particle size distributions of $CaCO_3$ feed and CaO product.

extremely reactive. He also reports that after analyzing limes from at least 20 mills, the products from our CFBC unit were the most reactive examined so far, followed closely by the lime produced in the "Fluo-Solids" calciner used by the Crestbrook Pulp Division. Further longer trials would be necessary to investigate the effect of various operating conditions (temperature, superficial velocity, etc.) on the calcination and agglomeration processes in a CFBC calciner. However, the preliminary results obtained so far are very promising.

Chapter 4

GASEOUS POLLUTANT EMISSIONS

4.1 Multipoint Gas Sampling System

A multipoint gas sampling system was installed in order to study the mechanisms of pollutant formation. Sample gas can be withdrawn at five different heights along the combustor, as well as between the two cyclones and from the flue gas conduit, as shown in Figures 4.1 and 4.2.

For gas sampling from the reactor, sampled gas passes through a porous stainless steel filter, in which gas and solids are separated, then is cooled in a water-cooled heat exchanger. Condensed water is drained from the bottom of the exchanger. A drying tube filled with magnesium perchlorate ($Mg(ClO_4)_2$) is used to remove any residual moisture before the sample gas reaches the manifold on the control board. For flue gas sampling, gas must traverse a water trap (ice bath) after the filter, instead of passing through a water-cooled heat exchanger. All sampling lines were made of stainless steel and teflon. Air purges were used to flush out solids from the filters. Because the combustor is operated at small positive pressures, no vacuum pump is needed. A schematic of the complete sampling system is provided in Figure 4.2.

The oxygen and SO_2 gas analyzers used for the last contract (Grace and Lim, 1987) were replaced by more accurate analyzers (both made by Horiba). New analyzers for CO, CO_2, and CH_4 were also purchased. The key features of the gas analyzers are listed in Table 4.1. The concentration of N_2O in the flue gas was measured by using a gas chromatograph. Details of N_2O measurement and results are provided in Section 8.1.

The gas sampling tubes for in-reactor gas sampling are connected to their respective filters by flexible stainless steel tubing, allowing them to be moved to different radial positions. Three types of sampling probes were tried: bare stainless steel tube, outer-cooled probe and inner-cooled probe. The design of the outer-cooled probe in shown is Figure 4.3. Because of high moisture contents of the fuels, water-cooled probes caused sudden condensation due to high cooling rates which could in turn lead to the blockage of the sampling tube by wet solids. Hence, the gas concentration profiles in this report are from uncooled sampling tubes.

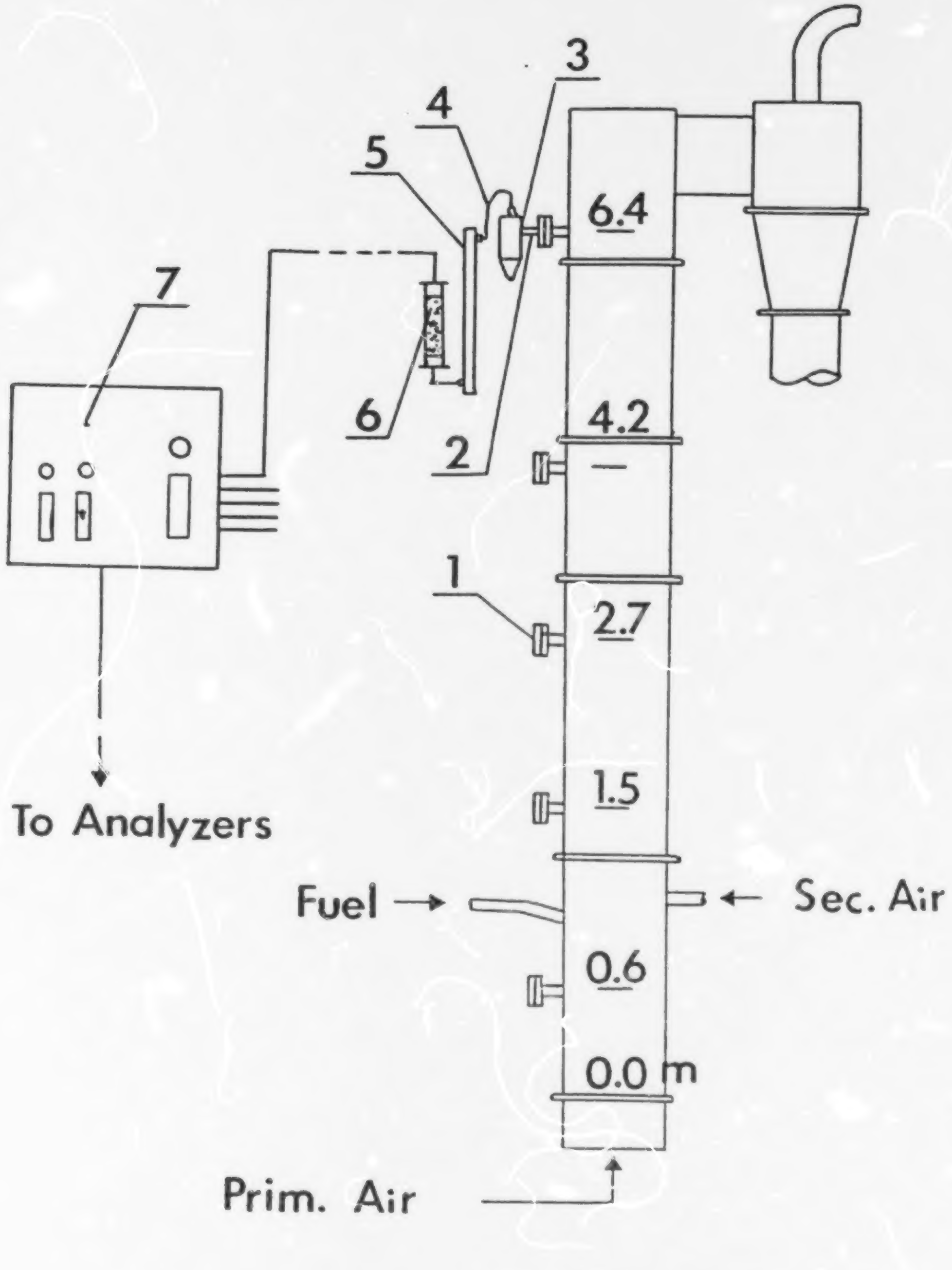
3
4
5
7
6
2
1
6.4
4.2
2.7
1.5
0.6
0.0 m
To Analyzers
Fuel
Sec. Air
Prim. Air

FIGURE 4.1: Vertical gas sampling positions and sampling trains. 1. Sampling port; 2. Sampling probe extending into reactor; 3. Gas filter; 4. Flexible stainless steel tubing; 5. Heat exchanger; 6. Dryer; 7. Control Panel. Note that only one of the five sampling trains is shown.

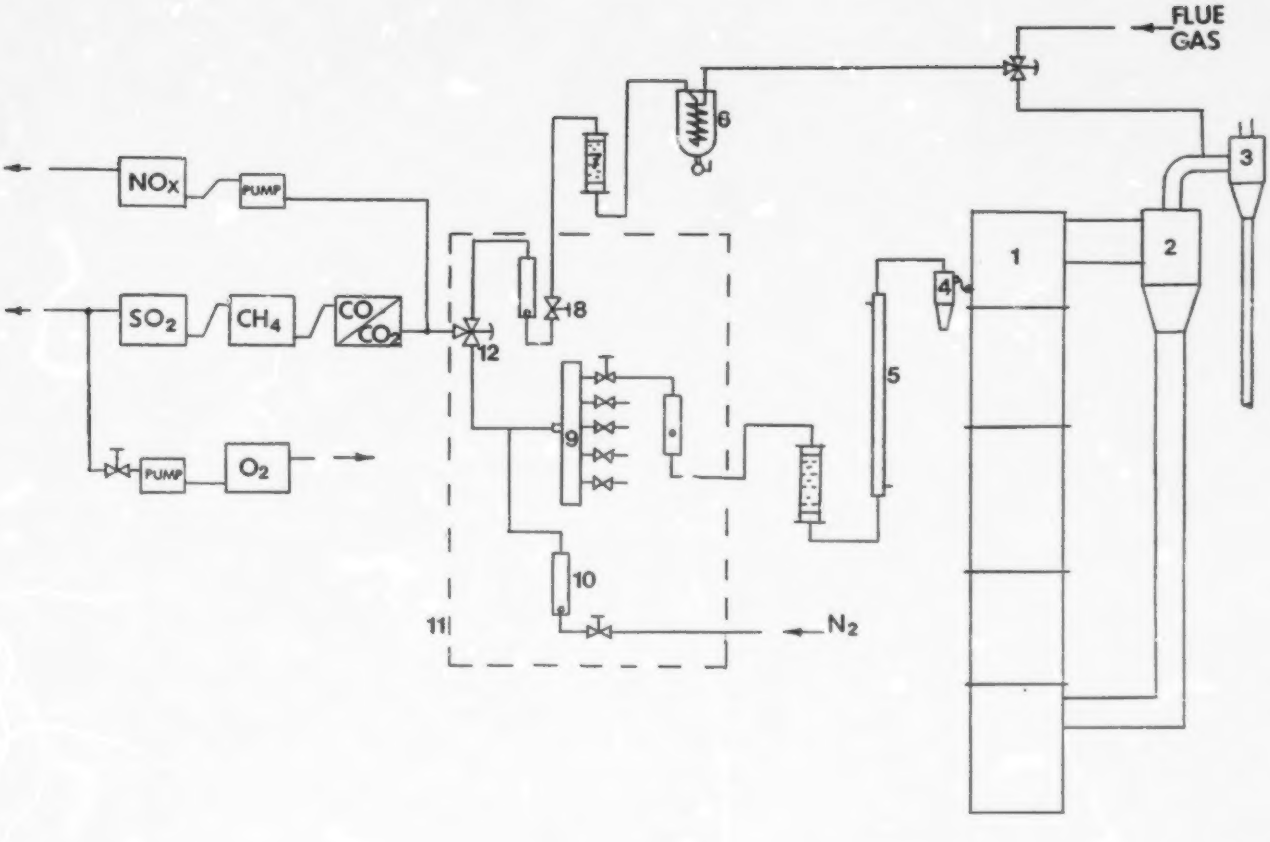
FLUE GAS
6
7
NOx
PUMP
3
2
1
SO2
CH4
CO
CO2
12
8
4
5
9
PUMP
O2
10
11
N2

FIGURE 4.2: Gas sampling system. 1. Reactor; 2. Primary cyclone; 3. Secondary cyclone; 4. Gas filter; 5. Heat exchanger; 6. Water trap; 7. Dryer; 8. Control valve; 9. Manifold; 10. Rotameter; 11. Control panel; 12. Three-way valve.

TABLE 4.1: Key Features of Gas Analyzers.

Gas	Principle	Range	Response Time	Accuracy
O_2	Paramagnetic	0–25% or 0–10%	20 s	1%
CO	NDIR*	0–1000	5 s	1%
CO_2	NDIR	0–20%	5 s	1%
CH_4	NDIR	0–0.2% or 0–0.5%	5 s	1%
SO_2	NDIR	0–1000 ppm, 0–3000 ppm or 0–5000 ppm	5 s	1%
NO	Chemiluminescence	0–250 ppm or 0–500	3 min	1%
NO_2	Chemiluminescence	0–50 ppm or 1–100 ppm	3 min	1%

* Non-dispersive infrared.

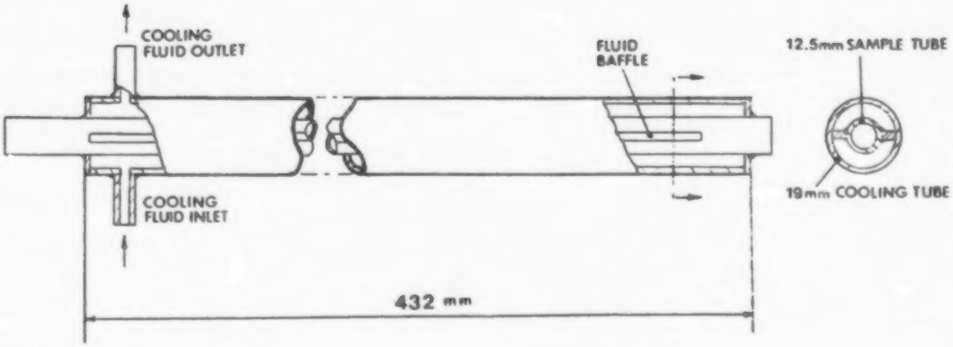
COOLING FLUID OUTLET
FLUID BAFFLE
12.5mm SAMPLE TUBE
COOLING FLUID INLET
19mm COOLING TUBE
432 mm

FIGURE 4.3: Gas probe with outer water-cooling.

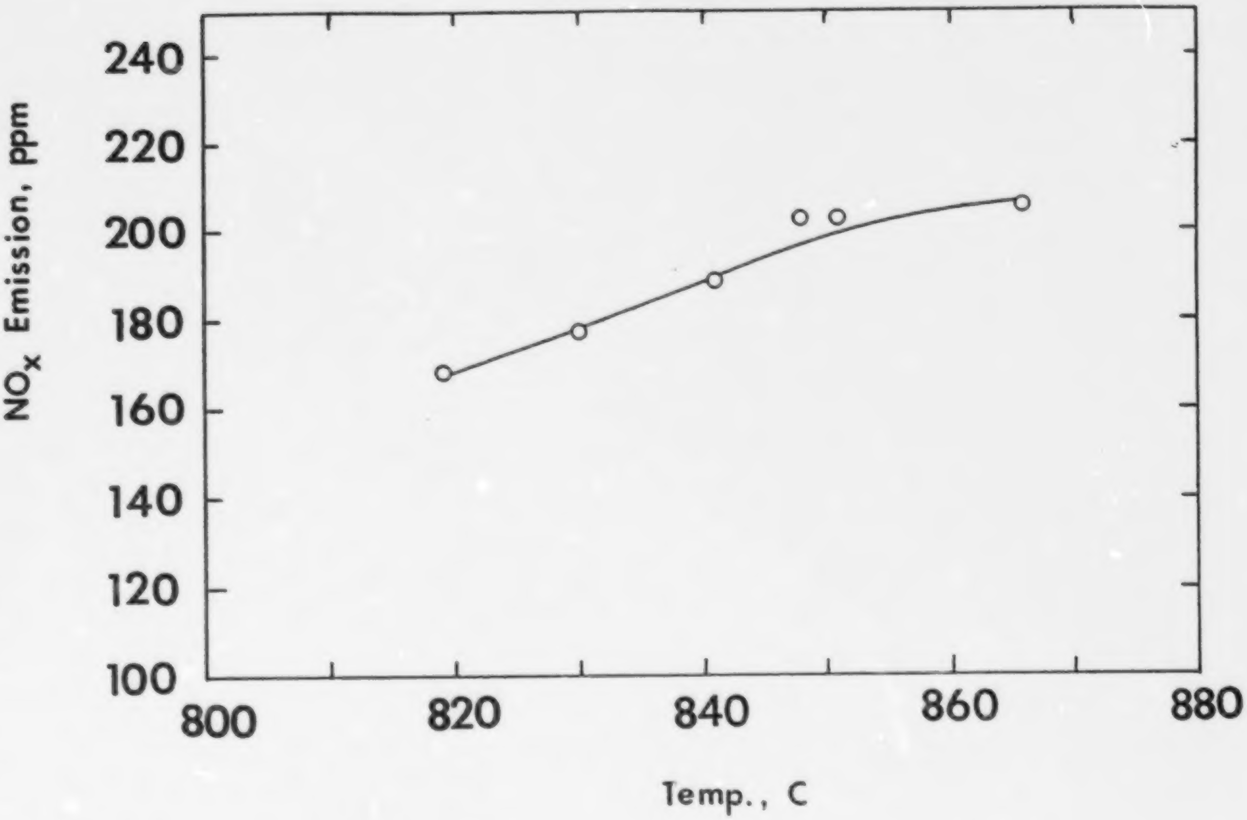

FIGURE 4.4: Temperature effect on NO_x emission for Highvale coal at U=8.4 m/s, Secondary/primary air ratio = 1.0.

4.2 NO_x Emission Results

Flue gas analyses for different combustion trials are given in Chapter 3. This section provides information on the effects of operating conditions on NO_x emissions.

4.2.1 Effect of temperature

Similar to findings in conventional (bubbling) fluidized bed combustion, NO_x emission levels increased with the operating temperature, although the effect appeared to be less strong. Figure 4.4 shows the influence of temperature on the NO_x concentration in the flue gas for Highvale coal. Figure 4.5 gives the variation of temperature and flue gas NO_x after a step decrease in the fuel feed rate during combustion of the lignite. The temperature in the combustor gradually decreased from 850 to 750°C over a period of two hours. It is seen that the

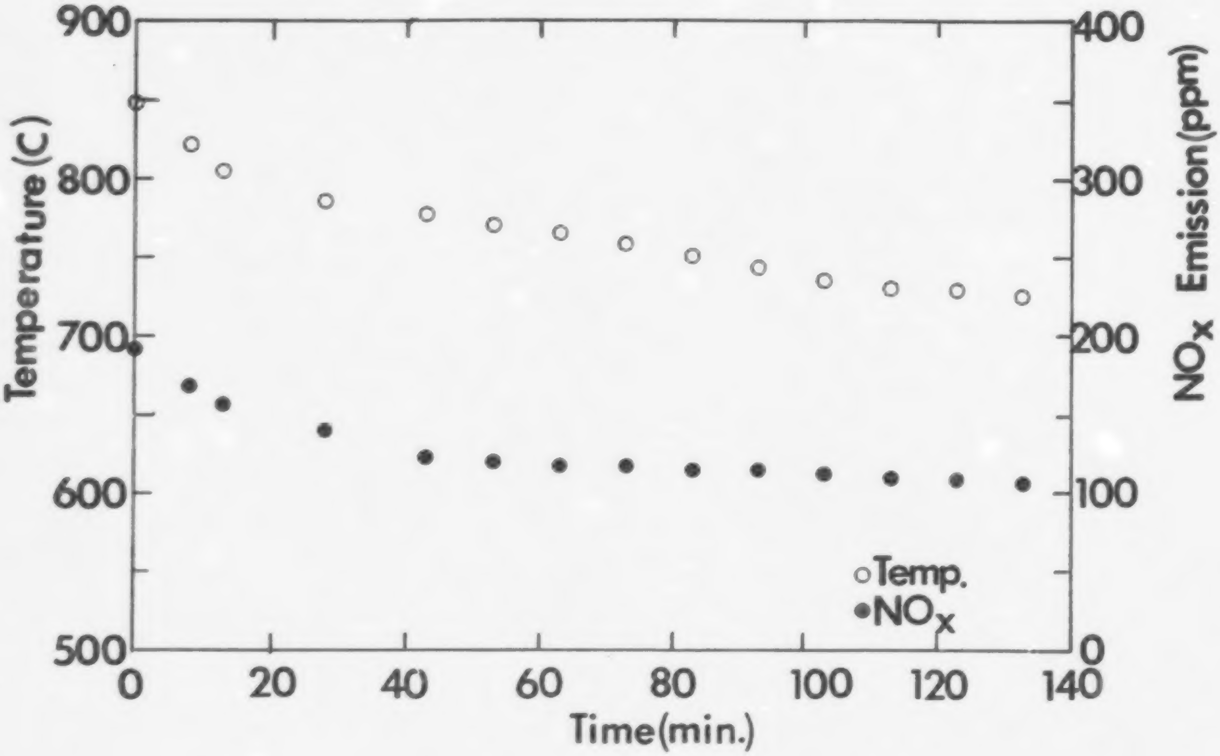

FIGURE 4.5: NO$_x$ emission and bed temperature versus time after step decrease in fuel feed rate: U = 6.0 m/s, oxygen in flue gas = 9.5%, secondary/primary air ratio = 1.6. (Lignite Run #15)

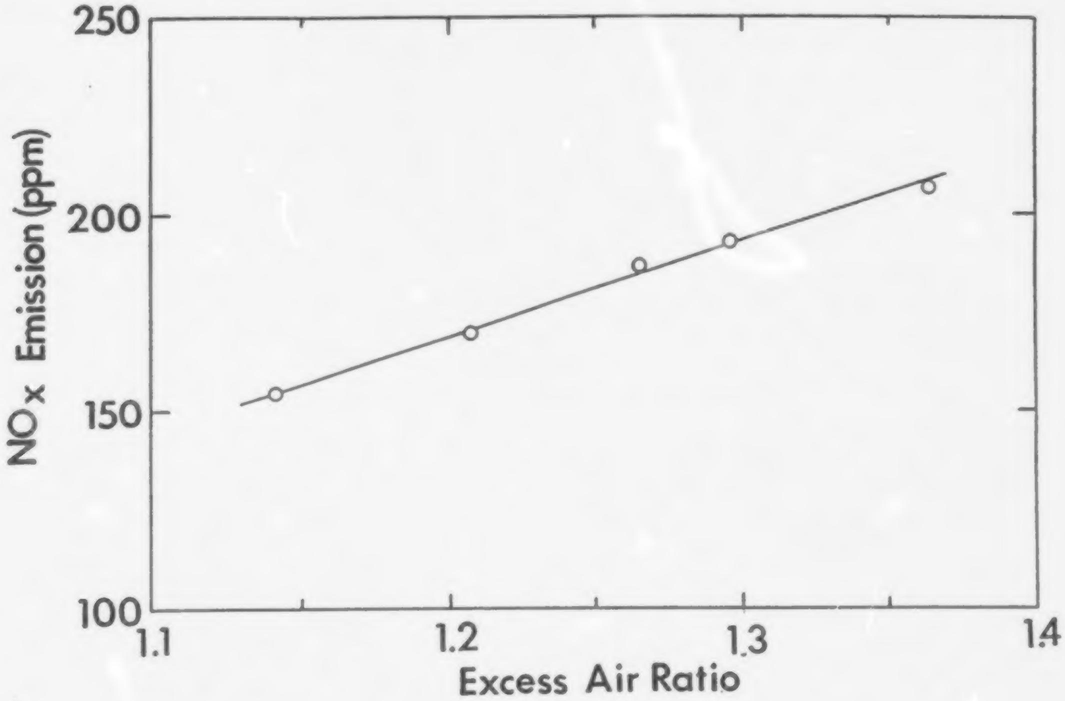

FIGURE 4.6: NO_x emission vs. excess air ratio for Highvale coal: U = 8.0 m/s, T = 870 °C, secondary/primary air ratio = 1.0.

concentration of NO_x in the flue gas decreased from 190 to 105 ppm. Note that the increase of CO level and carbon loading due to the lower temperature probably also contributed to the reduction of NO_x levels.

4.2.2 Effect of excess air ratio

Figure 4.6 shows the relationship between NO_x emission and excess air ratio for the combustion of Highvale coal. The apparent linear increase of NO_x level with excess air shows the importance of limiting excess air to reduce NO_x emissions. This finding is consistent with results from the literature (*e.g.* Hirama *et al.*, 1984).

4.2.3 Effect of staged combustion

There was no clear correlation between NO_x emission and secondary-to-primary air ratio for any of the fuels tested and conditions studied. Table 4.2 gives the NO_x emissions for

TABLE 4.2: NO_x Emissions from Combustion of Anthracite (3% oxygen).

Superficial Gas Velocity (m/s)	Bed Temperature (°C)	Sec./Prim. Air Ratio	NO_x (ppm)
7.7	872	1.0	80
7.8	875	0.5	80
7.9	884	2.0	97
6.0	874	2.0	86
6.2	882	1.0	90

combustion of anthracite with changing secondary-to-primary air ratios. The slight change of NO_x when secondary-to-primary air split is doubled shows that the influence of staged combustion is small for the geometry and conditions studied. In the current tests, secondary air was injected into the reactor only 0.9 m above the primary air (about 13% of the way up the reactor). It may be necessary for the secondary air entry to be much higher to have a noticeable staging effect. This will be investigated in future work. As pointed out by Hirama *et al.*, (1987), staged combustion in CFBC may be less effective than in conventional bubbling bed combustion.

4.2.4 Effect of Ca:S ratio

It was found that limestone addition has a strong impact on NO_x emissions, due to the catalytic effect of CaO. Typical results for Minto coal combustion appear in Table 3.4 (see Section 3.2.2). NO_x emission almost doubled when the molar Ca:S ratio increased from 0 to 3.0 for the conditions described. Similar results were obtained with CANMET pitch and H-Oil pitch.

4.2.5 Fuel character and NO_x emission

Since combustion tests started in 1986, a variety of fuels have been burned at the UBC–CFBC facility. NO_x emission levels have been found to be related not only to the nitrogen content of the fuel, but also to the fuel volatile content, presumably because larger portions of NO_x are formed by oxidation of the nitrogen compound from released volatiles. This is evident from Table 4.3. For example, the lignite, which contains less nitrogen but more volatiles compared to the anthracite, gives higher NO_x emissions. Table 4.3 also shows, despite the enormous differences between fuels, that a simple product, V_N, is strongly correlated to the NO_x emission level under the conditions studied (Zhao *et al.*, 1989). V_N is simply the product of the volatile matter from the primate analysis and the nitrogen content from the ultimate analysis of the same fuel (*i.e.* N% × Volatiles%). As shown in Table 4.3, NO_x emissions

TABLE 4.3: NO_x Emissions and Fuel Nitrogen-Volatiles Products, V_N (T = 820–880°C; Excess air = 10–25%; Secondary-to-primary air ratio = 0.5– 2.0; Superficial gas velocity = 7–10 m/s).

Fuel	N %	Volatile %	V_N	NO_x (ppm)
Hogfuel*	0.10	60.90	6.1	80–110
Anthracite	0.86	6.36	5.5	75–100
Lignite	0.60	35.65	21.4	125–145
Highvale	0.71	31.03	22.0	125–170
Minto	0.95	32.43	30.8	130–140
CANMET Pitch	1.10	67.70	74.5	145–164
H-Oil Pitch	1.00	n/a	n/a	170–180

* from Grace and Lim, 1987
n/a not available

are comparable for fuels with similar V_N (*e.g.* hogfuel and anthracite) and increase with increasing V_N.

4.3 SO_2 Emission and Sulphur Capture

Three of the fuels studied, Minto coal, CANMET pitch and H-Oil pitch had high sulphur contents (6.6, 2.8 and 2.3% respectively). Limestone was added during the combustion tests of these fuels. The sulphur capture results show that after the modifications of the combustion system (see Section 3.2.2) sulphur capture was substantially improved. Ninety-nine percent capture was achieved with a Ca:S molar ratio of 3.0 during the combustion of Minto coal. The sulphur dioxide concentration in the flue gas was about 50 ppm (35 mg/MJ approximately), far lower than the Canada Emission Standard (258 mg/MJ, Clean Air Act, 1981).

The results of sulphur capture for pitch runs are given in Section 3.2.5.

4.4 Gas Concentration Profiles

To assist in understanding the mechanisms of combustion and pollutant formation in CFB and to provide data for mathematical modelling, gas samples were withdrawn at different levels of the riser for some runs. With the system held at steady conditions, samples could be analyzed sequentially. At least three minutes are needed for each sampling at each position due to the length of the sampling lines and the response times of the gas analyzers.

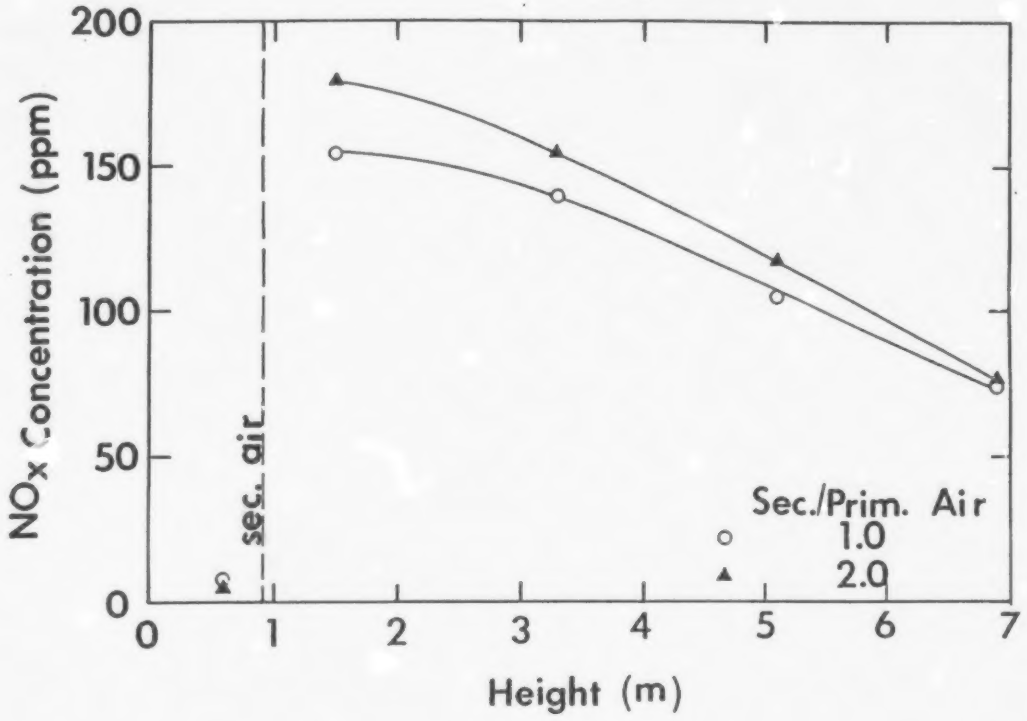

FIGURE 4.7: Axial NO_x concentrations at the wall for two secondary-to-primary air ratios for lignite combustion: U = 8.5 m/s, T = 870°C, oxygen in flue gas = 3.0%.

4.4.1 NO_x concentration profiles at outer wall

As shown in Figure 4.7, trends for axial NO_x profiles with samples taken at the wall were somewhat similar to those in bubbling beds, *e.g.* Beer *et al.*, 1980. At the bottom of the combustor, the NO_x concentration is very low. However, a fast build-up of NO_x was found above the secondary air entry. A maximum concentration occurred just above the secondary air. NO_x levels then decreased continuously over the upper part of the combustor. This pattern can be explained by the release of fuel nitrogen and subsequent reactions which may either enhance or abate the NO_x level. At the bottom, a turbulent dense bed exists. Fuels fed into the combustor need time to devolatize. Because of high superficial gas velocity, typically 4–5 m/s below and 8–10 m/s above the secondary air injection port, the volatiles are released at greater heights. Also, due to the reducing conditions at the bottom of the riser, there is limited oxygen for NO_x to form. The catalytic effect of limestone under reducing conditions tends to further suppress NO_x formation (Leckner and Amand, 1987). After a maximum NO_x is reached, reduction of NO_x by char causes the NO_x concentration to decrease substantially

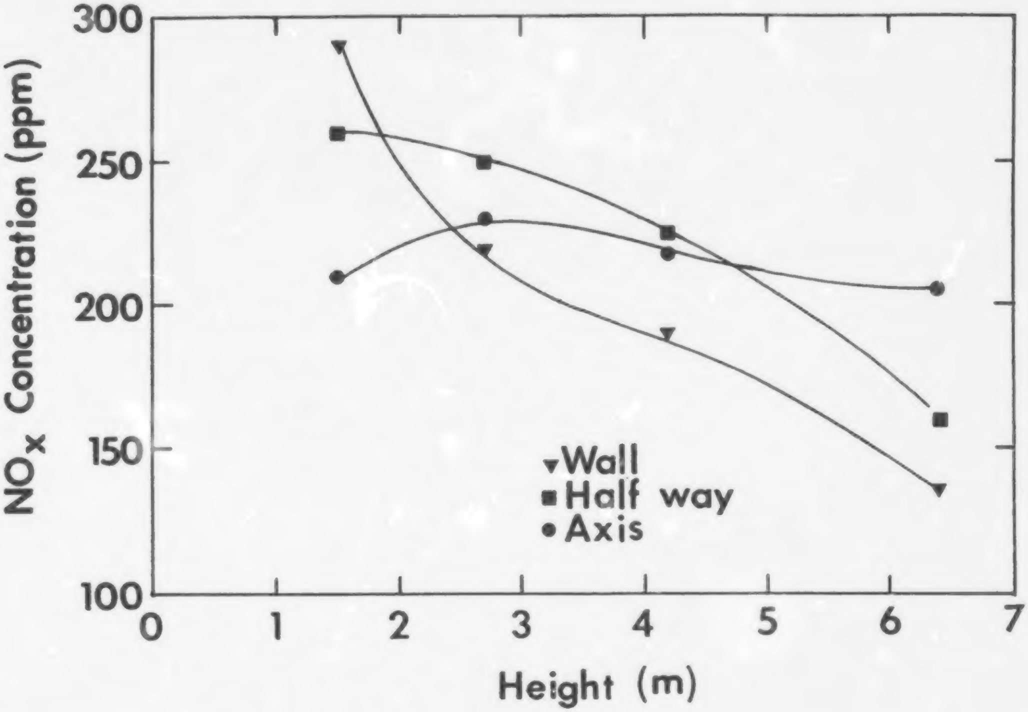

FIGURE 4.8: NO_x concentration profiles for Minto coal combustion: U = 7.6 m/s, T = 890°C, secondary to primary air ratio = 1.07, Ca/S = 3.0, oxygen in flue gas = 3.0%.

in the upper region. Increasing the secondary-to-primary air ratio led to higher NO_x levels above the secondary air entry point. However, NO_x levels converged (see Figure 4.7) and were essentially identical by the top of the column.

4.4.2 Profiles at other radial positions

Because of different hydrodynamics between bubbling and circulating fluidized beds, the spatial concentration distribution of gas components may be very different. The annulus-core flow pattern in circulating fluidized beds may be expected to cause radial gradients. Preliminary results from a combustion test of Minto coal, in which NO_x concentrations at three radial positions were measured, are shown in Figure 4.8. The concentration of NO_x was found to be almost uniform in the centre of the column. It is clear that the local suspension density (which determines carbon loading) strongly affects the profiles of NO_x and other gaseous components. With high suspension density near the wall, more carbon is available to react with NO_x, and there are less oxygen and more reducing species (C, CO, and CH_4) present. On the other hand, the reduction of NO_x was less effective in the dilute core of the combustor causing its concentration to drop much more slowly there.

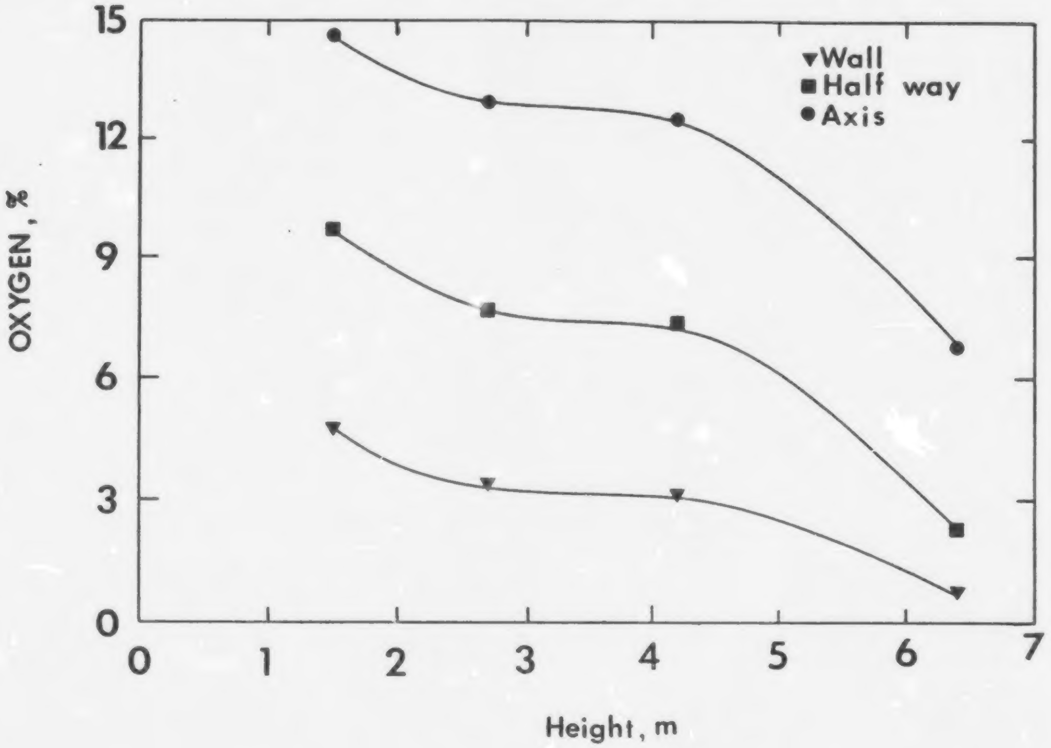

FIGURE 4.9: Oxygen concentration profiles for Minto coal combustion: U = 7.6 m/s, T = 890°C, secondary to primary air ratio = 1.07, Ca/S = 3.0, oxygen in flue gas = 3.0%.

4.4.3 Other gas concentration profiles

Typical oxygen concentration profiles at three radial positions are plotted in Figure 4.9. The low oxygen concentration near the wall is presumably due to the reaction of carbon in the solid layer moving along the wall. Relatively high CO concentrations near the wall (2000–4000 ppm compared to 50 ppm in the flue gas, as shown in Figure 4.10, are consistent with the reduced oxygen levels. It is interesting to note that the axial CO concentration profile, high at the bottom and again at the top (Figure 4.10), is similar to the suspension density profiles (see Section 5.1). The suspension density distribution clearly plays an important role in CFB combustion. A typical axial SO_2 concentration profile near the wall is shown in Figure 4.11. This shows that most sulphur capture occurs in the dense bed at the bottom, with the SO_2 concentration then remaining low throughout the rest of the reactor.

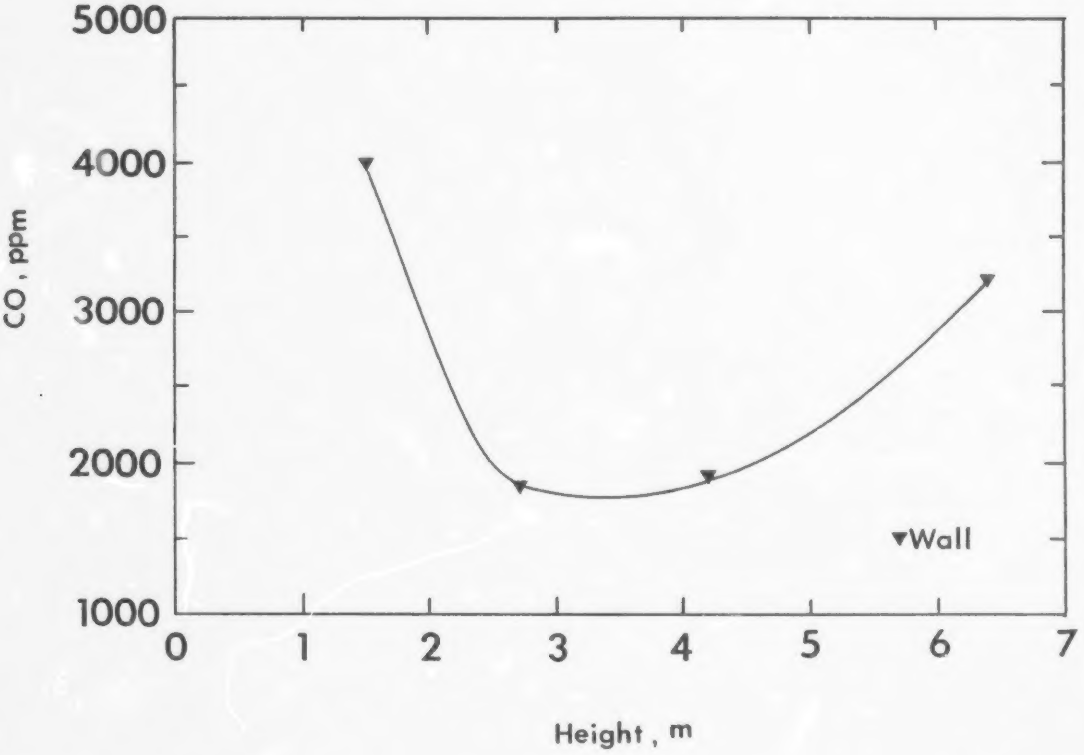

FIGURE 4.10: CO concentration profiles for Minto coal combustion: U = 7.6 m/s, T = 890°C, secondary to primary air ratio = 1.07, Ca/S = 3.0, oxygen in flue gas = 3.0%.

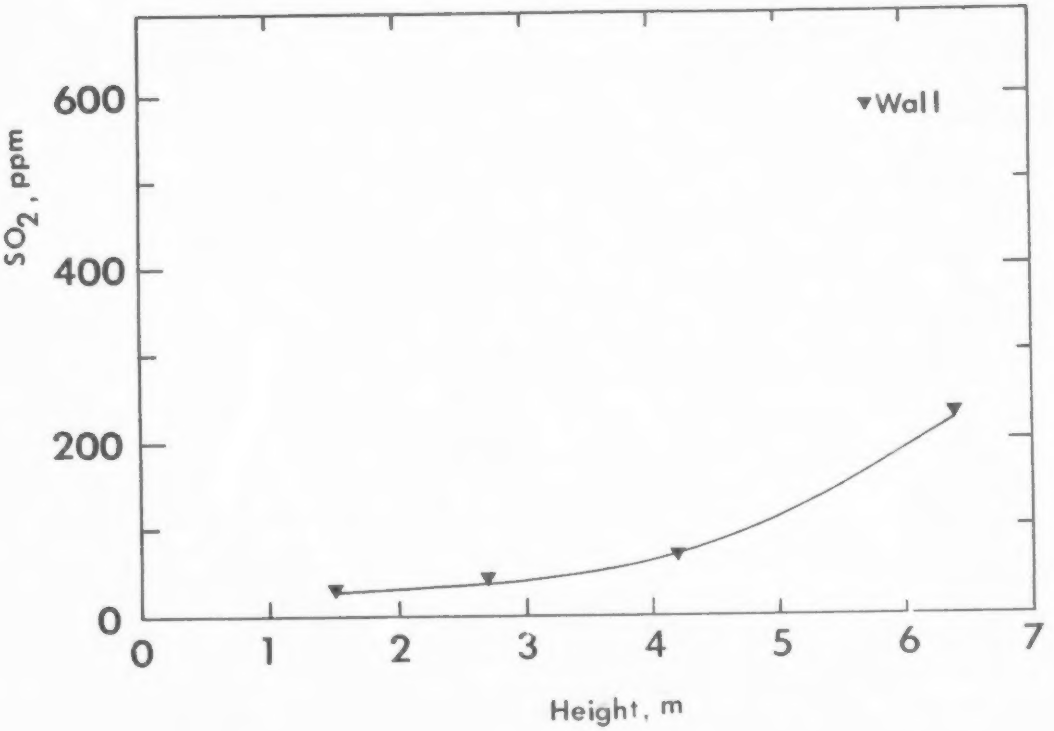

FIGURE 4.11: SO_2 concentration profiles for Minto coal combustion: U = 7.6 m/s, T = 890°C, secondary to primary air ratio = 1.07, Ca/S = 3.0, oxygen in flue gas = 3.0%.

Chapter 5

HYDRODYNAMIC STUDIES IN THE CFBC PILOT PLANT

5.1 Suspension Density Profiles in the Riser

The macrostructure of circulating fluidized beds is generally characterized by the variation of suspended solid density with height in the riser section. This density profile is an important feature from which one can determine the degree of gas/solids contacting within the riser. The suspension density profile is also very useful to infer hydrodynamic similarities for circulating fluidized beds of different sizes, which is important for scale-up work.

The suspension density profiles for the UBC pilot plant were obtained by direct measurements of differential pressures over seven intervals along the reactor shaft. The output from fast response pressure transducers was averaged for every 10 second interval. This practice eliminated the pressure fluctuations and gave very stable differential pressure data. However, during most of the combustor trials described in Chapter 3, it was difficult to obtain reliable pressure profiles in the reactor due to blocked pressure taps. Several improvements were therefore made to the pressure measurement system, such as the addition of controlled amounts of air purge to each pressure tap to keep solids from obstructing them, before valid density profile data could be recorded.

The CFBC pilot plant was specifically operated for the sole purpose of obtaining hydrodynamic results in Run #21. Highvale coal was used as fuel. The superficial velocity was varied in the range 5.7 to 10.5 m/s, secondary to primary air ratio between 0.70 and 1.00 and solids circulation flux from 19 up to 100+ kg/m^{2}s. The properties of the silica sand used as start-up bed materials are given in Table 2.4. The particle size distribution of the bed material collected at the end of the run is given in Table 5.1.

The axial density profiles obtained during Run #21 are shown in Figure 5.1. These show similar behaviour over the entire range of superficial velocity and solids circulation flux studied. The density first decreases rapidly over the lower part of the riser, then approaches a flat profile and finally increases again at the top. This behaviour is essentially identical to what has been observed in a cold CFB model (Brereton, 1987). The rise in density at the riser exit is due to the geometry of the outlet section. It is hoped to carry out further hydrodynamic tests with a smooth exit section to investigate the effect of the top geometry.

TABLE 5.1: Particle Size Distribution of Bed Materials at the End of the Hydrodynamic Run (Run #21).

Size Range (μm)	Weight Fraction (%)
5600 +	0
5600–4000	0.12
4000–2800	0.36
2800–2000	0.38
2000–1400	0.64
1400–1000	0.94
1000–710	1.22
710–500	1.15
500–355	3.18
355–250	25.12
250–180	44.96
180–125	14.56
125–90	4.07
90–53	1.44
53–45	0.37
45–0	1.49
Mean Particle Size (μm)	201

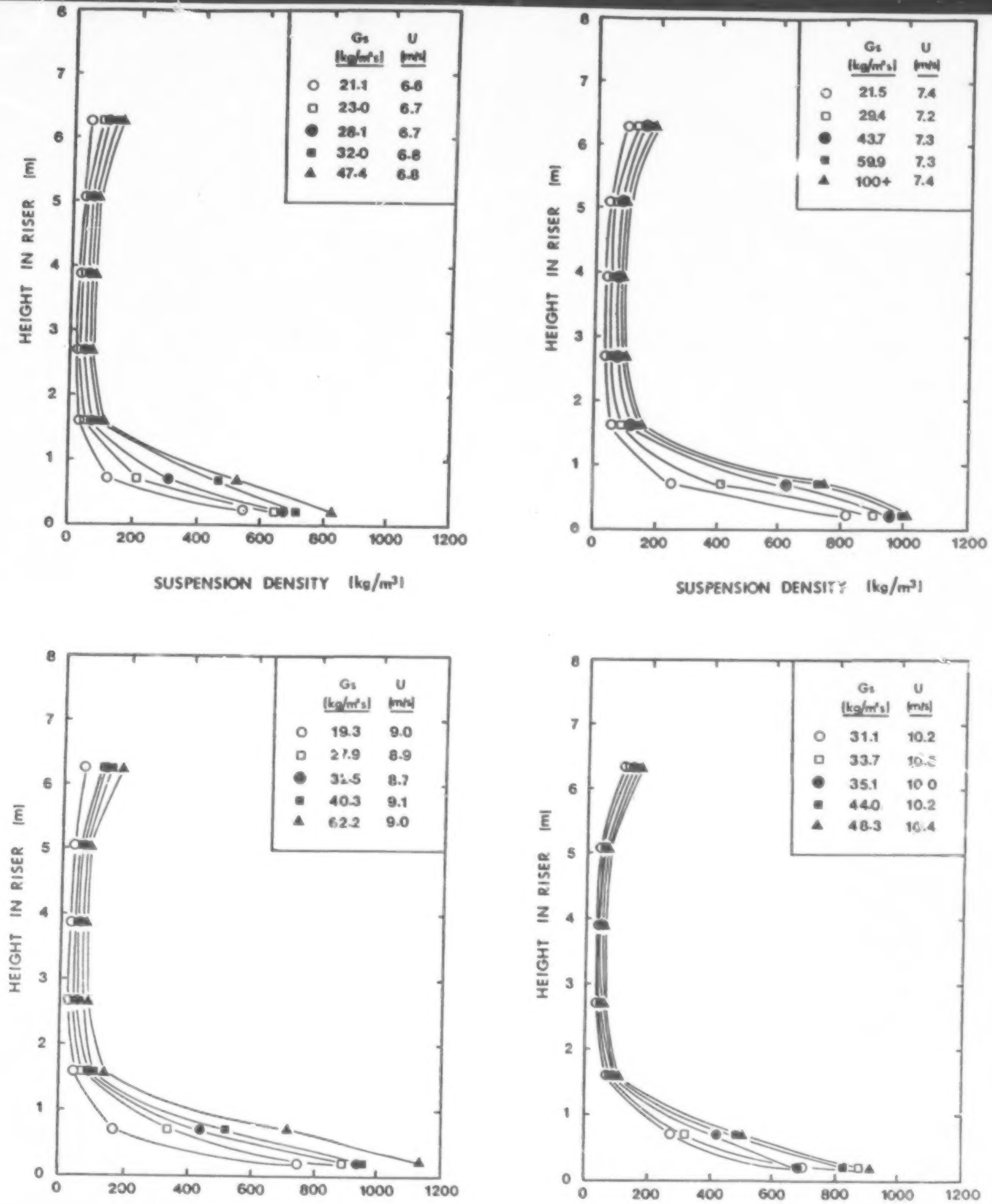

FIGURE 5.1: Axial density profiles. Silica sand particles and Highvale coal; temperature = 838–876°C; secondary to primary air ratio = 0.8–1.0.

5.2 Capacitance Probe Study

In order to fully understand the hydrodynamics of high velocity fluidized beds it is necessary to obtain hydrodynamic information more extensive than traditional plots of solids density versus height. The latter do not, for example, provide insight into whether solids are evenly distributed over a horizontal combustor cross section, or whether there is a substantial concentration of solids in the wall region. This information is required in order to understand heat transfer in circulating bed systems, and, pollutant formation in solids rich reducing zones.

One device that has been developed to give insight into solids distributions within gas-solids reactors is the capacitance probe. It has been used for detailed hydrodynamic studies in low temperature CFB systems (Brereton, 1987), but has yet to be applied in high temperature CFB reactors. One object of this study was to develop a high temperature capacitance probe suitable for use in a CFB combustor.

A capacitance probe, properly calibrated, is capable of measuring fluctuations in local solids loading with frequencies in the kHz range. The instantaneous loading itself may be resolved to an accuracy of approximately 10 kg/m^3 (Brereton, 1987). Hence, it can be used for two purposes:

1. To determine time average point densities by averaging the probe signal over a long time period.
2. To infer something of the nature of the local flow structure, (uniform or irregular), by analyzing the time variation of local density.

The probe functions by measuring the dielectric constant in a small control volume somewhere in the reactor. The dielectric constant is inferred from the capacitance of some appropriately shaped capacitor in which the measurement volume is the dielectric. Since the dielectric constant is a strong function of the solids loading it can be used to infer this parameter. Fast response can be obtained because capacitance may be determined very rapidly via electronic measurement.

The probe developed for this high temperature study is a so-called needle type. It is shown in Figure 5.2. The capacitance between a protruding "live" needle and a grounded "sheath", a control volume of approximately 1cm^3, is measured by commercially available capacitance measurement instrumentation sold to support fast response capacitative pressure transducers. The instrumentation is identical to that used by Brereton (1987).

The capacitance probe for use at high temperature must be structurally sound at the temperatures in question. This can be achieved either by building cooling into the design, or by using materials with suitable strength to withstand repeated solids impact at elevated temperature. In this case no cooling was used because, to introduce a cooled probe would have produced a unit so bulky that it would interfere with flow patterns within the reactor. A hot probe, however, has its own problems. In particular, dielectrics must be chosen to insulate the needle from the sheath which do not become too conductive at the high temperatures and high oscillating frequencies employed. Several probes were rejected because they

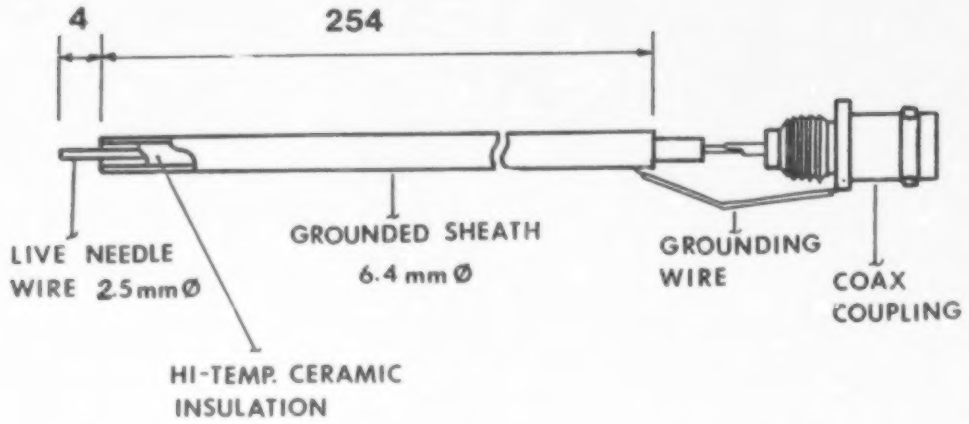

FIGURE 5.2: Capacitance probe used for high temperature work. All dimensions in mm.

"shorted out" due to ceramic dielectrics becoming too conductive in the 550–600°C range. Changing to a different dielectric used in high temperature thermocouples alleviated this problem and produced a satisfactory probe.

The study to date has produced a workable design which has given readings of density versus time in a 900°C circulating bed combustor. A typical result is shown in Figure 5.3 which illustrates a time trace of density half way up the combustor at a location immediately adjacent to the wall. The trace is similar to that seen in a room temperature unit showing a wall layer with higher density than an upflowing central core. The wall layer alternates in character between solids-rich and solids-lean regions. This confirms the basis of our modelling efforts.

Measurements were also obtained at other radial positions but are not included here due to drift. Ongoing work will focus on continued probe development and upon mapping the combustor in detail to elucidate the flow structures and validate the hydrodynamic models.

5.3 Erosion Probe Results

Fresh stainless steel tubes of 9.5mm O.D. were inserted horizontally at several axial locations into the combustor prior to two pitch (H-Oil) runs and one Highvale coal run. The purpose of these tubes or probes was to provide an indication of the extent of the regions in which

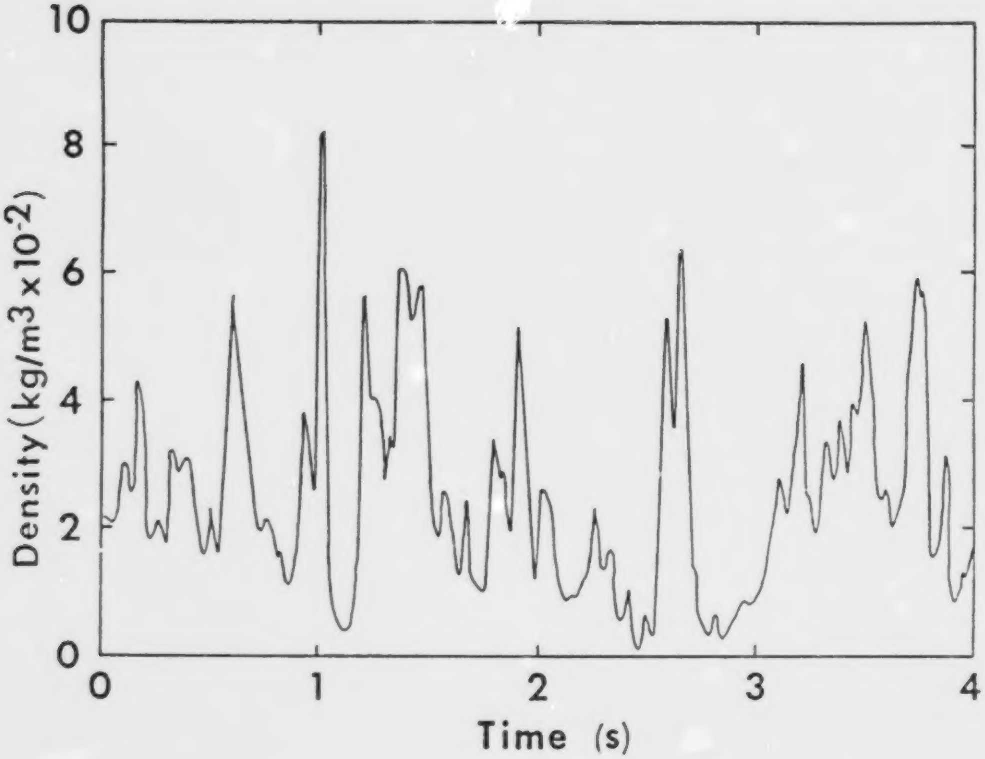

FIGURE 5.3: Time trace of density measured at the wall of the reactor, (Height = 4.1 m above primary air distribution) from capacitance probe. (Temperature = 860°C; superficial velocity = 7.5 m/s; secondary to primary air ratio = 1.0).

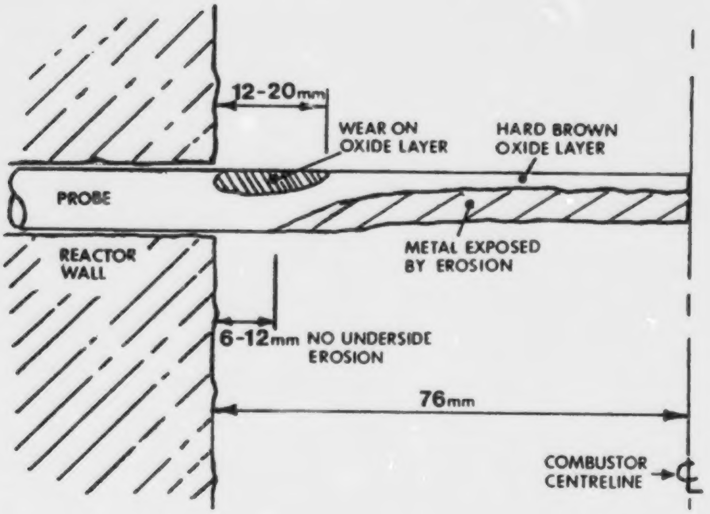

FIGURE 5.4: Typical erosion patterns observed after 24 hour exposure (Highvale coal, Temperature = 840–890°C; G_s = 60 kg/m^{2}s; 304 stainless steel).

the solids flow downwards adjacent to the wall and in which solids flow is predominantly upwards. The combustor was operated at nominal conditions of temperature 870°C, solids circulation 60 kg/m^{2}s and 16% excess air. Both 304 and 316 stainless steels were tested. The coal run and one pitch run lasted approximately one day while the duration of the other pitch run was approximately two days. After exposure to the combustor, the tubes were removed and examined.

The lower surfaces of the probes in the core of the combustor showed very heavy pitted erosion due to rapid upflow of particles. The probe wall thickness (2mm) was frequently fully eroded near the combustor centre. On the upper surface of the probe a dark brown hard oxide layer formed with little erosion evident, except sometimes near the wall. Near the combustor wall, the oxide layer was often tinged with the colour of other compounds. For high sulphur pitch runs, the interface between dark brown oxide layer and metal exposed by erosion was often tinged a mustard yellow. The whole oxide layer in the wall region often had a dark red colour after exposure to combustion of Highvale coal. The observed trends appeared to be independent of steel type.

Wear patterns of the oxide layer, presumably due to a downward flux of particles, were often observed on the upper region of the probes near the combustor wall. These patterns usually extended between 10 and 20 mm from the wall. The erosion of the probe underside usually extended to within 6 to 12 mm of the wall (Figure 5.4). Hence, there was a small region at the boundary between the outer annular region and the inner core, where solids

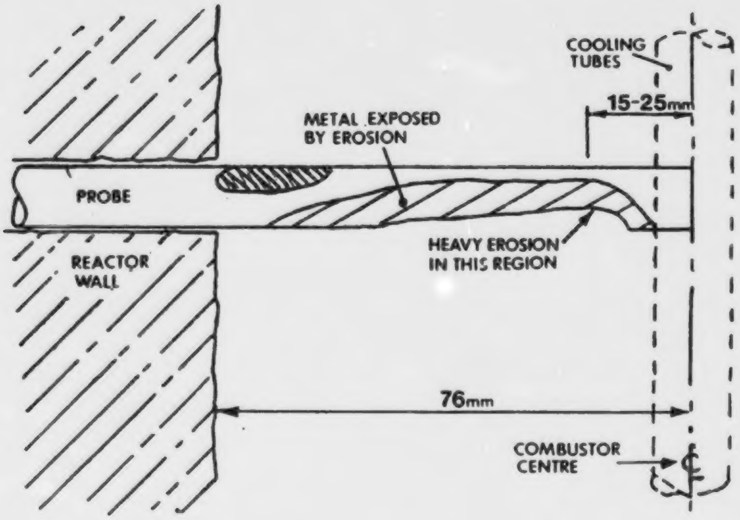

FIGURE 5.5: Erosion in the cooling tube region of the combustor after 24 hour exposure (Highvale coal; Temperature = 840–890°C; $G_s = 60$ kg/m^{2}s; 304 stainless steel).

could move alternatively upwards and downwards.

For all three runs, in-bed vertical cooling tubes were used for heat removal. The tubes, located at the centre of the bed between a vertical height of 4.6 and 5.7 m, diverted the upwardly moving solids into regions offset from the combustor centreline by 15 to 25 mm (Figure 5.5). Extremely high tube underside erosion was observed in these regions, probably due to increased gas (and hence solids) velocities associated with the reduction in cross-sectional area.

Most probes inserted in the combustor for the two day run were severely eroded, and bent upwards. They were generally too badly damaged to deduce erosion patterns. In contrast, erosion patterns were observable on most of the probes resident in the combustor for one day. Normally, due to wall roughness and chipped refractory at the probe ports, the exact location of the wall was not discernable to any greater accuracy than ±4 mm.

Combined capacitance probe and erosion probe work under controlled hydrodynamic conditions is planned to confirm the current interpretations of the probe erosion data. Use of alternative probe materials which could give increased erosion rates to allow data to be obtained more quickly is also being investigated.

Chapter 6

SOLID RESIDUES FROM HIGH SULPHUR COAL

6.1 Background

One of the principal advantages of CFBC is the ability to capture sulphur in situ using limestone as a sorbent. The limestone is first calcined:

$$CaCO_3 \rightarrow CaO + CO_2 \tag{6.1}$$

The sulphur capture reaction is usually written in summary form as

$$CaO + SO_2 + \frac{1}{2}O_2 \rightarrow CaSO_4 \tag{6.2}$$

with most of the captured sulphur appearing as anhydrous calcium sulphate in the solid residue. However, there have also been reports (Dearborn, 1986; Anthony, 1986) of significant quantities of calcium sulphide. Since the solid wastes are intended for disposal to landfill sites, the presence of significant quantities of sulphide would represent a considerable problem for CFBC technology. Accordingly, tests were carried out on solid residues from two tests where a high sulphur fuel (Minto coal) was burned in conjunction with different limestones.

6.2 Test Procedures

Characterization tests were carried out by Ortech International Consultants on solid samples withdrawn at seven different positions (see Section 2.6), two (#'s 1 and 2) corresponding to the bottom of and top of the reactor, three (#'s 3–5) to the primary cyclone recirculation loop, one(#6) to the return from the secondary cyclone and the final one (#7) to the baghouse. Except for the baghouse samples, the solid samples were withdrawn under nitrogen purge conditions to prevent reactions which could occur if hot solids were allowed to cool in an oxidizing environment outside the reactor system. In practice, baghouse samples would sit for some time exposed to the flue gas at reduced temperatures. In our system, the baghouse was emptied approximately every 90 minutes. The sampling procedure adopted should therefore give information on the local in situ solids composition at each of the several positions during operation. Since the solids samples analyzed were only collected after three "bed turnovers" and with conditions in the reaction system held as steady as possible, the results should provide a good indication of steady state solids compositions.

The sampling ports and respective operating procedures are presented in Figures 2.12 and 2.13. The slot (in the sample device for position #2 (see Figure 2.12) was oriented downwards during sampling to collect the upflowing solids. A longer period, typically 1–2 min, was required to collect about 0.2 kg via this sampling device at the top of the reactor.

Once the sealed samples had been shipped to the Ortech Laboratories in Sheridan Park, Ontario, samples from position #'s 1 to 6 (see Figure 2.11) were individually blended, riffled and subsampled under dry nitrogen in a glove bag. Baghouse samples (position #7 in Figure 2.11) were handled in the laboratory atmosphere. Bed drain samples (position #1 in Figure 2.11) were separated manually into groups based on visual appearance under a low-power optical microscope. Baghouse samples were separated by flotation into two density fractions using a bromoform-ethanol solution of specific gravity 2.2 as the flotation medium.

Chemical analysis of the various samples was performed using ICP (inductively coupled plasma) spectrometry. Sulphides were determined by a method (AOAC, 1980) originally used for blast furnace slags. Phase compositions were analyzed using X-ray diffraction (XRD) and thermal analysis (TGA/DTG), while SEM/EDXA methods were employed to investigate the morphology and approximate elemental composition of representative individual particles.

6.3 Experimental Results

Key features of the two experimental tests are given in Table 6.1. Note that the operating conditions of the two runs were similar with the following exceptions:

(a) The limestones were different, a 76% Texlime/24% Elmtree blend in Run #3, and a Havelock limestone in the later run. As shown in Table 2.5, the chemical analyses of the various limestones were quite similar, whereas from Table 2.4 it is clear that the Havelock limestone was significantly coarser than the other two limestones.

(b) Steady conditions were maintained through the entire run in the earlier test, whereas there were some changes in operating conditions in the later run.

(c) At the end of Run #3, after the reactor had cooled down, it was discovered that there was a blockage in the line returning solids captured in the secondary cyclone. It was not clear whether this problem developed early or late in the run, but it is most likely that the blockage affected the operation over a considerable period of time. In the later run, after some modifications in the equipment and in diagnostics, we are certain that continuous return was maintained from the secondary (as well as the primary) cyclone throughout the entire run. As discussed below, continuous return of the solids from the secondary cyclone appears to have made a significant improvement in the sulphide levels in the waste solids.

Chemical analyses of each of the seven samples for both runs are given in Table 6.2. From the elevated MgO concentrations, it is clear that there were significant amounts of

TABLE 6.1: Key Details of Runs Where Solids Characterization was Carried Out. Further details are given in Table 3.3.

Run #	3	16
Date	March 5–7, 1988	Dec. 9–11, 1988
Fuel	Minto Coal	Minto Coal
Sorbent	76% Texlime 24% Elmtree Limestone	Havelock Limestone
Sup. Velocity, m/s	8.4	7.7–8.8
Secondary/Primary Air	1.2	0.96–1.9
Coal Feed, kg/h	21	18–20
Ca:S	3.0	1.8, 3.0
Temperature at Bottom, °C	875	872–904
Temperature in L-valve, °C	882	860–892
O_2 in Flue Gas, %	2.6	3.1–4.2
S-capture, %	89	86–99
Combustion Efficiency, %	93	94–97
Secondary Cyclone Return	blocked	functioning

the original olivine sand in the samples withdrawn from positions 1 to 5 (Figure 2.11), with small amounts in the finer solids captured in the secondary cyclone (position 6) and baghouse (position 7). There is relatively little variation between positions 1 to 5, indicating that the solids in the main reactor loop are well mixed. However, positions 6 and 7 show much more marked variations, especially for Run #3. In particular, the "downstream solids" (positions 6 and 7) tend to show significantly and consistently higher levels of loss on ignition, carbon and sulphide.

It is also clear that there were significant differences between Run #3 and Run #16 in the degree of variation between positions 1–5 and positions 6 and 7. In particular, the earlier run shows a marked increase in Ca, total S, carbon and sulphide in the secondary cyclone and baghouse solids, whereas these changes were considerably reduced for Run #16. While it is possible that these changes were partially due to the different sorbent employed or to changes in operating conditions, it is much more likely that blockage of the secondary cyclone was a key factor for Run #3. Continuous return of solids captured in the secondary cyclone in Run #16 led to improved carbon burnout and sulphur capture; the decrease in carbon in turn probably contributed to the strong drop in the level of sulphide in the solids from both position 6 (secondary cyclone: from 2.6 to 0.44%) and position 7 (baghouse: from 2.3 to 0.30%). It would appear that having good cyclone capture and solids return is critical, not only to obtaining favourable combustion efficiency and sulphur capture, but also to reducing the presence of sulphides in the solid residues. Differences between the results of Run #3 and results obtained in the 22MWe demonstration plant at Chatham have been interpreted (Anthony *et al.*, 1989) as indicating major differences between large and small CFBC units. It is clear that the Run #16 results are much closer to those obtained at Chatham, and this may

TABLE 6.2: Chemical Analyses (% by mass) of Solid Samples.

Species	Pos. 1	Pos. 2	Pos. 3	Pos. 4	Pos. 5	Pos. 6	Pos. 7
Run #3							
SiO_2	28.99	29.50	26.40	28.10	29.99	12.99	10.89
Al_2O_3	5.19	5.20	4.81	4.79	4.29	3.12	3.66
Fe_2O_3	9.58	9.20	9.05	9.21	9.18	8.48	10.56
CaO	27.78	27.95	28.07	29.07	26.16	48.97	50.09
MgO	14.76	15.60	13.88	15.08	19.97	3.80	0.71
Ma_2O	0.27	0.21	0.20	0.21	0.20	0.19	0.18
K_2O	0.43	0.14	0.15	< 0.10	0.10	< 0.10	< 0.10
LOI	0.15	0.41	-0.15	0.23	-0.19	7.52	7.99
Carbon	0.83	1.13	0.71	1.64	0.64	9.23	10.00
Sulphur	6.15	6.19	6.41	6.38	5.49	8.27	8.82
Sulphide	0.50	0.50	0.60	0.50	0.50	2.60	2.30
Run #16							
SiO_2	21.35	20.02	24.14	21.01	20.33	15.48	17.02
Al_2O_3	3.49	3.22	2.70	3.43	3.01	4.41	7.01
Fe_2O_3	6.94	6.84	7.94	7.22	6.42	12.00	21.96
CaO	31.68	32.91	28.56	31.83	32.39	39.36	25.97
MgO	13.62	13.74	18.47	13.67	14.02	1.22	0.48
Na_2O	0.17	0.12	0.13	0.13	0.12	0.14	0.18
K_2O	< 0.10	< 0.10	< 0.10	< 0.10	< 0.10	< 0.10	0.48
LOI	1.30	1.38	1.43	1.50	1.39	2.16	7.28
Carbon	0.20	0.38	0.14	0.49	0.35	1.48	5.32
Sulphur	8.03	8.77	7.36	8.11	8.64	9.64	8.11
Sulphide	0.30	0.27	0.20	0.23	0.20	0.44	0.30

well indicate that in order for pilot plant units to simulate large units, with their considerably greater heights and residence times, scrupulous attention is required to ensure that excellent solids capture and return are maintained. In other words, the large units are likely to be more forgiving given the longer time to burn out carbon in a single pass, whereas small units require more efficient solids recirculation to ensure carbon conversion. The conversion of the reducing carbon species simultaneously decreases the reduction of sulphate to sulphide by reactions such as

$$CaSO_4 + 4C \rightarrow CaS + 4CO$$

$$CaSO_4 + 2C \rightarrow CaS + 2CO_2$$

or

$$CaSO_4 + 4CO \rightarrow CaS + 4CO_2$$

Since solid-solid reactions tend to be slow, reduction of $CaSO_4$ by gaseous species like CO, generated by oxidation of unburnt carbon, appears to be the most likely route for sulphide generation.

Other measured characteristics of the solid residues and speculation regarding reactions which lead to CaS formation are provided by Berry *et al.* (1989a, 1989b) and in Appendix C of this report. Some of the conclusions are as follows:

(a) There was no evidence of significant quantities of sulphides other than CaS.

(b) Solid residues are complex, showing the presence of olivine sand, calcined and sulphated lime, uncombusted coal, and inorganic material including ash derived from the combusted portion of the coal or imbedded with the coal. Bed drain material can, for example, be visually separated into four distinguishable types of particles, which show clear chemical differences.

(c) The baghouse catch material can be separated by gravity separation into fractions that correspond largely to carbon (S.G. < 2.2) and inorganic materials (S.G. > 2.2) (principally spent and partially sulphated limestone).

(d) The precise reactions by which sulphides are formed are not clear, but secondary reactions appear to be likely. The baghouse is probably at a temperature too low for significant reaction to occur there. The presence of CaS appears to be closely associated with the availability of carbon. It appears that CaS formation is not favoured if the local carbon:sulphur molar ratio remains below about 2.

While the Minto runs have been helpful in delineating some of the factors which affect solids properties, it is clear that more work is required on the chemistry of the various reactions and on optimum conditions for preventing CaS formation.

Chapter 7

HEAT TRANSFER STUDIES

7.1 Membrane Wall

All heat transfer data were obtained by using a single 1.59 m long by 148 mm wide water-cooled membrane wall as the heat transfer surface, beginning 4.27 m above the distributor on one wall of the column. This surface consisted of four identical, half-embedded, vertical, schedule-80 stainless steel tubes connected longitudinally by flat fins to form a membrane wall (see Figure 2.7). The fins were flush with the refractory surface above and below. One of the central tubes was instrumented with ten thermocouples approximately 150 mm apart. Both the temperature profile and flow rate of the water inside the tube were recorded.

Although the predominant heat transfer resistance for the present conditions is on the circulating bed side of the heat transfer surface, results reported here are suspension-to-exposed surface values, where the water-side resistance estimated from Sleicher and Louse (1975) and the tube resistance have been subtracted. Heat transfer coefficients are based on the total exposed areas of the tubes and the fins.

Highvale coal was used as the fuel in the membrane wall experiments. In all the experiments, Olivine sand was used as the inert bed materials. Relevant physical properties of the sand and coal are given in Chapter 2. Detailed particle size analyses for the runs are given in Table 7.1.

7.2 Results

The variations of average overall heat transfer coefficient with local suspension density are shown in Figure 7.1 for three suspension temperatures. In all cases, the average coefficient increases linearly with suspension density. The lines shown are least squares best fit lines. The similarity in the slopes for the three lines suggests that radiation is relatively independent of suspension density.

Figure 7.1 is cross-plotted in Figure 7.2 to show the variation of the overall time-mean heat transfer coefficient with suspension temperature at four different suspension density levels. It can be seen from Figure 7.2 that radiation starts to become a significant factor beyond a suspension temperature of about 400°C.

TABLE 7.1: Particle Size Analyses of Bed Materials for the Heat Transfer Runs (Run #6)

Size Range (μm)	C1 (wt. %)	C2 (wt. %)
1410+	0.0	0.0
1410 - 1000	0.0	0.0
1000 - 707	0.2	0.0
707 - 500	0.3	0.0
500 - 354	2.6	5.8
354 - 250	38.0	48.6
250 - 177	45.6	36.1
177 - 125	10.1	6.6
125 - 88	1.9	1.7
88 - 53	0.8	1.2
53 - 44	0.1	0.0
44 - 0	0.4	0.0
Mean Particle Size (μm)	216	238

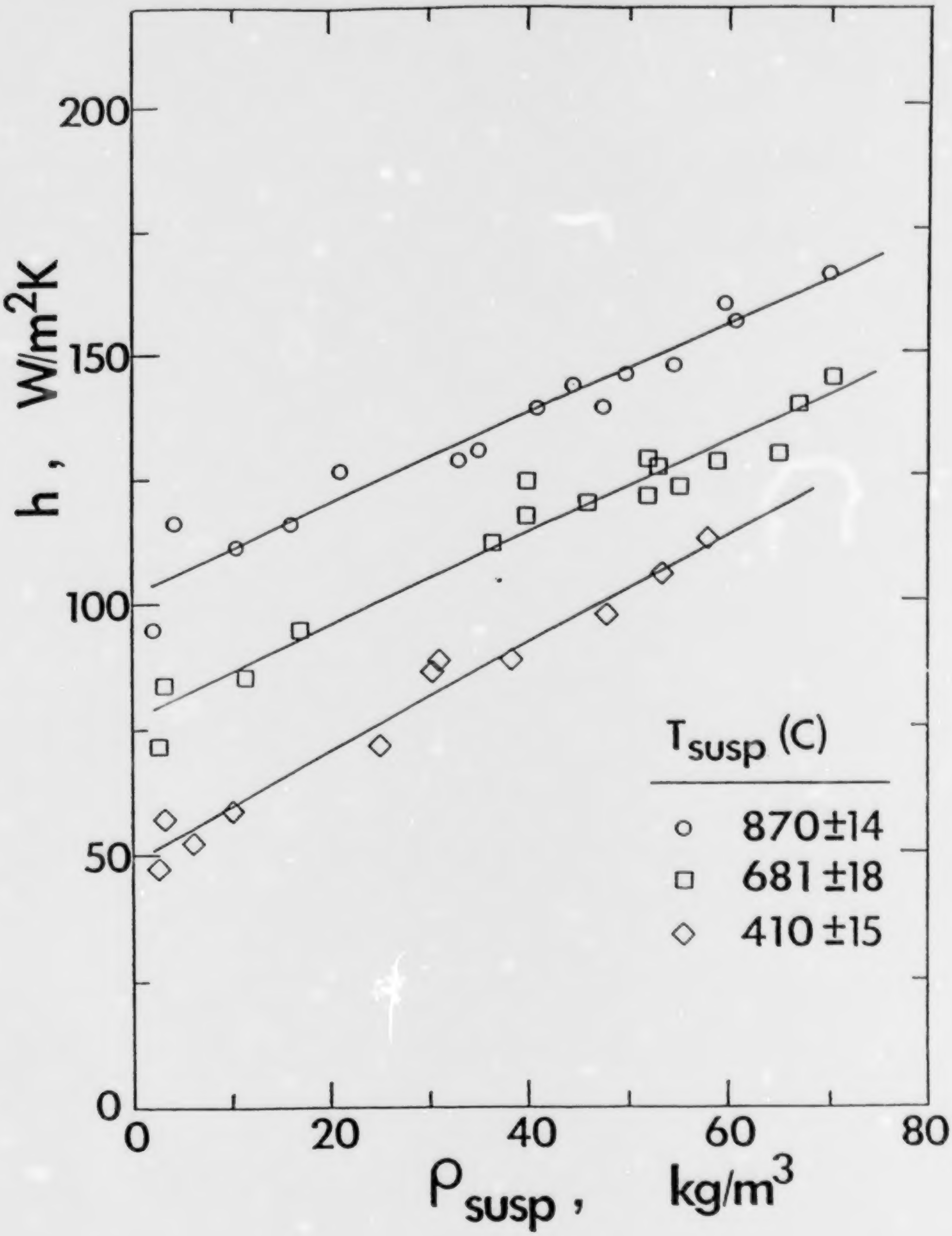

FIGURE 7.1: Overall heat transfer coefficient for the membrane wall versus suspension density at three suspension temperatures: Bottom line: Run #6, C1 in Table 7.1; U=7.5 m/s. Other lines: Run #6, C2 in Table 7.1; U=8.8–9.5 m/s.

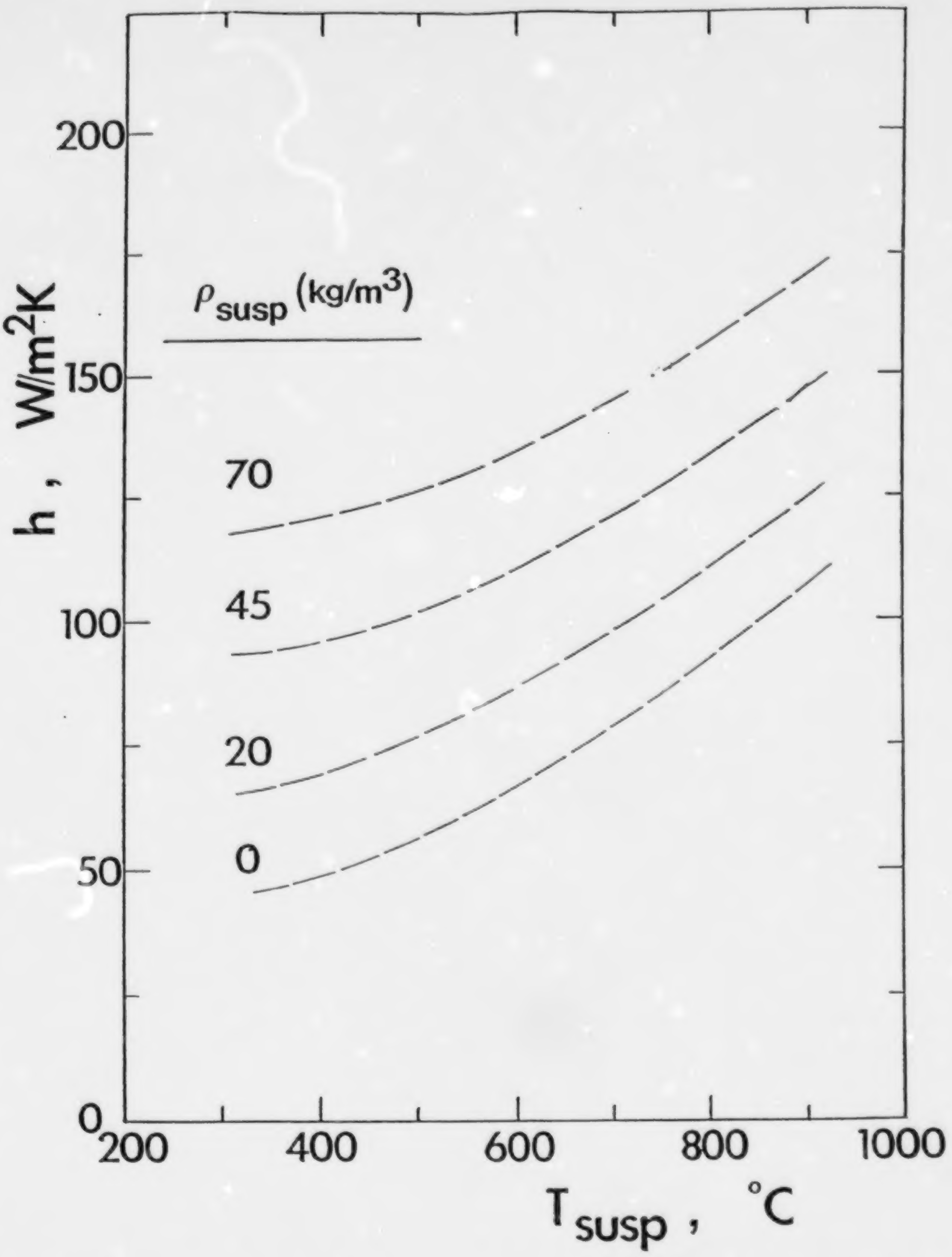

FIGURE 7.2: Cross-plot of overall heat transfer coefficient versus suspension temperature for membrane wall at four suspension density levels.

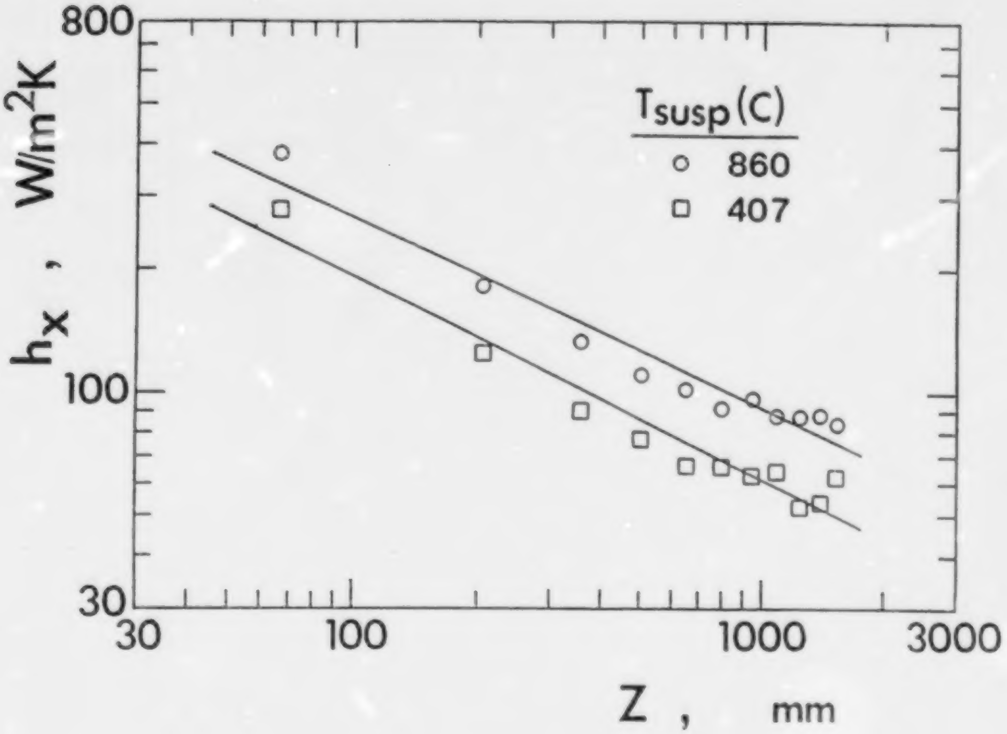

FIGURE 7.3: Local heat transfer coefficient along membrane wall versus z for two suspension temperatures. $\rho_{susp} = 54$ kg/m^3, Run #6, C1 in Table 7.1.

In addition to the overall heat transfer coefficients, local heat transfer coefficients along the membrane wall were also obtained for two suspension temperatures. The profiles are plotted in Figure 7.3 on a log-log scale where z is the distance along the membrane wall measured from its top downwards. Similar to the trend reported previously (Wu *et al.*, 1987), the local heat transfer coefficient decreases with increasing z, consistent with a predominantly downflowing wall layer next to the membrane wall surface, with fresh hot solids coming into contact with the top part of the surface. The slopes for both profiles are very close to -0.5 suggesting that there is little renewal in this wall layer of particles. As the two curves are obtained for the same suspension density, their differences are predominantly due to the effect of temperature. The larger differences near the top of the surface compared to the bottom are probably due to some cooling of the wall layer particles as they traverse the membrane wall surface, thus reducing the radiation transfer to the surface.

As discussed by Wu *et al.* (1989), the heat transfer coefficients for the membrane wall tend to be somewhat smaller than those for a single 12.7 mm o.d. tube (see Grace and Lim,

1987) obtained in the same system. The difference is probably due to limited effectiveness of the fins and the restricted view factor of the membrane surfaces.

Chapter 8

PRELIMINARY RESULTS OF FURTHER STUDIES

8.1 Determination of N_2O Emission Levels

Nitrous oxide has long been regarded as an innocuous gas, with the result that it has always been excluded in NO_x reporting and very few measurements have been taken of N_2O in combustion systems. However, with current worldwide concern regarding depletion of the ozone layer, attention has been focussed on N_2O since it catalyses the destruction of ozone. N_2O also acts as an absorber of infrared radiation, thereby acting as a "greenhouse gas" to warm the global climate. There are no major sinks once it enters the atmosphere, and N_2O has an estimated lifetime of about 150 years in the atmosphere.

Attention was drawn to possible elevated emissions of N_2O during CFB combustion by some work from Sweden (Fredericks, 1988) which indicated emissions of the order of 200–300 ppm, much higher than levels achieved in pulverized coal combustion. However, subsequent work has led to considerable uncertainty regarding these claims. There are no standard analysis techniques for N_2O. The favoured technique has been gas chromatography, but there is no consensus on the optimum detector, column or carrier gas. Moreover, N_2O can be formed if flue gas samples containing NO and SO_2 are allowed to sit for periods as short as 2 h (Muzio and Kramlich, 1988; de Soete, 1989). These analytical differences and problems probably account for much of the variation in reported N_2O values from a high of several hundred ppm, as noted above, to a low of 4 ppm from the TVA AFBC unit (Wheeldon, 1989).

With these factors in mind, a preliminary study was carried out to determine N_2O levels from our pilot plant unit. The study was subcontracted to Dr. K.C. Teo, whose report is included as Appendix A of this report. Conclusions must be regarded as tentative. The key findings are:

(a) Of the analytical techniques investigated, all using gas chromatography, the best sensitivity was found with a thermal conductivity detector, a 4 m long column of Chromosorb 102, and helium as the carrier gas. However, sensitivity was not very good using any of the combinations investigated. Calibration was carried out with gas samples prepared to contain 100 and 200 ppm N_2O.

(b) To avoid the problems of N_2O formation in stored samples, all samples were processed immediately. N_2O was confirmed to be present in all samples.

(c) If one excludes some preliminary data obtained with molecular sieve columns, which are believed to produce some N_2O from NO_x, the flue gas levels of N_2O determined are from about 35 to 60 ppm (with an average of 46 ppm) for a test with Highvale coal and 8 to 14 ppm (with an average of 12 ppm) in a subsequent Highvale coal run.

It is not clear why the two Highvale runs should have differed so much from each other, but levels of several hundred ppm certainly seem to be unlikely. Further work to determine the mechanisms of N_2O formation (Andersson *et al.*, 1988) and the factors influencing its formation is certainly required. Standard analytical techniques are also clearly needed to resolve some of the uncertainty regarding N_2O levels and possible differences between CFBC and other combustion techniques.

8.2 Development of a CFBC Reactor Model

The primary aim of the UBC CFB modelling work is to develop a mathematical model which reasonably predicts the performance of CFB combustion reactors for a given combustor geometry, fuel and set of operating conditions. Among the quantities to be predicted are:

1. heat release and transfer patterns within the riser, solids separators and solids return lines.
2. the levels of pollutants such as NO_x and SO_2 within and exiting the combustor system.
3. key combustion performance measures such as carbon loading and burnout and sulphur capture.

Description of the complex riser gas and solids flow patterns, and the gas and heterogeneous reactions within the system is required to meet these modelling goals.

Numerous investigators (*e.g.* Hartge *et al.*, 1988; Bader *et al.*, 1988; Horio *et al.*, 1988) have demonstrated that there exists a high degree of radial non-uniformity in a riser under typical combustion conditions. Sheets or streamers of particles are often detected falling down at the wall of the riser. Riser geometry has been demonstrated to have a large effect on axial solids bulk density profiles by Brereton (1987). Riser hydrodynamics are complex, and even the simplest modelling effort should be able to:

1. distinguish between a denser wall region and more dilute core region.
2. allow for both upward and downward fluxes of solids wherever they occur.
3. allow for radial and axial interchange of particles between different regions.

If these criteria are not met by a simple model, then the usefulness of such a model may be greatly restricted. Predicted data such as heat transfer rates and the effect of riser geometry may be in error.

Most circulating bed riser models proposed thus far are simple one dimensional zone models which satisfy mass balance constraints. Fett *et al.* (1987) proposed a model which represented the riser as a series of CSTR's stacked upon each other, with solids flow into each CSTR allowed from CSTR's both immediately above and below. This model assumes radial uniformity which contradicts experimental observations. Kwauk *et al.* (1988) proposed a model whereby a dilute solids phase flows up the riser and denser 'clusters' of particles diffuse upward and fall down by virtue of buoyancy and gravity. However, the Kwauk model also has no allowance for radial non-uniformity, and his axial bulk density correlations make no allowance for riser geometry. Rhodes (1989) recognizes the importance of a flux of particles to the wall in describing axial density profile decay with height. However, there is no allowance for a flux of particles from the wall to the core. This counterflux must occur to produce the increase in bulk density with height observed in risers with sharp exit geometries (*e.g.* see Figure 5.1).

The initial UBC mathematical modelling effort over the contract period described in this report has been largely involved with hydrodynamics. The preliminary work carried out at UBC initially involved developing a model constrained only by mass balances. This mass balance model has been developed with fitted hydrodynamic parameters that may be physically interpreted, and thus predicted by comprehensive energy/mass/momentum modelling performed in future work. The UBC mass balance model assumes that the region of the riser below the secondary air ports may be modelled as a well mixed turbulently fluidized bed. Above the secondary air ports the riser is divided into core and wall regions (Figure 8.1). A dilute stream of particles is assumed to flow rapidly up the core. The wall region contains 'streamers' of particles slowly moving downwards. The wall streamers may vary in cross-sectional area as dictated by mass balances. An important consequence of this variation is that both the thickness of the dense 'wall layer' containing streamers and the fraction of the wall covered by these streamers may vary simultaneously (Figure 8.2). It is possible at low solids circulations for the streamer thickness to decay to zero, in which case the riser becomes a dilute pneumatic conveyer. The streamers are assumed to be constant in density. Gas velocity in the core is assumed constant across the core cross-section. On the other hand, the time mean gas velocity in the region at the wall containing both streamers and dilute particle upflow is assumed to increase linearly with radius from a zero wall velocity to a maximum corresponding to the core velocity.

The model contains four fitted parameters. The first parameter is the velocity of the streamers down the wall. The model assumes this velocity to be constant. This velocity has been measured by several investigators (Hartge, 1988; Bader *et al.*, 1988), and is typically between -0.5 and -2.0 m/s. Presumably, solution of the interaction dynamics of gas, particle and wall will lead to prediction of this velocity at a given riser height. The particle slip velocity in the core is assumed to be the terminal velocity of the Sauter mean particle size.

Interchange of particles from streamers to core or vice versa is modelled by flux coefficients. For example, the flux from core region to wall streamers is:

$$\text{Flux}(kg/m^2 \cdot s) = \text{Flux Coefficient}(m/s) \times \text{Core Bulk Density}(kg/m^3)$$

The streamer to core flux coefficient is assumed to increase linearly with the thickness of the wall streamers. This increase allows for the formation of ripples, waves and instabilities which occur in the dense solids layers as they grow. High rates of particle entrainment are observed from the peaks of these 'waves'. This approach is similar to that used in two-phase

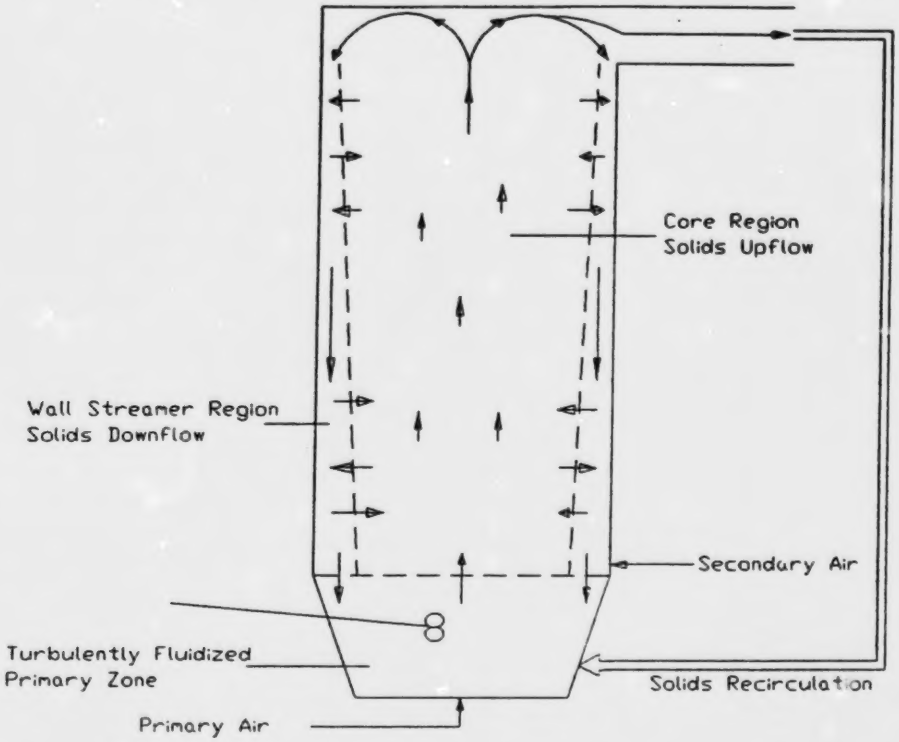
Core Region
Solids Upflow
Wall Streamer Region
Solids Downflow
Secondary Air
8
Turbulently Fluidized
Primary Zone
Solids Recirculation
Primary Air

FIGURE 8.1: CFBC reactor model schematic.

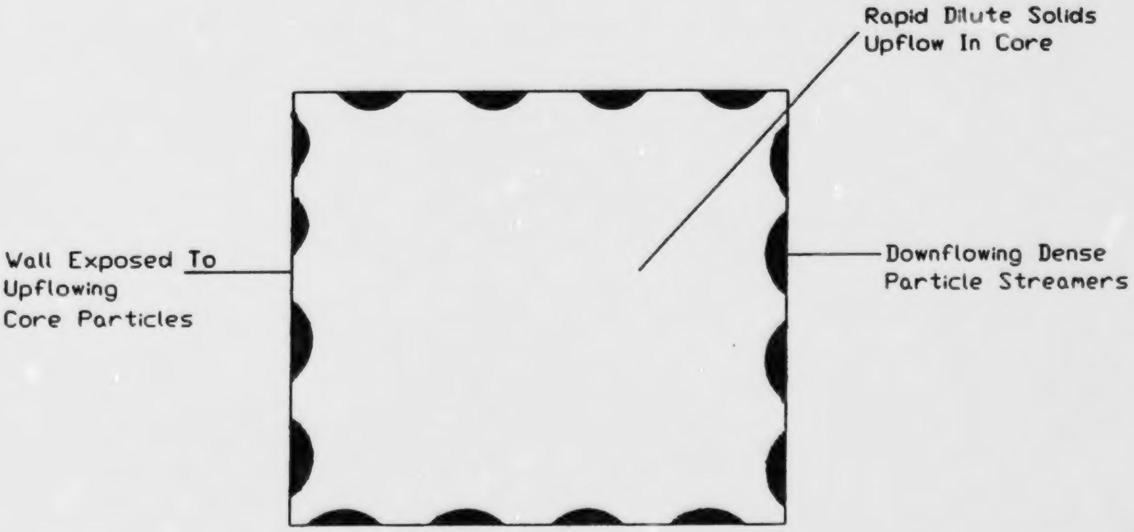
Rapid Dilute Solids Upflow In Core
Wall Exposed To Upflowing Core Particles
Downflowing Dense Particle Streamers

FIGURE 8.2: Riser cross-section showing streamer distribution.

gas-liquid annular flow. The rate at which the streamer to core flux coefficient increases is the second fitted model parameter. The riser core region above the secondary air ports is further divided into two sections. A small region immediately above the secondary air is termed the accelerating zone. The bulk density in this region decays rapidly with height due to rapid particle acceleration. The height of this region is given by the equations of Li *et al.* (1982), and the initial estimate of the density profile with height in this region is obtained from the equations of Kwauk *et al.* (1988). The core to streamer flux coefficient is allowed to vary in this region, and is found from solids mass balances.

Above the accelerating zone the core to streamer flux coefficient is assumed constant, and equal to the core-to-streamer flux coefficient at the top of the accelerating zone. The UBC model is then solved with these flux coefficient estimates to provide density profiles in the core and annulus zones above the secondary air ports. An output of the program predicting the density profile in the riser for one typical set of conditions is given in Appendix B. The model solution also provides data on wall coverage by streamers. The two simultaneous differential equations arising from the UBC model formulation are solved by a Runge-Kutta Fehlberg method with error control.

The fraction of upwardly travelling particles deflected down the wall at the riser top and the fraction successfully exiting the riser provide the model boundary condition at the top. The third fitted model parameter is the fraction of solids reflected at the riser exit. The inclusion of riser top geometry effects in the model allows for end effects. This is important when a high percentage of the solids reaching the top are reflected and an increase in bed density towards the top is predicted. Significant end effects are observed in the UBC combustor.

It is assumed that there exists a wall streamer thickness, above which 100% of the wall is covered by dense streamers. This thickness is the fourth fitted parameter in the model. It is envisaged that should the wall layer grow thicker than this maximum due to high core to streamer fluxes, then 'clumps' of particles may shear off the streamers and enter the core. These clumps or clusters may move down or up depending on their size. The model does not currently allow for the presence of clusters above the secondary air entry level.

A comparison of experimental and predicted density profiles for a particular set of conditions in the UBC combustor is given in Figure 8.3. It is seen that the correct trends are predicted by the model.

The UBC model was developed as the first stage of more detailed mathematical modelling work. The model has been used to explore the magnitude and interaction of key hydrodynamic properties such as solids radial fluxes, and axial and radial voidage distributions. Work has been begun to evaluate the model using pilot plant data to generate the fitted model parameters. A heat transfer sub-model will soon be added to the mass balance model. As the model describes radial solids fluxes and variations in wall bulk solids densities, it provides more information for wall heat transfer calculation than other models such as those of Kwauk *et al.* (1988), Fett *et al.* (1987), or Rhodes (1989).

A fully predictive CFBC hydrodynamic model must be based on sound studies of the dynamic interactions of gas, particles and riser surfaces. Current UBC work involves a fundamental study into particle-particle and gas-particle interactions. The mechanisms of gas-particle drag, particle-particle collision and turbulent particle diffusion are being investigated. Methods to mathematically represent these phenomena without inordinately large computational requirements are being tested.

A particle devolatilization model has also been developed for the CFB environment. Order of magnitude calculations indicate that significant internal particle temperature gradients exist in the fuel particles during heat up. The model is based on the model of Argawal *et al.* (1984). However, an improved heat transfer calculation procedure is incorporated. Intrinsic devolatization kinetics are modelled using the approach of Anthony *et al.* (1976) who assumed that devolatilization consisted of a very large number of series reactions whose activation energies formed a Gaussian distribution.

A program has also been developed which solves a simplified version of the particle equations of motion, whereby the wall layer thickness is assumed constant. The coupled hyperbolic partial differential equations are solved by the Method of Characteristics. The resulting par-

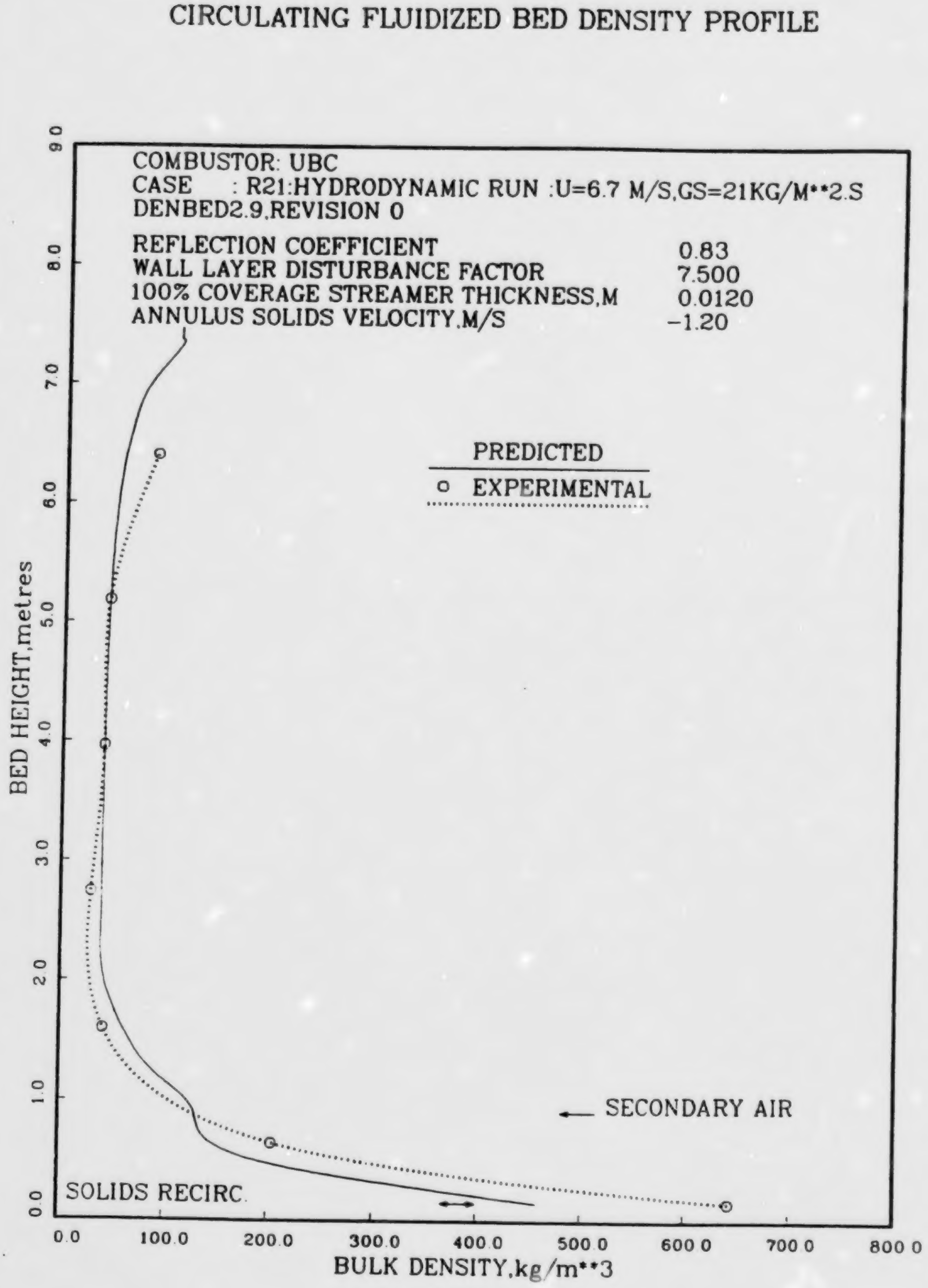

FIGURE 8.3: Comparison between predicted and experimental density profile.

ticle residence time versus combustor position data are combined with the volatiles release versus particle heat up time to predict heat release patterns, assuming heat transfer to the devolatilizing particle is independent of volatiles combustion.

8.3 Transient Studies and Initial Work on Control Strategies

Good automatic control is required to ensure both efficient and safe operation of equipment in any application. It is particularly important for the safe and reliable operation of CFBC boilers and power plants.

Foreknowledge of process transient behaviour is imperative for the design of operable control structures. As the study of the transient behaviour of CFB's is in its infancy, this research is concerned with the collection of transient data ultimately needed for the design of a control strategy that will be satisfactory for industrial or utility applications.

One preliminary transient test has been performed to date by interrupting the coolant to the tubes (see Figure 2.8) located in the upper part of the riser during a combustion trial with H-Oil pitch. The heat removal from the heat exchanger tubes was step decreased from 17.7 kW to 9.6 kW. The temperature response was a rise from an initial (steady-state) value of 820°C to a final steady-state value of 872°C. The temperature response curve for this test in shown in Figure 8.4 as the percent change in temperature versus time. The response is typical of an overdamped second order system and can be approximated with a first order plus dead-time model. The data indicate a first order time constant of 20 minutes, a 2.6 minute dead-time, and a process gain of 6.4°C/kW. Thus, the preliminary results suggest that the temperature response to a change in the heat removal can be represented by:

$$\frac{\Delta T}{\Delta q} = k(1 - e^{-(t-t_0)/\tau})$$

where:

ΔT = change in temperature from initial steady-state (°C)
Δq = change in heat removal (kW)
k = process gain (6.4°C/kW)
t = time after change from initial steady-state (min) ($t \geq t_0$)
t_0 = process dead-time (2.6 min)
τ = process time constant (20 min)

This is the first of many tests required. The first order plus dead-time model will have to be tested for various initial and final conditions over the entire range of CFB boiler operation to determine the degree of variation of process constants. If there is a large deviation, a more complex model will be required to approximate the transients. Other required tests include the effects of changes in primary air flow, secondary air flow, and L-valve aeration.

From the above tests, a process model will be developed which will be used to implement an initial control structure for the CFB boiler. As the research progresses, the model will be refined as required by the complexity of controller schemes investigated. Other transient

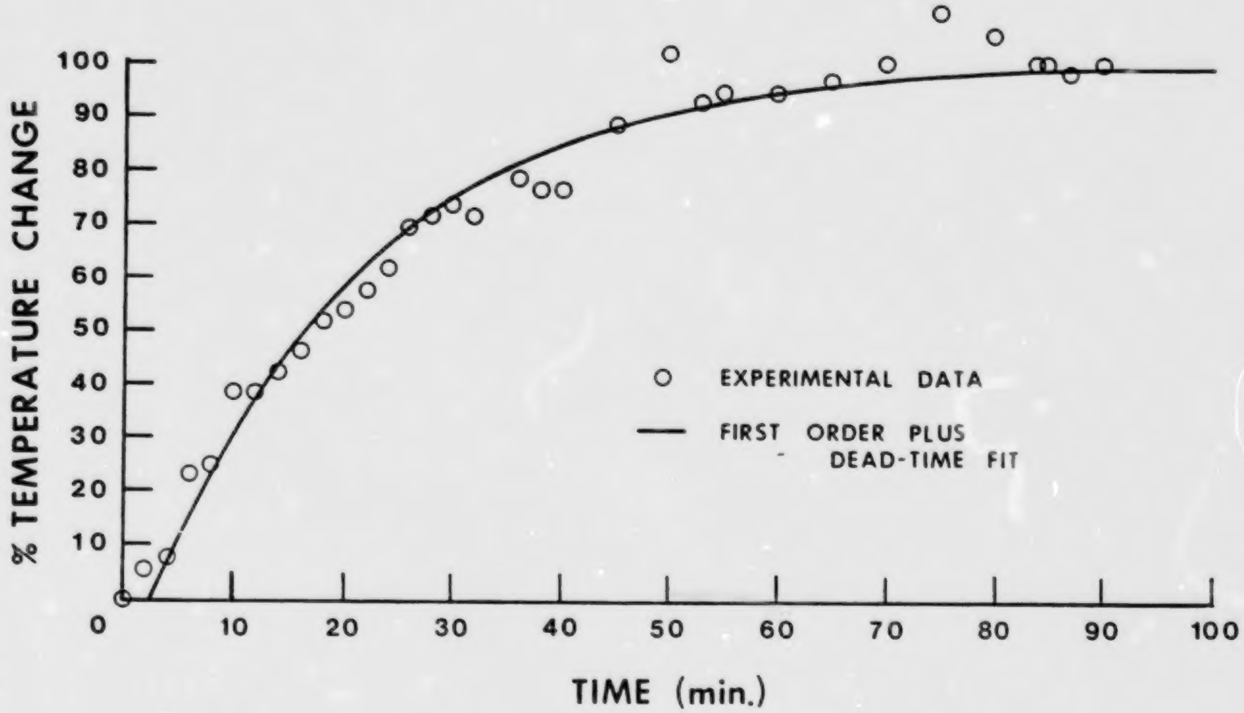

FIGURE 8.4: Transient response to a step decrease in heat removal of 8.1 kW.

Initial steady-state temperature = 820°C (0%)
Final steady-state temperature = 872°C (100%)
(Temperature was measured 1 m above the base of the riser)
Superficial velocity = 8.0 m/s
Average suspension density = 143 kg/m^3
Coal feed rate = 13.8 kg/h
Excess air = 19.8%
Secondary/primary air ratio = 0.80

results are discussed in Section 4.2.

8.4 Study of Combustion Behaviour in Cyclone

Cyclones are inertial separation devices which can effect a separation of solids of one density from a gas of another density. When used with a CFBC they take on a special significance. Their ability to capture fine coal and sorbent particles allows for the recycle of these fines, which means higher carbon efficiencies and improved sulphur capture ratios. A brief subinvestigation was carried out to measure gas concentration profiles at one level (just below the vortex finder) in the secondary cyclone to allow reactions in the cyclone to be assessed.

Examination of the combustion gases passing the primary and secondary cyclones usually reveals a substantial temperature increase. In addition, a reduction in CO concentration of 60 to 80% is commonly noted. Thus, two important parameters of a CFBC system are influenced by the cyclone stage, namely the temperature of the flue gas stream (important for NO_x formation and cycle efficiency) and the CO conversion. The preliminary results point to the combustion of captured particles at the wall with the combustion of fines and CO in the central turbulent regions of the cyclone.

Gas samples have been taken at different radial positions. Typical results for CO are shown in Figure 8.5. All gas analyses were performed with the system at steady state. These results show clearly that the CO concentration is higher near the outer wall of the cyclone (where higher solids concentrations occur) than near the core of the cyclone.

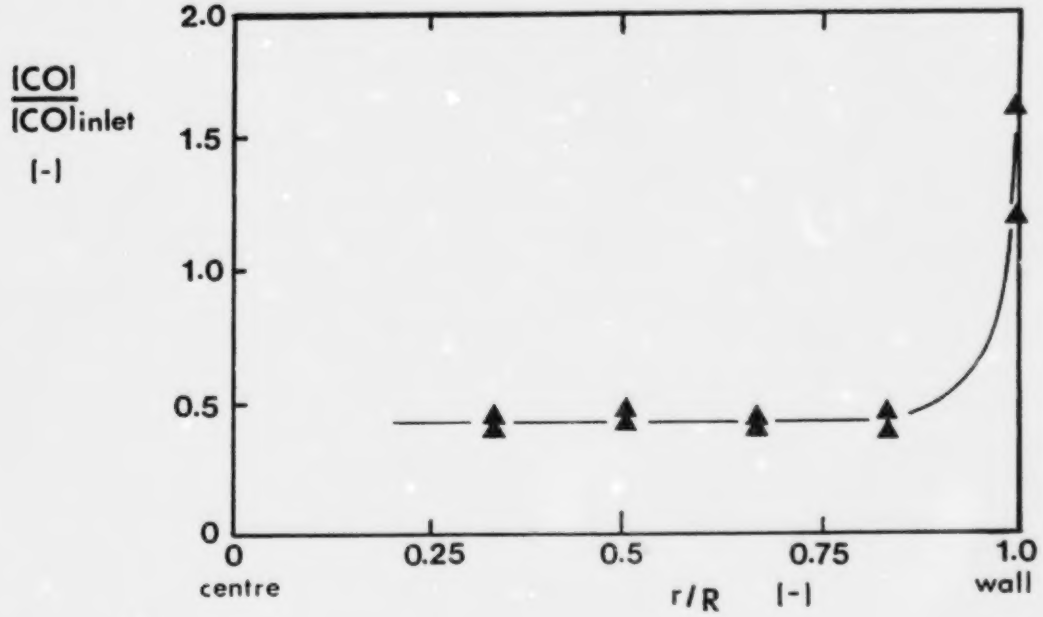

FIGURE 8.5: Radial CO concentration profile for secondary cyclone at a level of 203 mm below the top. Conditions: Superficial velocity = 7.5 m/s; Secondary to primary air ratio = 1.0; Reactor temperature = 872°C; Fuel: Highvale coal.

Chapter 9

CONCLUSIONS AND RECOMMENDATIONS

9.1 Conclusions

The UBC-CFBC pilot plant was extensively modified to allow greater flexibility for fuel testing and fundamental studies at high temperature. An improved gas sampling system was developed, which permits on-line measurement of O_2, CO_2, CO, NO_x, SO_2 and CH_4 concentrations from samples taken at several locations in the reactor. Successful recycling of the secondary cyclone catch was achieved with a jet eductor system. A baghouse was also installed to collect the finest particulate fractions leaving the system.

The pilot plant demonstrated its ability to burn a wide variety of fuels, several being considered as difficult to handle, such as a high sulphur coal (Minto), a low reactive anthracitic coal (Mt. Klappan), a low calorific lignite (Poplar River) and two pitches produced from heavy oil upgrading. Each fuel was burned successfully, and their combustion behaviour proved to be adequate for CFBC operation. For all the coals tested, the NO_x emissions without limestone addition were always below 200 ppm. The presence of limestone, increases in temperature and increases in excess air level, were all factors leading to a rise in NO_x emissions.

Sulphur capture results for Minto coal showed a strong improvement when the secondary recycle loop was operating. Values as high as 99% sulphur capture were observed at a Ca/S ratio of 3.0. Further trials are needed to confirm these results. Sulphur capture observed during the pitch combustion trials, however, were much lower than for Minto coal. The level of calcium sulphide in solids samples taken around the combustor system during the Minto trials, showed a strong drop when the secondary recycle loop operated efficiently. It also appeared that sulphide is not favoured if the local carbon:sulphur molar ratio remains below about 2. A mass balance on the vanadium during the CANMET pitch showed that most of it remains in the solids phase and is found mainly in the finest baghouse stream.

Combustion efficiencies were calculated for each fuel based on overall carbon conversion. The efficiencies ranged from 92.9% for the low reactive anthracite coal without secondary recycle, up to 99.9+% for the H-Oil pitch. The operation of the secondary recycle loop also led to an increase in combustion efficiency. In general, the various combustion trials in the pilot plant resulted in low NO_x emissions and excellent combustion efficiencies. The sulphur capture was greatly improved with the operation of the secondary recycle loop.

The CFBC pilot plant also showed its great flexibility during the calcium carbonate calcination trial. The product (lime) obtained from the primary recycle loop proved to have excellent characteristics for the recaustization process in a pulp mill.

Hydrodynamic studies showed that the axial density profile in the reactor at high temperature follows the same trends as in a cold model. The sharp exit caused a rise in solids density to occur at the top of the reactor. The top geometry is an important parameter in CFBC since it determines the amount of solids reflection into the reactor column. A capacitance probe capable of withstanding high temperatures was also developed. Preliminary results showed a two region flow structure with a dense annulus and a more dilute core. Examination of erosion probes also showed a slow downward moving flow of particles near the walls and a rapid upflow of particles in the centre.

Temperature profiles measured around the primary loop were relatively uniform for every fuel. The suspension membrane wall heat transfer coefficient was found to increase linearly with suspension density. Local heat transfer coefficients along the length of the membrane wall decreased with increasing distance from the top. This appears to be consistent with a layer of downflowing solids with little renewal. The heat transfer coefficients for the membrane wall are somewhat smaller than for a single tube exposed to identical conditions.

Other studies were also undertaken and are still in a preliminary stage. These include the investigation of N_2O levels in CFBC, the development of a reactor model and study of transients and control strategies for CFBC.

9.2 Recommendations

Before further tests are carried out in the CFBC pilot plant, the following modifications should be made:

(a) The gas sampling system must be modified to ensure that no condensation of water occurs in the sampling lines. This includes the use of insulated filters and heated sampling lines to keep the temperature above 100°C up to the point of water removal.

(b) A Gamma-ray density detector should be installed on the L-valve standpipe below the primary cyclone, to keep track of the solids level in the standpipe at all times.

(c) Secondary air ports should be installed higher in the reactor column to investigate the effect of staging on NO_x formation.

(d) The L-valve aeration air should be located one pipe diameter higher at the L-valve corner to possibly provide smoother solids recirculation.

Future work on the UBC–CFBC pilot plant will be concerned with the following aspects:

(a) NO_x generation and destruction during the combustion process. Determination of N_2O levels and factors leading to its formation will also be carried out.

(b) Further tests on the solid residues produced during combustion of a high sulphur fuel with limestone addition, will be performed to investigate further the issue of sulphide formation.

(c) Preliminary hot gas cleaning tests using a ceramic candle filter will be carried out.

(d) Development of a control strategy suitable for CFBC.

(e) Development of a complete CFBC reactor model with comparisons being made between experimental and predicted combustion results.

(f) The scale-up and scale-down laws for CFBC reactors will also be investigated.

References

Andersson, S., L-E. Amand and B. Leckner, "N_2O Emissions from Fluidized Bed Combustion", IEA AFBC Tech. Meeting, Amsterdam, November (1988).

Anthony, D.B. and J.B. Howard, "Coal Devolatilization and Hydrogasification", AIChE Journal, **22**:625–656 (1976).

Anthony, E.J., "The Presence of Calcium Sulphide in Solid Wastes From Circulating Fluidized Bed Combustors", CANMET Rept. ERP/ERL 86–53 (TR), (1986).

Anthony, E.J., G.G. Ross, E.E. Berry, R.T. Hemmings, R.K. Kissel and C.C. Doiron, "Characterization of Solid Wastes from Circulating Fluidized Bed Combustion," Proc. of the Tenth Conf. on Fluidized Bed Combustion, San Francisco, 131–139 (1989).

AOAC Method 1.013–1.015:Sulphide Sulphur (7) – Final Action, in Official Methods of the Association of Official Analytical Chemists, 13 ed., ed. W. Horwitz, Washington, D.C., (1980).

Argawal, P.K., W.E. Genetti and Y.Y Lee, "Model for Devolatilization of Coal Particles in Fluidized Beds", Fuel **63**:1157–1165 (1984).

Bader, R., J. Findlay and T.M. Knowlton, "Gas/Solids Flow Patterns in a 30.5 cm Diameter Circulating Fluidized Bed", in Circulating Fluidized Bed Technology II, ed. P. Basu and J.F. Large, Pergamon, Oxford, 123–137 (1988).

Becker, H.A. and R.K. Code, "Pilot Plant Trials on Atmospheric Fluidized Bed Combustion of High-Sulphur Eastern Canadian Coals (Minto and Devco) with Limestone Addition for Sulphur Capture, Tech. Rept. QFBC.TR.83.1, Queen's University, Kingston, Ontario, (1983).

Becker, H.A., R.K. Code and J.R. Stephenson, "Pilot Scale Trials on Atmospheric Fluidized Bed Combustion of a British Columbia Anthracite (Mt. Klappan)", Tech. Report QFBC.TR.87.4, Queen's University, Kingston, Ontario, (1987a).

Becker, H.A., R.K. Code and J.R. Stephenson, " Pilot Scale Trials on Atmospheric Fluidized Bed Combustion of a Western Canadian Sub-Bituminous Coal (Highvale)", Tech. Report QFBC.TR.87.3, Queen's University, Kingston, Ontario, (1987b).

Beer, J.M., A.F. Sarofim and Y.Y. Lee, "NO Formation and Reduction in Fluidized Bed Combustion of Coal", Proc. of the Sixth Intern. Conf. on Fluidized Bed Combustion, Atlanta, 942–955 (1980).

Berry, E.E., R.T. Hemmings and B.J. Cornelius, "Investigation of Sulphur Speciation in CFBC Solids", Rept. 89–0127 for Dearborn Chemical Company, (1989a).

Berry, E.E., R.T. Hemmings, B.J. Cornelius, and E.J. Anthony, "Sulphur Oxidation States in Residues From a Small-Scale Circulating Fluidized Bed Combustor", Materials Research Soc. Symp. Proc., **136**:9–22 (1989b).

Brereton, C.M.H., "Fluid Mechanics of High Velocity Fluidized Beds", PhD Dissertation, University of British Columbia, (1987).

Burkell, J.J., J.R. Grace, J. Zhao and C.J. Lim, "Measurement of Solids Circulation Rates in Circulating Fluidized Beds", in Circulating Fluidized Bed Technology II, ed. P. Basu and J.F. Large, Pergamon, Oxford, 501- -509 (1988).

Clean Air Act, Canada National Guidelines for New Stationary Sources, Canada Gazette Part II, April 25 (1981).

Dearborn Chemical Company, "Characterization of Circulating AFBC Wastes", CEA Rept. 432 G–494, December (1986).

de Soete, G.G., "Formation of Nitrous Oxide from NO and SO_2 During Solid Fuel Combustion", EPA/EPRI Joint Symposium on Stationary Combustion NO_x Control, San Francisco, March (1989).

Dorris, G., Private Communication, Pulp and Paper Research Institute of Canada, Pointe Claire, Quebec, (1989).

Fett, F.N., V. Weiss, H. Helmrich and K. Janssen, "Mathematical Modelling of Circulating Fluidized Bed Reactors by Reference to a Solids Decomposition Reaction and Coal Combustion", Chem. Eng. Process., **22**:79–90 (1987).

Fredericks, L., Studsvik Energy Rept. EP–88/14 (1988).

Geldart, D., "Types of Gas Fluidization", Powder Technol., **7**:285–292 (1973).

Gibbs, B.M., F.S. Pereira and J.M. Beer, "Coal Combustion and NO Formation in an Experimental Fluidized Bed", Inst. of Fuel Symp. Ser. No. 1, London, D6(1–13), (1975).

Grace, J.R., "Contacting Modes and Behaviour Classification of Gas-Solid and Other Two-Phase Suspensions", Can. J. Chem. Eng., **64**:353–363 (1986).

Grace, J.R. and C.J. Lim, "Circulating Fluidized Bed Combustion of Coal, Woodwastes and Pitch", Final Report, Prepared for Energy, Mines and Resources Canada, Contract 24ST.23400–6–9007, (1987).

Hamer, C.A., D.T. Liang and J.B. Kearns, "Combustion Trials with Syncrude Coke and Minto Coal in the Mineral Sciences Laboratories Circulating Fluidized Bed Combustor: Sulphur and Metals Capture and Metallic Corrosion", Rept. MSL 87–92 (1987).

Hartge, E.-U., D. Rensner, and J. Werther, "Gas/Solids Flow Patterns in a 30.5 cm Diameter Circulating Fluidized Bed", in Circulating Fluidized Bed Technology II, ed. P. Basu and J.F. Large, Pergamon, Oxford, 123–137 (1988).

Hirama, T., H. Takeuchi and M. Horio, "Nitric Oxide Emission from Circulating Fluidized-Bed Coal Combustion", Proc. of the Ninth Intern. Conf. on Fluidized Bed Combustion, Boston, 898–906 (1987).

Hirama, T., M. Tanita, M. Horio, T. Chiba and H. Kobayashi, "A Two-Staged Fluidized Bed Coal Combustion for Effective Reduction of NO_x Emission" in "Fluidization", eds. D. Kunii and R. Toei, Proc. of the Fourth Intern. Conf. on Fluidization, 443–450 (1984).

Horio, M., K. Morishita, O. Tachibana and N. Murata, "Solid Distribution and Movement in Circulating Fluidized Beds", in Circulating Fluidized Bed Technology II, ed. P. Basu and J.F. Large, Pergamon, Oxford, 147–154 (1988).

Kwauk, M., N. Wang, Y. Li, B. Chen and Z. Shen, "Fast Fluidization at ICM, in Circulating Fluidized Bed Technology II, ed. P. Basu and J.F. Large, Pergamon, Oxford, 89–103 (1988).

Leckner, B. and L.E. Amand, "Emission from a Circulating and a Stationary Fluidized Bed Boiler: A Comparison", Proc. of the Ninth Intern. Conf. on Fluidized Bed Combustion, Boston, 891–897 (1987).

Li, H. and M. Kwauk, "Hydrodynamics of V-Valve", Institute of Chemical Metallurgy, Academia Sinica, (1981).

Li, Y., B. Chen, F. Wang and Y. Wang, "Hydrodynamic Correlations for Fast Fluidization", Proc. of the First China-Japan Symposim on Fluidization, Hangzhou, China, 124–134, (1982).

Muzio, L.J. and J.C. Kramlich, "An Artifact in the Measurement of N_2O from Combustion Sources", Geophys. Research Lett., **15**:1369–1372 (1988).

Potkin, W., "Start-Up and Operation of a Fluo-Solids Calciner", Pulp and Paper Magazine of Canada, **71**(21):53–59 (1970).

Reh, L., "The Circulating Fluid Bed Reactor — A Key to Efficient Gas/Solid Processing", in Circulating Fluidized Bed Technology, ed. P. Basu, Pergamon, Toronto, 105–118 (1986).

Rhodes, M.J., "Modelling the Flow Structure of Upward-Flowing Gas- Solids Suspensions", (to be published), (1989).

Sleicher, C.A. and M.W. Rouse, "A Convenient Correlation for Heat Transfer to Constant and Variable Property Fluids", Intl. J. of Heat and Mass Transfer, **18**:677–683 (1975).

Tibbets, T.E. and W.J. Montgomery, "Evaluation of Canadian Commercial Coals", CANMET Rept. 76–40, Energy Research Laboratories, CANMET, Energy, Mines and Resources Canada, (1976).

Wheeldon, J., Personal communication to E.J. Anthony, June 5 (1989).

Wu, R.L., C.J. Lim, J. Chaouki and J.R. Grace, "Heat Transfer from a Circulating Fluidized Bed to Membrane Waterwall Surfaces", AIChE Journal, **33**:1888–1893 (1987).

Zhao, J., J.R. Grace, C.J. Lim, C. Brereton, R. Legros and E.J. Anthony, "NO_x Emissions in a Pilot Scale Circulating Fluidized Bed Combustor", EPA/EPRI Joint Symposium on Stationary Combustion NO_x Control, San Francisco, (1989).

Appendix A

Report on N_2O Measurement By Dr. K.C. Teo

METHODOLOGY DEVELOPMENT AND TESTING OF A GAS CHROMATOGRAPHIC METHOD FOR THE ANALYSIS OF NITROUS OXIDE (N_2O) IN FLUE GAS

1. INTRODUCTION

Several different gas chromatographic methods are available in principle for analysis of N2O in the gas phase. However, there are problems associated with the trace N2O analysis in flue gas or related samples. This is in part due to the more abundantly presence of CO2 (15-20%), excess air, unburnt hydrocarbons, mositure and NOx species. The concentration of N2O from literature and other technical information is general described to fall below 200ppm. or more likely to be within the range of 10-50ppm. for a well design combustor or incinerator under their optimal operationg conditions.

2. METHOD DEVELOPMENT

Within the context of this preliminary study gas chromatographic method was chosen for the need. In general, off-line or at-line flue gas analysis using GC offers the best and economical solution to the problem. Features of some candidate GC columns are collected in Figure 1 and Table 1. In terms of detector type, there are several different options, namely,

- Thermal conductivity detector (TCD):
  sensitivity - ppm range under carrier gas of hydrogen or helium.

- Electron capture detector (ECD):
  sensitivity - ppm to sub-ppm range under optimal operating conditions.

- Ultrasonic detector (USD):
  sensitivity - ppm to sub-ppm range under optimal operating conditions.

- Quadrapole mass spectrometer (QMS) detector:
  high sensitivity - sub-ppm to ppb or better

In this work the following GC columns have been attempted and evaluated:

a. Porapak N and Porapak R (organic polymeric solid phase).
b. Molecular Sieve 5A and 13X (zeolite, inorganic alumino-silicates).
c. Chromsorb 102 (an organic polymeric solid phase).

As N_2O is non-combustible therefore flame ionization detector (FID) is not a suitable detector for the application. The existing TCD in fact offers a reasonable optimal sensitivity detection range in the order of a few ppm under the helium carrier gas flow of 20-30 ml/min.

After some extensive exercises with the various column types as stated above, Chromosorb 102 was chosen as the best choice using the exisitng Varian GC system. The TCD was set to its highest sensitivity range 0.05 at 260°C with a detector current of 160mA. Separation of air, NO_x, CO_2 and N_2O can be achieved very well. NO_2, is an oxidant which present in flue gas together with NO might potentially react with the active sites of organic polymeric solid phase of a new GC column. There is also a concern about the possibility of hydrocarbon peak which might contaminate the N_2O peak and/or cause base-line drifting and obscure the quantitation of N_2O.

Calibration standards contain 100 and 200 ppm (by volume) in nitrogen gas were prepared by diluting 50 and 100μl of medical grade nitrous oxide with 500ml of nitrogen respectively. Estimated error of the standards is ±10%.

Gas samples were collected from the appropriate sampling line which carries an ice-bath condenser and an on-line anhydrous magnesium perchlorate drier. Moisture content of gas sample is expected to be less than 1ppm. Glass syringe which carries a Teflon plunger was used for all gas sampling. The collected gas samples were analysed within 1-5 hours.

Gas chromatrographic conditions:

Varian Gas Chromatrograph - model 6400
GC Column: Chromosorb 102 (12' x 1/8")
Carrier gas: 25.0ml helium/ min.
Detector: TCD/sensitivity range 0.05
Detector temperature: 260°C/ current 158mA.

3. RESULTS AND DISCUSSION

3.1 Linearity respond of TCD towards N2O as shown in Figure 2 was found in the early study under argon carrier gas. Linear correlation was also found for the TCD under helium gas flow with lower N2O concentration in the range of low % to 50ppm by volume.

3.2 The analytical performance of Chromsorb 102 for trace N2O was evaluated in terms of its capability to separate the major interferences such as carbon dioxide and NOx (Figures 3 to 6). At low N2O concentration (<200ppm), and under low plot attenuation (eg. 1 to 4x) one can identify the baseline drifting might be a concern for quantitation of a **weak** N2O chromatograhic peak. The estimated error is ±25%, and improve as the N2O level towards the high end.

3.3 CFB Test Run of lignite conducted on 3 November, 1988.

N2O was confirmed to be present in all the flue gas samples. Some samples seem to contain relatively high (cf. 100-550ppm) N2O (Table 2). Analytical data using Molecular Sieves (MS) 13X column on the same set of samples were also included in the same table for comparison. There is a general concern that MS might react with NOx to produce additional N2O, and thereby increase its appearent concentration. Calibrations on MS 13X are shown in Figure 8.

3.4 CBF Test Run of Highvale coal on 6 February, 1989.

The average at 45 ppm (Table 3) seems to be reasonable, and falls within the general literature range. Some typical GC outputs are shown in Figures 9A to 9E. Figure 9E illustrates the reproducible result of the analysis.

3.5 CBF Test Run of Highvale coal on 18 February, 1989.

The average at 11 ppm (Table 4) seems to be lower than the previous data (see 3.4), perhaps is due to different CFB operating conditions. Some typical GC outputs are shown in Figures 10A to 10D.

Prepared by K. C. Teo ***March 14, 1989***

FIGURE 2

LINEARITY CORRELATION OF TCD RESPOND AT HIGH CONCENTRATION OF N_2O

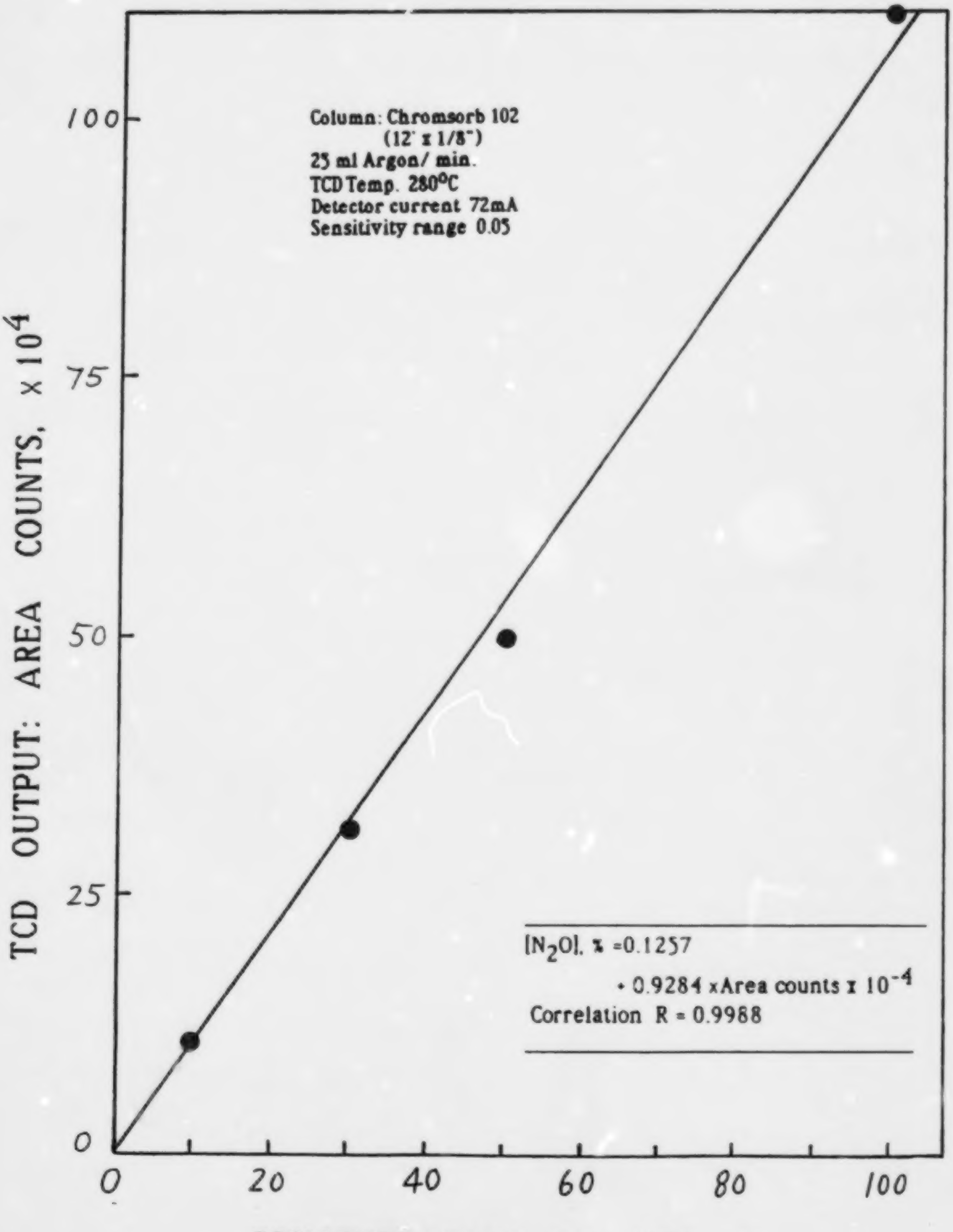

FIGURE 2B LINEARITY CORRELATION OF TCD RESPOND AND LOW CONCENTRATION OF N_2O

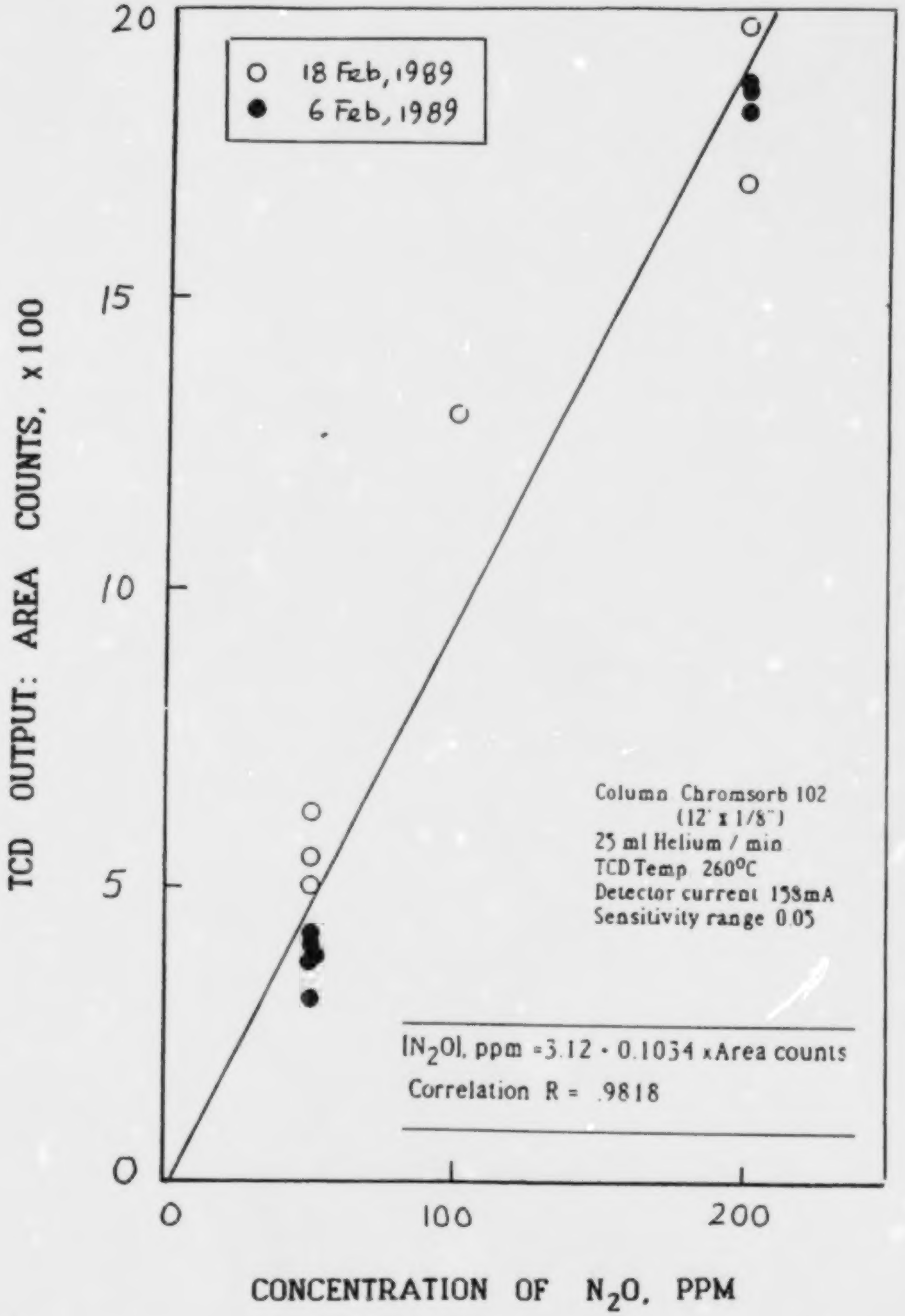

TABLE 1

ANALYTICAL METHODS USED BY OTHER RESEARCH GROUPS FOR ANALYSIS OF LOW CONCENTRATION NITROUS OXIDE (N2O) IN FLUE GAS SAMPLES

	Gas chromatographic conditions			
Ref. paper	Column type/ temp. °C	Carrier gas/ sample size	Detector type and temp. °C	Injector temp. °C
1.	Poraplot Q (fused SiO_2 column)/45	H_2/ 500µl	Electron capture detector (ECD) at 300 °C	150 °C
2.	Porasil B or C (2-3m x dia. 3mm)/ 45	5% CH_4 in Argon, 50 $ml\text{-}min^{-1}$/ N.A.	ECD at 350 °C	N.A.
3.	Molecular sieve 5A (3m x dia. 5mm)/ N.A.	Helium/ N.A.	Ultrasonic detector from Tracor/ N.A.	N.A.
4.	Chromosorb 101 (for CO_2 & N_2O separation only)	Helium/ N.A.	Thermal conductivity detector (TCD)	N.A.
5.	[A non-GC method]	--	Mass spectrometer detector	--

Ref.

1. Studsvik Arbetsrapport - Technical Note: EP-88/14.
2. D. Pieroth and R.A. Rasmussen (Journal??) 265 (1976).
3. Geophysical Research Letters 751 (1976) Dec.
4. FUEL 642 (67) 1988.
5. *ibid.*

TABLE 2

GAS ANALYSIS OF THE CFB TEST RUN COMBUSTION OF LIGNITE CONDUCTED ON 3 NOVEMBER, 1988

Flue gas sample[a]		Method 1 [b]		Method 2[c]
Label	Time (HR)	Direct output[d]	Peak area[e]	Peak area[e]
1.	16:55 B	553	552.5	113
2.	16:56 A	-	23	-
3.	17:03 B	-	27	-
4.	17:04 A	-	18	-
5.	17:10 B	139	135	62
6.	17:11 A	-	103	39
7.	17:15 A	-	11	26

(a) Port of sampling: A= after the drying tube; B= before the drying tube.

(b) Method A using Chromsorb 102 column (2m x 1/8").

(c) Method B using Molecular Sieves 13X (36" x 1/8") included for comparison.

(d) Calculated from direct area integration of the GC output.

(e) Calculated from the N_2O peak area using the trianglular method.

TABLE 3 GAS ANALYSIS OF CFB TEST RUN CONDUCTED ON 6 FEBRUARY, 1989

Gas sampling and analysis date: 6 February, 1989

Run number:

Fuel: Highvale Coal Conditions: #1

Gas	Sampling	Gas composition (a)					
sample	time, HR	N2O ppm	NOx ppm	O2 %	CO2 %	CO ppm	SO2 ppm
Flue gas stream:							
1.	17:37	36.2	140	≈4.	14.5	15	5
2.	17:42	52.6	162	3.9	17.6	24	5
3.	17:46	61.7	185	3.4	17.8	22	5
4.	17:54	44.9	175	4.2	18.5	18	5
5.	17:59	34.5	170	3.0	18.3	16	4
	average:	46.0	166	3.7	17.3	19	4.8
	std. dev.:	±10.2	±15	±0.4	±1.5	±3.5	±0.4
From outlet between cyclones							
6.	18:08	32.5	140	3.2	18.2	132	2
7.	18:13	36.4	195	3.3	18.3	133	0
8.	18:18	38.8	195	2.9	18.6	158	0
9.	18:23	61.1	195	2.8	18.0	195	0
	average:	42.2	181	3.1	18.3	155	0
	std. dev.	±11.1	±24	±0.2	±0.2	±26	

(a) N_2O by gas chromatographic analysis, all other gas species via on line analysers

TABLE 4 GAS ANALYSIS OF CFB TEST RUN CONDUCTED ON 18 FEBRUARY, 1989

Gas sampling and analysis date: February 18, 1989

Run number: **18** Fuel: Highvale Coal
Conditions: Primary air 42 SCFM Secondary air 26 SCFM
Pneumatic air 17 SCFM Sec/Primary = 1.0
U_r = 7.7 m/s Reactor T_r = 880°C

Gas sample	Sampling time, HR	Gas composition (a) N2O ppm	NOx ppm	O2 %	CO2 %	CO ppm	SO2 ppm
Flue gas stream:							
1.	14:35	8	160	3.6	18.0	34	15
2.	14:30	13	180	2.4	19.1	28	5
3.	14:46	<10	178	2.0	19.4	24	<3
4.	14:50	13	175	2.4	19.0	22	0
5.	14:54	14	180	2.6	18.7	22	0
	average: std. dev.	11.6 ±2.2	175 ±8	2.6 ±0.5	18.8 ±0.5	26 ±4.6	–
From outlet between cyclones							
6.	14:58	9	82	3.0	18.5	190	0
7.	15:04	≈5	85	3.3	18.1	198	20
8.	15:08	19	86	3.4	18.5	200	30
9.	15:11	13	78	3.7	18.3	200	30
10.	15:15	N/A	82	3.9	17.8	200	40
	average: std. dev.	11.5 ±5.2	82 ±3.	3.5 ±0.3	18.2 ±0.3	198 ±4.0	30 ±7.1

(a) N_2O by gas chromatographic analysis, all other gas species via on-line analysers

FIGURE 1 SOME TYPICAL N_2O AND NO_x ANALYSIS

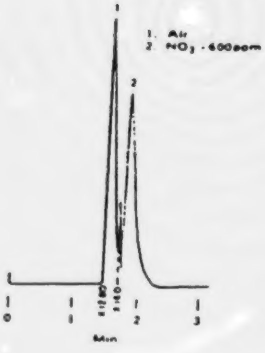

56
10% SF-96 on Fluoropak 80, 20′ × 1/8″ SS, 25°C, 84ml/min, N_2, EC.

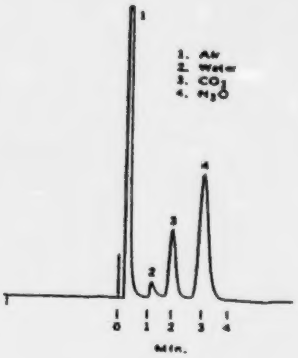

55
Carbosieve S, 60/80, 1.5′ × 1/8″ SS, 100°C, 40ml/min, He, TC.

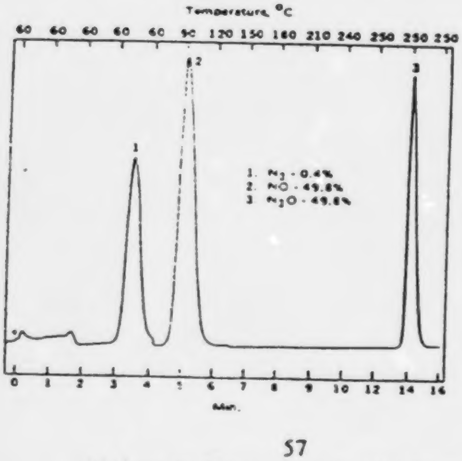

57
Molecular Sieve 5A (treated with NO), 6′ × 1/8″ SS, 4 min hold at 60°C, 30°C/min, to 250°C, 25ml/min, He, TC.

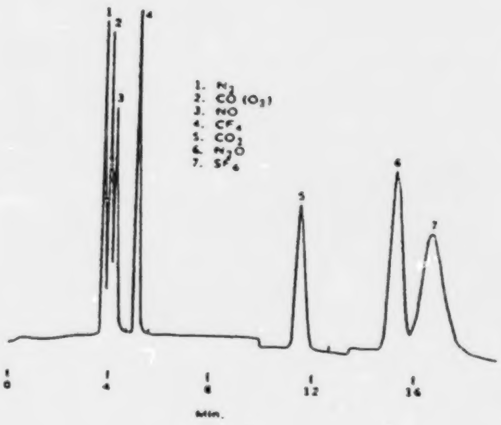

58
Chromosorb 102, 80/100, 20′ × 1/8″ SS, 35°C, 15ml/min, He, TC.

JOURNAL OF CHROMATOGRAPHIC SCIENCE•VOL SEPTEMBER 1978•387

FIGURE 2 LINEARITY CORRELATION OF TCD RESPONSE AND CONCENTRATION OF N_2O

Oct 24, 1988

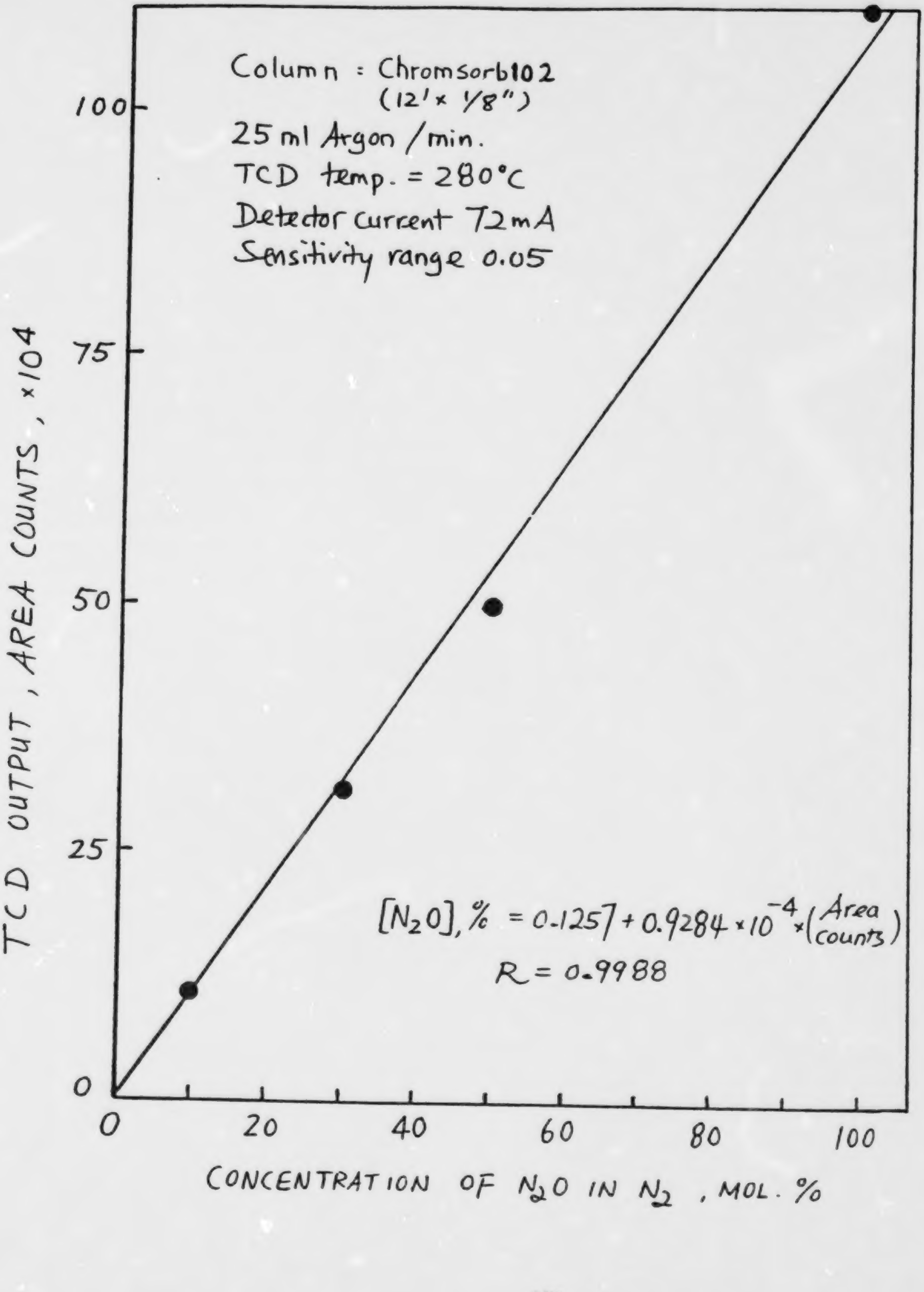

FIGURE 2B LINEARITY CORRELATION OF TCD RESPOND AND LOW CONCENTRATION OF N_2O

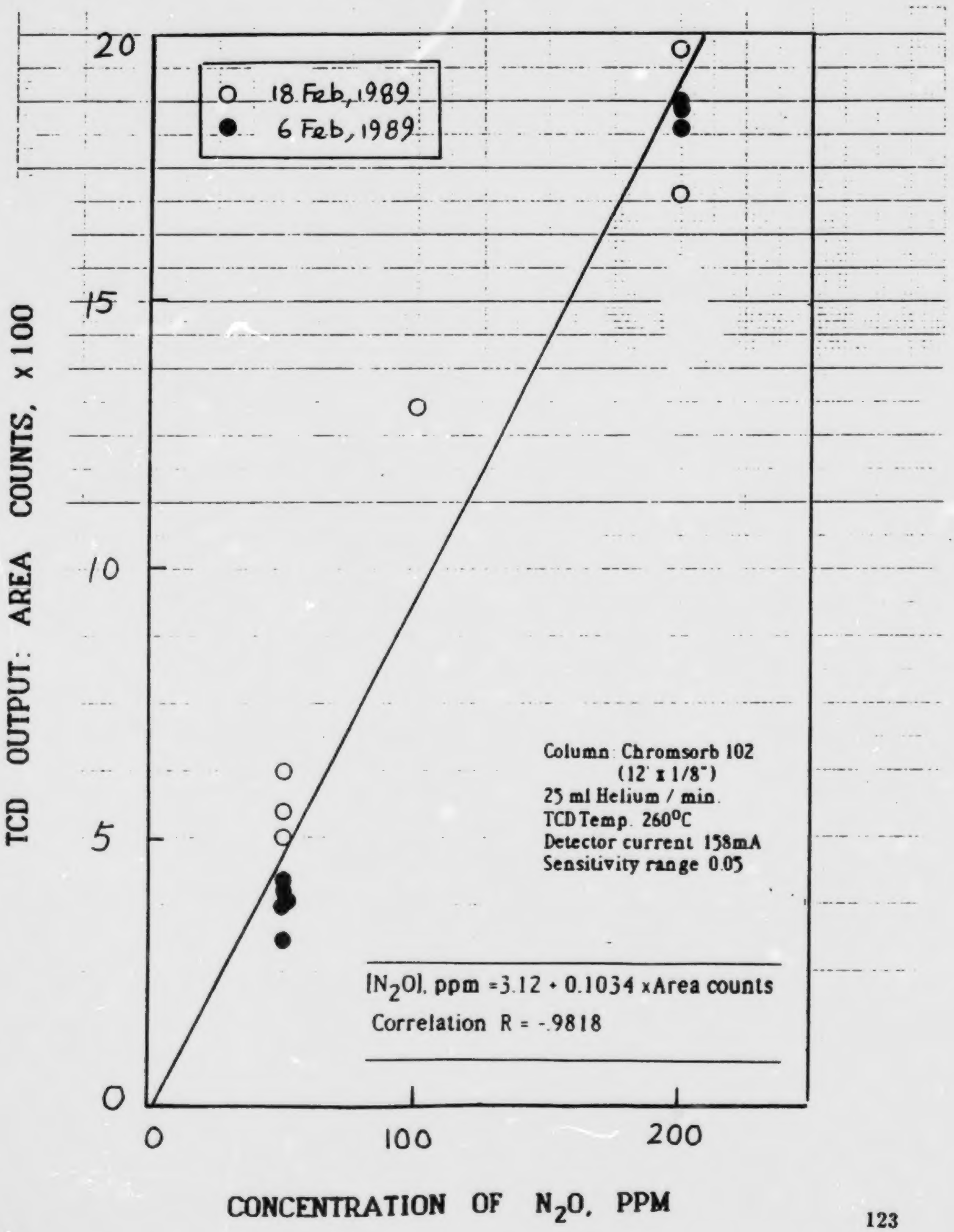

Column: Chromsorb 102
(12' x 1/8")
25 ml Helium / min.
TCD Temp. 260°C
Detector current 158mA
Sensitivity range 0.05

$[N_2O]$, ppm =3.12 + 0.1034 xArea counts
Correlation R = -.9818

FIGURE 3 N_2O ANALYSIS IN THE PRESENCE OF CO_2

(A)

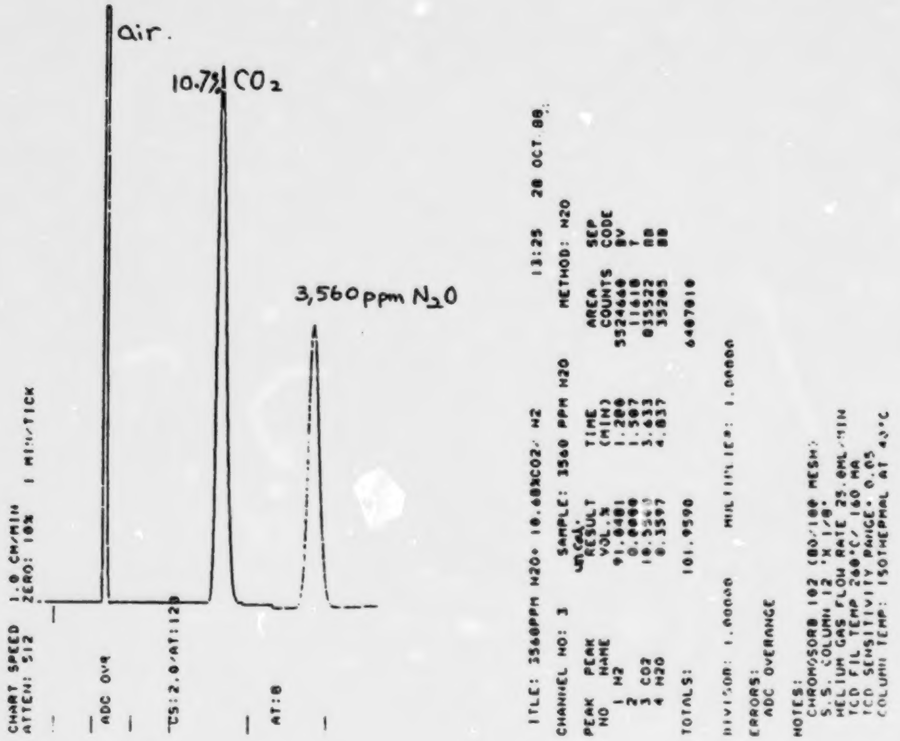

```
CHART SPEED  1.0 CM/MIN
ATTEN: 512   ZERO: 10%    1 MIN/TICK
ADC OVR
TS:2.0/AT:128
AT:8

ITLE: 3560PPM N20+ 10.68%CO2/ N2              13:25   28 OCT 80

CHANNEL NO: 3     SAMPLE: 3560 PPM N20     METHOD: N20
                  uncal.
PEAK  PEAK        RESULT       TIME         AREA     SEP
 NO   NAME        VOL.%        (MIN)        COUNTS   CODE
  1 N2            91.0401      1.200       5524660   BV
  2                0.0000      1.507         11618   T
  3 CO2           10.5560      3.633        835522   BB
  4 N20            0.3597      4.837         35205   BB

TOTALS:          101.9590                  6407010

DIVISOR: 1.00000     MULTIPLIER: 1.00000

ERRORS:
  ADC OVERANGE

NOTES:
  CHROMOSORB 102 (80/100 MESH)
  S.S. COLUMN 12 'X 1/8"
  HELIUM GAS FLOW RATE 25.0ML/MIN
  TCD FIL TEMP 260°C/ 160 MA
  TCD SENSITIVITY RANGE: 0.05
  COLUMN TEMP: ISOTHERMAL AT 40°C
```

(B)

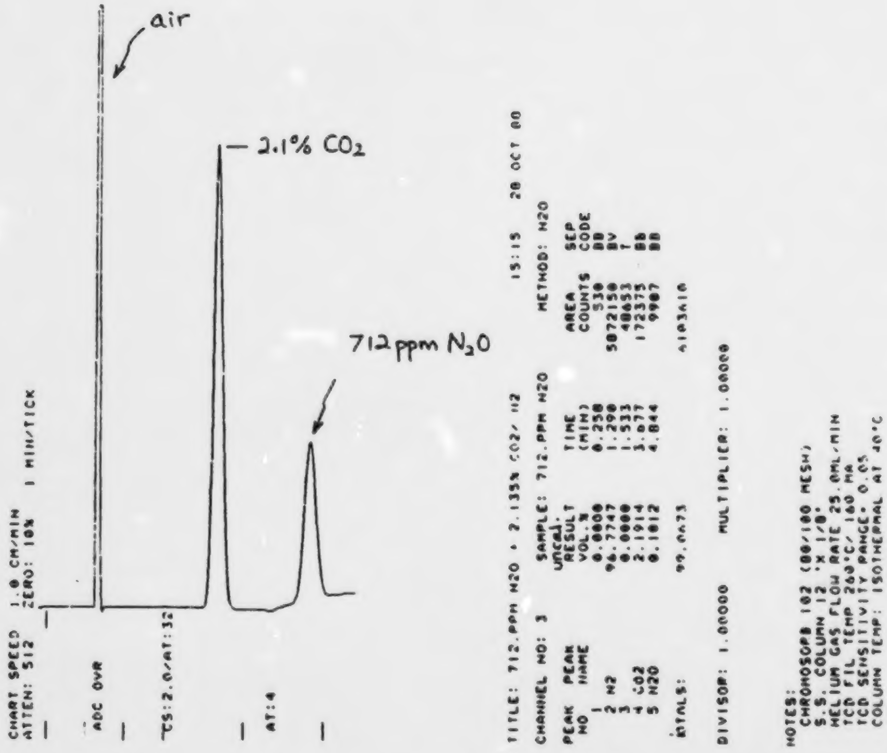

```
CHART SPEED  1.0 CM/MIN
ATTEN: 512   ZERO: 10%    1 MIN/TICK
ADC OVR
TS:2.0/AT:32
AT:4

TITLE: 712.PPM N20 + 2.135% CO2/ N2            15:15   28 OCT 80

CHANNEL NO: 3     SAMPLE: 712.PPM N20      METHOD: N20
                  uncal.
PEAK  PEAK        RESULT       TIME         AREA     SEP
 NO   NAME        VOL.%        (MIN)        COUNTS   CODE
  1                0.0000      0.250           530   BB
  2 N2            96.7747      1.290       5072150   BV
  3                0.0000      1.533         40653   T
  4 CO2            2.1914      3.677        172375   BB
  5 N20            0.1012      4.844          9907   BB

TOTALS:           99.0673                  6103610

DIVISOR: 1.00000     MULTIPLIER: 1.00000

NOTES:
  CHROMOSORB 102 (80/100 MESH)
  S.S. COLUMN 12 'X 1/8"
  HELIUM GAS FLOW RATE 25.0ML/MIN
  TCD FIL TEMP 260°C/ 160 MA
  TCD SENSITIVITY RANGE: 0.05
  COLUMN TEMP: ISOTHERMAL AT 40°C
```

FIGURE 4 LOW CONCENTRATION N_2O ANALYSIS IN THE PRESENCE OF CO_2

(A)

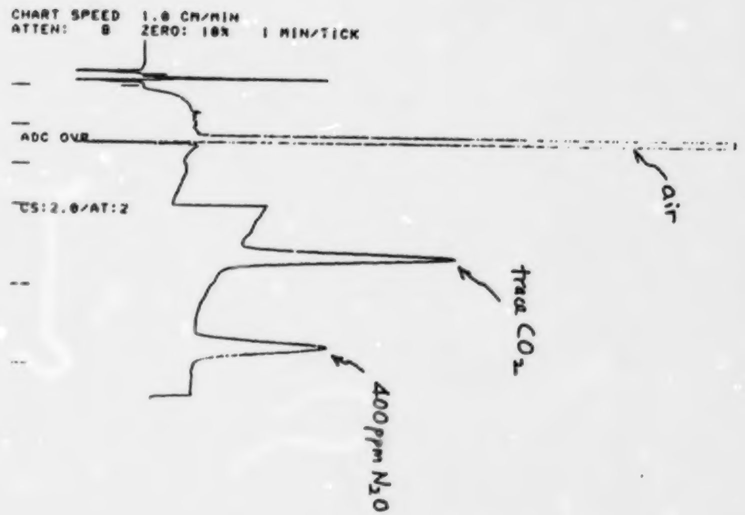

```
TITLE: LOW CONCN. N2O IN NITROGEN            17:48   28 OCT 88

CHANNEL NO: 3     SAMPLE: 400.PPM N2O     METHOD: N2O
                  uncal.
PEAK  PEAK        RESULT       TIME         AREA    SEP
 NO   NAME        VOL.%        (MIN)        COUNTS  CODE
   1              0.0000       0.653          273   BB
   2 N2          96.4313       1.267      5851310   BV
   3              0.0020       1.527        66086   T
   4 CO2          0.0658       3.642         5178   BB
   5 N2O          0.0421       4.789         4123   BB

TOTALS:          96.5392                  5926978

DIVISOR: 1.00000     MULTIPLIER: 1.00000


NOTES:
  CHROMOSORB 102 (80/100 MESH)
  S.S. COLUMN 12 'X 1/8"
  HELIUM GAS FLOW RATE 25.0ML/MIN
  TCD FIL TEMP 260°C/ 100 MA
  TCD SENSITIVITY RANGE= 0.05
  COLUMN TEMP: ISOTHERMAL AT 40°C
```

(B)

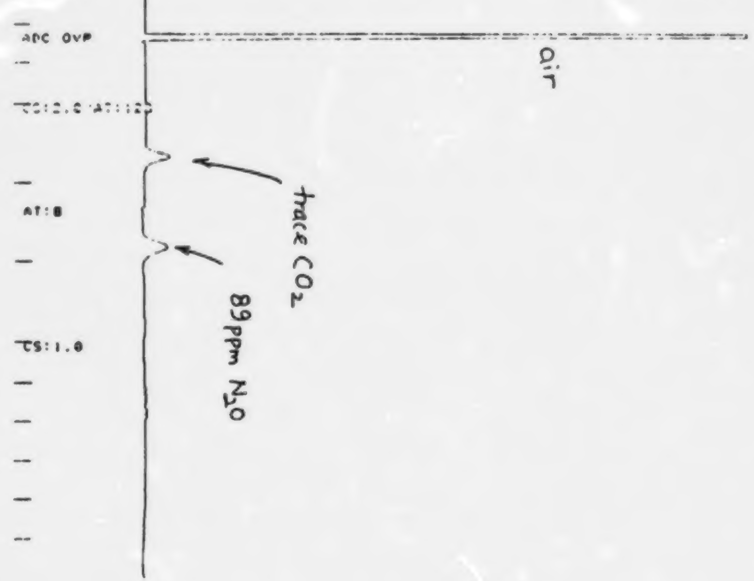

```
TITLE: 89.PPM N2O + 2670PPM CO2 / N2          16:18   28 OCT 88

CHANNEL NO: 3     SAMPLE: 89.PPM N2O      METHOD: N2O
                  uncal.
PEAK  PEAK        RESULT       TIME         AREA    SEP
 NO   NAME        VOL.%        (MIN)        COUNTS  CODE
   1              0.0000       0.697          336   BB
   2 N2          96.5646       1.270      5859390   BV
   3              0.0000       1.512        29267   T
   4 CO2          0.4538       3.665        35696   BB
   5 N2O          0.0299       4.819         2927   BB

TOTALS:          97.0483                  5927620

DIVISOR: 1.00000     MULTIPLIER: 1.00000

ERRORS:
  ADC OVERANGE

NOTES:
  CHROMOSORB 102 (80/100 MESH)
  S.S. COLUMN 12 '/ 1/8"
  HELIUM GAS FLOW RATE 25.0ML/MIN
  [illegible]
```

FIGURE 5 N_2O ANALYSIS IN THE PRESENCE OF NO_x

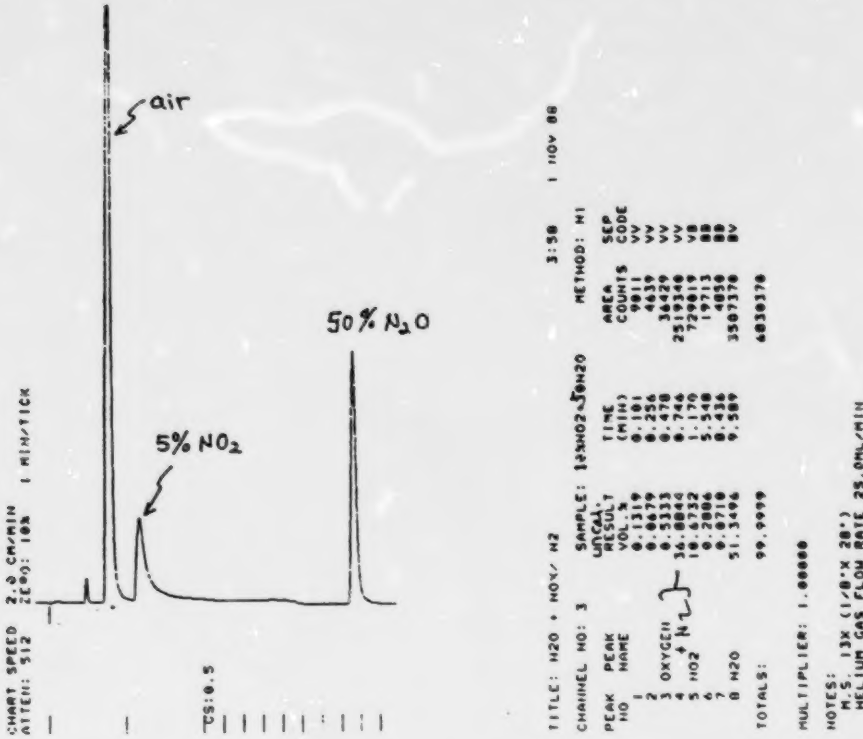

```
CHART SPEED  2.0 CM/MIN
ATTEN: 512   ZERO: 10%   1 MIN/TICK

TITLE: H20 + NOX/ N2                                    3:58     1 NOV 88

CHANNEL NO: 3      SAMPLE: 12%NO2+50%N20      METHOD: N1
                   uncal.
PEAK  PEAK         RESULT       TIME           AREA    SEP
 NO   NAME         VOL.%        (MIN)          COUNTS  CODE
   1               0.1319       0.101          9011    VV
   2               0.0679       0.256          4639    VV
   3 OXYGEN  }     0.5333       0.478          36429   VV
   4      + N2 }- 36.0044       0.746        2519340   VV
   5 NO2          10.6732       1.179         729019   VB
   6               0.2006       5.548          19713   BB
   7               0.0710       0.436           4050   BB
   8 N20          51.3496       9.509        3507370   BV

TOTALS:           99.9999                    6830370

MULTIPLIER: 1.00000

NOTES:
  M.S. 13X (1/8"X 20')
  HELIUM GAS FLOW RATE 25.0ML/MIN
  TCD FIL. TEMP 260°C/ 150MA
  TCD SENSITIVITY RANGE- 0.05
  COLUMN TEMP: 40°C/4M- R-30°C/M- 160°C
```

FIGURE 6 ANALYSIS OF 1000ppm N_2O

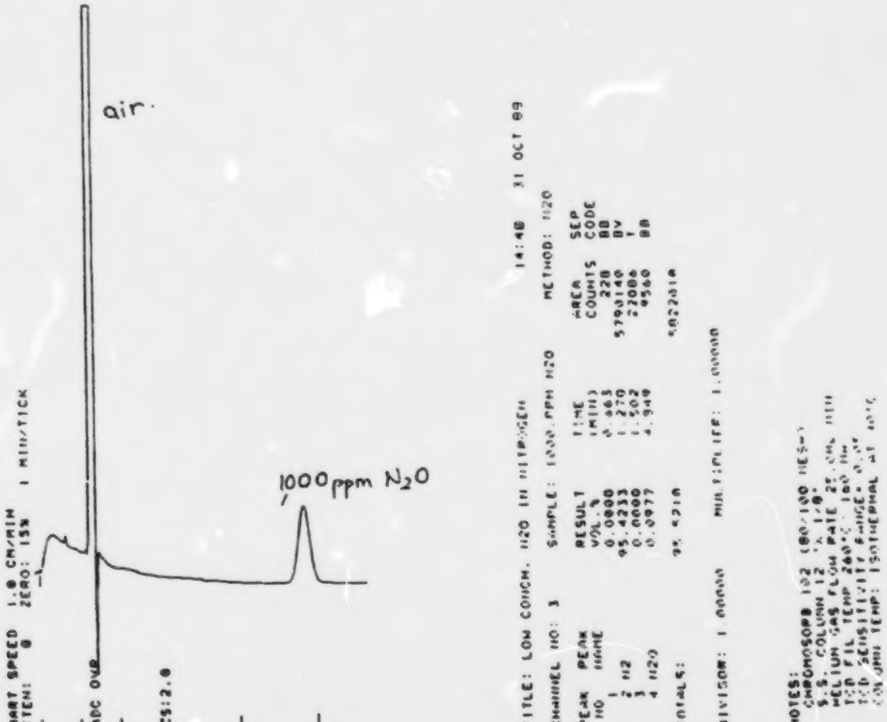

```
CHART SPEED  1.0 CM/MIN
ATTEN:   0   ZERO: 15%   1 MIN/TICK

TITLE: LOW CONCN. N20 IN NITROGEN                    14:48    31 OCT 89

CHANNEL NO: 3      SAMPLE: 1000.PPM N20      METHOD: N20

PEAK  PEAK         RESULT       TIME           AREA    SEP
 NO   NAME         VOL.%        (MIN)          COUNTS  CODE
   1               0.0000       0.663            220   BB
   2 N2           95.4233       1.270        5790140   BV
   3               0.0000       1.502          22006   T
   4 N20           0.0977       4.949           9560   BB

TOTALS:           95.5210                    5822010

DIVISOR: 1.00000      MULTIPLIER: 1.00000

NOTES:
  CHROMOSORB 102 (80/100 MES-)
  S.S. COLUMN 12 'X 1/8'
  HELIUM GAS FLOW RATE 25.0ML MIN
  TCD FIL TEMP 260°C  160 MA
  TCD SENSITIVITY RANGE- 0.05
  COLUMN TEMP: ISOTHERMAL AT 40°C
```

FIGURE 7 N_2O ANALYSIS OF FLUE GAS FROM CFB TEST RUN OF 3 NOVEMBER, 1988

(A) 100 ppm N_2O Calibration

```
CHART SPEED   1.0 CM/MIN
ATTEN:    4   ZERO: 10%    1 MIN/TICK
```

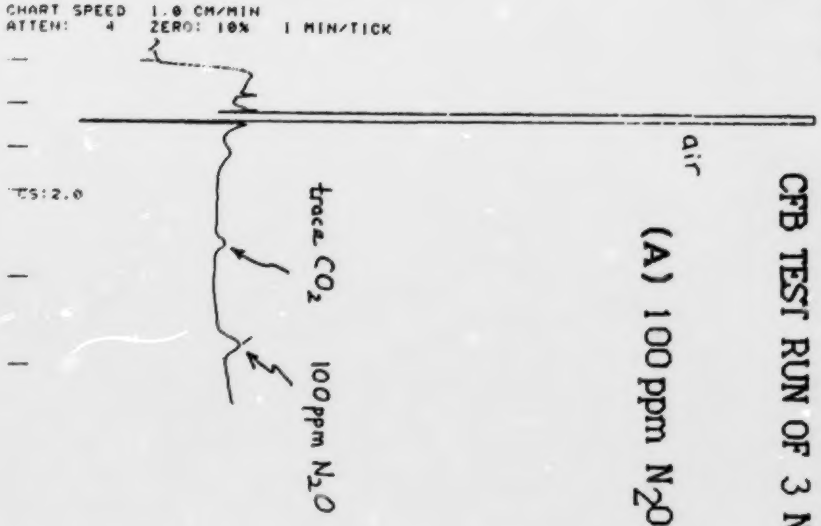

```
RECALC
TITLE: FLUE GAS ANALYSIS                          20:14    3 [illegible] 88

CHANNEL NO: 3       SAMPLE: 100.PPM N2O        METHOD: N2
                    unnml.
PEAK  PEAK          RESULT        TIME            AREA    SEP
 NO   NAME          VOL.%         (MIN)           COUNTS  CODE
   1                0.0050        0.000              289  BB
   2     air —     99.6951        1.227          5794960  BV
   3                0.2812        1.459            16347  T
   4     N2O —      0.0107        4.755             1086  BB

TOTALS:           100.0000                       5812680

MULTIPLIER: 1.00000

NOTES:
  CHROMSORB 102 (12'X1/8")
  HELIUM GAS FLOW RATE 25.0ML/MIN
  TCD FIL. TEMP 260°C/ 150MA
  TCD SENSITIVITY RANGE= 0.05
  COLUMN TEMPERATURE: ISOTHERMAL AT 40°C
```

(B) Analysis of Sample #1

```
CHART SPEED   1.0 CM/MIN
ATTEN:    4   ZERO: 10%    1 MIN/TICK
```

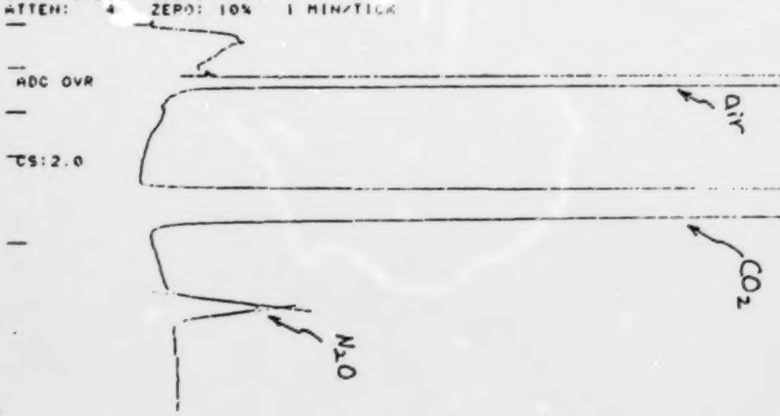

```
TITLE: FLUE GAS ANALYSIS                          21:10    3 NOV 88

CHANNEL NO: 3       SAMPLE: #1/1655 HP D       METHOD: N2

PEAK  PEAK          RESULT        TIME            AREA    SEP
 NO   NAME          VOL.%         (MIN)           COUNTS  CODE
   1                0.0065        1.001              451  BV
   2                0.0063        1.147              439  VV
   3 O2+N2         78.2178        1.233          5415160  VB
   4 CO2          21.6931        3.498          1501060  BB
   5 N2O            0.0762        4.709             5275  BB

TOTALS:            99.9999                       6923180

MULTIPLIER: 1.00000

NOTES:
  CHROMSORB 102 (12'X1/8")
  HELIUM GAS FLOW RATE 25.0ML/MIN
  TCD FIL. TEMP 260°C/ 150MA
  TCD SENSITIVITY RANGE= 0.05
  COLUMN TEMPERATURE: ISOTHERMAL AT 40°C
```

FIGURE 7

(C) Analysis of Sample #4

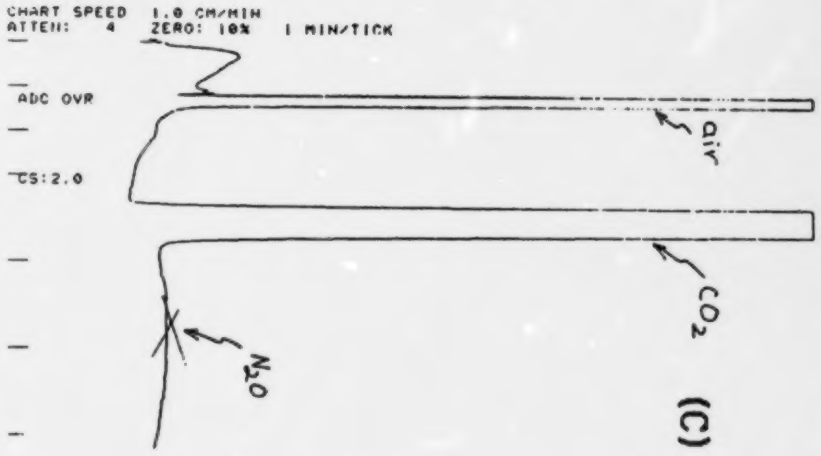

```
TITLE: FLUE GAS ANALYSIS                                  21:31    3 NOV

CHANNEL NO: 3      SAMPLE: #4/1704 HR A      METHOD: N2

PEAK  PEAK          RESULT      TIME          AREA    SEP
 NO   NAME          VOL.%       (MIN)         COUNTS  CODE
   1                0.0069      1.072           483   BV
   2                0.0061      1.137           427   VV
   3 O2+N2         78.4821      1.223       5454260   VB
   4 CO2           21.5048      3.486       1494520   BB

TOTALS:            99.9999                  6949690

MULTIPLIER: 1.00000


 OTES:
  CHROMSORB 102 (12'X1/8")
  HELIUM GAS FLOW RATE 25.0ML/MIN
  TCD FIL. TEMP 260°C/ 150MA
  TCD SENSITIVITY RANGE- 0.05
  COLUMN TEMPERATURE: ISOTHERMAL AT 40°C
```

(D) Analysis of Sample #5

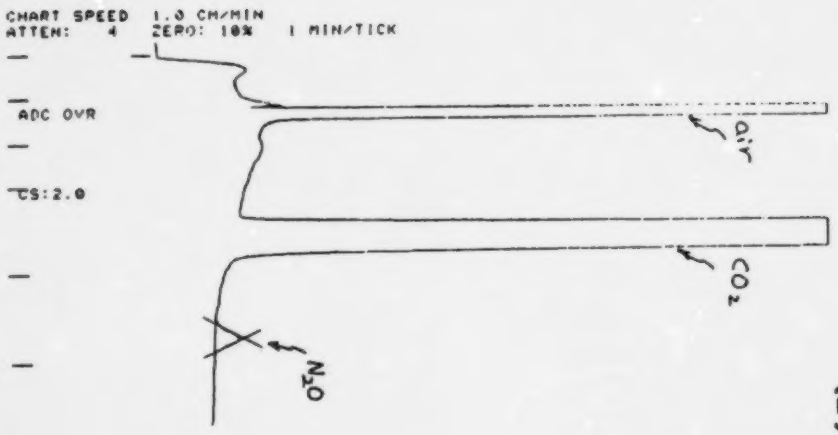

```
TITLE: FLUE GAS ANALYSIS                                  20:46    3 NOV 83

CHANNEL NO: 3      SAMPLE: #5/1710HR B        METHOD: N2
                   uncal.
PEAK  PEAK          RESULT      TIME          AREA    SEP
 NO   NAME          VOL.%       (MIN)         COUNTS  CODE
   1                0.0125      1.147           852   BV
   2     air -     83.9165      1.233       5730290   VB
   3     CO2 -     16.0511      3.526       1096060   BB
   4     N2O -      0.0198      4.719          1354   BB

 OTALS:            99.9999                  6828560

MULTIPLIER: 1.00000


NOTES:
  CHROMSORB 102 (12'X1/8")
  HELIUM GAS FLOW RATE 25.0ML/MIN
  TCD FIL. TEMP 260°C/ 150MA
  TCD SENSITIVITY RANGE- 0.05
  COLUMN TEMPERATURE: ISOTHERMAL AT 40°C
```

FIGURE 8 N_2O ANALYSIS USING A MOLECULAR SIEVE 13X COLUMN

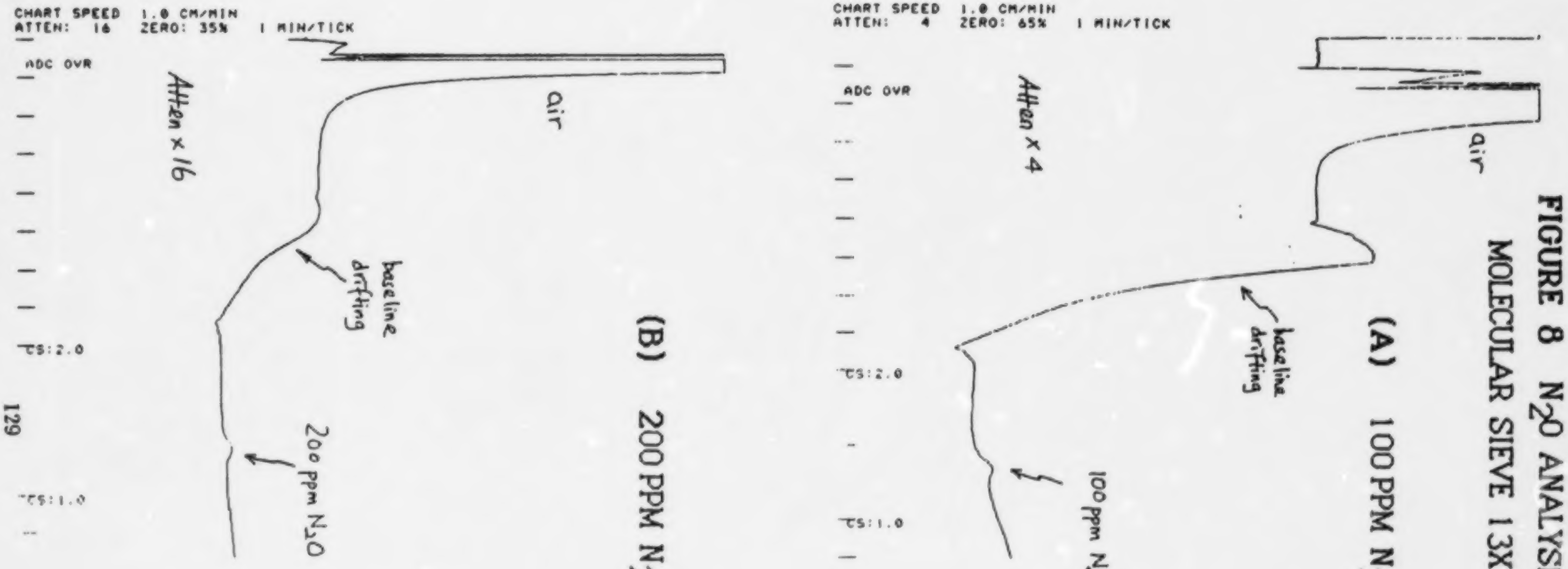

(A) 100 PPM N_2O

```
TITLE: FLUE GAS ANALYSIS                          19:33

CHANNEL NO: 3      SAMPLE: 100.PPM N2O      METHOD: N2O
                   uncal.
PEAK  PEAK         RESULT       TIME          AREA    SEP
 NO   NAME         VOL.%        (MIN)         COUNTS  CODE
   1               0.0000       0.060           1894  BV
   2               0.0000       0.117          16178  VV
   3 OXYGEN        0.3079       0.430          27543  VV
   4 NITROGEN     90.0735       0.587        6998950  VB

TOTALS:           90.3814                    7044560

DIVISOR: 1.00000      MULTIPLIER: 1.00000
```

(B) 200 PPM N_2O

```
TITLE: NITROUS OXIDE CALIBRATION                 14:13     3 NOV 83

CHANNEL NO: 3      SAMPLE: 200.PPM N2O      METHOD: N2O
                   uncal.
PEAK  PEAK         RESULT       TIME          AREA    SEP
 NO   NAME         VOL.%        (MIN)         COUNTS  CODE
   1               0.0000       0.059           1884  BV
   2               0.0000       0.101          15000  VV
   3 OXYGEN        0.4625       0.419          33036  VV
   4 N2          103.9010       0.500        6992700  VB
   5 N2O           0.0301       5.3[illegible]          2699  BB

TOTALS:          104.3940                    7045330

DIVISOR: 1.00000      MULTIPLIER: 1.00000
```

FIGURE 9

N_2O ANALYSIS FOR CFB TEST RUN OF 6 FEBRUARY, 1989

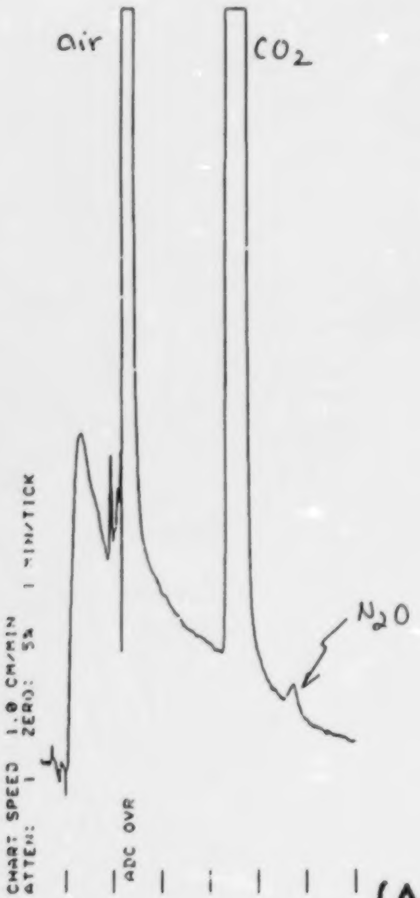

(A) Sample \#3

```
TITLE: N20 ANALYSIS: FLUE GAS/ JRG              19:53     6 FEB 89
CHANNEL NO: 3       SAMPLE: =3/ FLUE GAS        METHOD: TC
                     uncal.
PEAK  PEAK           RESULT        TIME          AREA      SEP
 NO   NAME           VOL.%         (MIN)         COUNTS    CODE
  1                0.183643        0.303          13479    BV
  2                0.018802        0.945           1380    VV
  3                0.019033        1.087           1397    VV
  4                0.009265        1.148            680    VV
  5                78.50560        1.237        5762130    VB
  6                21.26370        3.523        1560700    BB

TOTALS:            100.0000                     7339770
```

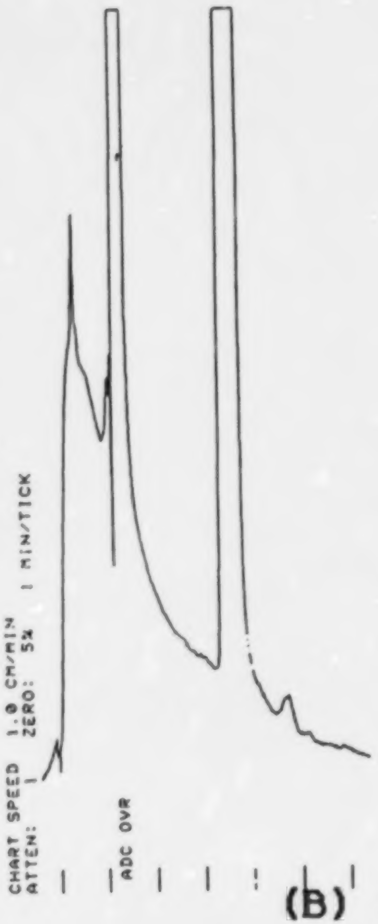

(B) Sample \#2

```
TITLE: N20 ANALYSIS: FLUE GAS/ JRG              18:48     6 FEB 89
CHANNEL NO: 3       SAMPLE: =2/ FLUE GAS        METHOD: TC
                     uncal.
PEAK  PEAK           RESULT        TIME          AREA      SEP
 NO   NAME           VOL.%         (MIN)         COUNTS    CODE
  1                0.189714        0.387          13951    BV
  2                0.103037        0.617           7577    VV
  3                0.040089        1.087           2948    VV
  4                0.015693        1.151           1154    VV
  5                77.78540        1.237        5720110    VB
  6                21.85960        3.526        1607490    BB
  7                0.006473        4.733            476    BB

TOTALS:            100.0000                     7353710
```

FIGURE 9

N_2O ANALYSIS FOR CFB TEST RUN OF 6 FEBRUARY, 1989

(C) Sample #4

```
CHART SPEED  1.0 CM/MIN
ATTEN:   1    ZERO:  5%    1 MIN/TICK
```

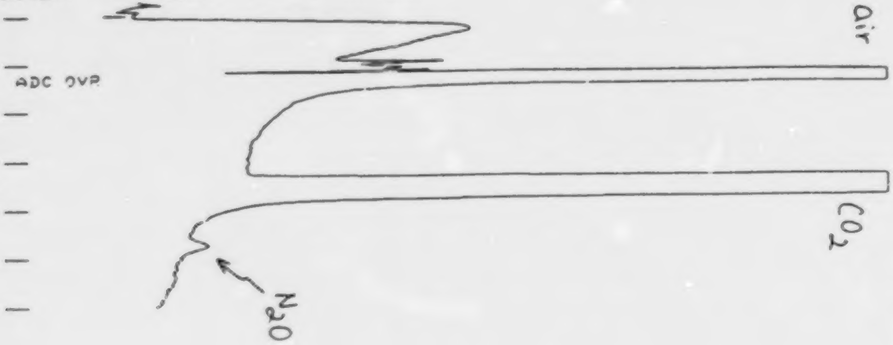

```
TITLE: N20 ANALYSIS: FLUE GAS/ JPG              20:25    6 FEB 39

CHANNEL NO: 3      SAMPLE: #4 / FLUE GA      METHOD: TC
                   uncal.
PEAK  PEAK         RESULT         TIME            AREA     SEP
 NO   NAME         VOL.%          (MIN)           COUNTS   CODE
   1             0.198115        0.307            14619    BV
   2             0.018946        0.931             1398    VV
   3             0.016018        1.094             1192    VV
   4             0.006917        1.149              658    VV
   5             76.29960        1.237          5630190    VB
   6             23.45390        3.517          1730670    BB
   7             0.004526        4.731              334    BB

TOTALS:          100.0000                       7379050
```

(D) 50ppm N_2O

```
CHART SPEED  1.0 CM/MIN
ATTEN:   1    ZERO: 20%    1 MIN/TICK
```

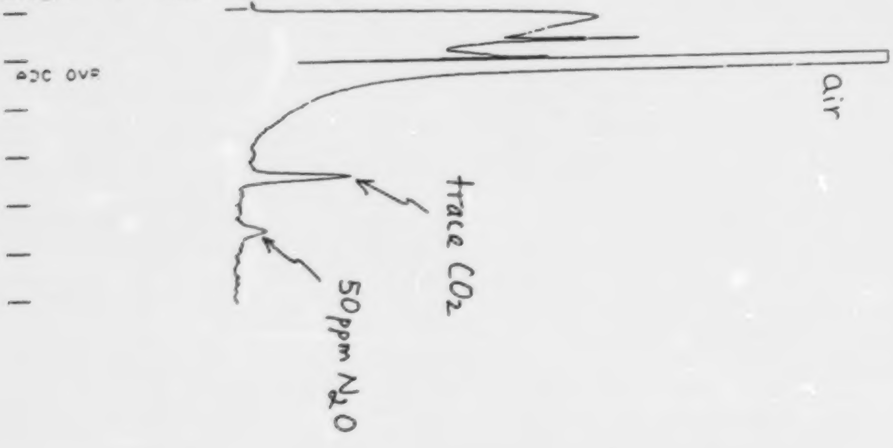

```
TITLE: N20 ANALYSIS: FLUE GAS/ JRG              16:16    7 FEB 89

CHANNEL NO: 3      SAMPLE: 50.PPM N20       METHOD: TC
                   uncal.
PEAK  PEAK         RESULT         TIME           AREA     SEP
 NO   NAME         VOL.%          (MIN)          COUNTS   CODE
   1             0.221505        0.337           13382    BV
   2             0.066111        0.785            3994    VV
   3             0.048598        1.130            2936    VV
   4             99.63660        1.213         5019440    VB
   5             0.020426        3.532            1234    BB
   6             0.006787        4.646             410    BB

TOTALS:          100.0000                      5841400

MULTIPLIER: 1.00000


NOTES:
  HE 25.0ML/MIN: 80PSI
  CHROMOSOPB 102(12'X 1/8')
  TCD: SEN RANGE 0.05/ TEMP-260. 150MA
```

FIGURE 9

N_2O ANALYSIS FOR CFB TEST RUN OF 6 FEBRUARY, 1989

(E) Duplicated Analysis for Sample *6

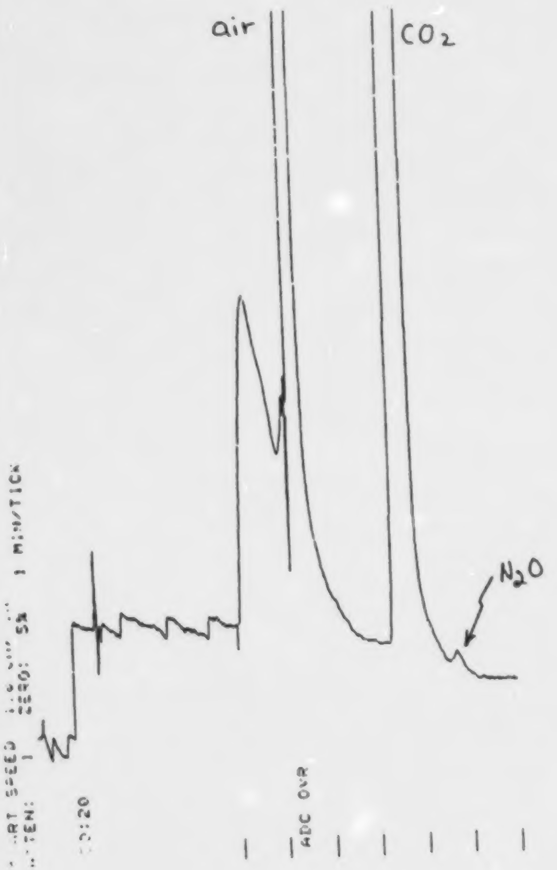

```
TITLE: N2O ANALYSIS: FLUE GAS/ JRG              21:11      6 FEB 89

CHANNEL NO: 3       SAMPLE: =6/ BTW. CYL      METHOD: TC
                    uncal.
PEAK  PEAK          RESULT       TIME          AREA     SEP
 NO   NAME          VOL.%        (MIN)         COUNTS   CODE
                    0.241809     0.324         17807    BV
  1                 0.032401     1.090          2386    VV
  2                 0.011923     1.1<7           878    VV
  3                77.06080      1.257       5674810    VB
  4         CO2 -  22.64990      3.522       1667950    BB
  5         N2O  -  0.003123     4.725           230    BB
  6

TOTALS:           100.0000                   7364060
```

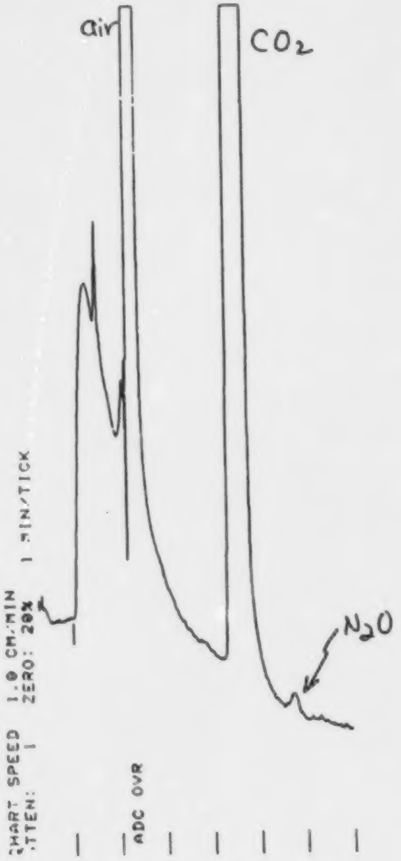

```
TITLE: N2O ANALYSIS: FLUE G-S/ JRG              21:24      6 FEB 8°

CHANNEL NO: 3       SAMPLE: =6/ BTW. CYL      METHOD: TC
                    uncal.
PEAK  PEAK          RESULT       TIME          AREA     SEP
 NO   NAME          VOL.%        (MIN)         COUNTS   CODE
                    0.124352     0.322          9160    BV
  1                 0.123850     0.550          9123    VV
  2                 0.037659     1.090          2774    VV
  3                 0.012788     1.152           942    VV
  4                77.01050      1.240       5672730    VV
  5         CO2 -  22.68760      3.517       1671210    BB
  6         N2O -   0.003272     4.738           241    BB
  7

TOTALS:           100.0000                   7366180
```

FIGURE 10

N_2O ANALYSIS FOR CFB TEST RUN OF 18 FEBRUARY, 1989

(A) 50 and 100ppm N_2O Calibration

```
NOTES:
 HE 25.0ML/MIN: 80PSI
 CHROMOSORB 102(12'X 1/8")
 TCD: SEN RANGE 0.05/ TEMP-260. 158MA
```

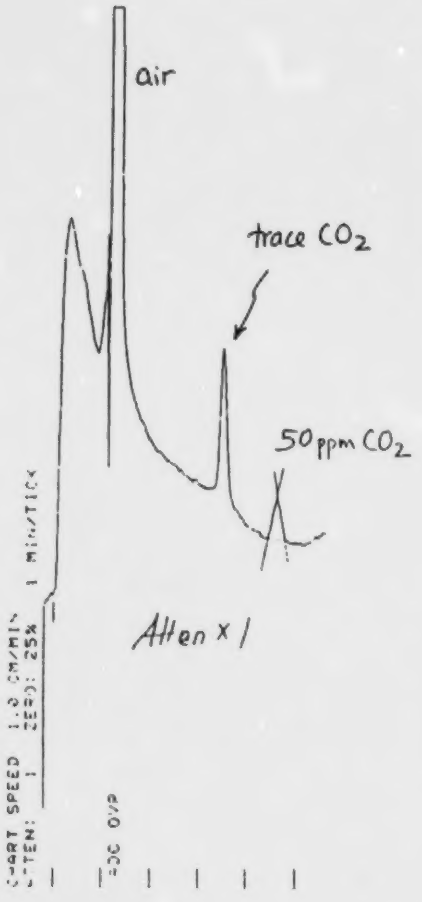

```
TITLE: N20 ANALYSIS: FLUE GAS/ JRG             20:57   18 FEB 89

CHANNEL NO: 3      SAMPLE: 50.PPM N20        METHOD: TC
                   uncal
PEAK   PEAK        RESULT        TIME          AREA     SEP
 NO    NAME        VOL.%         (MIN)         COUNTS   CODE
  1                0.175869      0.326          10118   BV
  2                0.117031      0.530           6733   VV
  3                0.056543      1.103           3253   VV
  4                99.60880      1.183        5730650   VV
  5                0.030922      3.513           1779   BB
  6                0.010864      4.631            625   BB

TOTALS:            100.0000                   5753160
```

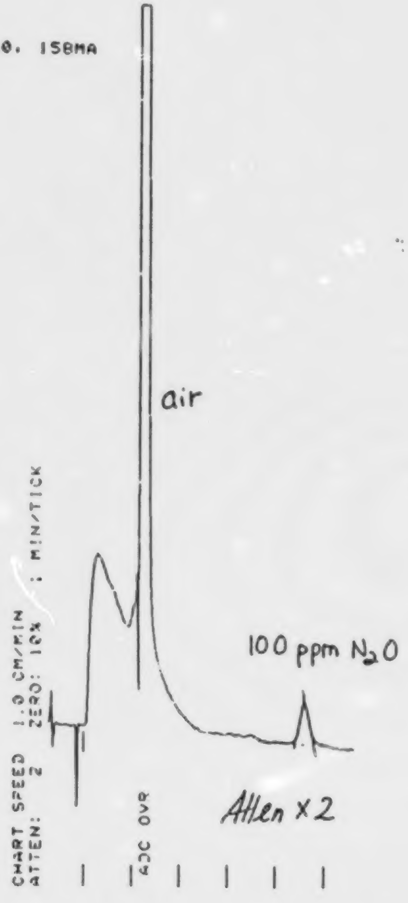

```
TITLE: N20 ANALYSIS: FLUE GAS/ JRG             15:56   18 FEB 89

CHANNEL NO: 3      SAMPLE: 100 PPM N20       METHOD: TC
                   uncal.
PEAK   PEAK        RESULT        TIME          AREA     SEP
 NO    NAME        VOL.%         (MIN)         COUNTS   CODE
  1                0.301926      0.300          17376   BV
  2                0.061737      1.111           3553   VV
  3                99.61370      1.193        5732820   VB
  4                0.022676      4.614           1305   BB

TOTALS:            100.0000                   5755050
```

FIGURE 10

N_2O ANALYSIS FOR CFB TEST RUN OF 18 FEBRUARY, 1989

(B) Sample #2

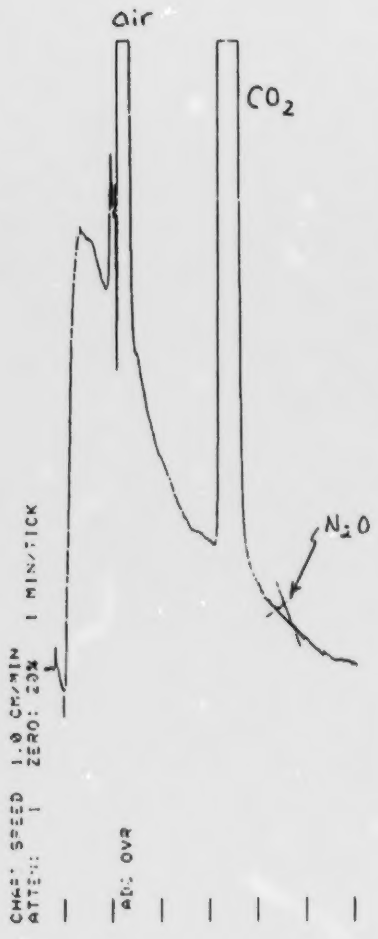

```
TITLE: N2O ANALYSIS: FLUE GAS/ JRG            18:55   18 FEB 89

CHANNEL NO: 3      SAMPLE: #2/1440HR/FL      METHOD: TC
                   uncal.
PEAK  PEAK         RESULT       TIME         AREA      SEP
 NO   NAME         VOL.%        (MIN)        COUNTS    CODE
  1                0.026528     0.385          1824    BB
  2                0.016609     1.030          1142    BV
  3                0.007737     1.106           532    VV
  4                79.10900     1.209       5439350    VV
  5                20.84010     3.412       1432920    BB

TOTALS:            100.0000                 6875770
```

(C) Sample #5

```
NOTES:
  HE 25.0ML/MIN: 60PSI
  CHROMOSOPB 102(12'X 1/8")
  TCD: SEN RANGE 0.05, TEMP-200. 150MA
```

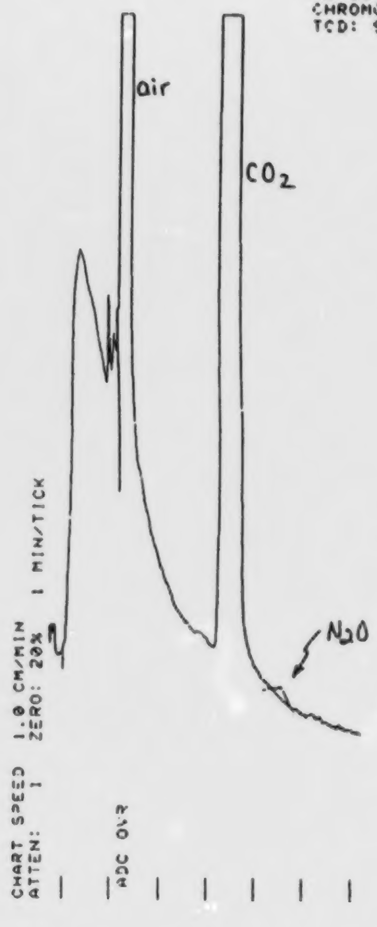

```
TITLE: N2O ANALYSIS: FLUE GAS/ JRG            18:28   18 FEB 89

CHANNEL NO: 3      SAMPLE: #5/1454HR/FL      METHOD: TC
                   uncal.
PEAK  PEAK         RESULT       TIME         AREA      SEP
 NO   NAME         VOL.%        (MIN)        COUNTS    CODE
  1                0.270512     0.335         18727    BV
  2                0.030797     0.946          2132    VV
  3                0.026622     1.053          1843    VV
  4                0.015326     1.117          1061    VV
  5                78.23900     1.200       5416330    VV
  6                21.41770     3.411       1482710    BB

TOTALS:            100.0000                 6922800
```

FIGURE 10

N_2O ANALYSIS FOR CFB TEST RUN OF 18 FEBRUARY, 1989

(D) Sample *9

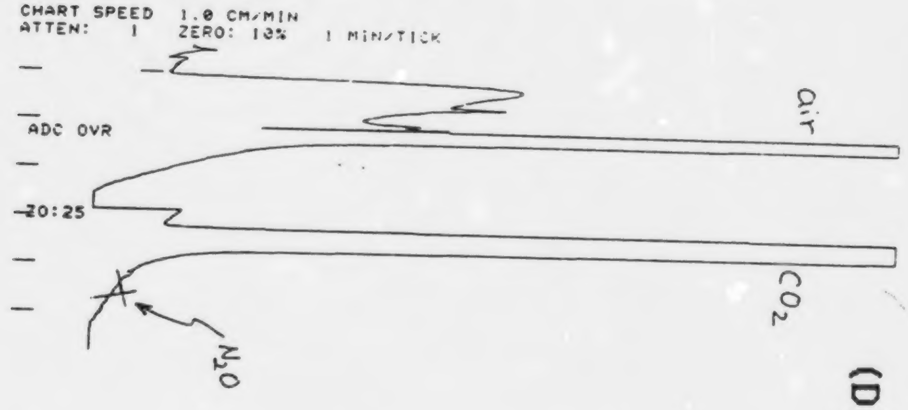

```
TITLE: N2O ANALYSIS: FLUE GAS/ JRG                 22:25    18 FEB 89

CHANNEL NO: 3        SAMPLE: #9/1511HR/CY       METHOD: TC
                     uncal.
PEAK  PEAK           RESULT       TIME          AREA     SEP
 NO   NAME           VOL.%        (MIN)         COUNTS   CODE
  1                  0.187518     0.291         12918    BV
  2                  0.091480     0.687          6302    VV
  3                  0.034926     1.050          2406    VV
  4                  0.017172     1.113          1183    VV
  5                  81.36520     1.197       5605180    VB
  6                  18.30370     3.424       1260930    BB

TOTALS:              100.0000                 6888920

MULTIPLIER: 1.00000


NOTES:
  HE 25.0ML/MIN: 80PSI
  CHROMOSORB 102(12'X 1/8")
  TCD: SEN RANGE 0.05/ TEMP-260. 150MA
```

Appendix B

Output of Computer Program for Predictions of Axial Density Profiles in Riser

```
            CIRCULATING FLUIDIZED BED RISER DENSITY PROFILE
            -----------------------------------------------

            RUN RESULTS OF PROGRAM DENBED,VERSION 2.9


COMBUSTOR: UBC
CASE     : R21:HYDRODYNAMIC RUN :U=6.7 M/S,GS=21KG/M**2.S

MEAN COMBUSTOR GAS TEMPERATURE=     1143.0         DEG.C
MEAN COMBUSTOR GAS PRESSURE=      101325.0         PA
GAS DENSITY AT COMBUSTOR TEMP=         0.309       KG/M**3
GAS VISC. AT COMBUSTOR TEMP=           0.453E-04   KG/M.S
BED PARTICLE DENSITY=               2500.0         KG/M**3
SAUTER MEAN PARTICLE SIZE=             0.219       MM
RISER CROSS SECTIONAL AREA=            0.02320     M**2
MIN. WALL STREAMER THICKNESS FOR
      100% WALL COVERAGE=             0.012        M
WALL STREAMER MEAN VELOCITY=         -1.20         M/S
RISER TOP REFLECTION COEFFICIENT=      0.83


         BULK DENSITIES,KG/M**3
         ----------------------

PRIMARY ZONE AT SOLIDS RECIRCULATION ENTRY POINT     457.9
PRIMARY ZONE AT FUEL FEED LOCATION                   178.5
MEAN PRIMARY ZONE BULK DENSITY                       309.4
MEAN CORE ZONE                                        12.5
WALL STREAMER ZONE                                  1000.0
MEAN SECONDARY ZONE                                   52.6
MEAN FOR ENTIRE RISER                                 74.9
RISER EXIT REGION                                    106.6

       HEIGHT ABOVE      CORE        STREAMERS       FULL CSA
       SEC.AIR
          M            KG/M**3       KG/M**3         KG/M**3
         0.00            27.9         1000.0          129.1
         0.32            20.0         1000.0           91.1
         0.64            14.6         1000.0           63.8
         0.96            11.4         1000.0           47.1
         1.28            10.0         1000.0           39.3
         1.60            10.0         1000.0           39.4
         1.92            10.0         1000.0           39.4
         2.24            10.0         1000.0           39.6
         2.56            10.1         1000.0           39.7
         2.88            10.1         1000.0           40.0
         3.20            10.2         1000.0           40.3
         3.52            10.3         1000.0           40.8
         3.84            10.4         1000.0           41.5
         4.16            10.6         1000.0           42.5
         4.48            10.9         1000.0           44.0
         4.80            11.3         1000.0           46.2
         5.12            11.9         1000.0           49.6
         5.44            12.9         1000.0           54.8
         5.76            14.5         1000.0           63.3
         6.08            17.4         1000.0           78.0
         6.40            23.1         1000.0          106.6
```

CIRCULATING FLUIDIZED BED RISER DENSITY PROFILE cont.

MASS FLUX COEFFICIENTS,M/S

HEIGHT ABOVE SEC. AIR M	CORE TO STREAMERS M/S	STREAMERS TO CORE M/S
0.00	0.6382	0.0142
0.32	0.5462	0.0099
0.64	0.4347	0.0071
0.96	0.3183	0.0055
1.28	0.2117	0.0050
1.60	0.2117	0.0051
1.92	0.2117	0.0051
2.24	0.2117	0.0051
2.56	0.2117	0.0051
2.88	0.2117	0.0051
3.20	0.2117	0.0052
3.52	0.2117	0.0053
3.84	0.2117	0.0054
4.16	0.2117	0.0055
4.48	0.2117	0.0058
4.80	0.2117	0.0061
5.12	0.2117	0.0067
5.44	0.2117	0.0075
5.76	0.2117	0.0090
6.08	0.2117	0.0119

STREAMER CROSS SECTIONAL AREA AND WALL COVERAGE

HEIGHT ABOVE SEC. AIR M	STREAMER AREA M**2	STREAMER WALL COVERAGE %
0.00	0.0024	0.65
0.32	0.0017	0.54
0.64	0.0012	0.45
0.96	0.0008	0.38
1.28	0.0007	0.35
1.60	0.0007	0.35
1.92	0.0007	0.35
2.24	0.0007	0.35
2.56	0.0007	0.35
2.88	0.0007	0.35
3.20	0.0007	0.35
3.52	0.0007	0.35
3.84	0.0007	0.36
4.16	0.0007	0.36
4.48	0.0008	0.37
4.80	0.0008	0.38
5.12	0.0009	0.39
5.44	0.0010	0.41
5.76	0.0011	0.45
6.08	0.0014	0.50
6.40	0.0020	0.59

```
          CIRCULATING FLUIDIZED BED RISER DENSITY PROFILE cont.
          -----------------------------------------------------

GAS VELOCITIES,M/S
------------------
SEC. ZONE SUPERFICIAL VELOCITY                   6.79
MEAN CORE INTERSTITIAL VELOCITY                  7.03
MEAN STREAMER INTERSTITIAL VELOCITY              3.51
SEC ZONE MEAN INTERSTITIAL VELOCITY              6.94
PRIMARY ZONE MEAN INTERSTITIAL VELOCITY          4.80
```

Appendix C

Characterization of Solid Residues by Ortech International

SUMMARY

Significant concentrations (~6%, as CaS) of sulphides or other reduced-sulphur species in solid residues from a small-scale circulating fluidized bed (CFB) combustor have been reported in the literature. Their presence in similar quantities in residues from a utility-scale combustor would present significant difficulties with handling, disposal or utilization of the residues. This report describes the findings of an investigation of the chemical nature of sulphur present in solid samples extracted during operation from a pilot-scale CFB combustor. The work was conducted on materials obtained from a pilot-scale CFB combustor at the University of British Columbia. Minto coal from New Brunswick, Eastern Canada, with ~7% sulphur was burned in a circulating bed formed from a blend of 76% Texlime and 24% Elmtree limestone. The purpose of this study has been to investigate the oxidation states of the major sulphur-containing species, and their location and mode of formation in a circulating fluid bed.

Chemical analysis, thermal analysis and X-ray diffraction were used to examine samples of the circulating bed, secondary cyclone catch, and baghouse solids that were removed during operation of the combustor. Optical and scanning electron microscopy were used to investigate the morphology of different particle types.

The chemical and mineralogical data, showed the samples to be of two general types as follows:

(a) The circulating particulate materials were of similar composition regardless of the sampling location in the bed, with 26–30% SiO_2, 26–30% CaO, total carbon ranging from 0.7 to 1.7% and total sulphur ranging from 5.5 to 6.4%. All of the circulating particulate samples showed low sulphide content (<0.6% as S^{2-}).

(b) Samples from the secondary cyclone and the baghouse showed lower silicon content (10–13% as SiO_2), increased calcium (~50% as CaO), and high levels of total carbon (~10% C), total sulphur (~8.5% S), and sulphide (~2.5% as S^{2-}).

Corresponding differences were noted by X-ray diffraction, from which it was found that all of the circulating bed samples were predominantly composed of lime (CaO), anhydrite

($CaSO_4$), "olivine sand" (use as a start-up bed), and quartz. In addition, materials from the secondary cyclone and the baghouse showed the presence of small quantities of $CaCO_3$, $Ca(OH)_2$, and CaS.

The following conclusions have been drawn from this study:

- Though sulphur is captured or retained in solid phases throughout the combustor largely as sulphate, its state of combination can be altered by secondary reactions.

- Consistent with previously reported work, the bulk of the sulphur in the circulating bed materials is present as $CaSO_4$, intimately mixed with CaO from calcined limestone.

- Circumstances can exist in some CFB combustors whereby reduced sulphur species are formed, or captured. Among these, sulphides have been identified that appear to be present largely as calcium sulphide.

- Calcium sulphide is predominantly present in the spent limestone particles collected from the secondary cyclone and baghouse. Its presence appears to be associated with that of unburned carbon in regions where reduction conditions may develop. It is proposed that CaS is formed at about 850°C in the secondary cyclone, by reduction of $CaSO_4$ through reactions involving C, CO and CO_2. The presence of sulphide in the baghouse discharge is assumed to be a consequence of carry-over of fine particles from the secondary cyclone.

E.E. Berry, Ph.D., CChem.
Consultant

R.T. Hem

R.T. Hemmings, Ph.D., CChem.
Consultant

CONTENTS

Section **Page**

1. INTRODUCTION 1

2. EXPERIMENTAL DETAILS 1
  2.1 Combustion 1
  2.2 Materials 2
  2.3 Analytical methods 2

3. RESULTS AND DISCUSSION 3
  3.1 Examination of the Bulk Samples 3
  3.2 Examination of Fractionated Samples 4
    Bed-drain Material 5
    Baghouse Residue 6
    Phase Composition 6
  3.3 Sulphur Speciation and the Mechanism of Formation of CaS 8

4. CONCLUSIONS 11

Acknowledgments 11
References 12
Tables 13
Figures 16

APPENDICES

1. INTRODUCTION

The environmental problems associated with the combustion of low-grade or high-sulphur coals for thermal power generation are being widely investigated in North America. Of particular concern are emissions of sulphur oxides to the atmosphere and their contribution to "acidic rain." One approach to reducing acidic gas emissions is to burn such fuels in either a bubbling or circulating atmospheric pressure fluidized bed (AFB) combustor containing crushed limestone. During combustion, the products from oxidation of the sulphur in the fuel are absorbed into the calcined bed material and discharged as a solid residue, rather than with the combustion gases.

Most of the sulphur captured by the limestone in AFB combustors is present in the discharged residues as anhydrous calcium sulphate ($CaSO_4$) [1-4]. However, significant accumulations of sulphide have been reported in residues from some small- and pilot-scale circulating fluidized bed combustors [5,6]. The presence of sulphide in residues from a full-scale, utility fluidized bed combustion (FBC) system would present considerable problems during waste utilization or disposal. Therefore, it is important to establish the nature of sulphides or other sulphur species in CFBC residues, and the mechanisms by which they might from or prevented from forming. This report describes an investigation of the nature of sulphur in solid phases extracted, during operation, from a pilot-scale CFB combustor. The purpose of this study has been to investigate the oxidation states of the major sulphur-containing species, and their location and mode of formation in a circulating fluid bed.

2. EXPERIMENTAL DETAILS

2.1 Combustion

The work was conducted on materials obtained from a pilot-scale CFB combustor at the University of British Columbia (Fig. 1). Full details of this installation have been reported by Grace et al. [7]. Fig. 2 shows a schematic representation of the circulating combustor system, together with the average temperatures and locations at points from which samples were withdrawn (points 1–7) while the combustor was operating. Because the CFBC solids are potentially sensitive to both oxidation and hydration when exposed to the atmosphere, sampling methods were developed by researchers at the University of British Columbia that permitted collection of solids from the operating combustor under a dry N_2 atmosphere. For this purpose, two devices (Fig. 3) were used, as appropriate, to obtain samples from points 1 to 6 (Samples 1–6). Because they are exposed to air during normal operations, samples from the baghouse discharge (Sample 7) were collected without protection by N_2. All samples discussed in this paper were withdrawn from the combustor during a run conducted during the period March 5 - 7, 1988. Sampling took place ~28 hours after "thermal steady state" had been achieved when it was apparent from combustion monitoring that a "composition steady-state" had been attained (estimated to be after 3 bed turnovers).

2.2 Materials

The fuel used during this experiment was a Minto coal from New Brunswick, Eastern Canada, with ~7% sulphur, other characteristics of which are given in Table I. The limestone used in this study, which was a blend of two high-Ca materials, comprised of 76% Texlime and 24% Elmtree. Chemical compositions of the raw materials and the ash from Minto coal are given in Table II. As is the case with all pilot-scale CFBC units, it was necessary to employ a "start-up" bed heated by propane gas, to raise the temperature of the system prior to addition of limestone and coal. In the UBC unit, an "olivine sand" (Fig. 4.) was used, an XRD pattern of which is shown in Fig. 5. This suggests that the sand is composed primarily of clinohumite ($Mg_9(SiO_4)_4(F,OH)$), quartz, forsterite and magnetite.

To obtain materials for laboratory examination, Samples 1–6 were individually blended, riffled and subsampled under dry N_2 in a glove bag. Samples from point 7 were handled in the laboratory atmosphere. Fractions from Sample 1 (bed-discharge) were collected by manual separation of particles into groups based on visual appearance under a low-power optical microscope. The separation was conducted under dry N_2 in a glove bag. Fractions from the baghouse material (Sample 7) were obtained by the density-flotation separation technique [8] using bromoform-ethanol media at a specific gravity of 2.2.

2.3 Analytical Methods

Chemical analyses for major elements in the solid residues were performed by inductively coupled argon plasma (ICP) spectrophotometry. Solids were prepared for analysis by fusion with lithium carbonate followed by dissolution in nitric acid. Total carbon and sulphur in the solids were detrmined by the combustion technique using a LECO CS244 analyzer calibrated with NBS Standards. A standard technique, originally devised for analysis of blast furnace slags [9] was used to determine sulphide in the solids. Details of this method are given in Appendix 1. X-ray diffraction (XRD) and thermogravimetry (TGA/DTG) in a dry N_2 atmosphere were used to determine phase compositions. The morphology and approximate elemental composition of some individual particles were examined using both optical microscopy and SEM-EDXA methods.

3. RESULTS AND DISCUSSION

3.1 Examination of the Bulk Samples

Chemical compositions of the seven bulk samples (Samples 1–7) are given in Table III, reported as major oxides, total sulphur, sulphide (as S^{2-}) and total carbon. Corresponding XRD patterns shown in Fig. 6. From the chemical and mineralogical data, it is clear that the samples may be categorized into two general groups as follows:

(a) The materials from the circulating particulate load (Samples 1–5) are of generally similar composition regardless of the sampling location. Chemically, the circulating solids may be considered as a single type with 26–30% SiO_2, 26–30% CaO and <0.4% loss on ignition. Total carbon ranged from 0.7–1.7% and total sulphur ranged from 5.5–6.4% in these samples, all of which also showed relatively low sulphide content (i.e. <0.6% as S^{2-}).

(b) The materials from the secondary cyclone and the baghouse (Samples 6 and 7 respectively) showed quite different characteristics. In comparison with the circulating solids, the silicon content is much lower (10–13% SiO_2), calcium is increased (~50% CaO), and the materials exhibited substantial loss-on-ignition (7–8%). These samples were distinguished further from the circulating materials by the presence of high levels of total carbon (~10% C), total sulphur (~8.5% S), and sulphide (~2.5% S^{2-}). Clearly, much of the unburnt carbon, the captured sulphur and the sulphide were accumulated in the solids secondary cyclone and the baghouse during combustion.

Corresponding differences were noted from the XRD data (Fig. 6). The diffraction patterns from all of the samples were dominated by lines attributable to lime (CaO), anhydrite ($CaSO_4$), "olivine sand" and quartz (SiO_2). Samples 6 and 7 from the secondary cyclone and the baghouse respectively, showed the presence of substantially more CaO than Samples 1–5 from the circulating particulates. Detailed consideration of the diffraction data is given in a subsequent section of this report.

hermogravimetric analysis was conducted on Samples 2, 6 and 7, primarily to confirm the resence of $CaCO_3$ and $Ca(OH)_2$ in the baghouse and secondary cyclone solids. From the sulting thermal curves (Fig. 7 and Appendix 2), three regions of mass loss are noted:

- A small mass loss over the range 350–500°C, attributable to the presence of minor quantities of $Ca(OH)_2$.
- A mass loss, that was substantial from Samples 6 and 7 and minor for Sample 2, occurred in two stages over the range 600–800°C. This is attributed to the calcination of calcium carbonate.
- An extensive mass loss occurred at temperatures >800°C and was not complete at 1000°C (the maximum temperature to which the TGA equipment could be raised).

t the present time, the origin of the mass loss above 800°C has not been established. It is ossible that it resulted from the decomposition of calcium sulphate:

$$CaSO_4 \rightarrow CaO + SO_3$$

his reaction is known to occur for pure $CaSO_4$ at temperatures over 1200°C but it may be ıfficiently accelerated by the presence of a number of compounds (including silicates and arbon) to proceed almost to completion in the TGA experiment at lower temperatures [10-5]. Alternatively, the mass loss may have resulted from the reduction of $CaSO_4$. The eactions involved in this process are discussed in a subsequent section of this paper.

he general morphology of particles from samples 3, 6 and 7 was investigated by scanning lectron microscopy (Figs. 8a-g.). Other electron micrographs are presented in Appendix .

.2 Examination of Fractionated Samples

he circulating bed materials, the solids recovered from the secondary cyclone return, and ıe baghouse catch are all expected to be heterogeneous mixtures of the following omponents:

- residual olivine sand from the start-up bed;

- limestone in various states of calcination and sulphation;
- uncombusted coal;
- coal-related inorganics, including ash, derived from the combusted portion of the fuel, and calcined shale-like minerals which were interbedded with the coal.

The distribution of these particle types through the combustor system may be expected to vary from point to point. In particular, low density and fine particulate fractions would be anticipated in the solids taken from the secondary cyclone and the baghouse (i.e. Samples 6 and 7). Coarser, more dense particles are expected to accumulate in the circulating mass (Samples 1–5). In a conventional CFB combustor, the only materials discharged during operation correspond to the bed-drain (Sample 1) and baghouse (Sample 7) residues. Because of the practical interest in the bed-drain and baghouse streams, these samples were examined for speciation among constituent particle types.

Bed-Drain Material

Examination of the bed-drain material under a low-power (Fig. 9), optical microscope showed it to be composed of a number of particle types, of which four (in addition to olivine sand) were visually distinguishable by colour or shape (Figs. 10a-d), as follows:

Type I	Black irregularly shaped particles assigned as incompletely burned coal.
Type II	Irregularly shaped particles, grey in colour.
Type IIIa	Light-coloured particles, of rounded form, with a golden/brown coating.
Type IIIb	Light-coloured particles, of rounded form, with a golden/brown coating, similar to Type IIIa, but showing evidence of expansion and fracturing.

Particles of Types II and IIIa were collected by manual manipulation under a low-power microscope and were examined by chemical analysis (Table IV). The major element content was used as an indicator of the probable origin of both particle types, as follows.

- Type II particles were clearly of aluminosilicate origin, with 61% SiO_2 and 19.6% Al_2O_3. These are presumed to have originated from coal-associated minerals. Consideration of the magnesium content (2.99%, as MgO) suggests that contamination by olivine sand (43.3% MgO) was minimal in the sample analysed. The Type II particles were found to contain little total sulphur (0.22%), of which more than half was present was as sulphide (0.16% as S^{2-}).

- The Type IIIa particles contained ~57% CaO, indicating them to be spent (i.e. sulphated/calcined) limestone. These particles were substantially sulphated (13.3% total S) and contained 0.64% of sulphide (as S^{2-}). It is considered probable that the particles of Types IIIa and IIIb are both composed of reacted limestone, Type IIIb particles being those that had expanded due to minor hydration or carbonation during handling. This was confirmed by observation of Type IIIa particles exposed to the laboratory atmosphere, whence similar expansion and fracturing was seen.

Baghouse Residue

The chemical composition of the baghouse catch (Sample 7: 50% CaO, 10% C) suggests that it is largely comprised of unburned carbon and a heterogeneous mixture of fine inorganic constituents, most of which originated from the spent limestone with minor quantities of coal shale/ash. In principle, sulphur in the sulphide state could be associated with either the unburnt carbon or the spent limestone particles in Samples 6 and 7. To investigate this further, a separation of the baghouse catch solids was made by flotation in a bromoform-ethanol mixture of specific gravity 2.2. The "float" and "sink" fractions were collected and analysed for major elements, total carbon, total sulphur and sulphide (Table IV). Consideration of the analytical data shows that the "float" material (SG <2.2) was largely carbon (73%, total C), with 2.7% total sulphur and minor sulphide content (0.18% as S^{2-}). The "sink" fraction (SG ≥2.2) was largely inorganic, principally comprising spent limestone (52% CaO), with 8.9% total S, 2.4% S^{2-} and 2.0% total C. Thus, the chemical analyses of the density fractions showed that most of the sulphide in the baghouse catch was associated with the spent limestone particles, rather than with the carbon.

Phase composition

X-ray diffraction and TGA data serve to identify the major components in the combustor solids as CaO, $CaSO_4$, $Ca(OH)_2$ and $CaCO_3$, with quartz and "olivine". A diffraction line at 3.05 Å is consistent with the presence of $CaCO_3$ in the secondary cyclone and baghouse solids, with more calcite present in Sample 6. No significant evidence was seen of $CaCO_3$ in the circulating solids, and a small quantity of $Ca(OH)_2$ was indicated in Samples 6 and 7.

Given the overall composition of the solids, it is reasonable to anticipate that much of the sulphide may be present as CaS. The XRD data were examined to investigate this expectation. Three problems hinder the identification of CaS in the presence of major quantities of $CaSO_4$:

- Calcium sulphide (CaS) has a simple cubic structure, it thus shows only a few strong X-ray diffraction lines in its spectrum.
- There is extensive correspondence of line positions in the published powder patterns of CaS and $CaSO_4$ [16].
- CaS may be poorly crystalized when produced in the combustor solids.

Table V shows the d-spacings and estimated intensities for the lines close to 2.00 Å in the diffraction patterns from Samples 1 and 7, compared with the published values for $CaSO_4$ and CaS. Within the limits of resolution of the method , only one low intensity, CaS line at 1.42 Å does not correspond with a line also assignable to $CaSO_4$. On the basis of observation of this line alone it would be difficult to confirm the presence of CaS with certainty. However, when the diffraction patterns are compared in detail in the 2.00 Å region (Table V, Fig. 11), it is clear that relative to the line at 1.86 Å (a well-defined $CaSO_4$ line), the line at 2.02 Å is much more intense for Sample 7 than for Sample 1. Similarly, when the intensity of the line at 2.85 Å (for which correspondence exists for the two compounds) is compared in each pattern relative to that of the line at 3.49 Å (a $CaSO_4$ line), diffraction from the baghouse material appears to be enhanced by CaS. It is concluded, on this basis, that both the baghouse and secondary cyclone solids contain crystalline CaS in addition to anhydrite ($CaSO_4$), the latter being the predominant sulphur-containing phase.

Table VI summarizes calculated values for the phase composition of Samples 2, 6 and 7 in terms of carbon, CaO, $Ca(OH)_2$, $CaCO_3$, $CaSO_4$ and CaS contents. These calculations are based on the data from chemical analysis and TGA, supplemented by the qualitative information from XRD. In making these calculations it has been assumed that all of the sulphide detected was present as CaS in the samples. This may not be the case, especially in the presence of substantial quantities of iron in various valence and combination states. However, no evidence has been found for other sulphide species.

3.3 Sulphur Speciation and the Mechanism of Formation of CaS

The chemical analyses clearly showed that sulphur captured from the combustion gases was present in all of the bulk samples, regardless of their point of collection from the combustion system. The solids forming the circulating mass (Samples 1–5) contained total sulphur at levels in the range 5.5–6.5% S. The materials removed from the combustion gases by the secondary cyclone and the baghouse contained more sulphur in total (8.3 and 8.8% S, respectively).

The oxidation state of sulphur was found to be markedly dependent on the location of the solids in the system. Solids from the circulating bed were relatively homogeneous, with sulphide contents in the range 0.47–0.60% S^{2-} by mass. This would indicate that in addition to the general similarity of composition among samples from different locations, there existed relatively similar conditions of oxidation in the circulating materials during combustion. This conclusion is further supported by the similarity in carbon content among these materials. In contrast, the high carbon content and the relatively high sulphide content of Samples 6 and 7 indicate that reducing or low-oxidation conditions existed in the secondary cyclone and/or baghouse during the combustion conditions prevailing when the samples were removed.

The presence of CaS in fluidized bed combustor residues has been previously identified [17,18]. However, concentrations in these reported cases were so low that Sun et al. [18] state that it is not a problem for once-through FBC systems. The situation with some circulating fluidized bed combustors appears to be less clear. From the present data and previously reported observations [5,6], it is clear that circumstances exist in some CFB combustors that permit formation of CaS and its accumulation in the discharged solids. If CaS formation is to be avoided in commercial CFBC operations, it is important that an understanding is developed of the conditions under which it can be formed.

A number of reactions which are capable of producing CaS at elevated temperatures are possible in the CFB system, including the following:

$$CaO + H_2S \rightarrow CaS + H_2O \tag{1}$$

To generate H_2S in a CFB combustor would require reducing conditions similar to those existing in a fixed bed or fluidized gasifier. Overall, the CFBC process operates under oxidizing conditions, except in regions where accumulations of carbon or CO may occur. Under these circumstances a number of reactions can lead to reduction of $CaSO_4$ with formation of CaS. A part of the extension of the early Leblanc process for producing soda ash involved recovery of sulphur by reaction of $CaSO_4$ with carbon, with the overall stoichiometry:

$$CaSO_4 + 4C \rightarrow CaS + 4CO \tag{2}$$

By this reaction, CaS can be produced at temperatures from 700–1000°C. Turkdogan and Vinters [19] have examined the reduction of $CaSO_4$ by carbon in some detail under conditions where either CaS or SO_2 is the principal product of reduction. The following reactions, with their associated free energy changes, were proposed:

$$CaSO_4 + 2C \rightarrow CaS + 2CO_2 \qquad (\Delta G^\circ = 33{,}820\text{-}77.69T \text{ cal.mole}^{-1};\ \Delta G^\circ = 0,\ T = 162^\circ C) \tag{3}$$

$$2CaSO_4 + C \rightarrow 2CaO + 2SO_2 + CO_2 \qquad (\Delta G^\circ = 128{,}660\text{-}115.22T \text{ cal.mole}^{-1};\ \Delta G^\circ = 0,\ T = 843^\circ C) \tag{4}$$

Because the solid-solid reactions are inherently slow, the reduction to CaS or SO_2 is expected to proceed via intermediate reaction products, CO and CO_2:

$$CaSO_4 + 4CO \rightarrow CaS + 4CO_2 \tag{5}$$

$$CO_2 + CaS \rightarrow CaO + SO_2 + 3CO \tag{6}$$

$$CO_2 + C \rightarrow 2CO \tag{7}$$

Experimentally, Turkdogan and Vinters [19] found that SO_2 evolution and loss of CaS continued in systems with low carbon content even after all of the carbon had been consumed. This lead them to propose a further competing solid-solid reaction:

$$3CaSO_4 + CaS \rightarrow 4CaO + 4SO_2 \qquad (\Delta G^\circ = 223{,}500\text{-}182.51T \text{ cal.mole}^{-1};\ \Delta G^\circ = 0,\ T = 951^\circ C) \tag{8}$$

The overall reaction process was shown by Turkdogan and Vinters [19] to preferentially produce either CaS or SO_2 depending on the amount of carbon present and its reactivity. In mixtures where the ratio of carbon to sulphur (C:S) was approximately 0.5, complete conversion to SO_2 was attained. Where C:S was slightly above the stoichiometric value of 2 for reaction 3, conversion to CaS was attained with less than 1% loss as SO_2.

The reactivity of the carbon was found to have a marked effect on the product. When graphite was used, even at high C:S levels, most of the sulphate was converted to SO_2, because of the slow oxidation of graphite to CO. The reverse behaviour was found for coconut charcoal. The authors concluded that the rate of conversion to CaS is determined by the rate of oxidation of carbon by CO_2. In their studies, it was found [that coal] "...is reactive and well suited for this purpose."

If reduction of $CaSO_4$ is the means whereby CaS is produced in the CFB combustor, it remains to be considered where in the system the reaction occurs. The chemical analyses of the solids from this study show that sulphide and carbon both accumulate in spent limestone particles that are captured in the secondary cyclone and the baghouse. The major part of the combustor, the loop containing the circulating solids, is largely under oxidizing conditions maintained by the primary (fluidizing) air and the introduction of secondary air below the L-valve (Fig. 2). It is unlikely that CaS would form by reduction in these regions of the system, as is consistent with the observed low sulphide-content of Samples 1-5.

The baghouse operates at a gas temperature of 80–120°C. Thus, despite the availability of carbon, it is not considered likely on free energy or kinetic grounds that $CaSO_4$ reduction could take place in the baghouse catch.

The secondary cyclone operates at a gas temperature close to 850°C, at which, according to reaction 3, $\Delta G^\circ = -53{,}438$ cal.mole^{-1}. The ratio C:S in the discharged solid (Sample 6) was 2.98, well in excess of the minimum stoichiometric requirement for reduction to CaS to predominate. It must be concluded that the potential exists for reduction of $CaSO_4$ by carbon to form CaS in the secondary cyclone. Its presence in the baghouse discharge is assumed to be a consequence of carry-over of fine particles from the secondary cyclone.

4. CONCLUSIONS

As a result of this study, the following conclusions as to the nature of sulphur capture in CFBC can be drawn:

1. It is clear that whereas sulphur is captured and retained in solid phases throughout the circulating bed, its state of combination can be altered by secondary reactions.

2. Consistent with previously reported work, the bulk of the captured sulphur in the bed materials is present as $CaSO_4$, intimately mixed with CaO from calcined limestone.

3. Circumstances can exist in some CFB combustors whereby reduced sulphur species are formed, or captured. Among these, sulphides have been identified that appear to be present largely as calcium sulphide.

4. Calcium sulphide is predominantly present in the solids collected from the secondary cyclone and baghouse. Its presence appears to be associated with the availability of carbon in regions where reduction conditions may prevail. At present, indications are that it is formed at about 850°C in the secondary cyclone, by reduction of $CaSO_4$ through a complex sequence of reactions involving C, CO and CO_2. The presence of sulphide in the baghouse discharge is assumed to be a consequence of carry-over of fine particles from the secondary cyclone.

ACKNOWLEDGMENTS

This work was conducted at the Ontario Research Foundation (now ORTECH International) as part of a joint project with the University of British Columbia (UBC) on behalf of CANMET, Energy, Mines and Resources Canada. The authors wish to thank Dr. J.R. Grace and his colleagues in the Department of Chemical Engineering, UBC, for the careful collection of sample materials and for many helpful discussions during the course of the project.

REFERENCES

1. J. McLaren and D.F. Williams, J.Inst. Fuel, 303, August 1969.
2. J.L. Minnick, Development of Potential Uses for the Residue from Fluidized Bed Combustion Processes, Reports under Contract No. EF-77-C-01-2549.
3. J.L. Minnick, Development of Potential Uses for the Residue from Fluidized Bed Combustion Processes, Reports under Contract No. DE-AC21-77-ET10415.
4. R.J. Collins, J. Testing and Evaluation 8, 259 (1980).
5. Dearborn Chemical Company, Characterization of Circulating AFBC Wastes, Canadian Electrical Association Report No. 432 G-494, December 1986.
6. E.J. Anthony, The Presence of Calcium Sulphide in Solid Wastes from Circulating Fluidized Bed Combustors, CANMET Division Report ERP/ERL 86-53(TR), Sept. 1986.
7. J.R. Grace and C.J. Lim, Circulating Fluidized Bed Combustion of Coal, Woodwastes and Pitch, Final Report under Energy, Mines and Resources Canada, Contract 24St.23440-6-9007, December 1987.
8. R.T. Hemmings and E.E. Berry, in Fly Ash and Coal Conversion By-Products: Characterization, Utilization and Disposal II, edited by G.J. McCarthy, F.P. Glasser and D.M. Roy, Mat. Res. Soc. Symp. Proc. Vol. 65 (Materials Research Society, Pittsburgh, 1986) pp. 91-104.
9. "AOAC Method 1.013 -1.015: Sulfide Sulfur (7)-Final Action," in Official Methods of the Association of Official Analytical Chemists, 13th Edition, W. Horwitz, ed., (Association of Official Analytical Chemists, Washington, D.C., 1980).
10. E.E. Berry, J. Appl. Chem. Biotechnol. 22, 673 (1972).
11. H.O. Hofmann and W. Mostowitsch, Trans. Am. Inst. Min. Metall. Engrs. 39, 628 (1908).
12. M.L. Bedwell, Rep. R. Inst. Chem. 3, (1952).
13. J.H. Frydlender, Rev. Prod. Chim. 29, 613 (1926).
14. G. I. Higson, Chem. Eng. News 29, 4469 (1951).
15. J. Manning, Proc. Fertil. Soc. 15, (1951).
16. *Powder Diffraction File,* W.F. McClune, Editor-in-Chief, (JCPDS-International Center for Diffraction Data, Swarthmore, PA).
17. L.S. Ryan, R.G. Beimer and R.F. Maddalone, Level 2 Chemical Analysis of Fluidized Bed Combustor Samples, EPA Report, EPA-600/7-79-0636 (1979).
18. C.C.Sun, C.H. Peterson and D.L. Keairns, Experimental/Engineering Support for EPA's FBC Program: Final Report - Vol.III, Solid Residue Study EPA -600/7-80-015C (1980).
19. E.T. Turkdogan and J.V. Vinters, Trans. Inst. Mining and Met., Section C, 85, C117 (1976).

Table I

Characteristics of Minto Coal*

Property	As Analyzed	Dry at 105°C	Dry, Ash Free
Proximate Analysis (mass%):			
Moisture, as analyzed	1.53	..	..
Ash	18.78	19.07	..
Volatile	33.91	33.42	41.30
Fixed carbon	46.78	47.51	58.70
Ultimate Analysis (mass%):			
Carbon	63.78	64.77	80.04
Hydrogen	4.13	4.19	5.18
Nitrogen	0.67	0.68	0.84
Sulphur, total	7.09	7.20	8.90
Oxygen by difference	4.02	4.09	5.04
Calorific Analysis (cal/g)	6527	6623	8184

* Data courtesy of CANMET Energy Research Laboratories.

Table II

Chemical Analyses (mass %) of CFBC Raw Materials*

Element Oxide	Start-up Bed Olivine Sand	··········Limestones·········· Texlime	Elmtree	Minto Coal Ash
SiO_2	41.48	0.00	0.00	39.32
Al_2O_3	0.76	0.62	1.43	12.52
Fe_2O_3	8.58	0.45	0.56	39.80
CaO	0.14	54.57	54.32	2.64
MgO	48.08	0.34	0.60	0.43
Na_2O	0.05	0.05	0.05	0.20
K_2O	0.01	0.16	N.A.	1.58
SO_3	0.54	1.17	N.A.	2.09

* Data courtesy of University of British Columbia.

Table III

Chemical Analysis (mass %) of Bulk Samples of FBC Residues

Element	Sample Number*						
Oxide	1	2	3	4	5	6	7
SiO_2	28.89	29.50	26.40	28.10	29.99	12.99	10.89
Al_2O_3	5.19	5.20	4.81	4.79	4.29	3.12	3.66
Fe_2O_3	9.58	9.20	9.05	9.21	9.18	8.48	10.56
CaO	27.78	27.95	28.07	29.07	26.16	48.97	50.09
MgO	14.76	15.60	13.88	15.08	19.97	3.80	0.71
Na_2O	0.27	0.21	0.20	0.21	0.20	0.19	0.18
K_2O	0.43	0.14	0.15	<0.10	0.10	<0.10	<0.10
LOI	0.15	0.41	-0.15	0.23	-0.19	7.52	7.99
Sulphur	6.15	6.19	6.41	6.38	5.49	8.27	8.82
Sulphide (S^{2-})	0.50	0.50	0.60	0.50	0.50	2.60	2.30
Carbon (total)	0.83	1.13	0.71	1.64	0.64	9.23	10.00

* Sample numbers correspond to points shown in Fig. 2.

Table IV

Chemical Analysis (mass %) of Fractionated FBC Residues

Element	Particle Fractions			
Oxide	Sample 1–Type II	Sample 1–Type IIIa	Sample 7–Float	Sample 7–Sink
SiO_2	60.8	4.13	5.60	14.05
Al_2O_3	19.6	1.20	2.48	2.65
Fe_2O_3	5.31	1.32	1.60	10.44
CaO	4.70	57.24	1.45	52.15
MgO	2.99	0.58	0.14	0.93
Sulphur	0.22	13.3	2.72	8.87
Sulphide (S^{2-})	0.16	0.64	0.18	2.40
Carbon	..	..	72.8	2.04

Table V

X-Ray Diffraction Lines from $CaSO_4$ and CaS

Observed Lines		Reported Lines*			
Sample 1	Sample 7	$CaSO_4$		CaS	
Å	Å	Å	I	Å	I
3.49 vs	3.49 vs	3.498	100		
2.85 m	2.85 vs	2.849	33	2.846	100
2.08 w	2.08 w	2.086	10		
2.01 w	2.02 m	1.993	6	2.013	68
1.94 w	1.94 w	1.938	4		
1.86 w	1.86 w	1.869	15		
1.64 w	1.64 w	1.648	14	1.644	21
	1.42 w			1.424	9

* Ref [16].

Table VI

Calculated Phase Composition (mass %) of FBC Residues

Element	Sample Number						
Oxide	1	2	3	4	5	6	7
CaS	1.13	1.13	1.35	1.13	1.13	5.85	5.18
$CaSO_4$	24.01	24.18	24.69	24.99	21.21	24.10	27.71
$CaCO_3$		0.18				13.03	6.74
$Ca(OH)_2$		0.74				4.85	5.47
CaO		16.45				25.45	23.36
Carbon		1.11				7.67	9.19

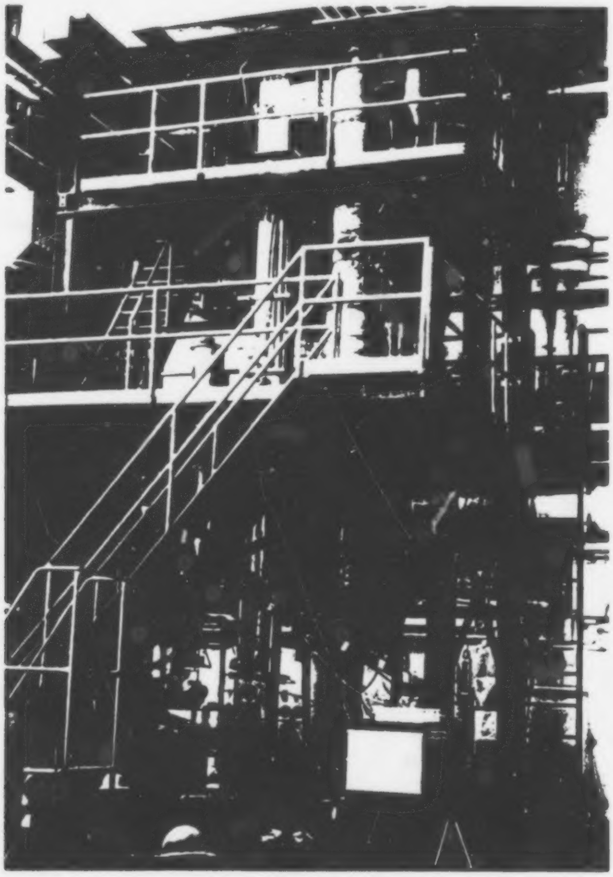

Figure 1. The University of British Columbia pilot-scale fluidized bed combustor

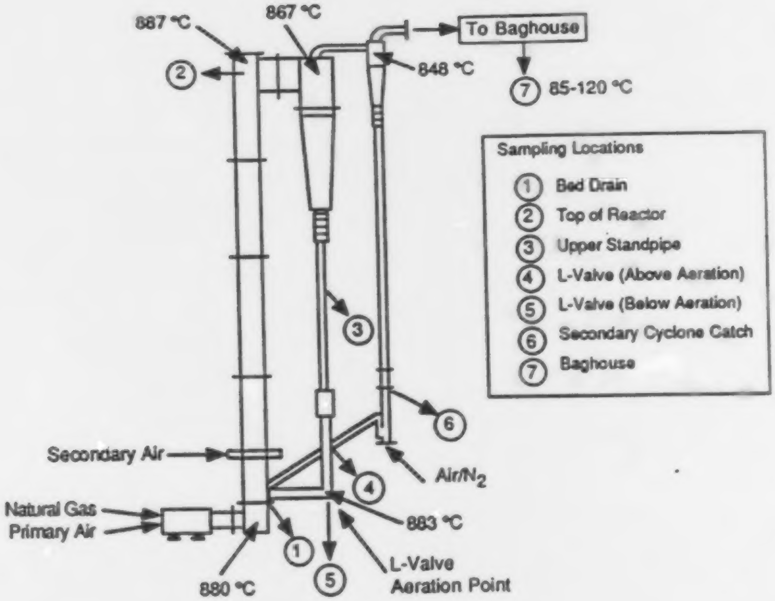
887 °C
867 °C
To Baghouse
848 °C
⑦ 85-120 °C
②
Sampling Locations
① Bed Drain
② Top of Reactor
③ Upper Standpipe
④ L-Valve (Above Aeration)
⑤ L-Valve (Below Aeration)
⑥ Secondary Cyclone Catch
⑦ Baghouse
③
⑥
Secondary Air
Air/N2
④
Natural Gas
Primary Air
883 °C
①
⑤
L-Valve
Aeration Point
880 °C

Figure 2. Schematic diagram of the University of British Columbia pilot-scale fluidized bed combustor showing the sampling points and corresponding temperature regimes (adapted from Grace et al. [7]).

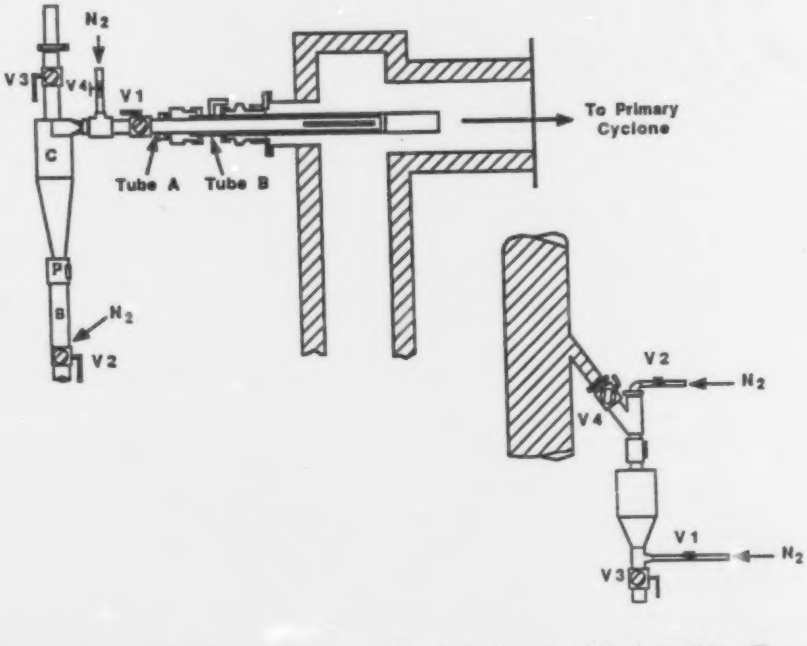
N2
V3
V4
V1
C
Tube A
Tube B
To Primary Cyclone
P
B
N2
V2
V2
N2
V4
V1
N2
V3

Figure 3. Inert atmosphere sample collection devices (designed by Grace et al.).

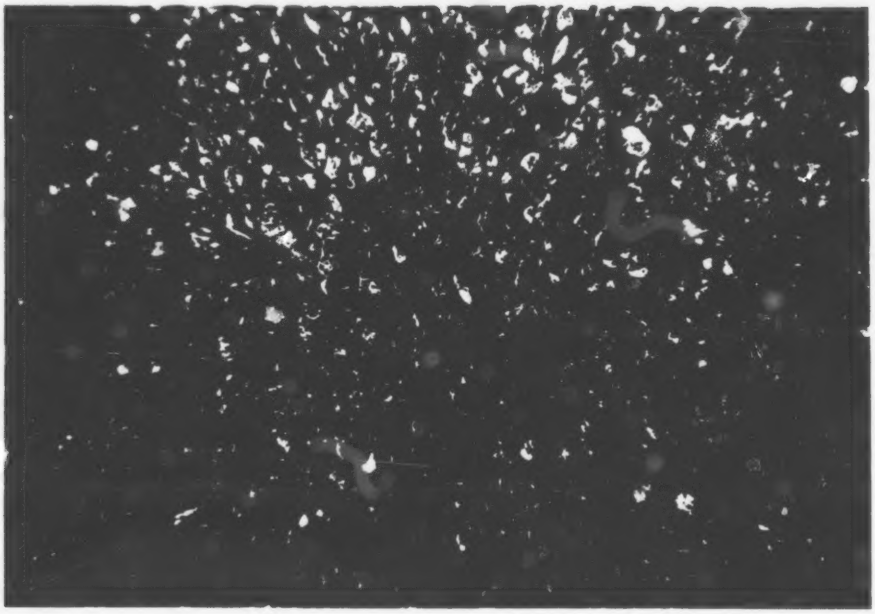

Figure 4. Olivine sand used as start-up bed in CFB combustor.

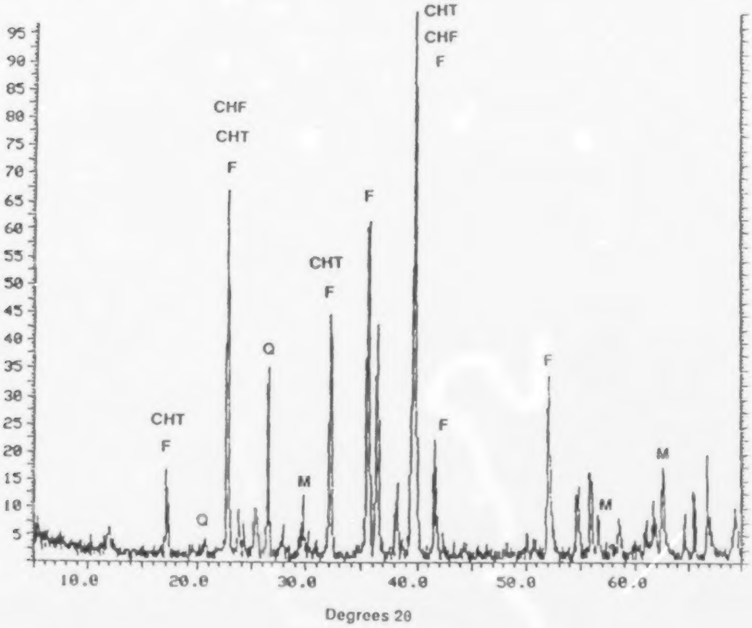

Figure 5. X-ray diffraction pattern from "olivine sand": **Q**, quartz; **CHT**, clinohumite (hydroxyl); **CHF**, clinohumite (fluoride); **F**, forsterite; **M**, Fe_3O_4.

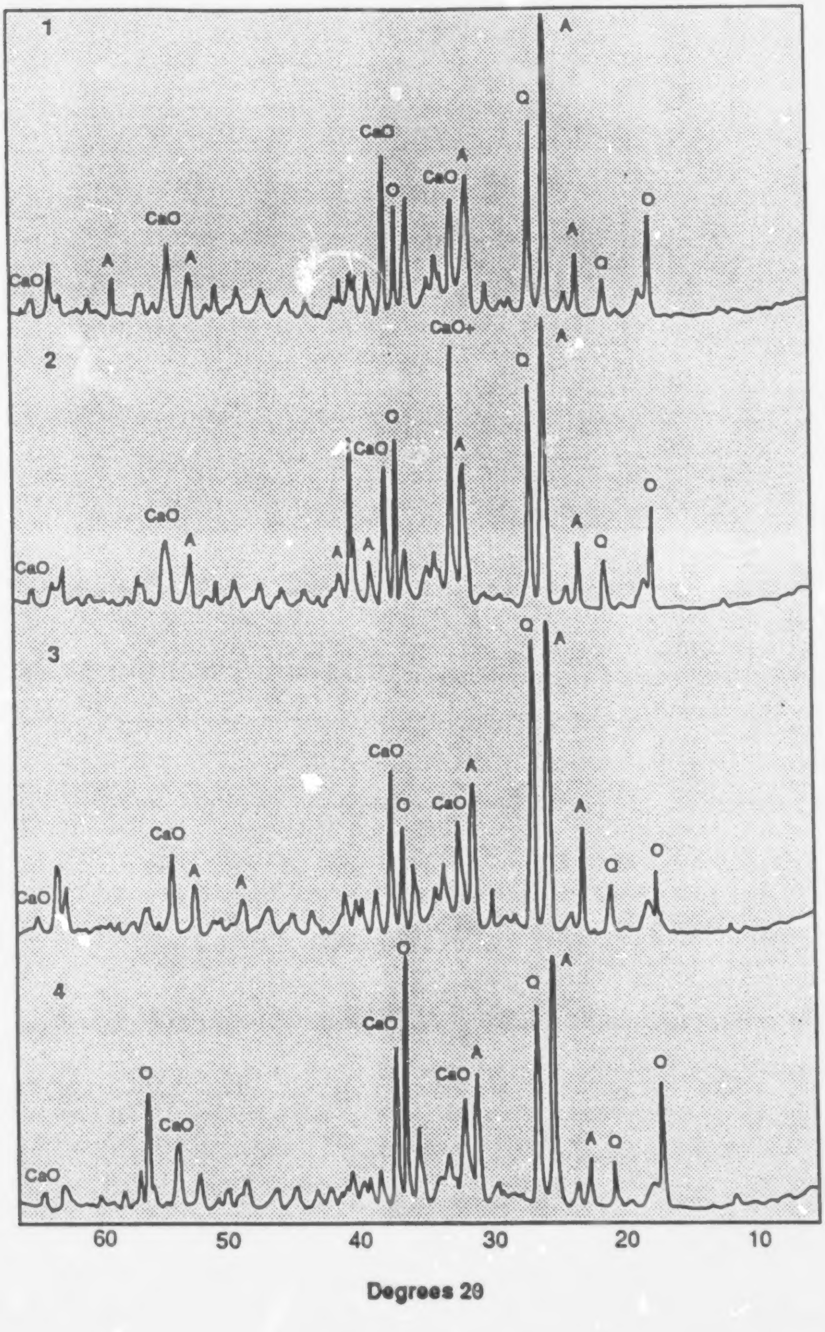

Figure 6. X-ray diffraction patterns (CuK_α) from samples 1 to 4: **Q**, quartz; **Ol**, "olivine sand"; **A**, anhydrite.

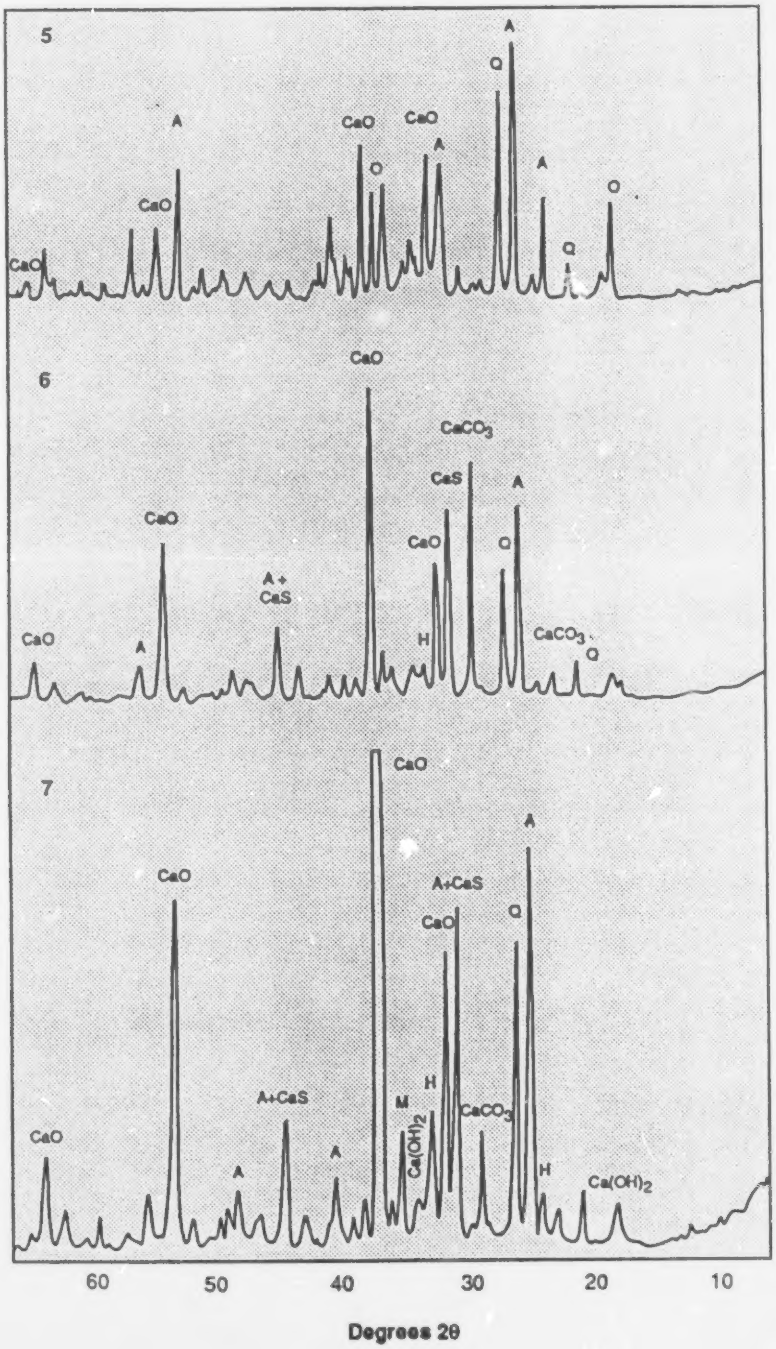

Figure 6(cont). X-ray diffraction patterns (CuK$_\alpha$) from samples 5 to 7: **Q**, quartz; **Ol**, "olivine sand"; **A**, anhydrite.

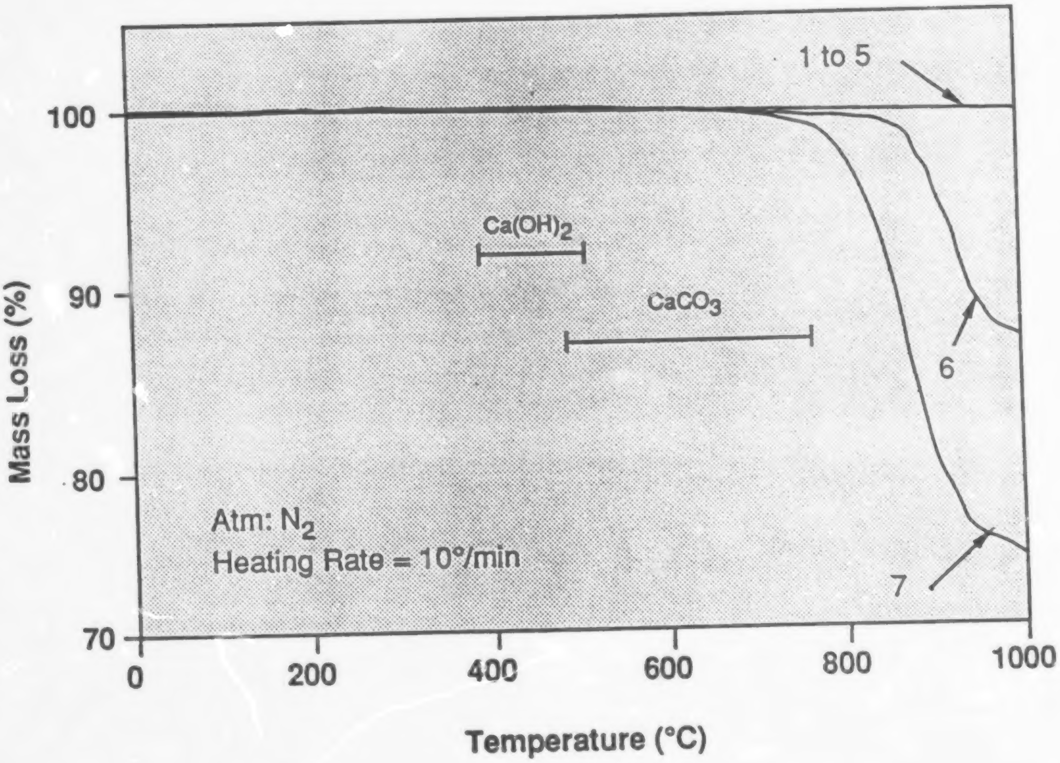

Figure 7. Thermogravimetric analysis curves from selected CFBC residues showing mass loss above 800°C.

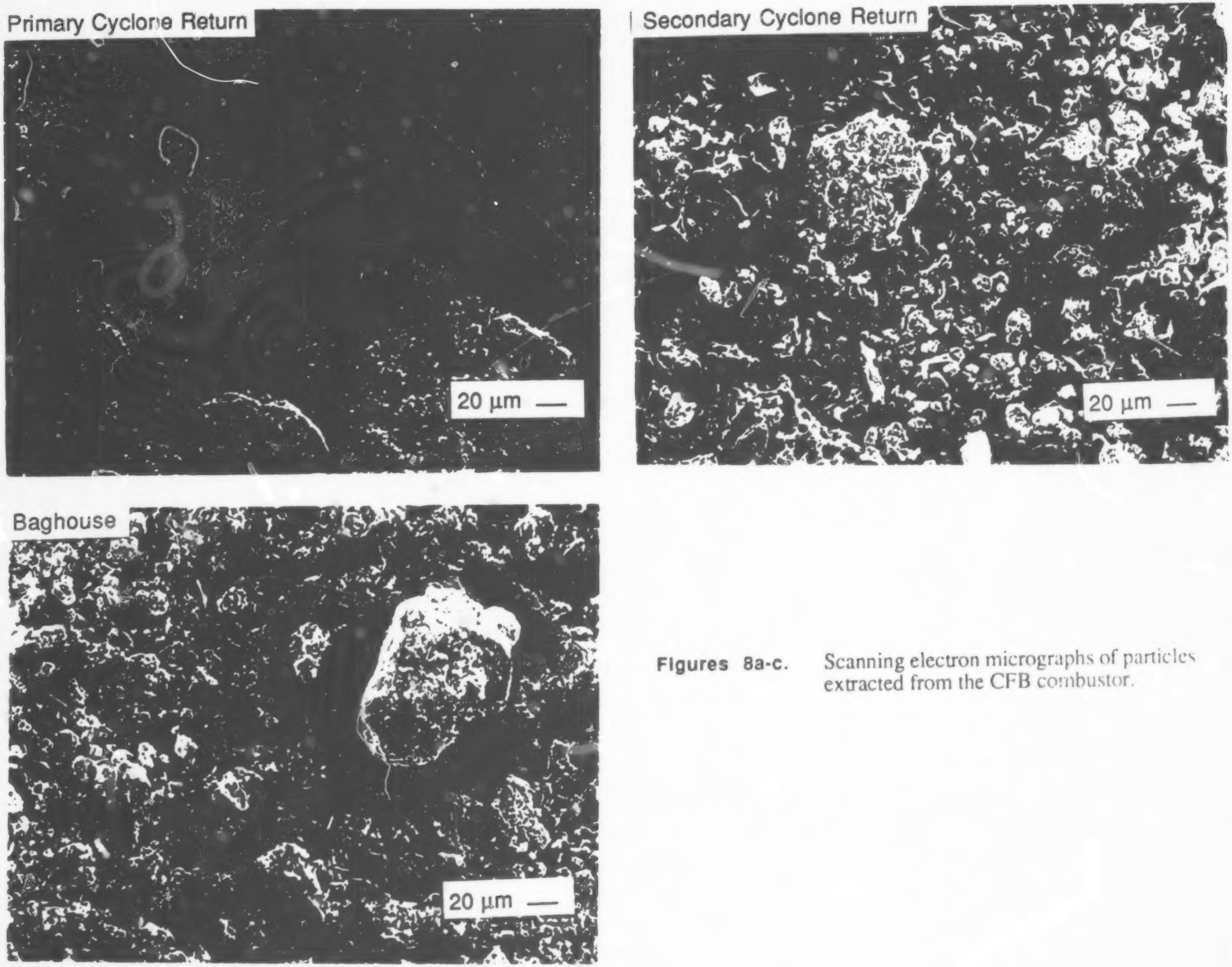
Primary Cyclone Return
20 µm
Secondary Cyclone Return
20 µm
Baghouse
20 µm

Figures 8a-c. Scanning electron micrographs of particles extracted from the CFB combustor.

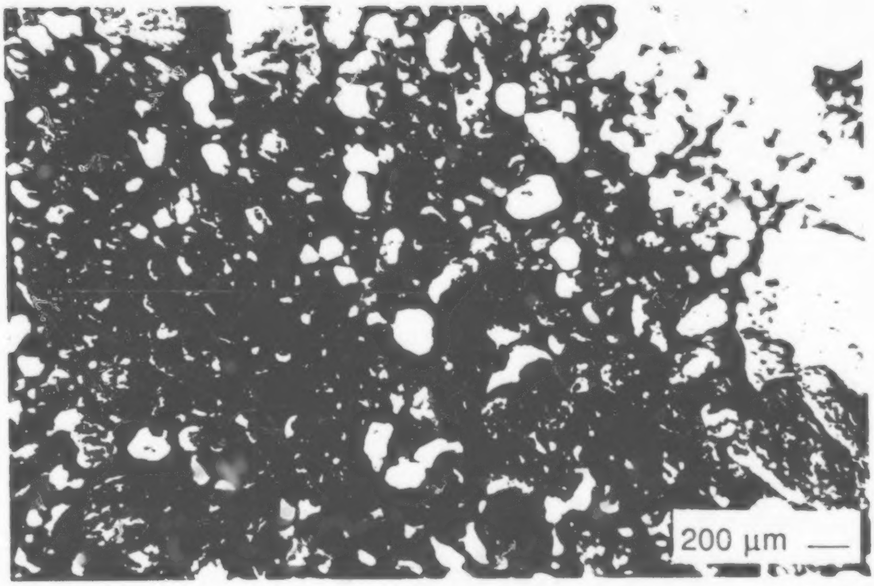

Figure 9. Optical photo-micrograph of bed-drain particles extracted from the UBC CFB combustor.

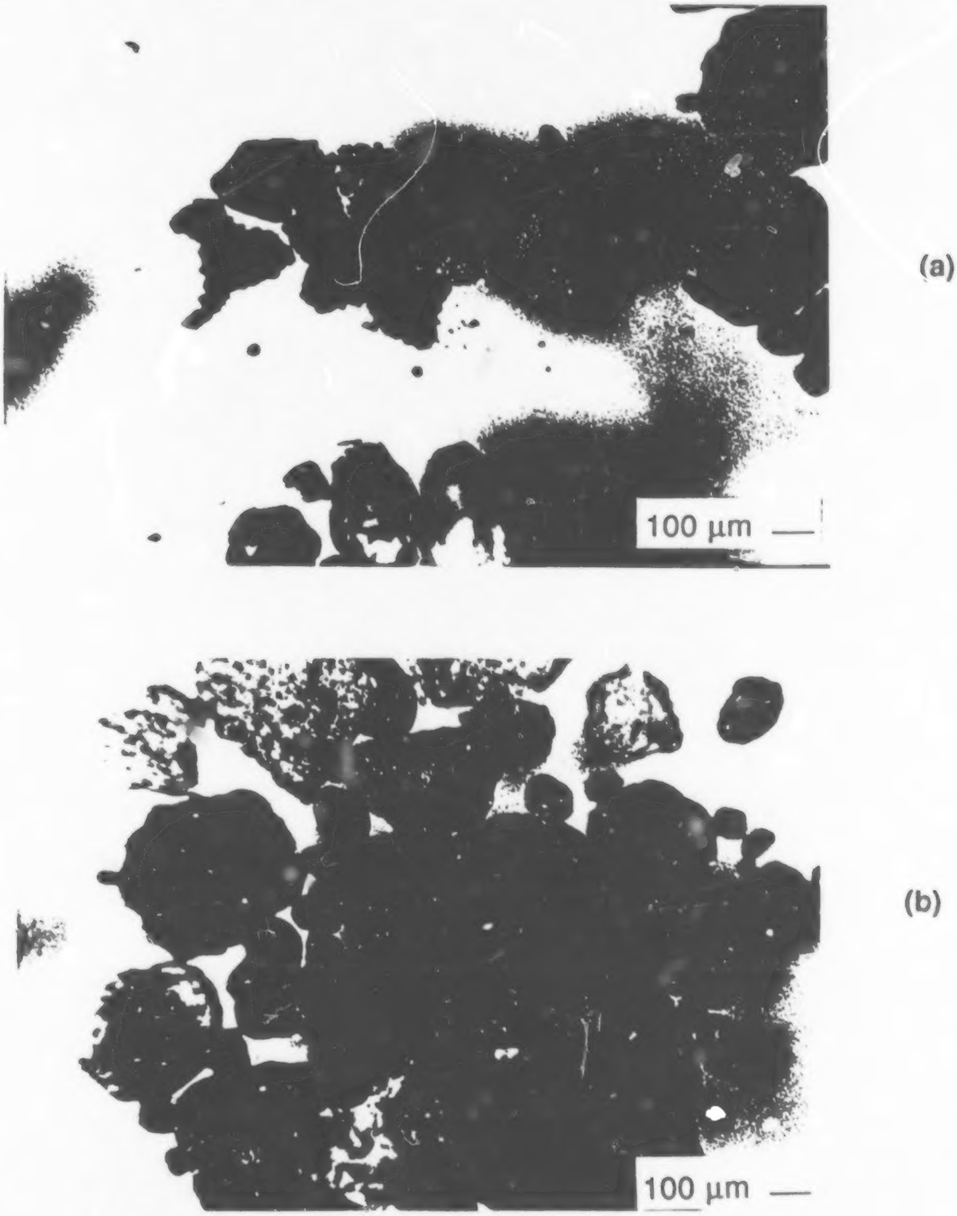

Figure 10. Optical photo-micrographs of particles selected from bed-drain material: (a) Type I particles (carbon); (b) Type II particles ("shale").

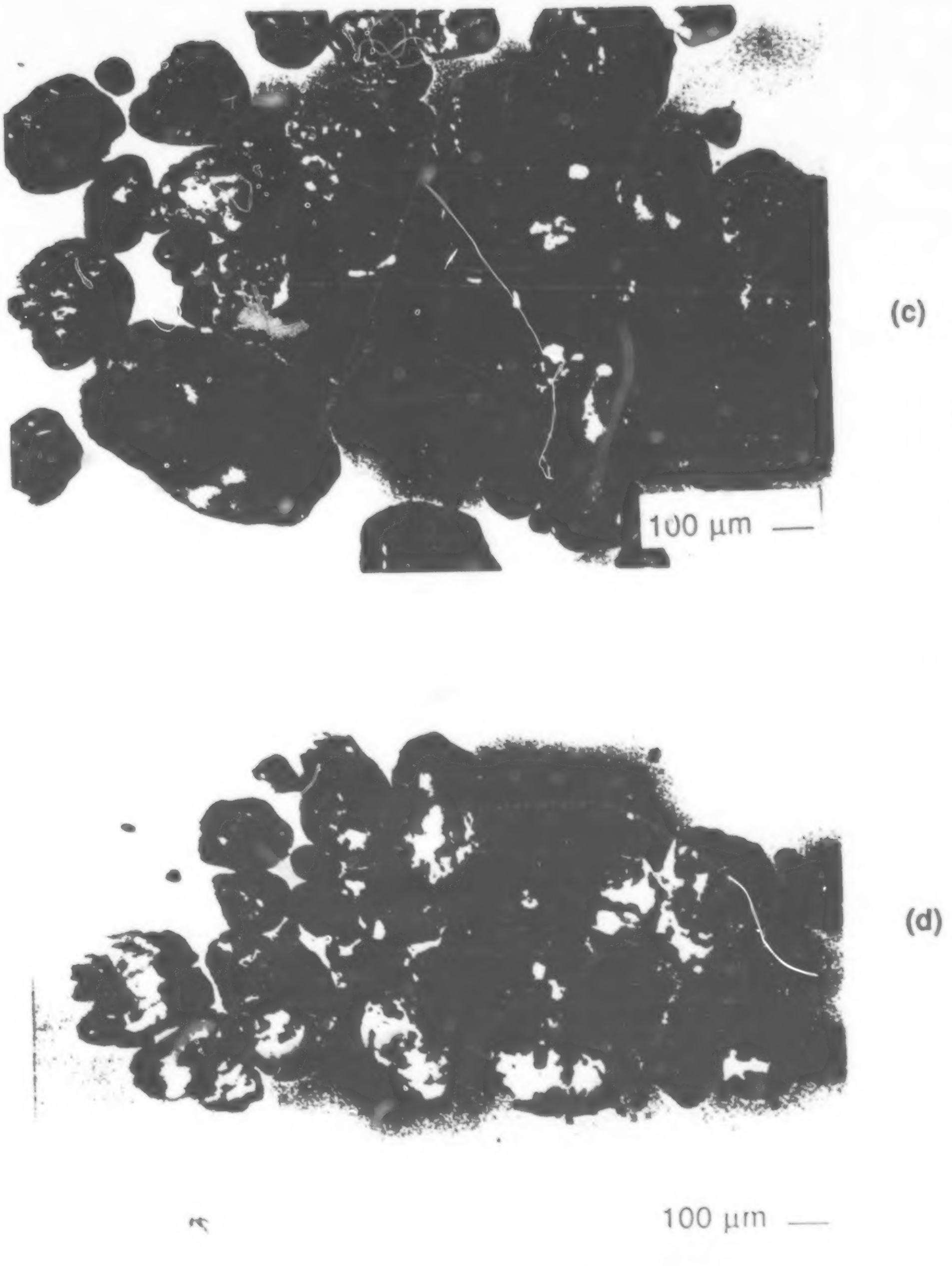

Figure 10 (cont). Optical photo-micrographs of particles selected from bed-drain material: (c) Type IIIa particles ; (d) Type IIIb particles.

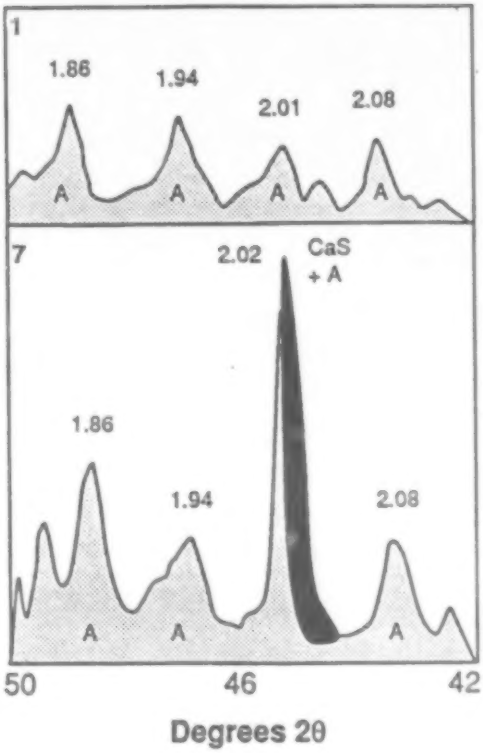

Figure 11. Details of the XRD patterns for Samples 1 and 7 in the 2.00 Å region showing the overlap of diffraction lines due to anhydrite (A) and calcium sulphide (CaS).

APPENDIX 1

METHOD USED FOR ANALYSIS OF SULPHIDE CONTENT

Sulfide Sulfur (7)—Official Final Action

(*Note:* $CdSO_4$ is toxic: *see also* **51.084.**)

1.013 ***Reagents***

(a) *Zinc dust.*—Low in Pb.

(b) *Absorbent soln.*—Dissolve 20 g $CdSO_4 \cdot 2\frac{2}{3}H_2O$ in H_2O and dil. to 1 L. Adjust to pH 5.6 potentiometrically or colorimetrically. If colorimetrically, match sep. 50 mL aliquot to buffer of same pH, **50.010**.

(c) *Sodium hydroxide std soln.*—0.1*N*. Prep. and stdze as in **50.032–50.036**.

(d) *Std acid.*—0.1*N* HCl. Stdze against std alkali, (c), using Me red.

(e) *Methyl red indicator.*—Dissolve 0.2 g Me red in 100 mL alcohol.

1.014 ***Apparatus***

Fit 250 mL erlenmeyer with 2-hole No. 5.5 stopper. Insert thru stopper 60 mL separator with stem drawn out to 2 mm and bent upward at tip, adjusting separator so stem is 6 mm from bottom of flask. Also insert thru stopper 6 mm glass outlet tube. Connect with amber rubber tubing to inlet of 25 × 150 mm tube half filled with H_2O and heated to near bp before and during detn. Connect in series 2 addnl tubes of same size, each contg 25 mL absorbent soln and held in 600 mL beaker filled with cold H_2O.

1.015 ***Determination***

Fill absorbent tubes with absorbent soln and heat H_2O tube to gentle boiling. Weigh 1 g slag, ground to pass No. 80 sieve, into evolution flask, add 1 g Zn dust, and wash down sides with 5–10 mL H_2O; mix with flat-end rod and connect flask to app. Add 50 mL HCl (1+4) to separator and let acid flow into reaction flask while swirling contents. If necessary, apply pressure to transfer acid and close stopcock while a little of the acid is still above it. Heat to bp; then regulate to maintain active but not too vigorous boiling for 10 min. Swirl flask frequently after adding acid and for first 5 min of boiling. To disconnect, hold inlet in first absorbent tube firmly with one hand and quickly pull off rubber tubing with other hand without pinching.

Filter CdS suspension by gravity thru 9 cm paper into 250 mL erlenmeyer and wash with H_2O to vol. of 100 mL. Add 4 drops Me red indicator and agitate vigorously while titrg slowly with 0.1*N* NaOH to exact tint of *ref. soln* (50 mL absorbent soln dild to 100 mL, with identical indicator concn, in 250 mL erlenmeyer). If end point is passed so that $Cd(OH)_2$ ppts, add 1–2 mL 0.1*N* HCl, let stand until ppt disappears, and complete titrn dropwise, agitating vigorously.

% $CaCO_3$ equivalence of sulfide *S* in sample = net mL 0.1*N* NaOH/2

g Sulfide S/detn = mL 0.1*N* NaOH × 0.0016

% Sulfide S = g sulfide S × 100

From Ref: [9].

APPENDIX 2

THERMOGRAVIMETRIC ANALYSIS DATA

University of British Columbia
Report No. 64-10966

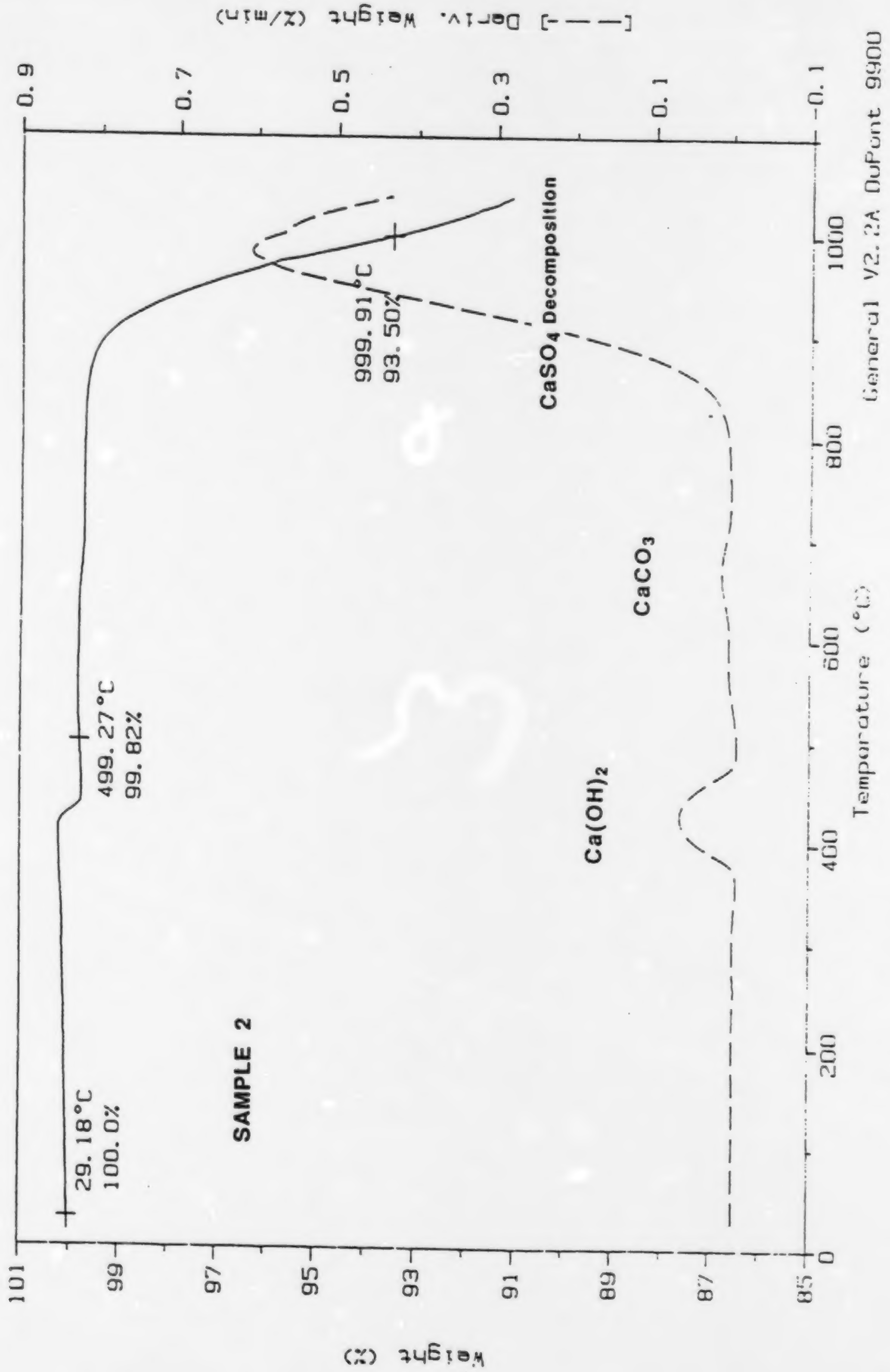

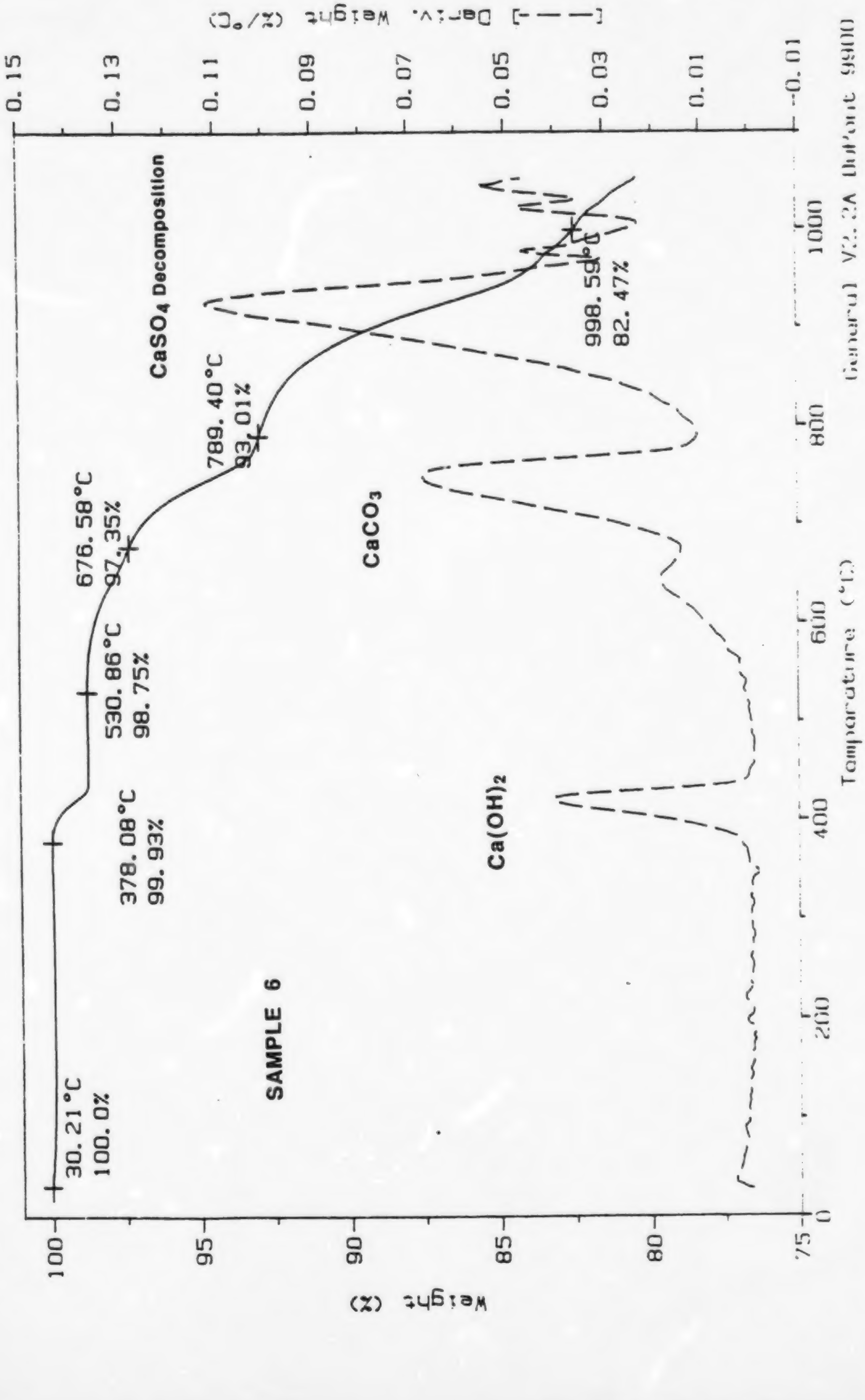
SAMPLE 6
30.21°C
100.0%
378.08°C
99.93%
530.86°C
98.75%
676.58°C
97.35%
789.40°C
93.01%
998.59°C
82.47%
Ca(OH)$_2$
CaCO$_3$
CaSO$_4$ Decomposition
Weight (%)
[– – –] Deriv. Weight (%/°C)
Temperature (°C)
General V2.2A DuPont 9900
100
95
90
85
80
75
0
200
400
600
800
1000
0.15
0.13
0.11
0.09
0.07
0.05
0.03
0.01
-0.01

University of British Columbia
Report No. 64-10966

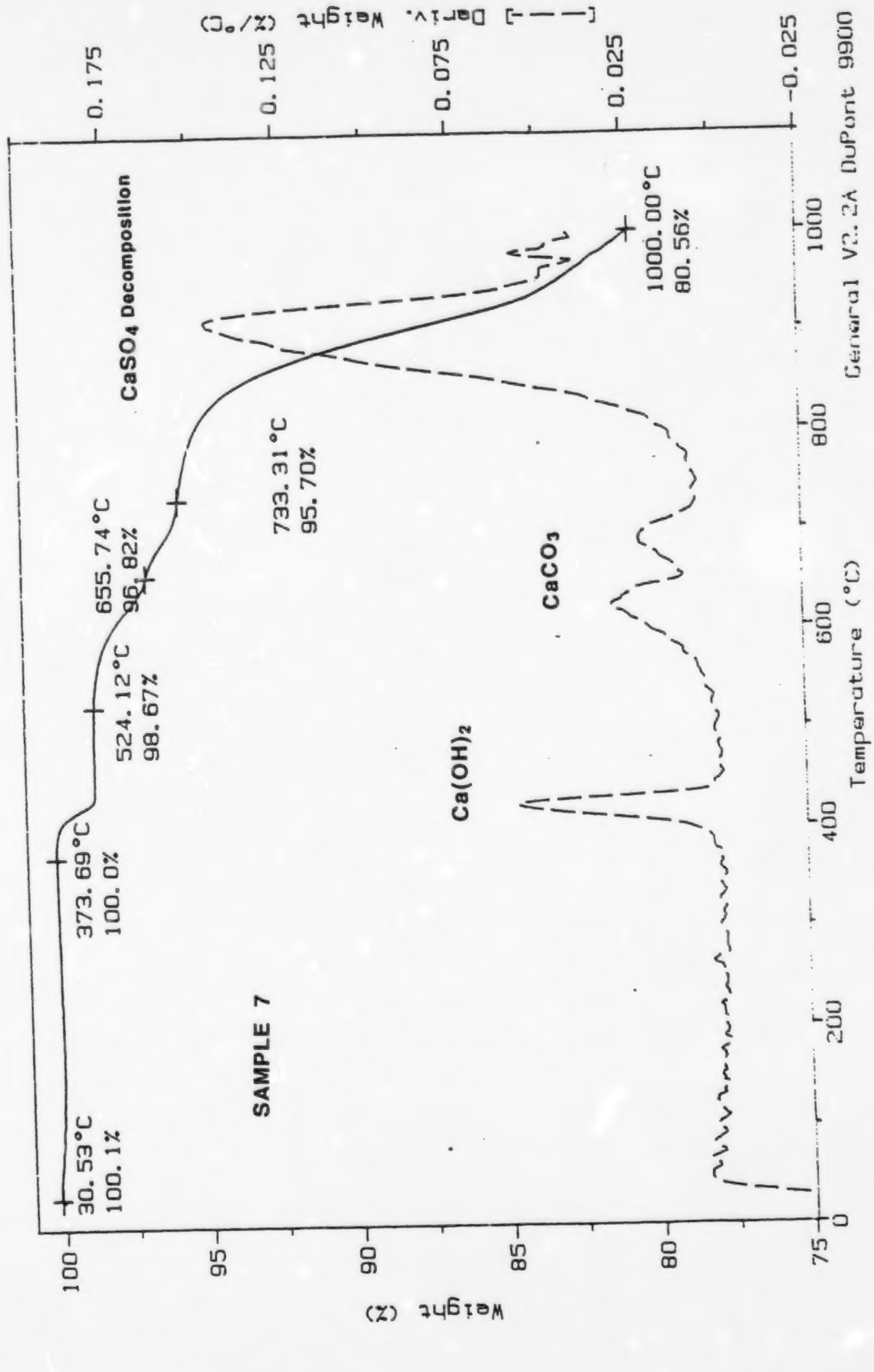

APPENDIX 3

SCANNING ELECTRON MICROGRAPHS

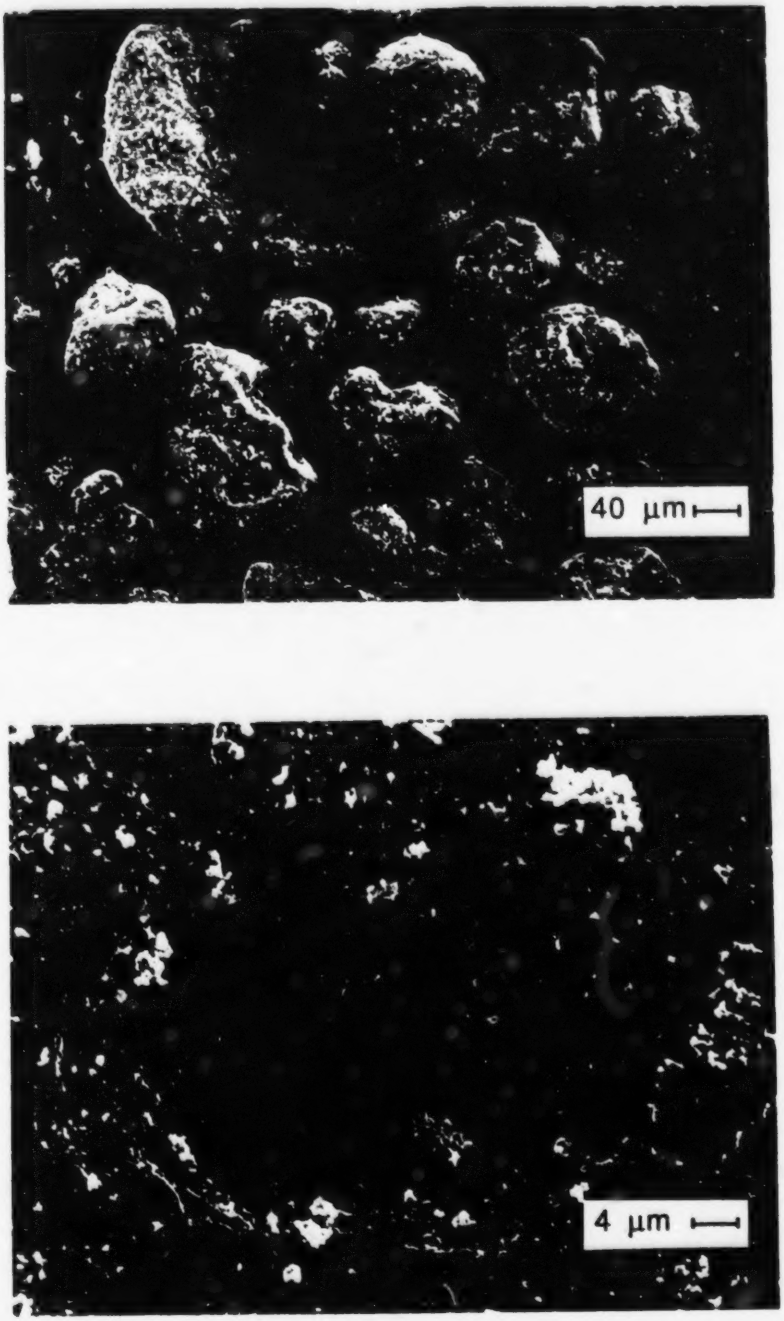

Scanning electron micrographs from primary cyclone return materials (Sample 3)

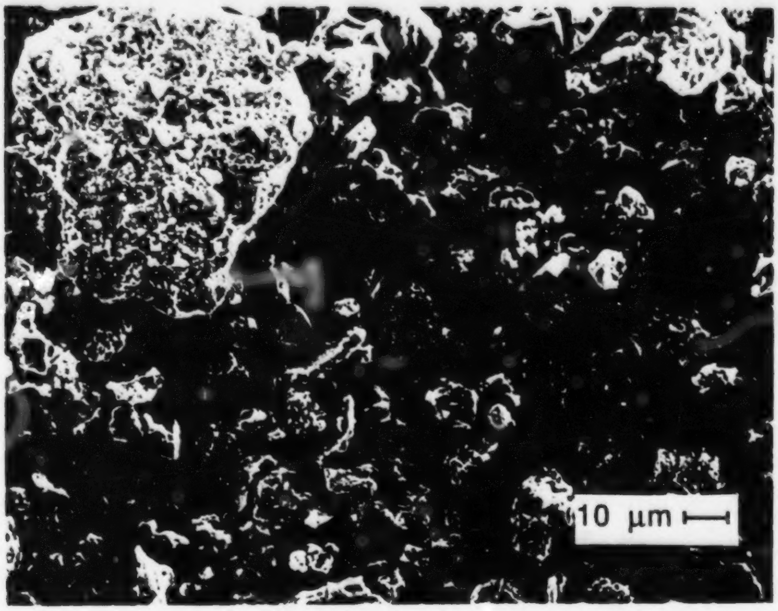

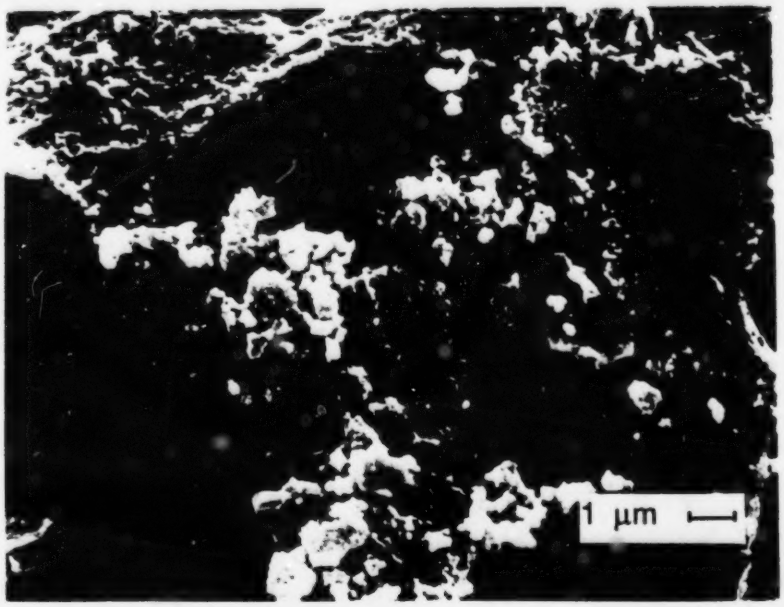

Scanning electron micrographs from secondary cyclone return materials (Sample 6)

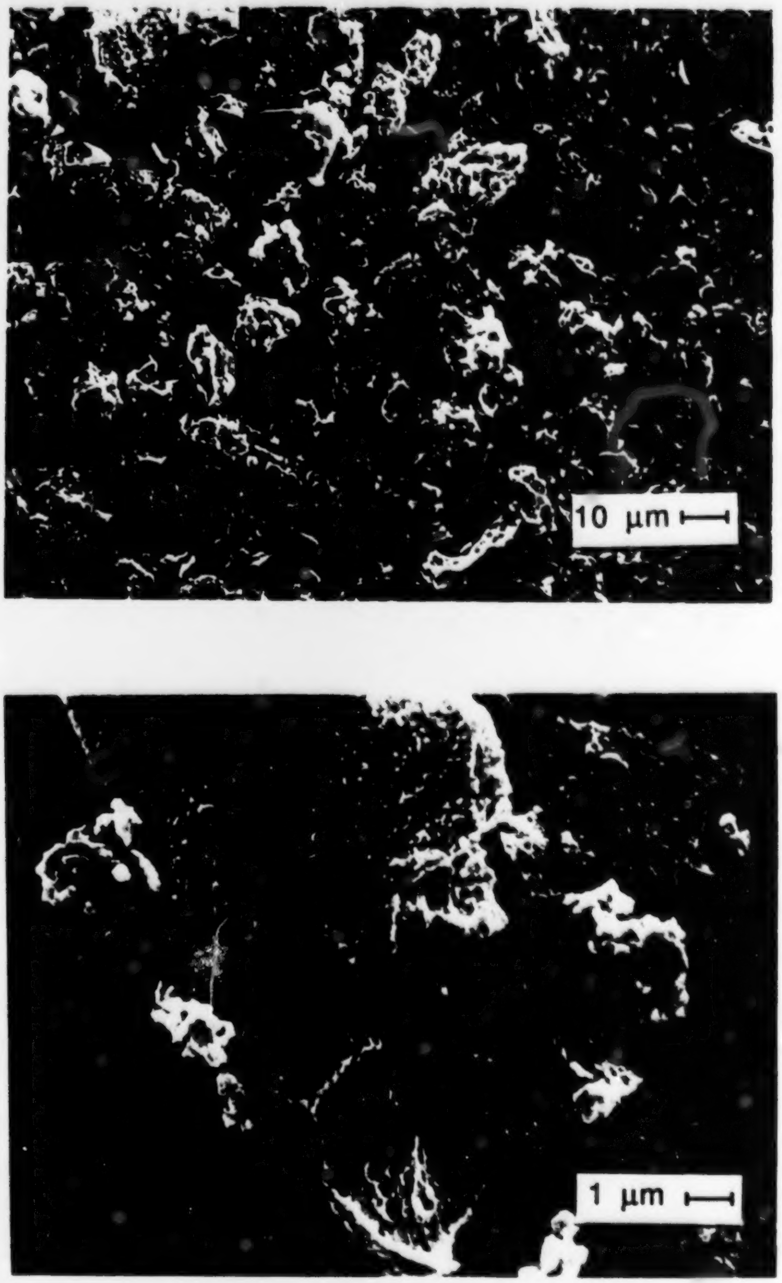

Scanning electron micrographs from baghouse discharge materials (Sample 7)